NNLO QCD⊗QED corrections to unpolarized and polarized SIDIS

By

Vaibhav Pathak

PHYS10201905001

The Institute of Mathematical Sciences, Chennai

A thesis submitted to the

Board of Studies in Physical Sciences

In partial fulfilment of requirements

For the Degree of

DOCTOR OF PHILOSOPHY

of

HOMI BHABHA NATIONAL INSTITUTE

Apr, 2026

Homi Bhabha National Institute

Recommendations of the Viva Voce Board

As members of the Viva Voce Board, we certify that we have read the dissertation prepared by Mr. Vaibhav Pathak entitled "NNLO QCD⊗QED corrections to unpolarized and polarized SIDIS" and recommend that it maybe accepted as fulfilling the dissertation requirement for the Degree of Doctor of Philosophy.

Sanatan Digal
______________________________ Date: 10.08.2026
Chair - Sanatan Digal

V. Ravindran
______________________________ Date: 10.08.2026
Guide/Convener - V. Ravindran

______________________________ Date:
Co-guide -

______________________________ Date: 10.08.2026
Member 1 - Rajesh Ravindran

SSharma
______________________________ Date: 10.08.2026
Member 2 - Sayantan Sharma

______________________________ Date: 10.08.2026
Member 3 - Meduri C. Kumar

______________________________ Date: 10.08.2026
External Examiner - Satyajit Seth

Final approval and acceptance of this dissertation is contingent upon the candidate's submission of the final copies of the dissertation to HBNI.

I hereby certify that I have read this dissertation prepared under my direction and recommend that it may be accepted as fulfilling the dissertation requirement.

Date: 10.08.2026

V. Ravindran

Place: IMSc, Chennai Guide - V. Ravindran

STATEMENT BY AUTHOR

This dissertation has been submitted in partial fulfilment of requirements for an advanced degree at Homi Bhabha National Institute (HBNI) and is deposited in the Library to be made available to borrowers under rules of the HBNI.

Brief quotations from this dissertation are allowable without special permission, provided that accurate acknowledgement of source is made. Requests for permission for extended quotation from or reproduction of this manuscript in whole or in part may be granted by the Competent Authority of HBNI when in his or her judgment the proposed use of the material is in the interests of scholarship. In all other instances, however, permission must be obtained from the author.

Vaibhav Pathak

Vaibhav Pathak

DECLARATION

I, hereby declare that the investigation presented in the thesis has been carried out by me. The work is original and has not been submitted earlier as a whole or in part for a degree / diploma at this or any other Institution / University.

Vaibhav Pathak

Vaibhav Pathak

CERTIFICATION ON ACADEMIC INTEGRITY

Undertaking by the Student

1. I, Vaibhav Pathak, HBNI Enrolment number: PHYS10201905001, hereby declare that the Thesis, titled "NNLO QCD⊗QED corrections to unpolarized and polarized SIDIS" is prepared by me and is the original work undertaken by me.

2. I also hereby undertake that this document has been duly checked through a plagiarism detection tool and the document is found to be plagiarism free as per the guidelines of the Institute/ UGC.

3. I am aware and undertake that if plagiarism is detected in my thesis at any stage in the future, suitable penalty will be imposed as per the guidelines of the Institute/ UGC.

Date:

Vaibhav Pathak

Vaibhav pathak

Endorsed by the Thesis Supervisor:

I certify that the thesis written by the researcher is plagiarism free as mentioned above by the student.

Date:

V. Ravindran

V. Ravindran

Professor-I

Theoretical Physics

IMSc, Chennai

List of Publications arising from the thesis

Journal

1. "**NNLO QCD Corrections to Semi-Inclusive Deep-Inelastic Scattering**"

   Saurav Goyal, Sven-Olaf Moch, Vaibhav Pathak, Narayan Rana, V. Ravindran;

   PhysRevLett.132.251902

2. "**NNLO QCD corrections to unpolarized and polarized SIDIS**"

   Saurav Goyal, Roman N. Lee, Sven-Olaf Moch, Vaibhav Pathak, Narayan Rana, V. Ravindran ;

   PhysRevD.111.094007

3. "**NNLO QCD⊗QED corrections to unpolarized and polarized SIDIS**"

   Saurav Goyal, Roman N. Lee, Sven-Olaf Moch, Vaibhav Pathak, V. Ravindran ;

   arxiv:2510.18872

List of other Publications, Not included in the thesis

Journal

1. "**NNLO QCD Corrections to Polarized Semi-Inclusive Deep-Inelastic Scattering**"

   Saurav Goyal, Roman N. Lee, Sven-Olaf Moch, Vaibhav Pathak, Narayan Rana, V. Ravindran ;

   PhysRevLett.133.211905

2. "**NNLO phase-space integrals for semi-inclusive deep-inelastic scattering**"

   Taushif Ahmed, Saurav Goyal, Syed Mehedi Hasan, Roman N. Lee, Sven-Olaf Moch, Vaibhav Pathak, Narayan Rana, Andreas Rapakoulias, V. Ravindran;

   PhysRevD.10.1103/22x4-dmmp

3. "**Soft and virtual corrections to semi-inclusive DIS up to four loops in QCD**"
   Saurav Goyal, Sven-Olaf Moch, Vaibhav Pathak, Narayan Rana, V. Ravindran;
   PhysRevD.10.1103/p81j-bq5t

Preprint

1. "**Soft and Jet Functions for SCET at Four Loops in QCD**"
   Saurav Goyal, Sven-Olaf Moch, Vaibhav Pathak, V. Ravindran;
   PhysRevD.10.1103/p81j-bq5t

Vaibhav Pathak

Vaibhav Pathak

List of presentations and participations at conferences

1. A Talk on *"Next-to-Soft-virtual resummation for SIDIS to NNLO+$\overline{NNLL}$"*, at Matter to the Deepest 2025, Sept 14-19, Katowice,Poland.

2. A Talk on *"Next-to-Soft-virtual resummation for SIDIS to NNLO+$\overline{NNLL}$"*, at DAE-Symposium 2024, Dec 19-23, 2024, Banaras Hindu University, Varanasi, India.

3. A Talk on *"NNLO QCD correction to SIDIS"*, at Advanced School & Workshop on Multiloop Scattering Amplitudes, Jan 15-19, 2024, NISER, Bhubaneswar, India.

4. Organised a school *"Advanced Methods in Precision Studies"*, July 1-6, 2025, IMSc, Chennai, India.

5. Attended *"Computer Algebra and Particle Physics (CAPP 2025)"*, Mar 24-28, 2025, DESY, Hamburg,Germany.

6. Attended *"IMSc Spring School on High Energy Physics "*, 24 Feb-7 Mar, 2025, IMSc, Chennai,India.

7. Attended *"Frontiers in Particle Physics 2024"*, Aug 9-11, 2024, IISc, Bangalore, India.

8. Attended *"Advanced School & Workshop on Multiloop Scattering Amplitudes"*, Jan 15-19, 2024, NISER, Bhubaneswar, India.

9. Attended *"Theory Challenges in the Precision Era of the Large Hadron Collider"*, Aug 28-Oct 13, 2023, Galileo Galilei Institute, Florence, Italy.

10. Attended *"DAE-Symposium 2022"*, Dec 12-16, 2022, IISER Mohali, India.

11. Attended *"GIAN Course: Recent Advances in Perturbative Quantum Chromodynamics"*, Nov 2-9, 2022, Mumbai University, Mumbai, India.

Research visits and seminars

1. Seminar on *"NNLO QCD $\otimes$ QED correction to unpolarized and polarized SIDIS"*, Oct 1-4,2025 at University of Milan,Italy.

2. Seminar on *"NNLO QCD $\otimes$ QED correction to unpolarized and polarized SIDIS"*, Sept 27-29,2025 at University of Cosenza,Italy.

3. Seminar on *"NNLO QCD $\otimes$ QED correction to unpolarized and polarized SIDIS"*, Sept 20-23,2025 at wigner institute of Physics, budapest,Hungary.

To those who inspired me

ACKNOWLEDGEMENTS

Though research often unfolds in solitude, no journey of understanding is truly solitary; it is shaped by the guidance of mentors, the companionship of friends, and the unwavering faith of family.

While this thesis carries a single author's name, its journey has been shaped by many-mentors who guided my thinking, friends who enriched the path, and family whose faith never wavered.

I would like to begin by expressing my deepest appreciation to V. Ravindran. I will never forget the day he agreed to let me begin my PhD journey under his supervision; it was a defining moment for which I am profoundly grateful. He has helped me evolve immensely, both as a researcher and as a person. Beyond the equations and the physics, he has taught me invaluable life lessons that I hope to carry with me always. I am especially thankful for his extraordinary patience; no matter how many times I approached him with the same questions, he always took the time to explain everything with care and clarity. During the many instances when I felt frustrated or overwhelmed by the challenges of research, he was always there to reassure me, telling me not to worry and helping me maintain my focus. I truly feel that I can never fully repay the debt of gratitude I owe him for the kindness, guidance, and support he has extended to me throughout these years. I am immensely grateful for his unwavering academic support and constant encouragement.

I would like to express my sincere gratitude to my collaborators: Saurav Goyal, Prof. Sven-Olaf Moch, Prof. Roman N. Lee, Prof. Narayan Rana, and Prof. Taushif Ahmed. My PhD journey has been significantly enriched by their valuable suggestions and the deep insights they shared throughout our work together. Working with such a distinguished group has been a profound learning experience for me. I am truly thankful for the opportunity to have learned so much from each of them. I would also like to express my sincere gratitude to Aparna Sankar and Surbhi Tiwari. I am truly grateful for the valuable

time they dedicated to me during my initial days of the PhD. Their support and guidance were instrumental in helping me navigate the early challenges of my research journey, and I deeply appreciate the kindness they showed me as I was starting out. My journey would be incomplete without mentioning Saurav Goyal. We set forth on this path together as researchers and have witnessed each other's evolution along the way. Working alongside him has taught me the true value of teamwork, which consistently brings out the best in every individual.

I am also deeply grateful to my seniors for their invaluable guidance and support. I would like to specifically thank Anurag Tripathi, Manoj Kumar Mandal, Maguni Mahakhud, Taushif Ahmed, Narayan Rana, Pulak Banerjee, Prasanna Kumar Dhani, Amlan Chakraborty, Pooja Mukherjee, and Ajjath A.H., Aparna Sankar and Surbhi Tiwari for the insights they shared throughout my time in the group. Furthermore, I would like to express my sincere gratitude to Satyajit Seth, M.C. Kumar, Ambresh Shivaji, Goutam Das, Gauhar Abbas, Saurav Pal, and Kajal Samanta. I am truly thankful for our occasional interactions and for the valuable guidance and support they provided throughout my journey.

I am also profoundly thankful to Amlan Chakraborty. Our numerous academic and non-academic discussions have had a lasting impact on me, and his views have changed my perspective in many meaningful ways. I am truly grateful for his guidance and support throughout my entire PhD journey.

I would like to express my sincere thanks to the members of my Doctoral Committee: Prof. D. Indumathi, Prof. Sanatan Digal, Prof. V. Ravindran, Prof. R. Rajesh, Prof. Sayantan Sharma, and Prof. M.C. Kumar. I am grateful for their oversight and for the constructive feedback they provided throughout my research. I would also like to thank Prof. Shrihari Gopalakrishna, Padmanath M. and Prof. Syed Hasan for attending my DC meetings and for their valuable comments and insights. I also would like to thank Prof. Nemani, Prof. Alok for their encouragement.

I am grateful to my friends among the IMSc postdoctoral fellows, especially Ratan, Biswajit, Tousik, Purushottam and Navdeep. I truly appreciated our academic and non academic discussions. I would like to thank Ratan, Biswajeet, Toushik,Saurav and Bhaskar for the weekend dinners that provided much-needed breaks and a sense of camaraderie. I would also like to thank Pritam Sen, Prabhat Butola, and Shivam Gola for our many stimulating discussions on particle physics. Furthermore, I am thankful to the members of the IMSc Pheno-Journal Club; the group provided a wonderful platform for valuable discussions that significantly broadened my understanding of the field.

I am also deeply grateful to the IMSc lunch group: Indumathi, Shrihari, Ravindran, Shibashish, Saurav, Prem, Hitesh, Krishna, Amit, Tausik, Biswajit, Ratan and Prabhat. I truly cherished our daily conversations covering a wide variety of topics; it was a rare and wonderful space where one could express opinions freely.

I would like to thank Prof. German Rodrigo for fruitful discussions during RADCOR, and Prof. Stefan Weinzierl for enlightening discussions on Master Integrals. I am grateful to Prof. George Sterman and Prof. Lance Dixon for wonderful discussions during my GGI visit. I also thank Prof. Gábor Somogyi for his hospitality and discussions, and Prof. Giancarlo Ferrera for the wonderful exchange on resummation during my visit to Milan. A special thanks goes to Prof. Sven-Olaf Moch for his warm hospitality in Hamburg and for his kind invitations to Europe.

I am grateful to my school teacher, Gayatri Prasad Tiwari, for making physics interesting for me and setting me on this path. I would like to thank my school friends: Shivam, Harshit, Himanshu, Akash, Yogesh, Ranjan, Utkarsh, Manish, Avinash and many more. I am also deeply thankful to my undergraduate friends Omkar, Sudheer, Ravikant, Ansh, Sukesh, Avinash, Vinit and Rajan for the companionship, joy, and laughter we shared. I am thankfull to my undergraduate roommates Shreyansh, Anand, Adarsh, Shivam , as well as my friends Anshuman, Vikas, and Krishna, for their support during those formative years.

I would like to thank all the administrative and non-academic staff at IMSc. In particular, I am grateful to the Ex-Director, Prof. V. Ravindran and Director Prof. Amritanshu Prasad, as well as to Ms. Indra, Ms. Prema, Mr. Johnson, Mr. Vasan, and Mr. Chandru for their support and assistance throughout various stages of my PhD. I also extend my sincere thanks to the canteen staff and housekeeping personnel, whose tireless efforts ensured that we were well-fed and that our surroundings remained clean and comfortable. Their dedication played a vital role in making day-to-day life at the institute smooth and welcoming.

I would like to thank my senior Gopal Prakash for teaching me how to use 'vim' and also would like to thank Sumit Shaw for teaching me many physics concepts and life lessons. I would like to thank my imsc friends : Amit Kumar, Chandrani, Vinay, Koyena, Souvik, Pavitra, Farina, Tanmoy, Kalyani, Ananta, Vishwajeet, Bhabani, Adarsh Vishwakarma and many more whose names I may have inadvertently missed.

During my time at IMSc, I was fortunate to be surrounded by a group of wonderful friends who were a constant source of warmth, encouragement and support. I would like to express my heartfelt thanks to Samim, Hitesh, Jatin, Krishna, Prem, Ravi, Tanishk, Adarsh, Amit (The Wild group) and Rakesh for being cheerful, dependable, and spirited companions throughout this journey. Their friendship provided me with the strength to navigate the inevitable ups and downs of a PhD, and their enthusiasm and positivity brought lightness to even the most challenging times. Whether it was our Friday night gatherings, Saturday movie evenings, trips, and parties filled with laughter and conversation, these moments created a sense of belonging and community that I will always cherish. The memories we built together remain among the most treasured aspects of my time at IMSc.

Last but certainly not least, my deepest and most heartfelt thanks go to my Grandparents, Parents, Uncles, Aunts, and Bua for their unwavering faith in me to pursue my dreams and their constant support through every stage of my life. Their belief in my abilities gave me the strength to persevere, even during the most difficult times. I am eternally grateful to my siblings- Garima, Gaurav, Akanksha, Sachin, Vikas, Stuti, Nitin, Aman, Shreyas, and Abhay and my sister-in-law Renuka - without whom this long and challenging PhD journey would not have been possible. Finally, a special mention to Anvi, Vashishtha, and Shambhvi for the joy they bring and for making me a proud uncle.

Contents

Summary

Understanding the internal structure of hadrons in terms of its fundamental constituents, quarks and gluons, is one of the central goals of modern high-energy physics. Quantum Chromodynamics (QCD), the non-abelian gauge theory describing the strong interaction, provides the theoretical framework to study the dynamics of quarks and gluons inside hadrons. However, due to the nonperturbative nature of QCD at low energy scales, a complete description of hadronic structure requires a combination of perturbative calculations from theory side and phenomenological inputs from experimental measurements.

Deep-inelastic scattering (DIS) has played a important role in revealing the partonic structure of nucleons. In inclusive DIS, only the scattered lepton is detected in the final state, and the process provides access to parton distribution functions (PDFs), which describe the probability of finding a parton carrying a given fraction of the nucleon momentum. Although inclusive DIS has played a crucial role in determining PDFs with high precision, it provides only limited information about the hadronization process through which partons form observable hadrons.

Semi-inclusive deep-inelastic scattering (SIDIS) offers a more detailed probe of the nucleon structure. In SIDIS, in addition to the scattered lepton, a hadron produced in the final state is also detected. This additional information allows simultaneous access to both PDFs and fragmentation functions (FFs). While PDFs describe the momentum distribution of partons inside the nucleon, FFs characterize the process through which partons fragment into observable hadrons. The study of SIDIS therefore provides a opportunity to

investigate both the partonic structure of nucleons and the dynamics of hadron formation.

Within the framework of QCD factorization, the cross section for SIDIS can be written as a convolution of perturbatively calculable coefficient functions (CFs) with PDFs and FFs. The CFs encode the short-distance partonic dynamics and can be computed systematically within perturbative QCD as a power series in the strong coupling constant. Achieving high theoretical precision requires the computation of these CFs to higher orders in perturbation theory.

For inclusive DIS, coefficient functions and splitting functions have been computed up to very high orders in perturbation theory, providing a solid theoretical foundation for global analyses of PDFs. In contrast, the semi-inclusive case is much more involved. The presence of an additional detected hadron introduces extra kinematic variables and a more complicated phase-space structure, making higher-order calculations significantly more challenging. As a consequence, for a long time the SIDIS coefficient functions were known exactly only up to next-to-leading order (NLO) in QCD.

In recent years, the increasing precision of experimental measurements has motivated the need for improved theoretical predictions for SIDIS processes. In particular, future facilities such as the Electron-Ion Collider (EIC) are expected to provide high-precision data over a wide kinematic range. To fully exploit the potential of these measurements, it is essential to reduce theoretical uncertainties by incorporating higher-order perturbative corrections.

The main objective of this thesis is to advance the theoretical understanding of semi-inclusive deep-inelastic scattering by computing higher-order corrections within the framework of perturbative QCD and QED. In particular, this work focuses on the evaluation of next-to-next-to-leading order (NNLO) contributions to the SIDIS coefficient functions. These calculations represent an important step toward achieving precision predictions that match the accuracy of present and future experimental data.

The computation of higher-order corrections involves the evaluation of multi-loop Feynman diagrams and the treatment of infrared and collinear singularities that arise in intermediate steps of the calculation. Modern techniques in perturbative quantum field theory, including integration-by-parts identities, reduction to master integrals, and differential equation methods, are employed to systematically evaluate the relevant Feynman integrals. These methods allow the complicated loop integrals to be expressed in terms of a finite set of master integrals, which can then be computed analytically or semi-analytically.

In addition to QCD corrections, electromagnetic effects can also play an important role in precision studies of SIDIS. Although QED corrections are typically smaller than the corresponding QCD contributions, their inclusion becomes increasingly important when aiming for high theoretical accuracy. In this thesis, NNLO QED corrections as well as mixed QCD$\otimes$QED contributions are also investigated for both unpolarized and polarized SIDIS observables. These corrections provide a more complete theoretical description of the process and contribute to reducing the overall theoretical uncertainties.

The results obtained in this work improve the perturbative description of SIDIS and provide important ingredients for future phenomenological analyses. In particular, the higher-order corrections computed in this thesis contribute to stabilizing the perturbative expansion and reducing the dependence of theoretical predictions on the choice of renormalization and factorization scales. This improvement in theoretical precision is essential for reliable extractions of PDFs and FFs from experimental data.

Furthermore, the results presented in this thesis are expected to play an important role for upcoming high-precision measurements at facilities such as the Electron-Ion Collider (EIC). The EIC will provide unprecedented access to the 3-d structure of nucleons and nuclei, and accurate theoretical predictions will be necessary for fully exploiting the scientific potential of this facility.

In summary, this thesis contributes to the ongoing effort to achieve precision theoretical predictions for SIDIS. By computing higher-order QCD and QED corrections to SIDIS coefficient functions, this work provides inputs for future global analyses of parton distribution and fragmentation functions and helps bridge the gap between theoretical developments and experimental measurements in the study of hadronic structure.

List of Figures

Chapter 1

Introduction

Contents

Understanding the fundamental structure of matter and the interactions governing its constituents has been a main theme in physics. Over the past century, experiments involving high-energy particle collisions have played a vital role in revealing the microscopic structure of matter. By accelerating particles to extremely high energies and allowing them to collide, physicists are able to probe smaller distance scales, hence uncovering the fundamental building blocks of nature.

These experimental efforts have led to the development of the Standard Model of particle physics, a theoretical framework that successfully describes three of the four known fundamental interactions: the electromagnetic, weak, and strong forces. Within this framework, matter consists of fermions (quarks and leptons), while interactions between them are mediated by gauge bosons. The discovery of the Higgs boson confirmed the mechanism responsible for providing masses to particles and became an important milestone in validating the Standard Model.

Among the fundamental interactions, the strong interaction plays a unique role in shaping the structure of visible matter. It is responsible for binding quarks into hadrons such as protons and neutrons and for holding these nucleons together within atomic nuclei. The theory describing the strong interaction is QCD, a non-Abelian gauge theory based on the symmetry group $SU(3)_c$. In this theory, quarks carry a color charge and interact through the exchange of gluons, the gauge bosons of the strong force. A hallmark of QCD is the phenomenon of *asymptotic freedom* [1–5]: at short distances, corresponding to large momentum transfers, the strong coupling decreases and the interaction becomes weak, allowing the use of perturbative techniques. And, at larger distance scales the coupling grows strong, confining quarks and gluons within color-neutral bound states. This interplay between perturbative and nonperturbative dynamics makes QCD a rich and interesting theory.

Although protons and neutrons are often treated as elementary particles in low-energy phenomena, they are in fact highly dynamic objects composed of quarks and gluons. Understanding how these constituents contribute to the observable properties of the proton remains one of the central challenges in strong interaction physics. In particular, determining how the momentum, spatial distribution, and spin of the proton arise from its quark and gluon degrees of freedom is an active area of research.

An example of this challenge is the proton spin puzzle [6,7]. Early measurements revealed that the intrinsic spins of quarks account for only a fraction of the total spin of the proton. This observation raised fundamental questions about how the remaining spin is distributed among gluon contributions and the orbital angular momentum of quarks and gluons. This problem requires precise experimental measurements together with accurate theoretical calculations within the framework of QCD.

Future experimental facilities are expected to significantly advance our understanding of hadronic structure. One of the most ambitious projects in this direction is the Electron-Ion Collider (EIC) [8, 9], a next-generation accelerator designed to collide electrons with protons and nuclei. The EIC will provide unprecedented accuracy and a wide kinematic reach, allowing detailed studies of the internal structure of nucleons and nuclei. Among its primary scientific goals are the determination of the spin and spatial structure of the proton, the mapping of the momentum distributions of quarks and gluons, and the investigation of QCD in high parton density regime.

At very high energies and small values of the Bjorken variable x, gluons are expected to dominate the internal structure of hadrons. In this regime, gluon densities can become extremely large, leading to collective phenomena that cannot be described within the framework of dilute partonic systems. This region may be characterized by a novel state of matter known as the Color Glass Condensate (CGC), where gluon fields form a dense and coherent system governed by nonlinear QCD dynamics. Investigating this regime represents one of the key objectives of the EIC physics program.

To interpret the results of such experiments, precise theoretical predictions are required. At sufficiently large momentum transfer, many scattering processes can be described within perturbative QCD. In this framework, physical observables are computed as expansions in the strong coupling constant. In modern precision calculations, electromagnetic effects described by QED may also contribute and are often included together with QCD corrections when higher theoretical accuracy is required. These calculations provide the connection between experimentally measured cross sections and the underlying partonic structure of hadrons.

1.1 Lagrangian

The fundamental interactions among quarks and leptons at the energy scales relevant to high-energy scattering processes are described by two gauge field theories: Quantum Chromodynamics (QCD) and Quantum Electrodynamics (QED) [10–15]. QCD governs the dynamics of the strong interaction, while QED accounts for the electromagnetic interactions of electrically charged particles. Together they form the gauge structure $SU(N_c) \times U(1)$, which is responsible for the interactions of quarks and leptons with gluons and photons.

QCD is a non-Abelian gauge field theory based on the local symmetry group $SU(N_c)$ with $N_c = 3$, corresponding to the three color charges carried by quarks. In this theory, quarks interact through the exchange of gluons, which are the gauge bosons associated with the strong force. Because gluons themselves carry color charge, they interact with one another, giving rise to nonlinear dynamics responsible for *asymptotic freedom* and *confinement*.

The gauge-invariant classical Lagrangian density of QCD is given by

$$\mathcal{L}_{\mathrm{QCD}}^{\mathrm{classical}} = -\frac{1}{4} G^{a}_{\mu\nu} G^{\mu\nu}_{a} + \sum_{f=1}^{n_f} \bar{\psi}_f \left(i\gamma^\mu D_\mu - m_f \right) \psi_f \,, \tag{1.1}$$

where ψ_f denotes the quark field of flavor f with mass m_f, and G^a_μ represents the gluon field in the adjoint representation of $SU(N_c)$. The gluon field-strength tensor is defined as

$$G^a_{\mu\nu} = \partial_\mu G^a_\nu - \partial_\nu G^a_\mu + g_s f^{abc} G^b_\mu G^c_\nu \,, \tag{1.2}$$

where f^{abc} are the structure constants of the $SU(N_c)$ group and g_s is the strong coupling constant. The nonlinear term proportional to g_s reflects the self-interaction among gluons.

The covariant derivative appearing in the quark kinetic term is

$$D_\mu = \partial_\mu - i g_s G^a_\mu T^a \,, \tag{1.3}$$

where T^a are the generators of $SU(N_c)$ in the fundamental representation, satisfying the Lie algebra

$$\left[T^a, T^b\right] = i f^{abc} T^c \,. \tag{1.4}$$

The generators are normalized as $\mathrm{Tr}(T^a T^b) = T_F\,\delta^{ab}$ with $T_F = \frac{1}{2}$, and they satisfy the completeness relation

$$\sum_a T^a_{ij} T^a_{kl} = T_F \left(\delta_{il}\,\delta_{kj} - \frac{1}{N_c}\,\delta_{ij}\,\delta_{kl}\right) . \tag{1.5}$$

Two important quadratic Casimir operators of $SU(N_c)$ arise frequently in perturbative calculations:

$$\sum_a (T^a T^a)_{ij} = C_F\,\delta_{ij} \,, \qquad \sum_{c,d} f^{acd} f^{bcd} = C_A\,\delta^{ab} \,, \tag{1.6}$$

where $C_A = N_c$ is the Casimir of the adjoint representation and $C_F = (N_c^2 - 1)/(2N_c)$ is the Casimir of the fundamental representation. For QCD, $N_c = 3$ gives $C_A = 3$ and $C_F = 4/3$.

Under a local $SU(N_c)$ gauge transformation $U(x) \in SU(N_c)$, the quark and gluon fields transform as

$$\psi_f(x) \to U(x)\,\psi_f(x) \,, \qquad G_\mu(x) \to U(x)\,G_\mu(x)\,U^{-1}(x) + \frac{i}{g_s}\,(\partial_\mu U(x))\,U^{-1}(x) \,. \tag{1.7}$$

The quantization of a non-Abelian gauge theory faces an immediate difficulty: due to gauge invariance, gauge fields contain redundant degrees of freedom which prevents unique construction of the gauge field propagator. This is resolved by fixing the gauge, which in the covariant formulation introduces two additional contributions to the Lagrangian: a gauge-fixing term and a ghost term arising from the Faddeev-Popov procedure.

The full quantized QCD Lagrangian reads

$$\mathcal{L}_{\rm QCD} = \mathcal{L}_{\rm QCD}^{\rm classical} - \frac{1}{2\xi_g}\left(\partial^\mu G^a_\mu\right)^2 + \left(\partial^\mu \bar{c}^a\right)\left(\partial_\mu \delta^{ad} - g_s f^{abd} G^b_\mu\right) c^d\,, \tag{1.8}$$

where ξ_g is the gluon gauge-fixing parameter and c^d, $\bar{c}^a$ are the anticommuting Faddeev-Popov ghost and anti-ghost fields. These ghost fields are unphysical scalar fields obeying fermionic statistics; they never appear as external states but must be included in loop calculations to cancel unphysical degrees of freedom of the gauge field and maintain unitarity of the theory. The choice $\xi_g = 1$ corresponds to the Feynman gauge, which is often used in perturbative calculations, physical observables are independent of ξ_g.

The electromagnetic interaction is described by QED, an Abelian gauge theory based on the local symmetry group $U(1)$. Unlike gluons in QCD, photons do not carry electric charge and therefore do not self-interact. The QED Lagrangian for a set of n_f quark flavors and n_L leptons is

$$\mathcal{L}_{\rm QED} = -\frac{1}{4}F_{\mu\nu}F^{\mu\nu} - \frac{1}{2\xi_e}\left(\partial^\mu A_\mu\right)^2 + \sum_{f=1}^{n_f}\bar{\psi}_f\left(i\gamma^\mu\partial_\mu + eQ_f \not{A} - m_f\right)\psi_f + \sum_{\ell=1}^{n_L}\bar{\psi}_\ell\left(i\gamma^\mu\partial_\mu + e\not{A} - m_\ell\right)\psi_\ell\,, \tag{1.9}$$

where A_μ is the photon field, e is the electromagnetic coupling constant, Q_f is the electric charge of quark flavor f in units of the proton charge, ψ_ℓ denotes the lepton field of flavor ℓ with mass m_ℓ, and ξ_e is the photon gauge-fixing parameter. The electromagnetic field-strength tensor is

$$F_{\mu\nu} = \partial_\mu A_\nu - \partial_\nu A_\mu\,. \tag{1.10}$$

Since photons are electrically neutral, $F_{\mu\nu}$ is linear in A_μ and contains no self-interaction terms. Under the Abelian $U(1)$ gauge transformation by a local scalar $\alpha(x)$, the fields transform as

$$\psi_f(x) \to e^{-ieQ_f\alpha(x)}\,\psi_f(x)\,, \qquad A_\mu(x) \to A_\mu(x) - \partial_\mu\alpha(x)\,. \tag{1.11}$$

Because the $U(1)$ gauge group is Abelian, no ghost fields are required for the consistent quantization of QED.

When both strong and electromagnetic interactions are simultaneously present, quarks carry both color charge and electric charge, and the full theory is based on the gauge group $SU(N_c) \times U(1)$. The covariant derivative acting on a quark field of flavor f with electric charge Q_f then takes the form

$$D_\mu = \partial_\mu - ig_s G^a_\mu T^a - ieQ_f A_\mu \,, \tag{1.12}$$

which couples the quark simultaneously to both the gluon and photon fields, extending eq. (1.3) to the combined $SU(N_c) \times U(1)$ theory. The combined Lagrangian after gauge fixing is

$$\begin{aligned}\mathcal{L} = &\sum_{f=1}^{n_f} \bar{\psi}_f \left(i\gamma^\mu \partial_\mu - g_s \gamma^\mu G^a_\mu T^a - eQ_f \gamma^\mu A_\mu - m_f\right) \psi_f + \sum_{\ell=1}^{n_L} \bar{\psi}_\ell \left(i\gamma^\mu \partial_\mu + e\gamma^\mu A_\mu - m_\ell\right) \psi_\ell \\ &- \frac{1}{4} G^a_{\mu\nu} G^{\mu\nu}_a - \frac{1}{4} F_{\mu\nu} F^{\mu\nu} - \frac{1}{2\xi_g} \left(\partial^\mu G^a_\mu\right)^2 - \frac{1}{2\xi_e} \left(\partial^\mu A_\mu\right)^2 + \left(\partial^\mu \bar{c}^a\right) \left(\partial_\mu \delta^{ad} - g_s f^{abd} G^b_\mu\right) c^d \,,\end{aligned} \tag{1.13}$$

The corresponding propagators and interaction vertices derived from this Lagrangian are shown below.

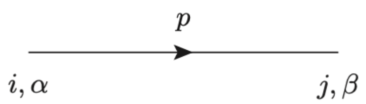

$$= \frac{i\,\delta_{ij}\,(\not{p} + m_f)_{\alpha\beta}}{p^2 - {m_f}^2 + i\epsilon}$$

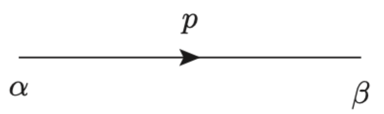

$$= \frac{i\,(\not{p} + m_\ell)_{\alpha\beta}}{p^2 - {m_\ell}^2 + i\epsilon}$$

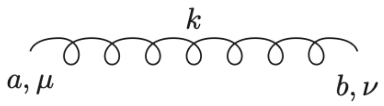

$$= \frac{i\,\delta^{ab}}{k^2 + i\epsilon}\left[-\,g_{\mu\nu} + (1-\xi_g)\frac{k_\mu k_\nu}{k^2}\right]$$

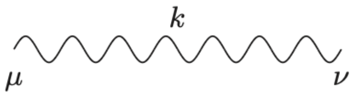

$$= \frac{i}{k^2 + i\epsilon}\left[-\,g_{\mu\nu} + (1-\xi_e)\frac{k_\mu k_\nu}{k^2}\right]$$

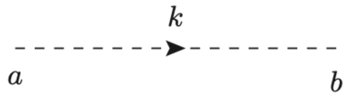

$$= \frac{i\,\delta^{ab}}{k^2 + i\epsilon}$$

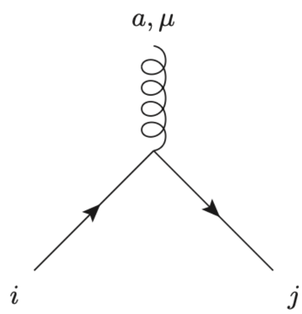

$$= \; i\,g_s\,(T^a)_{ij}\,\gamma^\mu$$

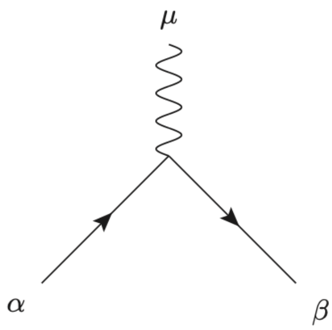

$$= \; i\,e\,\gamma^\mu_{\alpha\beta}$$

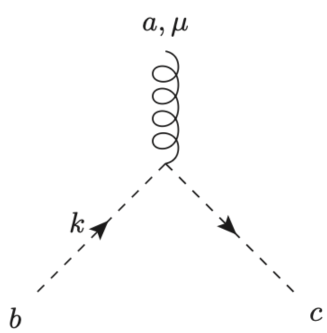

$$= \; g_s\,f^{abc}\,k^\mu$$

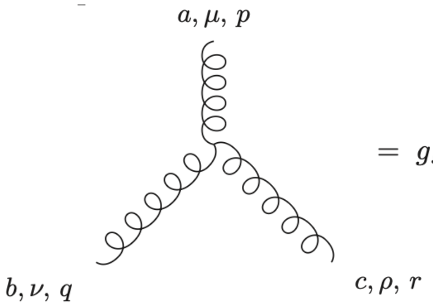

$$= g_s f^{abc}[g^{\mu\nu}(p-q)^\rho + g^{\nu\rho}(q-r)^\mu + g^{\rho\mu}(r-p)^\nu]$$

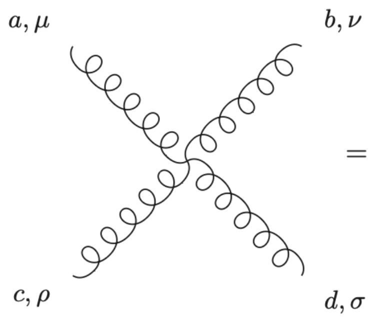

$$= -i\, g_s^2 \Big[f^{abe} f^{cde} (g^{\mu\rho} g^{\nu\sigma} - g^{\mu\sigma} g^{\nu\rho}) + f^{ace} f^{bde} (g^{\mu\nu} g^{\rho\sigma} - g^{\mu\sigma} g^{\nu\rho}) + f^{ade} f^{bce} (g^{\mu\nu} g^{\rho\sigma} - g^{\mu\rho} g^{\nu\sigma}) \Big]$$

This Lagrangian encodes the full dynamics of quarks and leptons interacting through both strong and electromagnetic forces, and provides the theoretical starting point for higher-order perturbative calculations.

1.1.1 Renormalization

Perturbative calculations in QCD and QED generate ultraviolet (UV) divergences from loop integrals, as well as infrared (IR) divergences associated with massless gluons, massless photons, and (nearly) massless quarks and leptons. A consistent and Lorentz-invariant method for handling these divergences is *dimensional regularization* [16–18], in which the spacetime dimension is analytically continued to

$$D = 4 + \varepsilon\,, \tag{1.14}$$

where ε is a small parameter. UV and IR divergences appear as poles $1/\varepsilon^n$. Because the coupling constants g_s and e acquire a mass dimension in $D \neq 4$, an arbitrary mass scale μ is introduced to keep the couplings dimensionless. In the modified minimal subtraction ($\overline{\text{MS}}$) scheme, renormalized couplings absorb the UV poles along with the combination $\ln(4\pi) - \gamma_E$, where $\gamma_E \simeq 0.5772$ is the Euler-Mascheroni constant. This is encoded in the factor

$$S_\varepsilon = \exp\left[\frac{(\gamma_E - \ln 4\pi)\,\varepsilon}{2}\right]. \tag{1.15}$$

The $\overline{\text{MS}}$ scheme is the standard choice in modern multi-loop computations due to its simplicity and the absence of large logarithms at the renormalization scale.

To make physical observables finite, all bare (unrenormalized) fields and parameters in the Lagrangian are expressed in terms of renormalized quantities through multiplicative renormalization constants. The quark, lepton, gluon, and photon fields are renormalized as

$$\psi_q = Z_{2q}^{1/2}\,\psi_q^r\,, \quad \psi_\ell = Z_{2\ell}^{1/2}\,\psi_\ell^r\,, \quad G_\mu^a = Z_3^{1/2}\,G_{\mu,r}^a\,, \quad A_\mu = Z_{3\gamma}^{1/2}\,A_{\mu,r}\,, \tag{1.16}$$

where Z_{2q}, $Z_{2\ell}$, Z_3, and $Z_{3\gamma}$ are the quark-field, lepton-field, gluon-field, and photon-field renormalization constants,

The coupling constants and masses are renormalized as

$$g_s = Z_g\, g_s^r\,, \quad e = Z_e\, e^r\,, \quad m_q = Z_{m_q}\, m_q^r\,, \quad m_\ell = Z_{m_\ell}\, m_\ell^r\,. \tag{1.17}$$

All renormalized quantities are designated with a superscript r. Here, Z_g, Z_e, Z_{m_q}, and Z_{m_ℓ} are the QCD-coupling, QED-coupling, quark-mass, and lepton-mass renormalization constants. Inserting these relations into the Lagrangian and collecting all terms proportional to $\delta Z \equiv Z - 1$ yields the counterterm Lagrangian. Since $Z_{a_c} = Z_{g_c}^2$ (with $c \in \{s, e\}$), the renormalization of the coupling constants can equivalently be expressed in terms of the rescaled dimensionless couplings

$$a_s = \frac{\alpha_s}{4\pi}\,, \qquad a_e = \frac{\alpha_e}{4\pi}\,, \tag{1.18}$$

with $\alpha_s = g_s^2/(4\pi)$ and $\alpha_e = e^2/(4\pi)$ being the strong and electromagnetic fine-structure constants, respectively. the $\overline{\mathrm{MS}}$ factor S_ε, the unrenormalized couplings $\hat{a}_c$ are therefore related to the renormalized ones through

$$\frac{\hat{a}_c}{(\mu^2)^{\varepsilon/2}}\, S_\varepsilon = \frac{a_c(\mu_R^2)}{(\mu_R^2)^{\varepsilon/2}}\, Z_{a_c}\big(a_s(\mu_R^2),\, a_e(\mu_R^2),\, \varepsilon\big)\,, \tag{1.19}$$

where μ is the arbitrary scale and μ_R is the renormalization scale. the renormalization group equation (RGE) for Z_{a_c}:

$$\mu_R^2 \frac{d}{d\mu_R^2} \ln Z_{a_c} = -\frac{\beta_{a_c}(a_s(\mu_R^2),\, a_e(\mu_R^2))}{a_c(\mu_R^2)}\,, \tag{1.20}$$

where the β-functions admit double expansions in a_s and a_e:

$$\beta_{a_s} = -\sum_{i,j=0}^{\infty} \beta_{ij}^s\, a_s^{i+2}\, a_e^j\,, \qquad \beta_{a_e} = -\sum_{i,j=0}^{\infty} \beta_{ij}^e\, a_e^{j+2}\, a_s^i\,, \tag{1.21}$$

with the coefficients β^s_{ij} and β^e_{ij} accounting for contributions from pure QCD, pure QED, and mixed QCD ⊗ QED interactions. Solving eq. (1.20) perturbatively and using the expansions eq. (1.21), one obtains the renormalization constants up to third order [19,20]:

$$
\begin{aligned}
Z_{a_s} = 1 &+ a_s\left(\frac{2\beta^s_{00}}{\varepsilon}\right) + a_s a_e\left(\frac{\beta^s_{01}}{\varepsilon}\right) + a_s^2\left(\frac{4(\beta^s_{00})^2}{\varepsilon^2} + \frac{\beta^s_{10}}{\varepsilon}\right) + a_s a_e^2\left(\frac{2\beta^e_{00}\beta^s_{01}}{3\varepsilon^2} + \frac{2\beta^s_{02}}{3\varepsilon}\right) \\
&+ a_s^2 a_e\left(\frac{4\beta^s_{00}\beta^s_{01}}{\varepsilon^2} + \frac{2\beta^s_{11}}{3\varepsilon}\right) + a_s^3\left(\frac{8(\beta^s_{00})^3}{\varepsilon^3} + \frac{14\beta^s_{00}\beta^s_{10}}{3\varepsilon^2} + \frac{2\beta^s_{20}}{3\varepsilon}\right) + \cdots
\end{aligned} \tag{1.22}
$$

$$
\begin{aligned}
Z_{a_e} = 1 &+ a_e\left(\frac{2\beta^e_{00}}{\varepsilon}\right) + a_e a_s\left(\frac{\beta^e_{10}}{\varepsilon}\right) + a_e^2\left(\frac{4(\beta^e_{00})^2}{\varepsilon^2} + \frac{\beta^e_{01}}{\varepsilon}\right) + a_e a_s^2\left(\frac{2\beta^s_{00}\beta^e_{10}}{3\varepsilon^2} + \frac{2\beta^e_{20}}{3\varepsilon}\right) \\
&+ a_e^2 a_s\left(\frac{4\beta^e_{00}\beta^e_{10}}{\varepsilon^2} + \frac{2\beta^e_{11}}{3\varepsilon}\right) + a_e^3\left(\frac{8(\beta^e_{00})^3}{\varepsilon^3} + \frac{14\beta^e_{00}\beta^e_{01}}{3\varepsilon^2} + \frac{2\beta^e_{02}}{3\varepsilon}\right) + \cdots
\end{aligned} \tag{1.23}
$$

where "$\cdots$" denotes terms of order $a_s^i a_e^j$ with $i + j > 3$. The renormalization constants eqs. (1.22)-(1.23) are sufficient to make all UV divergences finite; they are organized as double power series in a_s and a_e.

1.1.2 Running Coupling Constants

A fundamental consequence of renormalization is that the coupling constants become scale-dependent quantities, commonly referred to as *running couplings*. This scale dependence follows directly from the RGE [21, 22] eq. (1.20): the bare coupling $\hat{a}_c$ be independent of renormalization scale μ_R leads to the evolution equation

$$
\mu_R^2 \frac{d\,a_i(\mu_R^2)}{d\mu_R^2} = \beta_i(a_s, a_e)\,, \qquad i \in \{s, e\}\,, \tag{1.24}
$$

where β_i are the β-functions defined in eq. (1.21).

The QCD β-function encodes the running of the strong coupling. Its leading coefficient, which governs the one-loop running, is

$$
\beta^s_{00} = \frac{11}{3} C_A - \frac{4}{3} T_F\, n_f\,, \tag{1.25}
$$

where $C_A = N_c = 3$, $T_F = \frac{1}{2}$, and n_f is the number of active quark flavors. For $n_f \leq 16$ (and in particular for the Standard Model value $n_f = 6$), this coefficient is positive, so the QCD β-function is negative:

$$\beta_{a_s} < 0 \quad \Longrightarrow \quad a_s(\mu_R^2) \text{ decreases as } \mu_R^2 \text{ increases.} \tag{1.26}$$

This is the phenomenon of *asymptotic freedom*: at short distances (high energies) quarks and gluons interact weakly, making perturbative QCD reliable for hard-scattering processes.

The electromagnetic coupling a_e also runs with the energy scale, although its variation is much milder than that of a_s. The leading coefficient of the QED β-function is

$$\beta_{00}^e = -\frac{4}{3}\left(N_c \sum_{q=1}^{n_f} e_q^2 + \sum_{\ell=1}^{n_L} e_\ell^2\right), \tag{1.27}$$

where e_q and e_ℓ are the electric charges of quarks and leptons in units of the proton charge, and n_L is the number of active leptons. The color factor N_c reflects the fact that each quark flavor contributes N_c times to the photon self-energy. Since $\beta_{00}^e < 0$, the QED β-function is positive:

$$\beta_{a_e} > 0 \quad \Longrightarrow \quad a_e(\mu_R^2) \text{ increases as } \mu_R^2 \text{ increases.} \tag{1.28}$$

This is the phenomenon of *charge screening*: the electromagnetic coupling grows logarithmically with the energy scale, though the effect is very mild over experimentally accessible energies since $\alpha_e \approx 1/137$ at low energies and $\approx 1/128$ at $\mu_R \sim M_Z$.

1.2 Factorization and the Parton Model

The application of perturbative QCD [11, 23] to processes involving hadrons is nontrivial due to the composite nature of hadronic states. Unlike leptons, which are elementary particles, hadrons are bound states of quarks and gluons whose interactions are governed by the strong force. At large distance scales the QCD coupling becomes large, making direct perturbative calculations unreliable. Hence, a purely perturbative description of hadronic observables is not possible in general.

Nevertheless, many scattering processes studied in high-energy experiments involve momentum transfers significantly larger than the strong interactions scale Λ_{QCD}. In this regime asymptotic freedom ensures that a_s is small, so the short-distance part of the interaction can be treated perturbatively. However, even at high energies, hadronic observables are influenced by both short-distance and long-distance physics, and therefore cannot be computed fully within perturbation theory.

A observable in a renormalizable QFT depends on the kinematic scale Q characterizing the scattering process, on the masses of the particles involved, and on the renormalization scale μ_R. The dependence on μ_R appears through logarithmic terms such as $\ln(Q/\mu_R)$ or $\ln(\mu_R/m)$, where m represents relevant mass scales. Although an appropriate choice of μ_R can reduce some of these logarithms, it cannot remove them completely. In particular, logarithmic terms of the form $\ln(Q/m)$ involving particle masses signal sensitivity to long-distance physics, where the strong coupling becomes large and perturbation theory breaks down. When such logarithms are large, terms of the form $a_s^n \ln^k(Q/m)$ (with $k \leq 2n$) can compensate the smallness of a_s at each order, making the fixed-order expansion unreliable. In such kinematic regimes, it becomes necessary to identify and resum these logarithmically enhanced contributions to all orders in perturbation theory. Systematic frameworks for carrying out this resummation, such as the Dokshitzer-Gribov-Lipatov-Altarelli-Parisi (DGLAP) evolution equations [24–26], Sudakov resummation [27], and Soft-Collinear Effective Theory (SCET) [28, 29], have been developed extensively in the literature. However, resummation [30] lies beyond the scope of the present work; we restrict ourselves to fixed-order perturbative calculations.

This interplay between short-distance and long-distance dynamics implies that hadronic cross sections generally contain both perturbative and nonperturbative contributions. A powerful theoretical framework that allows these contributions to be systematically separated is provided by the factorization theorem [11, 23]. The central idea is that physical observables involving hadrons can be expressed as a convolution of a perturbatively calculable short-distance part with universal nonperturbative functions that encode the internal structure of the hadrons.

The physical picture underlying factorization can be understood through the parton model. In this model, a fast-moving hadron is described as a collection of quasi-free constituents called partons: quarks, antiquarks, and gluons, each carrying a fraction of the hadron's momentum. When the hadron is probed by a highly energetic particle, such as a lepton in deep inelastic scattering, the interaction occurs on a timescale that is extremely short compared to the typical timescale of the strong interactions binding the partons together. As a consequence, the probe effectively interacts with a single parton rather than with the hadron as a whole.

During the short duration of the hard interaction, the internal dynamics of the hadron can be considered frozen. A parton participating in the hard scattering carries momentum $x_1 P^\mu$, where P^μ is the hadron momentum and the longitudinal momentum fraction x_1 satisfies $0 \le x_1 \le 1$.

A key ingredient of the parton model is the introduction of parton distribution functions (PDFs), usually denoted $f_i(x_1)$. These describe the probability density of finding a parton of type i carrying a fraction x_1 of the hadron momentum. The PDFs encode the long-distance structure of the hadron and are intrinsically nonperturbative: they cannot be calculated from first principles in perturbation theory but must be extracted from experimental measurements.

Within this framework, the cross section for a high-energy hadronic process can be expressed as an incoherent sum over the scattering of individual partons, each contribution weighted by the probability of finding the corresponding parton inside the colliding hadron. In a generic electron-hadron collision where one hadron appears in the final state, the differential cross section takes the schematic form

$$\frac{d^3\sigma}{dx\,dy\,dz} \approx x^{i-1} \sum_{a,b} \int_x^1 \frac{dx_1}{x_1} \int_z^1 \frac{dz_1}{z_1}\, f_{a/P}(x_1,\mu_F^2)\, D_{H'/b}(z_1,\mu_F^2)\, \mathcal{C}_{i,ab}\left(\frac{x}{x_1},\frac{z}{z_1},Q^2,\mu_F^2\right), \tag{1.29}$$

where $f_{a/P}(x_1,\mu_F^2)$ are the PDFs of the incoming hadron, $D_{H'/b}(z_1,\mu_F^2)$ are the fragmentation functions (FFs) describing how a final-state parton b hadronizes into the observed hadron H', and $\mathcal{C}_{i,ab}$ are the perturbatively calculable coefficient functions (CFs) encoding the short-distance partonic dynamics. The factorization scale μ_F separates the long-distance from the short-distance contributions and serves as the argument of the PDFs and FFs.

The factorized structure of eq. (2.24) clearly separates the perturbatively calculable partonic dynamics from the nonperturbative information contained in the PDFs and FFs. This separation is one of the central principles underlying the theoretical description of high-energy hadronic reactions.

1.3 Outline of the Thesis

In this thesis we investigate higher-order perturbative corrections to semi-inclusive deep-inelastic scattering (SIDIS) within the framework of perturbative QCD, and subsequently extend the calculation to include QED corrections. Precise theoretical predictions for SIDIS are essential for extracting detailed information about the internal structure of hadrons and for interpreting data from present and future high-energy scattering experiments. In particular, future facilities such as the EIC will provide high-precision measurements that demand theoretical predictions at the level of next-to-next-to-leading order (NNLO) accuracy. This thesis therefore focuses on the computation of higher-order corrections and their implications for phenomenology.

The structure of the thesis is organized as follows.

Chapter 1 introduces the physical motivation for studying SIDIS. The study of SIDIS plays a central role in understanding the partonic structure of hadrons because it provides access to more detailed information than inclusive deep-inelastic scattering. In particular, the detection of an identified hadron in the final state allows one to probe the fragmentation of partons in addition to their distributions inside the nucleon, making SIDIS a powerful tool for investigating PDFs, FFs, and the three-dimensional structure of hadrons. The chapter discusses the broader context of high-energy scattering experiments, the importance of precision measurements, and the relevance of SIDIS for understanding fundamental aspects of QCD such as the momentum and spin structure of the proton. The need for higher-order perturbative calculations, including NNLO QCD corrections and mixed QCD⊗QED effects, is motivated in the context of future precision programs, especially those planned at the EIC.

Chapter 2 provides the theoretical background necessary for the analysis carried out in this thesis. It begins by reviewing the kinematics of deep-inelastic scattering and its extension to semi-inclusive processes. The relevant kinematic variables, the formalism of the hadronic tensor and its decomposition in terms of structure functions, and the framework of collinear factorization are introduced. Within this framework, SIDIS cross sections are expressed as convolutions of perturbatively calculable coefficient functions with universal PDFs and FFs. The perturbative expansion of the coefficient functions in the strong coupling constant is discussed together with the role of renormalization and factorization scales.

Chapter 3 presents the computation of higher-order QCD corrections to the SIDIS process. Beyond leading order, contributions arise from purely virtual loop corrections, real emission processes, and mixed real-virtual contributions. At NNLO accuracy the calculation requires the evaluation of two-loop virtual amplitudes as well as real-virtual and double real emission processes. The chapter describes the techniques used to compute these contributions and to combine them into a consistent perturbative prediction, with particular attention to the treatment of UV and IR divergences. Ultraviolet divergences are removed through the renormalization procedure, while collinear singularities are absorbed into the PDFs and FFs via mass factorization. Numerical results illustrating the impact of the NNLO corrections on SIDIS observables are presented.

Chapter 4 extends the analysis by incorporating electromagnetic corrections. While QCD effects dominate, QED corrections become important when theoretical predictions reach high levels of precision, and the interplay between QCD and QED leads to mixed contributions that must be treated consistently within the perturbative framework. This chapter discusses the inclusion of pure QED as well as mixed QCD⊗QED corrections in the computation of SIDIS coefficient functions. A key methodological tool is the Abelianisation procedure, which allows the extraction of QED contributions from known QCD results by systematically modifying color structures and coupling constants. The treatment of the γ_5 matrix in dimensional regularization is also addressed. The phenomenological impact of these corrections on SIDIS observables is analyzed, with particular relevance for precision measurements of the spin structure of the nucleon.

Finally, Chapter 5 summarizes the main results obtained in this thesis and discusses their broader implications. The key theoretical developments are reviewed, with emphasis on the role of NNLO QCD and mixed QCD⊗QED corrections in improving the precision of SIDIS predictions. The relevance of the present work for the physics program of the EIC is highlighted, and an outlook on possible future directions is provided, including extensions of the present calculations to other observables and further refinements of perturbative predictions in the combined QCD and QED framework.

Chapter 2

Theoretical Framework

Contents

In the previous chapter, we discussed that several important aspects of QCD, such as the internal structure of the proton, the spin content of the proton, asymptotic freedom, and the color-glass condensate, are still not completely understood. Therefore, in order to make accurate theoretical predictions for collider experiments, it is essential to include higher-order perturbative corrections. One of the most powerful experimental tools for probing hadronic structure and testing QCD is Deep Inelastic Scattering. This chapter develops the theoretical framework required for the higher-order calculations presented in subsequent chapters. We begin by reviewing inclusive DIS and its extension to semi-inclusive processes, introduce the kinematic variables and tensor decompositions that characterize these processes, and establish the factorization framework through which structure functions are related to perturbatively calculable coefficient functions.

2.1 Deep Inelastic Scattering

In this section , we introduce deep inelastic scattering as the foundational experimental and theoretical framework from which our study of hadronic structure proceeds. We trace how DIS evolved from a discovery tool into a precision QCD laboratory, and establish the kinematic variables and cross-section structure that carry over directly into the semi-inclusive extension treated in the next section.

Deep inelastic scattering (DIS) [31–35] has played a fundamental role in the development of modern particle physics and in establishing our present understanding of the structure of hadrons. Historically, DIS has evolved through several important stages, each contributing to a deeper understanding of nucleon structure and the internal dynamics.

The first milestone came in the late 1960s with the electron-proton scattering experiments at the Stanford Linear Accelerator Center (SLAC). In these experiments, electrons with sufficiently high energies were scattered from nucleon targets at large momentum transfer. During the 1970s, neutrino-nucleon DIS experiments at CERN and Fermilab played an essential role in establishing the flavour structure of quarks and testing the electroweak theory. These experiments were particularly important because weak interactions could distinguish between quark flavours and probe the charged-current structure of the Standard Model.

With QCD, DIS became a precision tool for studying strong interactions. The discovery of scaling violations in structure functions (SFs) demonstrated that partons radiate gluons, confirming the QCD prediction of logarithmic Q^2 dependence. This led to the formulation of the DGLAP evolution equations, which describe the scale dependence of PDFs. A major advance occurred in the 1990s with the HERA electron-proton collider at DESY, which extended DIS measurements to previously unexplored regions of very small Bjorken-x and very large Q^2. HERA data provided precise information on the gluon density inside the proton and opened new directions in the study of small-x physics, parton saturation, and high-energy QCD dynamics.

In recent years, DIS has continued to evolve through polarized scattering experiments, which investigate the spin structure of the proton, and through semi-inclusive and exclusive processes that provide three-dimensional information on hadron structure via transverse momentum dependent distributions (TMDs) and generalized parton distributions (GPDs). Future facilities such as the Electron-Ion Collider (EIC) are expected to further deepen our understanding of nucleon structure and gluon-dominated matter.

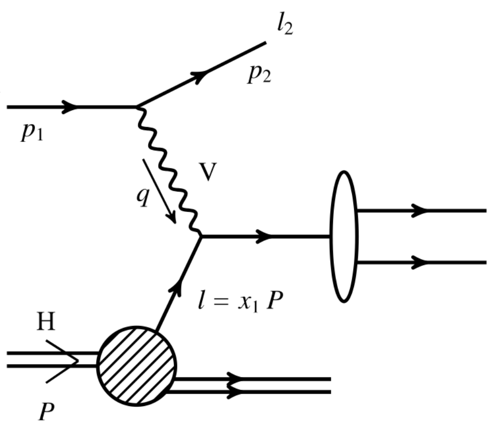

Figure 2.1: Deep Inelastic Scattering Process

The DIS process can be written schematically as

$$l(k_l) + P(P) \to l(k_l') + X \tag{2.1}$$

where the incoming lepton l carries momentum k_l, the incoming hadron P carries momentum P, and the outgoing lepton carries momentum k_l'. The remaining unobserved particles are collectively denoted by X. The four-momentum transfer is $q = k_l - k_l'$, and the virtuality of the exchanged boson is $Q^2 = -q^2$.

The SLAC experiments revealed a scaling behaviour when the cross section was expressed in terms of the dimensionless Bjorken variable

$$x = \frac{Q^2}{2P \cdot q} \tag{2.2}$$

where P denotes the momentum of the target nucleon. This phenomenon, known as Bjorken scaling, suggested that the nucleon contains point-like constituents that interact with the incoming lepton, later identified as quarks. Another important kinematic variable is the inelasticity,

$$y = \frac{P \cdot q}{P \cdot k_l} \tag{2.3}$$

which measures the fractional energy transferred from the incoming lepton to the hadronic system in the target rest frame.

The interpretation of DIS experiments led to the formulation of the parton model by Feynman. In this picture the nucleon is viewed as a collection of quasi-free constituents called partons. When a high-energy lepton scatters off the nucleon, the interaction effectively takes place with a single parton inside the hadron. The cross section can therefore be expressed as an incoherent sum over scattering processes involving the individual partons.

The discovery of asymptotic freedom in QCD provided the theoretical framework that explains the success of the parton model. In the QCD improved parton model the cross section for DIS can be expressed in terms of structure functions depending on x and Q^2, which encode information about the internal structure of the hadron. Within the framework of QCD factorization, they can be written as convolutions of non-perturbative PDFs and perturbatively calculable coefficient functions (CFs). PDFs describe the probability of finding a parton carrying a fraction x_1 of the hadron momentum; since they are non-perturbative, they must be extracted from experimental data. The differential cross-section of DIS are related to PDFs $f_{a/\mathrm{P}}$ and CFs $\mathcal{C}_{i,ab}$ through the QCD improved parton model:

$$\frac{d^2\sigma}{dx\,dy} \approx \sum_{a,b} \int_x^1 \frac{dx_1}{x_1} f_{a/P}(x_1, \mu_F^2)\, \mathcal{C}_{i,ab}\left(\frac{x}{x_1}, Q^2, \mu_F^2\right). \tag{2.4}$$

With the kinematic variables and the basic cross-section structure of DIS established, we have the foundation needed to extend the analysis to semi-inclusive processes. Inclusive DIS, however, does not directly probe the fragmentation of the struck parton into observable hadrons. To access this information and thereby gain sensitivity to FFs alongside PDFs, we must extend the process to detect a specific hadron in the final state. This is the subject of the next section.

2.2 Semi-Inclusive Deep Inelastic Scattering

In this section we extend the DIS framework to the semi-inclusive process, where a specific hadron is identified in the final state alongside the scattered lepton. We introduce the additional kinematic variable z that characterizes this hadron, define the FFs that describe parton hadronization, and establish the factorized form of the SIDIS cross section that forms the central object of this thesis.

Semi-inclusive deep inelastic scattering (SIDIS) is an extension of inclusive DIS in which, in addition to the scattered lepton, one observes a specific hadron in the final state. The SIDIS process can be written schematically as

$$l(k_l) + P(P) \to l(k_l') + H'(P_H) + X\,, \tag{2.5}$$

where the detected hadron H' has momentum P_H, while the remaining unobserved particles are collectively denoted by X.

The detection of a specific hadron in the final state provides sensitivity to the process of

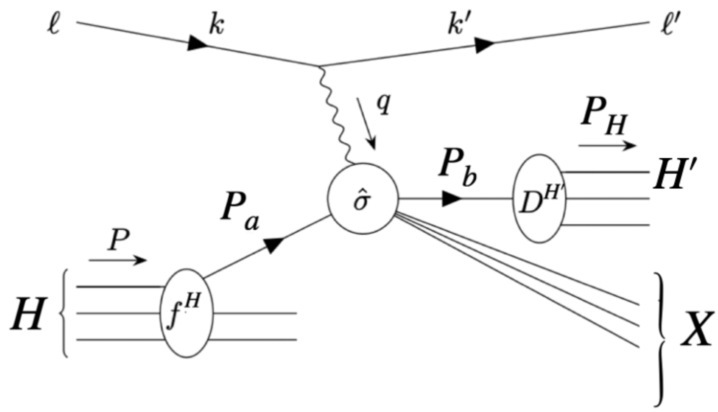

Figure 2.2: Semi-Inclusive Deep Inelastic Scattering Process

fragmentation, in which partons produced in the hard scattering transform into hadrons. To describe this process theoretically, one introduces FFs [36], which give the probability that a parton produced in the hard scattering fragments into a given hadron carrying a certain fraction of the parton momentum.

According to the QCD factorization theorem, the SIDIS cross section separates into three distinct components: parton distribution functions describing the structure of the incoming hadron, FFs describing the hadronization of the outgoing parton, and coefficient functions describing the short-distance hard scattering process. This factorization property makes SIDIS a powerful tool for studying both the partonic structure of hadrons and the mechanisms of hadron formation.

Experimentally, SIDIS measurements have been performed at several facilities including the HERMES experiment [37] at DESY and the COMPASS experiment [38] at CERN. The Electron-Ion Collider (EIC) at BNL and China is a new initiative to further explore the fundamental structure and dynamics of hadrons using high-energy electron and ion beams [39]. The SIDIS reaction will be one of the flagship measurements at the EIC, covering a large range of hadron kinematics in (x, Q^2) and (z, Q^2), for the simultaneous extraction of PDFs and FFs, in particular for the case of polarized beams, which will allow one to study spin-dependent PDFs in largely unexplored regions. In recent times, measurements from SIDIS experiments [40–42] have already been used [43–47] to directly constrain FFs, and also in combined fits of FFs and spin-dependent PDFs [48–50], most recently at NNLO accuracy [51, 52], improving earlier fits of polarized PDFs [53, 54].

The kinematics of the SIDIS process are described by several Lorentz-invariant variables. In addition to the DIS variables x and y already introduced, SIDIS requires a third variable: the fragmentation variable

$$z = \frac{P \cdot P_H}{P \cdot q}, \tag{2.6}$$

which describes the fraction of the virtual photon energy carried by the detected hadron. Together, x, y, and z fully characterize the SIDIS process in the collinear approximation. More details are available in Appendix **??**.

With the SIDIS process defined and its kinematic variables established, we have identified the three ingredients: PDFs, FFs, and coefficient functions (CFs),that enter the factorized cross section. To connect these ingredients to experimental observables, we need to develop the tensor formalism that relates the cross section to the underlying hadronic dynamics. This requires decomposing the cross section into leptonic and hadronic tensors, which is the subject of the next section.

2.3 Leptonic and Hadronic Tensors

In this section, we express the SIDIS cross section in a form that separates the calculable leptonic part from the non-perturbative hadronic part. We decompose the hadronic tensor into structure functions using symmetry constraints, and derive the explicit cross-section formulae in terms of those structure functions that will serve as the basis for the perturbative computation in the sections that follow.

In the one-photon exchange approximation the SIDIS, unpolarized and polarized (Δ) cross section factorizes into a leptonic tensor and a hadronic tensor. The leptonic tensor describes the interaction of the lepton with the virtual photon and can be calculated exactly using perturbation theory. The hadronic tensor encodes the non-perturbative structure of the hadron.

$$d(\Delta)\sigma = \frac{d^3k_l'}{(2\pi)^3 2k_l'^0}\frac{1}{4\sqrt{(k_l\cdot P)^2 - m^2M^2}}\,(\Delta)\mathcal{L}^{\mu\nu}(k_l,k_l',q)$$
$$\times\left(\frac{e^4}{Q^4}\right)(4\pi M)\,(\Delta)W_{\mu\nu}(q,P,P_H)\,, \tag{2.7}$$

where e denotes the electric charge and M (m) is the mass of the incoming hadron (lepton); we drop the lepton mass throughout. For unpolarized scattering the leptonic tensor takes the form

$$\mathcal{L}^{\mu\nu} = 2k_l^\mu k_l'^\nu + 2k_l'^\mu k_l^\nu - Q^2 g^{\mu\nu}\,, \tag{2.8}$$

while for polarized scattering the antisymmetric leptonic tensor is

$$\mathcal{L}_A^{\mu\nu} = -2i\lambda_\ell\,\varepsilon^{\mu\nu\alpha\beta}k_\alpha k_\beta'\,, \tag{2.9}$$

where λ_ℓ is the polarization of the incoming lepton and $\varepsilon^{\mu\nu\sigma\lambda}$ is the Levi-Civita tensor (with $\varepsilon^{0123} = +1$). More details are available in Appendix **??**.

2.3.1 Decomposition of the Hadronic Tensor

The non-perturbative information about the hadronic target in deep inelastic scattering is encoded in the hadronic tensor. For SIDIS it is defined as

$$W_{\mu\nu}(P,q,P_H) = \frac{1}{4\pi}\sum_X (2\pi)^4\delta^{(4)}(P+q-P_H-P_X)\langle P|J_\mu(0)|H'X\rangle\langle H'X|J_\nu(0)|P\rangle\,, \tag{2.10}$$

where $J_\mu(0)$ denotes the electromagnetic current operator evaluated at the spacetime point $x = 0$ and the sum runs over all unobserved hadronic final states X.

The hadronic tensor is constrained by Lorentz invariance, current conservation ($q^\mu W_{\mu\nu} = 0$), parity conservation, and time-reversal invariance. These symmetry constraints strongly restrict the possible tensor structures that may appear in the decomposition of $W_{\mu\nu}$.

Using these constraints, the (un)polarized hadronic tensor can be expanded in terms of two unpolarized structure functions $F_i(x, z, Q^2)$ and two polarized structure functions $g_i(x, z, Q^2)$ for $i = 1, 2$, see e.g. [55]:

$$W_{\mu\nu} = \sum_{i=1,2} W_i(x, z, Q^2)\, T_{i,\mu\nu}(P, q)\,, \tag{2.11}$$

$$\Delta W_{\mu\nu} = \sum_{i=1,2} g_i(x, z, Q^2)\, S_{i,\mu\nu}(P, q, S)\,, \tag{2.12}$$

where the tensor structures are

$$\begin{aligned} T_{1,\mu\nu} &= -g_{\mu\nu} + \frac{q_\mu q_\nu}{q^2}\,, \\ T_{2,\mu\nu} &= \frac{1}{M^2}\left(P_\mu - \frac{P\cdot q}{q^2} q_\mu\right)\left(P_\nu - \frac{P\cdot q}{q^2} q_\nu\right), \end{aligned} \tag{2.13}$$

and

$$\begin{aligned} S_{1,\mu\nu} &= -\frac{i}{P\cdot q}\,\varepsilon_{\mu\nu\sigma\lambda}\, q^\sigma S^\lambda\,, \\ S_{2,\mu\nu} &= -\frac{i}{P\cdot q}\,\varepsilon_{\mu\nu\sigma\lambda}\, q^\sigma \left(S^\lambda - \frac{S\cdot q}{P\cdot q} P^\lambda\right), \end{aligned} \tag{2.14}$$

with $S^2 = 1$ and $S \cdot P = 0$. Substituting $(\Delta)W_{\mu\nu}$ into eq. (2.7) and expressing the leptonic phase space in terms of x and y, we obtain the unpolarized cross section

$$\frac{d^3\sigma}{dx\,dy\,dz} = \frac{4\pi\alpha_e^2}{Q^2}\left[yF_1(x, z, Q^2) + \frac{1-y}{y} F_2(x, z, Q^2)\right], \tag{2.15}$$

where $\alpha_e = e^2/(4\pi)$, and the unpolarized structure functions F_i are related to W_i through $W_1 = F_1/M$ and $W_2 = F_2/(yE)$ with E the energy of the incoming lepton. The spin-dependent cross section is

$$\frac{d^3\Delta\sigma}{dx\,dy\,dz} = \frac{4\pi\alpha_e^2}{Q^2}(2-y)\, g_1(x, z, Q^2)\,, \tag{2.16}$$

where g_2 does not contribute since we restrict ourselves to longitudinally polarized hadrons in the initial state.

The (polarized) unpolarized structure functions are related to PDFs $(\Delta)f_{a/\mathrm{P}}$, FFs $D_{\mathrm{H}'/b}$, and CFs $(\Delta)\mathcal{C}_{i,ab}$ through the QCD improved parton model [23]:

$$\begin{aligned}(g_1)F_i(x,z,Q^2) = x^{i-1} \sum_{a,b=q,\bar{q},g,\gamma} \int_x^1 \frac{dx_1}{x_1} (\Delta)f_{a/\mathrm{P}}(x_1,\mu_F^2) \int_z^1 \frac{dz_1}{z_1} D_{\mathrm{H}'/b}(z_1,\mu_F^2) \\ \times (\Delta)\mathcal{C}_{i,ab}\left(\frac{x}{x_1}, \frac{z}{z_1}, Q^2, \mu_F^2\right),\end{aligned} \tag{2.17}$$

where $\Delta f_{a/\mathrm{P}} = f_{a(\uparrow)/\mathrm{P}(\uparrow)} - f_{a(\downarrow)/\mathrm{P}(\uparrow)}$. More technical details regarding the derivation can be found in Appendix **??**.

With the structure functions now expressed in terms of the three factorized components, the remaining task is to specify how the CFs are extracted from perturbative calculations. In practice this requires projecting the hadronic tensor onto individual SFs, which is achieved through a set of projection operators. These are introduced in the next subsection.

2.3.2 Projectors for Structure Functions

In perturbative calculations it is convenient to extract the structure functions from the hadronic tensor using appropriate projection operators. These projectors isolate the scalar functions multiplying the independent tensor structures in the decomposition of $W_{\mu\nu}$, avoiding the need to compute the full tensor structure of the scattering amplitude.

The projector tensors $P^{(1)}_{\mu\nu}$, $P^{(2)}_{\mu\nu}$, and $\Delta P^{(1)}_{\mu\nu}$ are defined by the orthonormality conditions

$$P^{(i)}_{\mu\nu}\, T^{(j)\mu\nu} = \delta_{ij}\,, \qquad \Delta P^{(1)}_{\mu\nu}\, S^{(1)\mu\nu} = 1\,, \tag{2.18}$$

so that contracting the hadronic tensor with these projectors directly yields

$$F_i = P^{(i)}_{\mu\nu}\, T_i^{\mu\nu}(P, q)\,, \qquad g_1 = \varDelta P^{(1)}_{\mu\nu}\, S_1^{\mu\nu}\,. \tag{2.19}$$

In d-spacetime dimensions the explicit forms are

$$\begin{aligned}
P^{(1)\mu\nu} &= \frac{1}{d-2}\left(-g^{\mu\nu} + \frac{q^\mu q^\nu}{q^2}\right), \\
P^{(2)\mu\nu} &= \frac{1}{(d-2)(P\cdot q)^2}\left(P^\mu - \frac{P\cdot q}{q^2} q^\mu\right)\left(P^\nu - \frac{P\cdot q}{q^2} q^\nu\right), \\
\varDelta P^{(1)\mu\nu} &= \frac{i}{(d-2)(d-3)}\, \varepsilon^{\mu\nu\sigma\lambda}\, \frac{q_\sigma P_\lambda}{P\cdot q}\,.
\end{aligned} \tag{2.20}$$

Applying these projectors to the perturbatively calculated bare partonic tensor yields the bare partonic structure functions F_1, F_2 and g_1. Ultraviolet divergences are then removed through renormalization of the strong coupling constant and electromagnetic coupling constant, and soft divergences immediately disappear once we add all the diagrams, after which the remaining collinear singularities are removed via mass factorization. This procedure yields the infrared-safe coefficient functions, which upon convolution with the PDFs and FFs give the physical structure functions. Further technical details are provided in Appendices **??** and C.

With both the decomposition of the hadronic tensor and the projection technique in hand, we have all the ingredients needed to perform explicit perturbative calculations. The next section describes how the coefficient functions entering eq. (2.17) are actually computed at higher orders in perturbation theory.

2.4 Perturbative Computation

The goal of this section is to describe how the CFs appearing in the factorized cross section are obtained from a perturbative calculation. We outline the treatment of UV divergences through renormalization, of collinear divergences through mass factorization via Altarelli-Parisi kernels, and present the double expansion of the coefficient functions in powers of a_s and a_e that organizes the corrections computed in the subsequent chapters.

The SFs appearing in the cross section can be expressed in terms of PDFs, FFs, and perturbatively calculable CFs. This decomposition follows from the QCD factorization theorem, which separates long-distance non-perturbative physics from short-distance perturbative dynamics. Within the collinear factorization framework the structure functions take the form

$$F_i(x,z,Q^2) = \sum_{a,b} f_{a/P} \otimes \mathcal{C}_{i,ab} \tilde{\otimes} D_{H'/b}\,, \qquad i = 1,2\,, \tag{2.21}$$

$$g_1(x,z,Q^2) = \sum_{a,b} \Delta f_{a/P} \otimes \Delta\mathcal{C}_{1,ab} \tilde{\otimes} D_{H'/b}\,, \tag{2.22}$$

where the double convolution is defined by

$$A(x) \otimes \mathcal{C}(x,z) \,\tilde{\otimes}\, B(z) = \int_x^1 \frac{dx_1}{x_1} \int_z^1 \frac{dz_1}{z_1} A(x_1)\, \mathcal{C}\left(\frac{x}{x_1}, \frac{z}{z_1}\right) B(z_1)\,. \tag{2.23}$$

The coefficient functions describe the short-distance partonic scattering processes and are computed from partonic cross sections using dimensional regularization. The CFs can be extracted from the parton-level subprocess cross sections $d(\Delta)\hat{\sigma}_{i,ab}/dx\,dy\,dz$ through the relation $x^{(1-i)}d(\Delta)\hat{\sigma}_{i,ab}/dx\,dy\,dz = (\Delta)\hat{\mathcal{C}}_{i,ab}$, where i labels the structure function and a, b denote the initial and final-state partons. The partonic cross sections are defined as,

$$\frac{d^3(\Delta)\hat{\sigma}_{i,ab}}{dxdydz} = \frac{(\Delta)\mathcal{P}_i^{\mu\nu}}{4\pi} \int \mathrm{dPS}_{X+b}\, \Sigma|(\Delta)M_{ab}|^2_{\mu\nu}\, \delta\left(\frac{z}{z_1} - \frac{p_a \cdot p_b}{p_a \cdot q}\right) \tag{2.24}$$

After UV renormalization, the CFs are free of UV poles in ε, but retain soft and collinear divergences [56, 57]. The soft divergences cancel upon summing over all contributing subprocesses and final states, as required by the Kinoshita-Lee-Nauenberg (KLN) theorem [58, 59]. The residual collinear singularities, which are of purely long-distance origin, do not cancel but instead factorize into universal Altarelli-Parisi (AP) splitting kernels $(\Delta)\Gamma$ and $\tilde{\Gamma}$ [25]. The mass factorization reads

$$(\Delta)\hat{\mathcal{C}}_{i,ab}(x,z,\varepsilon) = (\Delta)\Gamma_{c\leftarrow a}(x,\varepsilon) \otimes (\Delta)\mathcal{C}_{i,cd}(x,z,\varepsilon) \,\tilde{\otimes}\, \tilde{\Gamma}_{b\leftarrow d}(z,\varepsilon)\,, \tag{2.25}$$

where Γ and $\Delta\Gamma$ are the space-like AP kernels, including spin dependence for the latter, and $\tilde{\Gamma}$ are the corresponding time-like AP kernels. These kernels absorb all collinear divergences, so that the renormalized CFs $(\Delta)\mathcal{C}_{i,cd}$ are finite at every order in perturbation theory. The technical details of this procedure are described in Chapter 3.

After renormalization and mass factorization the CFs admit a double expansion in powers of the strong and electromagnetic coupling constants:

$$\begin{aligned}(\Delta)\mathcal{C}_{i,ab} = (\Delta)\mathcal{C}^{(0,0)}_{i,ab} + a_s(\mu_F^2)\,(\Delta)\mathcal{C}^{(1,0)}_{i,ab} + a_e(\mu_F^2)\,(\Delta)\mathcal{C}^{(0,1)}_{i,ab}\\ + a_s^2(\mu_F^2)\,(\Delta)\mathcal{C}^{(2,0)}_{i,ab} + a_e^2(\mu_F^2)\,(\Delta)\mathcal{C}^{(0,2)}_{i,ab} + a_s(\mu_F^2)\,a_e(\mu_F^2)\,(\Delta)\mathcal{C}^{(1,1)}_{i,ab} + \mathcal{O}(a_s^3, a_e^3)\,.\end{aligned} \tag{2.26}$$

The leading-order term $(\Delta)\mathcal{C}^{(0,0)}$ corresponds to the simple parton model picture, while higher-order terms arise from radiative corrections involving real and virtual processes. Setting $\mu_R = \mu_F$, the pure QCD CFs $\mathcal{C}^{(l,0)}_{i,ab}$ for $l = 0,1,2$ are derived in Chapter 3, while the pure QED CFs $(\Delta)\mathcal{C}^{(0,l)}_{i,ab}$ for $l = 1,2$ and the mixed QCD⊗QED CFs $(\Delta)\mathcal{C}^{(1,1)}_{i,ab}$ are derived in Chapter 4.

The calculation of higher-order corrections is essential for obtaining precise theoretical predictions. The CFs for SIDIS have been computed in perturbative QCD to next-to-leading order (NLO) long ago [60–65]. Beyond NLO, only partial results were available for a long time [66–69]. In the soft and collinear limit ($x \to 1$ and $z \to 1$), the dominant threshold logarithms have been obtained recently up to N^{3}LO accuracy in QCD [70, 71], and resummed to all orders to N^{3}LL accuracy [72–80], see also [12, 36, 81–99, 99–125, 125–168]. In particular, NNLO corrections significantly reduce theoretical uncertainties and improve the stability of perturbative predictions. The computation of these NNLO contributions for SIDIS processes [169–181] forms the central topic of this thesis .

With the factorization framework, projection technique, mass factorization procedure, and perturbative expansion all in place, this chapter has established the complete theoretical machinery needed for the higher-order calculations that follow. Chapter 3 uses this framework to carry out the explicit computation of the NNLO QCD coefficient functions, while Chapter 4 extends the analysis to include QED and mixed QCD⊗QED contributions.

Chapter 3

NNLO QCD Corrections to Unpolarised SIDIS

Contents

In the previous chapter we established the theoretical framework for SIDIS: the factorized cross section, the decomposition of the hadronic tensor into SFs, and the role of CFs as the perturbatively calculable short-distance kernels. The task of this chapter is to carry out the explicit NNLO computation of those CFs for unpolarised SIDIS. The calculation proceeds in three main stages. First, we identify and classify all partonic subprocesses that contribute up to second order in a_s and compute their squared matrix elements. Second, we reduce the resulting loop and phase-space integrals to a minimal set of master integrals (MIs) and evaluate them in dimensional regularization. Third, we perform UV renormalization and mass factorization to extract finite CFs, and present phenomenological results for the EIC.

3.1 Partonic sub-processes

We identify every partonic subprocess that contributes to the SIDIS CFs through NNLO, see also [94], generate the corresponding Feynman diagrams, and organize the squared matrix elements into the classes → VV, RV, and RR- that will be treated separately in the subsequent integration. This classification is the essential first step before any integral reduction or divergence analysis can be performed.

The computation of CFs requires parton level cross sections, the UV renormalization constants and the AP kernels to desired accuracy in the strong coupling constant (a_s) and ε. Since the latter are all known, we only need to compute the partonic cross sections in eq. (2.17) to second order in a_s. We use `QGRAF` [182] to generate Feynman diagrams for all the sub-processes. With a set of in-house routines written in `FORM` [183, 184], the output of `QGRAF` is converted into a suitable format to apply Feynman rules and to perform Dirac algebra, Lorentz contractions and simplifications of color factors. In the computation of partonic cross section beyond leading order (LO) in perturbation theory, we encounter both UV and IR divergences. The latter originate from soft and collinear partons due to massless gluons and quarks (anti-quarks). We work in $d = 4 + \varepsilon$ space-time dimensions to regulate them.

3.1.1 Amplitudes

We list all partonic subprocesses contributing to the CFs up to NNLO, organized by the number of loops and real emissions. This enumeration determines the complete set of squared matrix elements that must subsequently be integrated. In the following, we list the amplitudes corresponding to sub-processes that contribute to the CFs, up to NNLO level. We begin with the partonic sub-process at LO as shown in Fig. 3.1:

$$q(\bar{q}) + \gamma^* \to q(\bar{q})\,. \tag{3.1}$$

Here, the quark (antiquark) in the final state will fragment into hadron H′. At the NLO

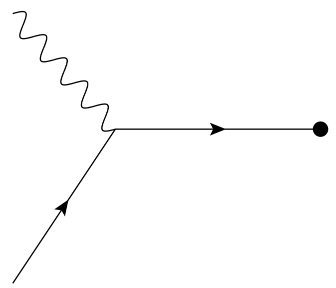

Figure 3.1: Feynman diagram for the LO process.

level, two types of processes contribute, namely the real parton emission sub-processes (R) and virtual gluon corrections (V) to the Born amplitude.

$$q(\bar{q}) + \gamma^* \to q(\bar{q}) + \text{one loop}\,, \tag{3.2}$$

$$q(\bar{q}) + \gamma^* \to q(\bar{q}) + g\,, \tag{3.3}$$

$$g + \gamma^* \to q + \bar{q}\,. \tag{3.4}$$

Any one of the final state partons in this list can fragment into the observed hadron H′. At

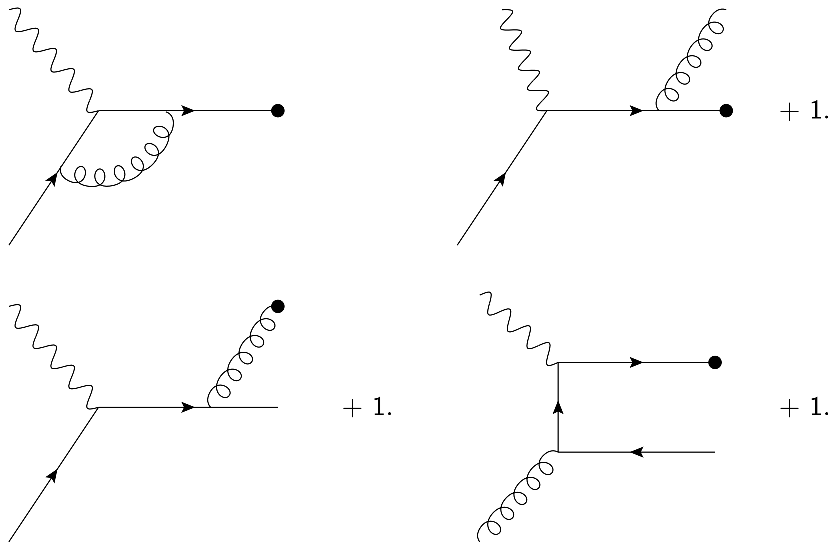

Figure 3.2: Sub-processes at NLO. The integers denote the numbers of additional diagrams to be considered.

NNLO, we encounter two-loop amplitudes, which we classify as VV. The sub-process is given by

$$q(\bar{q}) + \gamma^{*} \to q(\bar{q}) + \text{two loops}\,, \tag{3.5}$$

for which, the schematic Feynman diagrams are given as

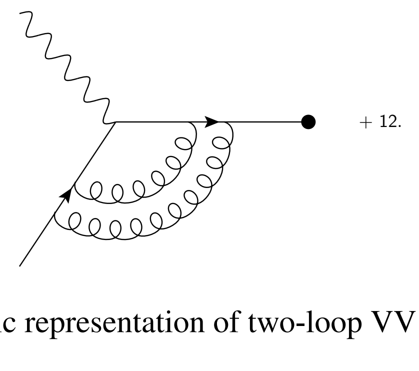

Figure 3.3: Schematic representation of two-loop VV Feynman diagrams.

The class RV consists of single real emission amplitudes with one-loop virtual correction, as given by:

$$q(\bar{q}) + \gamma^* \to q(\bar{q}) + g + \text{one loop}\,, \tag{3.6}$$

$$g + \gamma^* \to q + \bar{q} + \text{one loop}\,. \tag{3.7}$$

The Feynman diagrams can be drawn as:

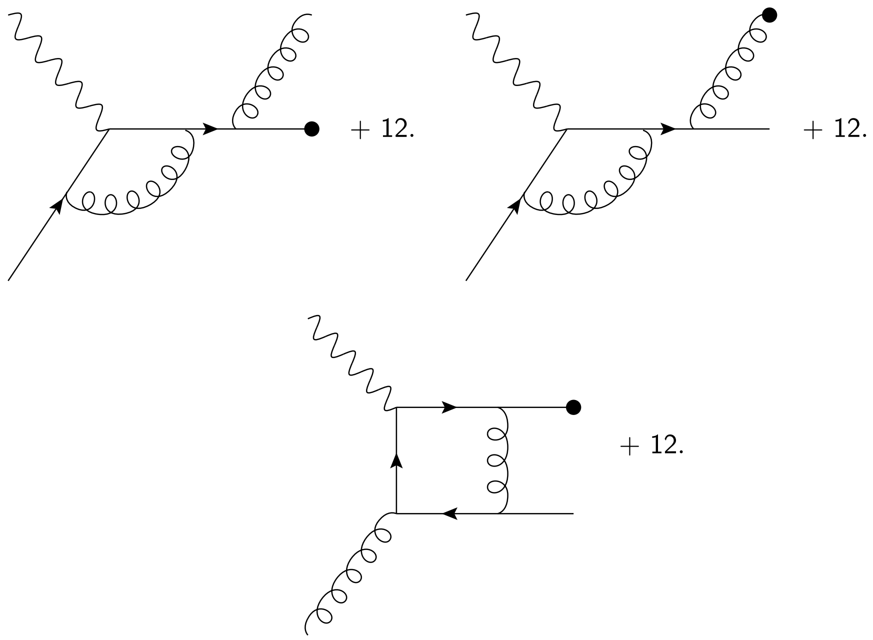

Figure 3.4: RV diagrams (one-loop with one real emission) at NNLO.

The list of sub-processes with two real emissions reads:

$$q(\bar{q}) + \gamma^* \to q(\bar{q}) + g + g\,, \tag{3.8}$$

$$g + \gamma^* \to g + q + \bar{q}\,, \tag{3.9}$$

$$q(\bar{q}) + \gamma^* \to q(\bar{q}) + q' + \bar{q}'\,, \tag{3.10}$$

$$q(\bar{q}) + \gamma^* \to q(\bar{q}) + q + \bar{q}\,. \tag{3.11}$$

Again, any one of the final state partons in the above list of sub-processes can fragment into hadron H′.

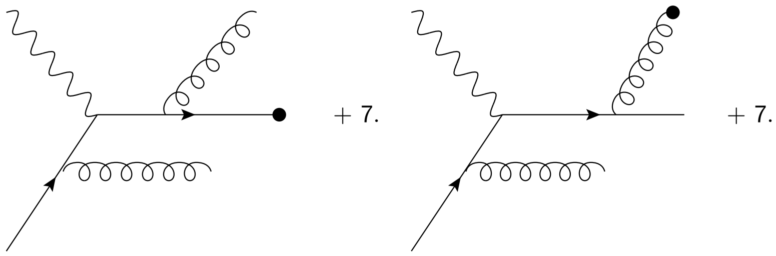

Figure 3.5: RR diagrams: emissions of two gluons. The integer indicates the number of additional diagrams.

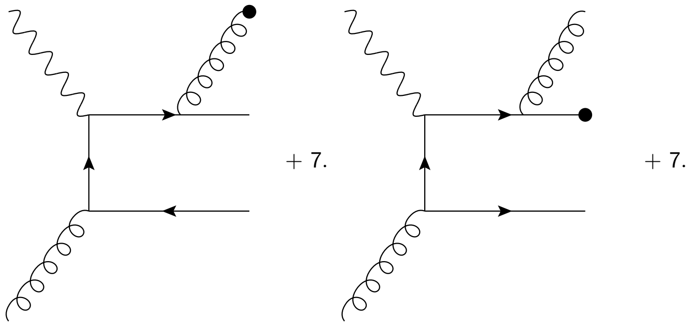

Figure 3.6: RR diagrams: gluon initiated processes. The integer indicates the number of additional diagrams.

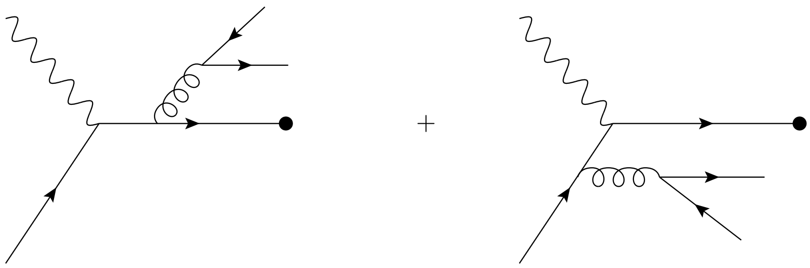

Figure 3.7: RR diagrams: A type as defined in the text.

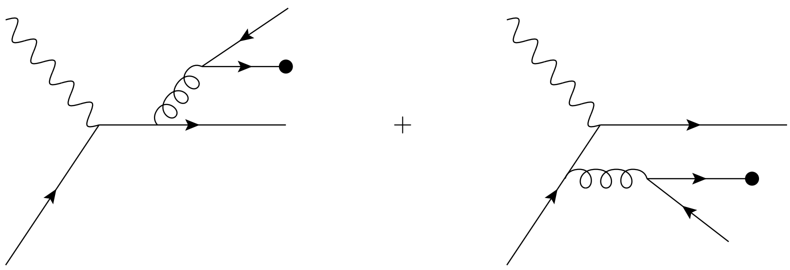

Figure 3.8: RR diagrams: B type as defined in the text.

At NNLO, the VV contributions are given by the two-loop virtual amplitudes, Fig. 3.3, and the square of one-loop virtual correction to the LO sub-process, cf. upper left diagram

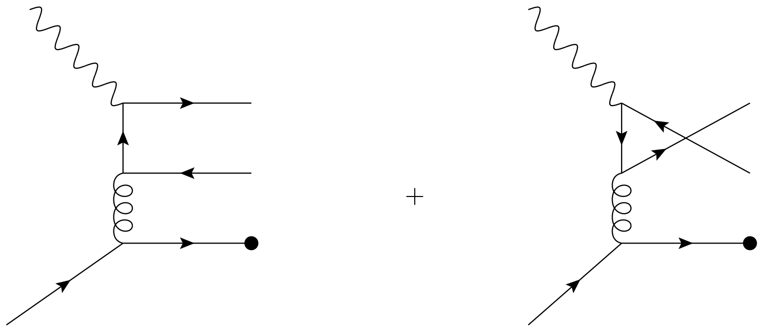

Figure 3.9: RR diagrams: C type as defined in the text.

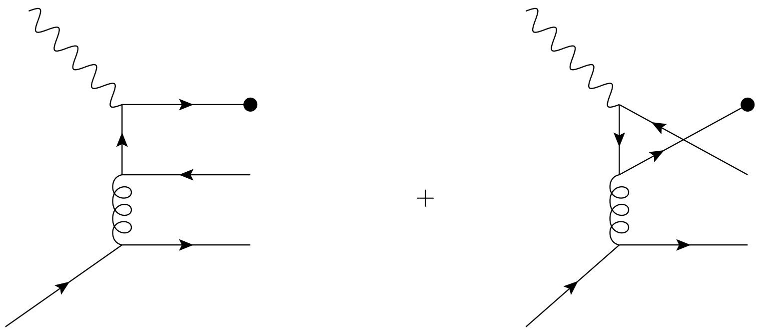

Figure 3.10: RR diagrams: D type as defined in the text.

in Fig. 3.2. The RV contributions arise from the interference of one loop-one real emission amplitudes, Fig. 3.4 with one real emission amplitudes Fig. 3.2.

The two-parton real emissions (RR) have three distinct sub-processes, namely the ones with a pair of gluons in the final state, cf. Fig. 3.5, those with one gluon along with a quark anti-quark pair Fig. 3.6, and the ones that have a final state quark anti-quark pair from gluon splitting. The latter type contains four different sub-processes denoted by A, B, C and D, shown in Figs. 3.7 – 3.10.

Having obtained the amplitudes and the squared matrix elements in d dimensions, we extract the SFs F_i, g_1 using appropriate projectors and perform loop as well as phase space integration as described in the next section.

3.1.2 Master Integrals

We reduce the large number of loop and phase-space integrals arising from the VV, RV, and RR squared matrix elements to a minimal set of master integrals (MIs) using integration-by- parts (IBP) identities, and to present the explicit analytic results for those MIs in dimensional regularization. We treat the three classes VV, RV, and RR in turn, since each requires its own family of propagators and reduction strategy.

Common Setup: Phase Space and IBP Framework

Before specifying the individual integral families, we establish the common framework for phase-space integration and IBP reduction that is used throughout.

The $n+1$-body phase space for scattering processes with momenta $p_a + q \to \sum_{i=1}^{n} k_i + p_b$ and a constraint on the momentum p_b of the fragmenting parton is given by

$$\int_{z'} [\mathrm{dPS}]_{n+1} = \prod_{i=1}^{n} \left(\int \frac{d^d k_i}{(2\pi)^{d-1}} \delta(k_i^2) \right) \int d^d p_b (2\pi) \delta(p_b^2) \\ \times \delta^d(p_b + K - p_a - q) \delta\left(z' - \frac{p_a \cdot p_b}{p_a \cdot q}\right) , \tag{3.12}$$

where $K = \sum_i^n k_i$ and $q = k_l - k_l'$. Note that we have introduced an additional delta function to define scaling variable $z' = z/z_1$ corresponding to the fragmenting parton.

In center-of-mass frame of p_a and q, the two-body phase space takes the simple form:

$$\int_{z'} [\mathrm{dPS}]_2 = \frac{2\pi}{(4\pi)^{\frac{d}{2}} \Gamma_{\frac{d}{2}-1}} \left(\frac{Q^2(1-x')}{x'} \right)^{\frac{d}{2}-2} \int_0^1 dw (w(1-w))^{\frac{d}{2}-2} \delta(w - z') , \tag{3.13}$$

where the integral $\int_{z'}$ implies the constraint on z' through $\delta(z' - p_a \cdot p_b / p_a \cdot q)$, which has been omitted for brevity, here $x' = x/x_1$. The Gamma function $\Gamma(n)$ is presented as Γ_n. Similarly, the three-body phase space for the scattering $p_a + q \to k_1 + k_2 + p_b$ in the center-of-mass frame of the momenta k_1 and k_2 is found to be (see [185–188])

$$\int_{z'} [\mathrm{dPS}]_3 = \frac{1}{(4\pi)^d \Gamma_{d-3}} \left(\frac{Q^2(1-x')}{x'} \right)^{d-3} \int_0^\pi d\theta (\sin\theta)^{d-3} \int_0^\pi d\phi (\sin\phi)^{d-4}$$
$$\times \int_0^1 dw \int_0^1 dz \, w^{\frac{d-4}{2}} (1-w)^{d-3} \big(z(1-z)\big)^{\frac{d-4}{2}} \delta(w-z') \,. \tag{3.14}$$

The computation of the phase space integrals with the constraint $z' = p_a.p_b/p_a.q$ is technically challenging compared to fully inclusive DIS. The significant number of parton level sub-processes for the RV and RR cases leave us with large number of phase space integrals, most of them related to each other, though. In order to find a set of basis integrals, called master integrals (MIs), we use integration by parts identities (IBP) [189–192]. To obtain IBP identities for phase space integrals, we use the method of reverse unitarity [193–196], convert all of them into loop integrals with the help of the identity,

$$(2\pi i)\delta(p^2) = \frac{1}{p^2 + i\epsilon} - \frac{1}{p^2 - i\epsilon} \,, \tag{3.15}$$

and then follow the standard approach that one uses for loop integrals to generate IBP identities. With the help of these identities, we can express all the phase space integrals in terms of a few phase space MIs. We group the integrals into families and generate IBP identities using the *Mathematica* package `LiteRed` [197–199].

VV Master Integrals

The VV part up to the NNLO level requires the two-loop contributions to the Born subprocess ($p_a + q \to p_b$). All integrals are known up to desired accuracy in a_s and ε, see [144, 185, 200–211] and details of their computation are listed here for completeness. At two loops, one encounters two families of integrals

$$\mathbb{B}_1\colon \{D_1^{\mathbb{B}}, D_2^{\mathbb{B}}, D_3^{\mathbb{B}}, D_4^{\mathbb{B}}, D_6^{\mathbb{B}}, D_7^{\mathbb{B}}, D_8^{\mathbb{B}}\} \;,$$
$$\mathbb{B}_2\colon \{D_1^{\mathbb{B}}, D_2^{\mathbb{B}}, D_3^{\mathbb{B}}, D_5^{\mathbb{B}}, D_6^{\mathbb{B}}, D_7^{\mathbb{B}}, D_9^{\mathbb{B}}\} \;,$$

where the propagators $D_i^{\mathbb{B}}$ are defined as,

$$
\begin{aligned}
&D_1^{\mathbb{B}}:(l_1)^2 && D_4^{\mathbb{B}}:(l_1+p_a)^2 && D_7^{\mathbb{B}}:(l_2+p_a)^2 \\
&D_2^{\mathbb{B}}:(l_2)^2 && D_5^{\mathbb{B}}:(l_1-p_b)^2 && D_8^{\mathbb{B}}:(l_2+p_a-p_b)^2 \\
&D_3^{\mathbb{B}}:(l_1-l_2)^2 && D_6^{\mathbb{B}}:(l_1+p_a-p_b)^2 && D_9^{\mathbb{B}}:(l_1-l_2-p_b)^2\,.
\end{aligned}
$$

Here, $D_7^{\mathbb{B}}$ and $D_5^{\mathbb{B}}$ serve as auxiliary propagators in the families $\mathbb{B}_1$ and $\mathbb{B}_2$, respectively. The two-loop integrals $J\left(\mathbb{B}_n, n_1, \cdots, n_7\right)$ for the family $\mathbb{B}_n$ are given by

$$
J\left(\mathbb{B}_n, n_1, \cdots, n_7\right)=\int \frac{d^d l_1}{(2\pi)^d}\frac{d^d l_2}{(2\pi)^d}\frac{1}{\left(D_{a_1}^{\mathbb{B}}\right)^{n_1}\cdots\left(D_{a_7}^{\mathbb{B}}\right)^{n_7}}\,, \tag{3.16}
$$

where again the propagators are to be taken from the ordered set of family $\mathbb{B}_n$. An IBP reduction leads to the following 4 MIs,

$$
\begin{aligned}
&J\left(\mathbb{B}_1;0,1,1,0,1,0,0\right) && J\left(\mathbb{B}_1;1,1,0,0,1,0,1\right) \\
&J\left(\mathbb{B}_1;0,1,1,1,0,0,1\right) && J\left(\mathbb{B}_2;1,1,1,0,1,1,1\right)\,.
\end{aligned}
$$

RV Master Integrals

The RV case [204, 212–215] consists of 3 families. They are given by

$$
\begin{aligned}
\mathbb{C}_1:&\quad \{D_1^{\mathbb{C}}, D_2^{\mathbb{C}}, D_3^{\mathbb{C}}, D_6^{\mathbb{C}}\} \\
\mathbb{C}_2:&\quad \{D_1^{\mathbb{C}}, D_2^{\mathbb{C}}, D_3^{\mathbb{C}}, D_5^{\mathbb{C}}\} \\
\mathbb{C}_3:&\quad \{D_1^{\mathbb{C}}, D_2^{\mathbb{C}}, D_4^{\mathbb{C}}, D_5^{\mathbb{C}}\}\,,
\end{aligned}
$$

where the propagators $D_i^{\mathbb{C}}$ are defined as,

$$
\begin{aligned}
&D_1^{\mathbb{C}}:\quad (l_1)^2 && D_2^{\mathbb{C}}:\quad (l_1-p_a)^2 \\
&D_3^{\mathbb{C}}:\quad (l_1+q)^2 && D_4^{\mathbb{C}}:\quad (l_1-p_a-q+k_1)^2 \\
&D_5^{\mathbb{C}}:\quad (l_1-p_a+k_1)^2 && D_6^{\mathbb{C}}:\quad (l_1+q-k_1)^2\,.
\end{aligned}
$$

We define an integral in the family $\mathbb{C}_n$ as

$$
\begin{aligned}
&J\left(\mathbb{C}_n, n_1, \cdots, n_4\right) = \\
&\int \frac{d^d l_1}{(2\pi)^d} \int_{z'} [\mathrm{dPS}]_2 \frac{1}{\left(D^{\mathbb{C}}_{a_1}\right)^{n_1} \cdots \left(D^{\mathbb{C}}_{a_4}\right)^{n_4}}\,,
\end{aligned} \tag{3.17}
$$

for propagators $D^{\mathbb{C}}_{a_1}, \cdots, D^{\mathbb{C}}_{a_4}$ taken from the ordered set of family $\mathbb{C}_n$. After IBP reduction using `LiteRed`, we obtain 7 MIs:

$$
\begin{array}{lll}
J(\mathbb{C}_1; 0,1,1,0) & J(\mathbb{C}_1; 1,0,0,1) & J(\mathbb{C}_1; 1,0,1,0) \\
J(\mathbb{C}_1; 1,1,1,1) & J(\mathbb{C}_2; 1,0,0,1) & J(\mathbb{C}_2; 1,1,1,1) \\
J(\mathbb{C}_3; 1,1,1,1) & &
\end{array}
$$

RR Master Integrals

In the case of RR at NNLO level [216], we have 8 independent propagators which give 13 families. Each family is denoted by $\mathbb{A}_i, i = 1, \cdots, 13$ and an ordered set,

$$
\begin{array}{llllll}
\mathbb{A}_1: & \{D^{\mathbb{A}}_1, D^{\mathbb{A}}_5, D^{\mathbb{A}}_6\} & \mathbb{A}_2: & \{D^{\mathbb{A}}_1, D^{\mathbb{A}}_5, D^{\mathbb{A}}_7\} & \mathbb{A}_3: & \{D^{\mathbb{A}}_1, D^{\mathbb{A}}_5, D^{\mathbb{A}}_8\} \\
\mathbb{A}_4: & \{D^{\mathbb{A}}_1, D^{\mathbb{A}}_6, D^{\mathbb{A}}_8\} & \mathbb{A}_5: & \{D^{\mathbb{A}}_1, D^{\mathbb{A}}_2, D^{\mathbb{A}}_4\} & \mathbb{A}_6: & \{D^{\mathbb{A}}_1, D^{\mathbb{A}}_2, D^{\mathbb{A}}_8\} \\
\mathbb{A}_7: & \{D^{\mathbb{A}}_1, D^{\mathbb{A}}_4, D^{\mathbb{A}}_5\} & \mathbb{A}_8: & \{D^{\mathbb{A}}_1, D^{\mathbb{A}}_4, D^{\mathbb{A}}_7\} & \mathbb{A}_9: & \{D^{\mathbb{A}}_1, D^{\mathbb{A}}_4, D^{\mathbb{A}}_8\} \\
\mathbb{A}_{10}: & \{D^{\mathbb{A}}_2, D^{\mathbb{A}}_4, D^{\mathbb{A}}_5\} & \mathbb{A}_{11}: & \{D^{\mathbb{A}}_2, D^{\mathbb{A}}_5, D^{\mathbb{A}}_7\} & \mathbb{A}_{12}: & \{D^{\mathbb{A}}_2, D^{\mathbb{A}}_5, D^{\mathbb{A}}_8\} \\
\mathbb{A}_{13}: & \{D^{\mathbb{A}}_2, D^{\mathbb{A}}_5, D^{\mathbb{A}}_6\} & & & &
\end{array}
$$

where the propagators ($D^{\mathbb{A}}_i$) are defined below.

$$
\begin{array}{llll}
D^{\mathbb{A}}_1 : (k_1 - p_a)^2 & D^{\mathbb{A}}_2 : (k_1 - q)^2 & D^{\mathbb{A}}_3 : (k_2 - p_a)^2 & D^{\mathbb{A}}_4 : (k_2 - q)^2 \\
D^{\mathbb{A}}_5 : (k_1 - p_a - q)^2 & D^{\mathbb{A}}_6 : (k_2 - p_a - q)^2 & D^{\mathbb{A}}_7 : (k_1 + k_2)^2 & D^{\mathbb{A}}_8 : (k_1 + k_2 - p_a)^2
\end{array}
$$

An integral $J(\mathbb{A}_n, n_1, n_2, n_3)$ in the family $\mathbb{A}_n$ is given by

$$J(\mathbb{A}_n, n_1, n_2, n_3) = \int_{z'} [\mathrm{dPS}]_3 \frac{1}{\left(D^{\mathbb{A}}_{a_1}\right)^{n_1} \left(D^{\mathbb{A}}_{a_2}\right)^{n_2} \left(D^{\mathbb{A}}_{a_3}\right)^{n_3}}, \tag{3.18}$$

where the propagators $D^{\mathbb{A}}_{a_1}, D^{\mathbb{A}}_{a_2}, D^{\mathbb{A}}_{a_3}$ are the elements from the ordered set of family $\mathbb{A}_n$. The solution of the IBP identities leads to the following 20 MIs,

$$\begin{aligned}
&J(\mathbb{A}_1;0,0,0),\ J(\mathbb{A}_1;0,0,1),\ J(\mathbb{A}_1;1,1,1), J(\mathbb{A}_2;1,1,1),\ J(\mathbb{A}_3;0,0,1),\\
&J(\mathbb{A}_3;1,1,1), J(\mathbb{A}_4;1,1,1),\ J(\mathbb{A}_5;0,0,1),\ J(\mathbb{A}_5;0,0,2), J(\mathbb{A}_5;0,1,1),\\
&J(\mathbb{A}_5;1,1,1),\ J(\mathbb{A}_6;0,1,1), J(\mathbb{A}_6;1,1,1), J(\mathbb{A}_7;0,1,1),\ J(\mathbb{A}_7;1,1,1),\\
&J(\mathbb{A}_8;1,1,1),\ J(\mathbb{A}_{10};1,1,1), J(\mathbb{A}_{11};1,1,1), J(\mathbb{A}_{12};1,1,1), J(\mathbb{A}_{13};1,1,1)\,.
\end{aligned} \tag{3.19}$$

The task to evaluate the MIs for the VV, RV and RR type diagrams in dimensional regularization to the desired accuracy in ε will be discussed next.

3.1.3 Results of MIs

The goal of this subsection is to provide the explicit analytic expressions for the MIs in dimensional regularization, discuss the analytic continuation required to extend the RV results to the full physical region, and identify the structure of IR singularities that must be removed by mass factorization.

VV and RV Master Integrals: Results

The two-loop MIs for the VV case to the required accuracy in ε can be found in [185, 200, 201, 217]. The MIs for the RV case have been listed in [185]. We also note that these phase-space integrals have been recently discussed in a publication [176], which expands on the previous findings presented in [218]. Additionally, in [175], we also have presented these integrals along with the complete computational details.

Unlike the pure virtual case (VV), the RV integrals require special care when using them in the physical regions spanned by the scaling variables x' and z'. We list these integrals below for arbitrary x' and z', and, subsequently, we express them in a form that can be used in different physical regions with the help of analytic continuation and analyticity properties of the integrals. For

$$J\left(\mathbb{C}_1;0,1,1,0\right) = -i\frac{2}{\varepsilon}\frac{C_\varepsilon}{(1+\varepsilon)}(-s)^{\varepsilon/2}\,, \tag{3.20}$$

$$J(\mathbb{C}_1;1,0,0,1) = -i\frac{2}{\varepsilon}\frac{C_\varepsilon}{(1+\varepsilon)}(-u)^{\varepsilon/2}\,, \tag{3.21}$$

$$J\left(\mathbb{C}_1;1,0,1,0\right) = -i\frac{2}{\varepsilon}\frac{C_\varepsilon}{(1+\varepsilon)}(Q^2)^{\varepsilon/2}\,, \tag{3.22}$$

$$J\left(\mathbb{C}_2;1,0,0,1\right) = -i\frac{2}{\varepsilon}\frac{C_\varepsilon}{(1+\varepsilon)}(-t)^{\varepsilon/2}\,, \tag{3.23}$$

$$\begin{aligned} J\left(\mathbb{C}_1;1,1,1,1\right) = -i\frac{8C_\varepsilon}{\varepsilon^2}\Bigg\{&\frac{(Q^2)^{\varepsilon/2}}{su}F_\varepsilon\left(\frac{Q^2t}{su}\right) \\ &-\frac{(-u)^{\varepsilon/2}}{su}F_\varepsilon\left(\frac{-t}{s}\right)-\frac{(-s)^{\varepsilon/2}}{su}F_\varepsilon\left(\frac{-t}{u}\right)\Bigg\}, \end{aligned} \tag{3.24}$$

$$\begin{aligned} J\left(\mathbb{C}_2;1,1,1,1\right) = -i\frac{8C_\varepsilon}{\varepsilon^2}\Bigg\{&\frac{(Q^2)^{\varepsilon/2}}{st}F_\varepsilon\left(\frac{Q^2u}{st}\right) \\ &-\frac{(-t)^{\varepsilon/2}}{st}F_\varepsilon\left(\frac{-u}{s}\right)-\frac{(-s)^{\varepsilon/2}}{st}F_\varepsilon\left(\frac{-u}{t}\right)\Bigg\}, \end{aligned} \tag{3.25}$$

$$\begin{aligned} J\left(\mathbb{C}_3;1,1,1,1\right) = -i\frac{8C_\varepsilon}{\varepsilon^2}\Bigg\{&\frac{(Q^2)^{\varepsilon/2}}{tu}F_\varepsilon\left(\frac{Q^2s}{tu}\right) \\ &-\frac{(-u)^{\varepsilon/2}}{tu}F_\varepsilon\left(\frac{-s}{t}\right)-\frac{(-t)^{\varepsilon/2}}{tu}F_\varepsilon\left(\frac{-s}{u}\right)\Bigg\}, \end{aligned} \tag{3.26}$$

where,

$$\begin{aligned} &F_\varepsilon(\xi) = {}_2F_1\left(1,\tfrac{\varepsilon}{2};1+\tfrac{\varepsilon}{2};\xi\right) = 1-\sum_{n=1}^{\infty}\left(-\tfrac{\varepsilon}{2}\right)^n \mathrm{Li}_n(\xi)\,, \\ &C_\varepsilon = \frac{1}{16\pi^2}\left(\frac{\Gamma(1-\frac{\varepsilon}{2})\Gamma^2(1+\frac{\varepsilon}{2})}{(4\pi)^{\frac{\varepsilon}{2}}\Gamma(1+\varepsilon)}\right), \\ &s = \frac{Q^2(1-x')}{x'}, \quad t = \frac{-Q^2(1-z')}{x'}, \quad u = \frac{-Q^2z'}{x'}\,. \end{aligned} \tag{3.27}$$

In the above formulas we imply that

$$(-s)^{\varepsilon/2} = (-s-i0)^{\varepsilon/2} = e^{-i\pi\varepsilon/2} s^{\varepsilon/2}.$$

Analytic Continuation of RV Integrals

The expressions (3.24)–(3.26) contain hypergeometric functions with arguments which can be larger than one when $x' \geqslant \min(z', 1-z')$. Therefore, in order to extend the applicability of these formulas to the whole physical region, one should perform an analytical continuation. Fortunately, it is easy to rewrite eqs. (3.24)–(3.26) in the form which is explicitly analytic in the whole physical region. For this purpose, we represent $\mathrm{F}_\varepsilon(\xi)$ for positive ξ as,

$$\mathrm{F}_\varepsilon(\xi) = \frac{\varepsilon^2(1-\xi)}{4\xi^{1+\frac{\varepsilon}{2}}}\widetilde{F}_\varepsilon(1-\xi^{-1}) - \frac{\varepsilon}{2\xi^{\varepsilon/2}}\left[\psi\left(\frac{\varepsilon}{2}\right) + \ln\left(\xi^{-1}-1\right) + \gamma_E\right], \tag{3.28}$$

where $\widetilde{F}_\varepsilon(z) = {}_3F_2\left(1,1,1+\varepsilon/2;2,2;z\right)$, $\psi(x) = \Gamma'(x)/\Gamma(x)$, and $\gamma_E = -\psi(1) = 0.577\ldots$ is the Euler constant.

Note that the only function in the right-hand side of eq. (3.28) which has a branching point on the interval $(0,+\infty)$ at $\xi = 1$ is $\ln\left(\xi^{-1}-1\right)$. Then it is easy to check that the branching logarithms cancel in eqs. (3.24)–(3.26). We have

$$\begin{aligned} J\left(\mathbb{C}_1;1,1,1,1\right) = &-\frac{2iC_\varepsilon}{(Q^2)^{2-\varepsilon/2}}\left(\frac{(1-z')x'}{(1-x')z'}\right)^{1-\frac{\varepsilon}{2}}\left\{\frac{x'-z'}{(1-z')^2}\left[\widetilde{F}_\varepsilon\left(\frac{x'-z'}{(1-z')x'}\right) - x'\widetilde{F}_\varepsilon\left(\frac{x'-z'}{1-z'}\right)\right]\right. \\ &\left.+\frac{4e^{-\frac{i\pi\varepsilon}{2}}x'(1-z')^{\varepsilon/2-1}}{\varepsilon^2 z'^{\varepsilon/2}}F_\varepsilon\left(\frac{z'-1}{z'}\right) - \frac{2x'\ln(x')}{\varepsilon(1-z')}\right\}, \end{aligned} \tag{3.29}$$

$$J\left(\mathbb{C}_2;1,1,1,1\right) = J\left(\mathbb{C}_1;1,1,1,1\right)|_{z'\to 1-z'}, \tag{3.30}$$

$$J\left(\mathbb{C}_3;1,1,1,1\right) = -\frac{2iC_\varepsilon}{(Q^2)^{2-\varepsilon/2}}\left(\frac{(1-x')\,x'}{(1-z')\,z'}\right)^{1-\frac{\varepsilon}{2}}\left\{\frac{x'\left(1-z'-x'\right)}{\left(1-x'\right)^2}\widetilde{F}_\varepsilon\left(\frac{1-z'-x'}{1-x'}\right)\right.$$

$$
+\frac{x'\,(z'-x')}{(1-x')^2}\,\widetilde{F}_\varepsilon\left(\frac{z'-x'}{1-x'}\right)+\frac{(z'-x')\,(1-z'-x')}{(1-x')^2}\,\widetilde{F}_\varepsilon\left(\frac{(z'-x')\,(1-z'-x')}{(x'-1)\,x'}\right)
$$

$$
\left.+\frac{2x'}{\varepsilon\,(1-x')}\left[\psi\,(\varepsilon/2)+\gamma_E-\ln\left(x'^{-1}-1\right)\right]\right\}. \tag{3.31}
$$

These new expressions are explicitly analytic in the whole physical region. More details are available in Appendix E. It is well known that the hypergeometric function $\widetilde{F}_\varepsilon(\xi)$ can be expanded in a power series in ε in terms of generalized [219] or harmonic [220–223] polylogarithms using,

$$
{}_3F_2\,(1,1,1+\varepsilon/2;2,2;z)=-\frac{1}{z}\sum_{n=0}^{\infty}(-\varepsilon/2)^n\,G(\underbrace{0,1,\ldots,1}_{n+2}|z)=\frac{1}{z}\sum_{n=0}^{\infty}(\varepsilon/2)^n\,H(2,\underbrace{1,\ldots,1}_{n}|z)\,. \tag{3.32}
$$

IR Divergence Structure

Our next task is to perform the mass factorization for the partonic cross sections $d\hat{\sigma}_{i,ab}$ in eq. (2.25) to obtain finite CFs. This removes collinear singularities arising from radiations off the incoming parton as well as off the fragmenting parton. The AP kernels $\Gamma_{c\leftarrow a}$ and $\tilde{\Gamma}_{b\leftarrow d}$ are pure counter-terms, containing only poles in ε which multiply '+'-distributions $\mathcal{D}_j(w)=(\ln^j(1-w)/(1-w))_+$, delta functions $\delta(1-w)$, and regular terms in w, where $w=x',z'$ (see, e.g. [169]). In order to cancel the collinear singularities in $d(\Delta)\hat{\sigma}_{1,ab}$ against those from AP kernels, we need to extract from the former ones the poles in ε in terms of the same '+'-distributions and regular functions.

The IR divergences in the partonic sub-cross section show up as $(1-x')^{-1}$ and/or $(1-z')^{-1}$. These terms originate either from MIs or their coefficients at the level of squared matrix elements and diverge in the respective threshold regions $x'\to 1$ and/or $z'\to 1$. In $d=4+\varepsilon$ dimensions, they are regulated by $(1-x')^{a\varepsilon}$ and $(1-z')^{b\varepsilon}$ respectively which originate from phase space and loop integrals.

At NNLO, we encounter IR singularities in sub-processes for the RR case through terms of the form

$$\frac{(1-x')^{\varepsilon}(1-z')^{\varepsilon}}{(1-x')(1-z')(z'-x')((1+x')^2-4x'z')} f_1(x',z',\varepsilon)\,. \tag{3.33}$$

After partial fractioning, it is easy to see that these terms contain only simple poles at the thresholds i.e. $x' \to 1$ and $z' \to 1$ when $\varepsilon \to 0$. Similarly, in integrals of RV type we find IR singular terms of the form

$$\frac{(1-x')^{a\varepsilon}(1-z')^{b\varepsilon}|z'-x'|^{c\varepsilon}|1-z'-x'|^{d\varepsilon}}{(1-x')(1-z')(z'-x')(1-z'-x')} f_2(x',z',\varepsilon)\,.$$

Here, a, b can take the values $1/2$ or 1 and c, d can be 0 or $-1/2$, while $f_i, i = 1, 2$ are regular in all their arguments.

After partial fractioning, we end up with the following combinations of denominators $\frac{1}{(1-x')(1-z')}$, $\frac{1}{(1-x')(z'-x')}$, $\frac{1}{(1-x')((1+x')^2-4x'z')}$, $\frac{1}{(1-x')}$, $\frac{1}{(1-z')}$ etc.

The extraction of the pole structure proceeds sequentially, first separating the singularity at $x' \to 1$ and then $z' \to 1$, or vice versa. For the RV case, the following form of IR singular terms is suitable for mass factorization.

$$\begin{aligned}
\frac{(1-x')^{a\varepsilon}(1-z')^{b\varepsilon}|z'-x'|^{c\varepsilon}}{(1-x')(1-z')} f(x',z') = {} & \frac{(1-x')^{a\varepsilon}_E}{1-x'}\frac{(1-z')^{b\varepsilon}_E}{1-z'}\bigg(|z'-x'|^{c\varepsilon}_E\, f(x',z') - (1-x')^{c\varepsilon}_E f(x',1) \\
& - (1-z')^{c\varepsilon}_E\big(f(1,z') - f(1,1)\big)\bigg) \\
& + \frac{(1-x')^{(a+c)\varepsilon}_E}{1-x'}\left[\frac{(1-z')^{b\varepsilon}}{1-z'}\right]_P f(x',1) \\
& + \frac{(1-x')^{a\varepsilon}_E}{1-x'}\left[\frac{(1-z')^{(b+c)\varepsilon}}{1-z'}\right]_P f(1,1) \\
& + \left[\frac{(1-x')^{a\varepsilon}}{1-x'}\right]_P\left[\frac{(1-z')^{(b+c)\varepsilon}}{1-z'}\right]_P f(1,1) \\
& + \left[\frac{(1-x')^{a\varepsilon}}{1-x'}\right]_P \frac{(1-z')^{(b+c)\varepsilon}_E}{1-z'}\big(f(1,z') - f(1,1)\big)
\end{aligned}$$

$$\frac{(1-x')^{a\varepsilon}(1-z')^{b\varepsilon}|z'-x'|^{c\varepsilon}}{(1-x')(z'-x')} f(x',z') = \frac{(1-x')^{a\varepsilon}_E}{1-x'}\frac{(1-z')^{b\varepsilon}_E}{z'-x'}\,|z'-x'|^{c\varepsilon}_E\, f(x',z')$$

$$
\begin{aligned}
&+\frac{(1-x')_E^{a\varepsilon}}{1-x'}\frac{(1-z')_E^{(b+c)\varepsilon}}{1-z'}\big(f(1,z')-f(1,1)\big)\\
&-\left[\frac{(1-x')^{a\varepsilon}}{1-x'}\right]_P\frac{(1-z')_E^{(b+c)\varepsilon}}{1-z'}\big(f(1,z')-f(1,1)\big)\\
&+\frac{(1-x')_E^{a\varepsilon}}{1-x'}\left[\frac{(1-z')^{(b+c)\varepsilon}}{1-z'}\right]_P f(1,1)\\
&-\left[\frac{(1-x')^{a\varepsilon}}{1-x'}\right]_P\left[\frac{(1-z')^{(b+c)\varepsilon}}{1-z'}\right]_P f(1,1)
\end{aligned}
\tag{3.34}
$$

In the RR case, the numerator $|z'-x'|^{c\varepsilon}$ is absent. Hence, we use the same identities after setting $c=0$ in eq. (3.34). The subscripts P and E in eq. (3.34) imply the shorthands as follows

$$
(\kappa)_E^{\eta\varepsilon} = \sum_{i=0}^{\infty}\frac{(\eta\varepsilon)^i}{i!}\ln^i(\kappa)\,, \tag{3.35}
$$

$$
\begin{aligned}
\left[\frac{(1-\kappa)^{\eta\varepsilon}}{1-\kappa}\right]_P &= \frac{1}{\eta\varepsilon}\delta(1-\kappa)+\left[\frac{(1-\kappa)_E^{\eta\varepsilon}}{1-\kappa}\right]_+\\
&= \frac{1}{\eta\varepsilon}\delta(1-\kappa)+\sum_{i=0}^{\infty}\frac{(\eta\varepsilon)^i}{i!}\left[\frac{\ln^i(1-\kappa)}{1-\kappa}\right]_+\,,
\end{aligned}
\tag{3.36}
$$

where the expansions should be properly truncated, since the IR singularities show up explicitly as poles in ε. The IR singularities in the individual contributions → VV, RV, and RR which consist of two physically distinct types: soft divergences, arising from the emission of zero-energy gluons, and collinear divergences, arising from emissions collinear to the incoming or outgoing massless partons. At NNLO, the unrenormalized partonic cross sections contain poles starting at $1/\varepsilon^4$, the highest power being generated by the double-soft and double-collinear limits of the VV,RV and RR contributions. However, a fundamental consequence of the KLN theorem guarantees that, upon summing all contributions at a given perturbative order: VV, RV, and RR, the soft poles cancel exactly. After this cancellation, one is left with poles of order $1/\varepsilon^2$ and $1/\varepsilon$, which are purely collinear in origin. These remaining poles have a well-defined structure: the $1/\varepsilon^2$ poles arise from simultaneous collinear singularities in the initial and final states, while the $1/\varepsilon$ poles arise from single collinear singularities off either the incoming parton or the fragmenting parton. To remove these residual collinear poles and absorb them into the non-perturbative PDFs and FFs, we employ mass factorization via the Altarelli-Parisi kernels introduced in eq. (2.25). The next section carries out this procedure explicitly and presents the resulting finite CFs order by order in a_s.

3.2 Mass Factorization

This section is to remove all remaining UV and IR divergences from the partonic cross sections through coupling renormalization and mass factorization, and to present the complete set of finite CFs $\mathcal{C}_{i,ab}^{(l,0)}$ at LO, NLO, and NNLO for all relevant partonic channels. At this stage all UV and IR divergences in the perturbative expansion of the partonic cross sections have been extracted as poles in ε. The UV divergences are removed by renormalization of the strong coupling ,

$$\hat{a}_s S_\varepsilon \left(\frac{1}{\mu^2}\right)^{\varepsilon/2} = a_s(\mu_R^2)\left(\frac{1}{\mu_R^2}\right)^{\varepsilon/2} Z_{a_s}(\mu_R^2)\,,$$

where the renormalization constant Z_{a_s} to order a_s is given by

$$Z_{a_s}(\mu_R^2) = 1 + a_s(\mu_R^2)\left(\frac{2\beta_{00}^s}{\varepsilon}\right) + O(a_s^2)\,, \tag{3.37}$$

with the one-loop coefficient of the QCD beta-function $\beta_{00}^s = \left(\frac{11}{3}C_A - \frac{2}{3}n_f\right)$.

The sub-processes involving emissions of on-shell partons contain soft and collinear divergences [57, 224, 225], with the soft ones canceling in the sum of all real emission and virtual contributions. The collinear divergences due to emissions from initial(final)-state partons are removed by space(time)-like AP-kernels. We apply eq. (2.25) to extract the collinear finite CFs $\mathcal{C}_i$ order by order in perturbation theory from the partonic sub-process cross sections computed in the previous section. The AP kernels can be expanded in powers of a_s

$$\mathbb{\Gamma}_{c\leftarrow d}(\xi,\mu_F^2,\varepsilon) = \delta_{cd}\delta(1-\xi) + \sum_{l=1}^{\infty} a_s^l(\mu_F^2)\, \mathbb{\Gamma}_{c\leftarrow d}^{(l,0)}(\xi,\varepsilon)\,, \tag{3.38}$$

where $\mathbb{\Gamma}$ denotes the set $\mathbb{\Gamma} \in \{\Gamma, \tilde{\Gamma}\}$, subject to a renormalization group evolution equation,

$$\mu_F^2 \frac{d}{d\mu_F^2} \mathbb{\Gamma}_{c\leftarrow d} = \frac{1}{2} \mathbb{P}_{ce}(a_s(\mu_F^2)) \otimes \mathbb{\Gamma}_{e\leftarrow d}\,,$$

where we abbreviate the splitting functions collectively by the set $\mathbb{P} \in \{P, \tilde{P}\}$. Their perturbative expansion reads $\mathbb{P}_{ce} = \sum_{l=1}^{\infty} a_s^l(\mu_F^2)\mathbb{P}_{ce}^{(l)}$ and they are all available in the literature to the required order and beyond, cf. e.g. refs. [79,226–229] for the space-like unpolarized splitting functions P, refs. [230, 231] for the time-like unpolarized ones $\tilde{P}$.

The AP kernels $\mathbb{\Gamma}_{c\leftarrow d}^{(l,0)}$ at NLO ($l = 1$ in eq. (4.18)) are given by,

$$\mathbb{\Gamma}^{(1,0)}_{q\leftarrow q} = \tfrac{1}{\varepsilon}\mathbb{P}^{(1,0)}_{qq}, \qquad \mathbb{\Gamma}^{(1,0)}_{g\leftarrow g} = \tfrac{1}{\varepsilon}\mathbb{P}^{(1,0)}_{gg},$$

$$\mathbb{\Gamma}^{(1,0)}_{\bar{q}\leftarrow g} = \mathbb{\Gamma}^{(1,0)}_{q\leftarrow g} = \tfrac{1}{\varepsilon}\mathbb{P}^{(1,0)}_{qg}, \qquad \mathbb{\Gamma}^{(1,0)}_{q\leftarrow \bar{q}} = 0,$$

$$\mathbb{\Gamma}^{(1,0)}_{g\leftarrow \bar{q}} = \mathbb{\Gamma}^{(1,0)}_{g\leftarrow q} = \tfrac{1}{\varepsilon}\mathbb{P}^{(1,0)}_{gq},$$

and at NNLO ($l = 2$ in eq. (4.18)),

$$\mathbb{\Gamma}^{(2,0)}_{q\leftarrow q} = \mathbb{\Gamma}^{(2,0),\mathrm{S}}_{q\leftarrow q} + \mathbb{\Gamma}^{(2,0),\mathrm{NS}}_{q\leftarrow q}, \qquad \mathbb{\Gamma}^{(2,0)}_{\bar{q}\leftarrow q} = \mathbb{\Gamma}^{(2,0)}_{q\leftarrow \bar{q}},$$

$$\mathbb{\Gamma}^{(2,0)}_{q\leftarrow \bar{q}} = \mathbb{\Gamma}^{(2,0),\mathrm{S}}_{q\leftarrow \bar{q}} + \mathbb{\Gamma}^{(2,0),\mathrm{NS}}_{q\leftarrow \bar{q}}, \qquad \mathbb{\Gamma}^{(2,0),\mathrm{S}}_{q\leftarrow \bar{q}} = \mathbb{\Gamma}^{(2,0),\mathrm{S}}_{q\leftarrow q},$$

$$\mathbb{\Gamma}^{(2,0)}_{\bar{q}'\leftarrow q} = \mathbb{\Gamma}^{(2,0)}_{q'\leftarrow q} = \mathbb{\Gamma}^{(2,0),\mathrm{S}}_{q\leftarrow q}, \qquad \{\text{for } q' \neq q\}$$

and are related to the splitting functions as,

$$
\begin{aligned}
\Gamma^{(2,0),\mathrm{NS}}_{q\leftarrow\bar q} &= \frac{1}{2\varepsilon}\mathbb{P}^{(2,0),-}_{qq}, \qquad \Gamma^{(2,0),\mathrm{S}}_{q\leftarrow q} = \frac{1}{2\varepsilon}\mathbb{P}^{(2,0),\mathrm{S}}_{qq} + \frac{1}{2\varepsilon^2}\Big(\mathbb{P}^{(1,0)}_{qg}\otimes\mathbb{P}^{(1,0)}_{gq}\Big),\\
\Gamma^{(2,0),\mathrm{NS}}_{q\leftarrow q} &= \frac{1}{2\varepsilon}\mathbb{P}^{(2,0),\mathrm{NS}}_{qq} + \frac{1}{2\varepsilon^2}\Big(2\beta^s_{00}\mathbb{P}^{(1,0)}_{qq} + \mathbb{P}^{(1,0)}_{qq}\otimes\mathbb{P}^{(1,0)}_{qq}\Big),\\
\Gamma^{(2,0)}_{g\leftarrow g} &= \frac{1}{2\varepsilon}\mathbb{P}^{(2,0)}_{gg} + \frac{1}{2\varepsilon^2}\Big(2\beta^s_{00}\mathbb{P}^{(1,0)}_{gg} + 2n_f\Big(\mathbb{P}^{(1,0)}_{gq}\otimes\mathbb{P}^{(1,0)}_{qg}\Big) + \mathbb{P}^{(1,0)}_{gg}\otimes\mathbb{P}^{(1,0)}_{gg}\Big),\\
\Gamma^{(2,0)}_{\bar q\leftarrow g} = \Gamma^{(2,0)}_{q\leftarrow g} &= \frac{1}{2\varepsilon}\mathbb{P}^{(2,0)}_{qg} + \frac{1}{2\varepsilon^2}\Big(2\beta^s_{00}\mathbb{P}^{(1,0)}_{qg} + \mathbb{P}^{(1,0)}_{qg}\otimes\mathbb{P}^{(1,0)}_{gg} + \mathbb{P}^{(1,0)}_{qq}\otimes\mathbb{P}^{(1,0)}_{qg}\Big),\\
\Gamma^{(2,0)}_{g\leftarrow\bar q} = \Gamma^{(2,0)}_{g\leftarrow q} &= \frac{1}{2\varepsilon}\mathbb{P}^{(2,0)}_{gq} + \frac{1}{2\varepsilon^2}\Big(2\beta^s_{00}\mathbb{P}^{(1,0)}_{gq} + \mathbb{P}^{(1,0)}_{gg}\otimes\mathbb{P}^{(1,0)}_{gq} + \mathbb{P}^{(1,0)}_{gq}\otimes\mathbb{P}^{(1,0)}_{qq}\Big).
\end{aligned}
$$

The required expressions for the splitting functions $\mathbb{P}^{(l,0)}_{ab}$ up to two loops are collected in Appendix D. Upon substitution of the AP kernels $\Gamma^{(l,0)}_{c\leftarrow d}$ in eq. (2.25) we can extract order by order the finite CFs $\mathcal{C}_i$ entering eq. (2.17),

$$
\mathcal{C}_{i,ab} = \mathcal{C}^{(0,0)}_{i,ab} + a_s(\mu_F^2)\,\mathcal{C}^{(1,0)}_{i,ab} + a_s^2(\mu_F^2)\,\mathcal{C}^{(2,0)}_{i,ab} + O(a_s^3(\mu_F^2))\,. \tag{3.39}
$$

For equal scales, setting $\mu_R = \mu_F$, the CFs $\mathcal{C}^{(l,0)}_{i,ab}$ for $l = 0,1,2$ are found to be following:

at LO ($l = 0$):

$q(\bar q) \to q(\bar q)$

$$
\mathcal{C}^{(0,0)}_{i,qq}(x',z') = \hat{\mathcal{C}}^{(0,0)}_{i,qq}(x',z') = \delta(1-x')\,\delta(1-z'),
$$

at NLO ($l = 1$):

$q(\bar q) \to q(\bar q)$

$$\mathcal{C}^{(1,0)}_{i,qq}(x',z') = \left(\frac{Q^2}{\mu_F^2}\right)^{\frac{\varepsilon}{2}} \hat{\mathcal{C}}^{(1,0)}_{i,qq}(x',z') - \delta(1-x')\,\tilde{\Gamma}^{(1,0)}_{q\leftarrow q}(z') - \Gamma^{(1,0)}_{q\leftarrow q}(x')\,\delta(1-z'),$$

$q(\overline{q}) \to g$

$$\mathcal{C}^{(1,0)}_{i,qg}(x',z') = \left(\frac{Q^2}{\mu_F^2}\right)^{\frac{\varepsilon}{2}} \hat{\mathcal{C}}^{(1,0)}_{i,qg}(x',z') - \delta(1-x')\,\tilde{\Gamma}^{(1,0)}_{g\leftarrow q}(z'),$$

$g \to q(\overline{q})$

$$\mathcal{C}^{(1,0)}_{i,gq}(x',z') = \left(\frac{Q^2}{\mu_F^2}\right)^{\frac{\varepsilon}{2}} \hat{\mathcal{C}}^{(1,0)}_{i,gq}(x',z') - \Gamma^{(1,0)}_{q\leftarrow g}(x')\,\delta(1-z'),$$

at NNLO ($l = 2$):

$q(\overline{q}) \to q(\overline{q})$

$$\begin{aligned}\mathcal{C}^{(2,0)}_{i,qq}(x',z') = {}& \left(\frac{Q^2}{\mu_F^2}\right)^{\varepsilon} \hat{\mathcal{C}}^{(2,0)}_{i,qq}(x',z') + \frac{2\beta^s_{00}}{\varepsilon}\left(\frac{Q^2}{\mu_F^2}\right)^{\frac{\varepsilon}{2}} \hat{\mathcal{C}}^{(1,0)}_{i,qq}(x',z') - \mathcal{C}^{(1,0)}_{i,qq}(x',z')\tilde{\otimes}\tilde{\Gamma}^{(1,0)}_{q\leftarrow q}(z') \\ & - \mathcal{C}^{(1,0)}_{i,qg}(x',z')\tilde{\otimes}\tilde{\Gamma}^{(1,0)}_{q\leftarrow g}(z') - \delta(1-x')\,\tilde{\Gamma}^{(2,0)}_{q\leftarrow q}(z') - \Gamma^{(2,0)}_{q\leftarrow q}(x')\,\delta(1-z') \\ & - \Gamma^{(1,0)}_{q\leftarrow q}(x')\,\tilde{\Gamma}^{(1,0)}_{q\leftarrow q}(z') - \Gamma^{(1,0)}_{q\leftarrow q}(x')\otimes\mathcal{C}^{(1,0)}_{i,qq}(x',z') \\ & - \Gamma^{(1,0)}_{g\leftarrow q}(x')\otimes\mathcal{C}^{(1,0)}_{i,gq}(x',z'),\end{aligned}$$

$q(\overline{q}) \to g$

$$\begin{aligned}\mathcal{C}^{(2,0)}_{i,qg}(x',z') = {}& \left(\frac{Q^2}{\mu_F^2}\right)^{\varepsilon} \hat{\mathcal{C}}^{(2,0)}_{i,qg}(x',z') + \frac{2\beta^s_{00}}{\varepsilon}\left(\frac{Q^2}{\mu_F^2}\right)^{\frac{\varepsilon}{2}} \hat{\mathcal{C}}^{(1,0)}_{i,qg}(x',z') - \mathcal{C}^{(1,0)}_{i,qq}(x',z')\tilde{\otimes}\tilde{\Gamma}^{(1,0)}_{g\leftarrow q}(z') \\ & - \mathcal{C}^{(1,0)}_{i,qg}(x',z')\tilde{\otimes}\tilde{\Gamma}^{(1,0)}_{g\leftarrow g}(z') - \delta(1-x')\,\tilde{\Gamma}^{(2,0)}_{g\leftarrow q}(z') - \Gamma^{(1,0)}_{q\leftarrow q}(x')\otimes\mathcal{C}^{(1,0)}_{i,qg}(x',z') \\ & - \Gamma^{(1,0)}_{q\leftarrow q}(x')\,\tilde{\Gamma}^{(1,0)}_{g\leftarrow q}(z'),\end{aligned}$$

$q(\overline{q}) \to \overline{q}(q)$

$$\begin{aligned}\mathcal{C}^{(2,0)}_{i,q\overline{q}}(x',z') = {}& \left(\frac{Q^2}{\mu_F^2}\right)^{\varepsilon} \hat{\mathcal{C}}^{(2,0)}_{i,q\overline{q}}(x',z') - \mathcal{C}^{(1,0)}_{i,qg}(x',z')\tilde{\otimes}\tilde{\Gamma}^{(1,0)}_{\overline{q}\leftarrow g}(z') - \delta(1-x')\,\tilde{\Gamma}^{(2,0)}_{\overline{q}\leftarrow q}(z') \\ & - \Gamma^{(1,0)}_{g\leftarrow q}(x')\otimes\mathcal{C}^{(1,0)}_{i,g\overline{q}}(x',z') - \Gamma^{(2,0)}_{\overline{q}\leftarrow q}(x')\,\delta(1-z'),\end{aligned}$$

$q(\overline{q}) \to q'(\overline{q}')$, for $\{q \neq q'\}$

$$\mathcal{C}^{(2,0)}_{i,qq'}(x',z') = \left(\frac{Q^2}{\mu_F^2}\right)^{\varepsilon} \hat{\mathcal{C}}^{(2,0)}_{i,qq'}(x',z') - \mathcal{C}^{(1,0)}_{i,qg}(x',z')\tilde{\otimes}\tilde{\Gamma}^{(1,0)}_{q\leftarrow g}(z') - \delta(1-x')\,\tilde{\Gamma}^{(2,0)}_{q'\leftarrow q}(z')$$

$$- \Gamma^{(1,0)}_{g\leftarrow q}(x') \otimes \mathcal{C}^{(1,0)}_{i,gq}(x',z') - \Gamma^{(2,0)}_{q'\leftarrow q}(x')\, \delta(1-z'),$$

$q(\overline{q}) \to \overline{q}'(q')$, for $\{q \neq q'\}$

$$\mathcal{C}^{(2,0)}_{i,q\overline{q}'}(x',z') = \left(\frac{Q^2}{\mu_F^2}\right)^{\varepsilon} \hat{\mathcal{C}}^{(2,0)}_{i,q\overline{q}'}(x',z') - \mathcal{C}^{(1,0)}_{i,qg}(x',z') \tilde{\otimes} \tilde{\Gamma}^{(1,0)}_{\overline{q}\leftarrow g}(z') - \delta(1-x')\, \tilde{\Gamma}^{(2,0)}_{\overline{q}'\leftarrow q}(z')$$
$$- \Gamma^{(1,0)}_{g\leftarrow q}(x') \otimes \mathcal{C}^{(1,0)}_{i,g\overline{q}}(x',z') - \Gamma^{(2,0)}_{\overline{q}'\leftarrow q}(x')\, \delta(1-z'),$$

$g \to q(\overline{q})$

$$\mathcal{C}^{(2,0)}_{i,gq}(x',z') = \left(\frac{Q^2}{\mu_F^2}\right)^{\varepsilon} \hat{\mathcal{C}}^{(2,0)}_{i,gq}(x',z') + \frac{2\beta^s_{00}}{\varepsilon}\left(\frac{Q^2}{\mu_F^2}\right)^{\frac{\varepsilon}{2}} \hat{\mathcal{C}}^{(1,0)}_{i,gq}(x',z') - \mathcal{C}^{(1,0)}_{i,gq}(x',z') \tilde{\otimes} \tilde{\Gamma}^{(1,0)}_{q\leftarrow q}(z')$$
$$- \Gamma^{(1,0)}_{q\leftarrow g}(x')\, \tilde{\Gamma}^{(1,0)}_{q\leftarrow q}(z') - \Gamma^{(1,0)}_{q\leftarrow g}(x') \otimes \mathcal{C}^{(1,0)}_{i,qq}(x',z')$$
$$- \Gamma^{(1,0)}_{g\leftarrow g}(x') \otimes \mathcal{C}^{(1,0)}_{i,gq}(x',z') - \Gamma^{(2,0)}_{q\leftarrow g}(x')\, \delta(1-z'),$$

$g \to g$

$$\mathcal{C}^{(2,0)}_{i,gg}(x',z') = \left(\frac{Q^2}{\mu_F^2}\right)^{\varepsilon} \hat{\mathcal{C}}^{(2,0)}_{i,gg}(x',z') - \mathcal{C}^{(1,0)}_{i,gq}(x',z') \tilde{\otimes} \tilde{\Gamma}^{(1,0)}_{g\leftarrow q}(z') - \mathcal{C}^{(1,0)}_{i,g\overline{q}}(x',z') \tilde{\otimes} \tilde{\Gamma}^{(1,0)}_{g\leftarrow \overline{q}}(z')$$
$$- \Gamma^{(1,0)}_{q\leftarrow g}(x')\, \tilde{\Gamma}^{(1,0)}_{g\leftarrow q}(z') - \Gamma^{(1,0)}_{\overline{q}\leftarrow g}(x')\, \tilde{\Gamma}^{(1,0)}_{g\leftarrow \overline{q}}(z')$$
$$- \Gamma^{(1,0)}_{q\leftarrow g}(x') \otimes \mathcal{C}^{(1,0)}_{i,qg}(x',z') - \Gamma^{(1,0)}_{\overline{q}\leftarrow g}(x') \otimes \mathcal{C}^{(1,0)}_{i,\overline{q}g}(x',z'). \tag{3.40}$$

For the subsequent discussion of the CFs with initial/final quarks of same or different flavor, it is useful to factor the dependence on the quark electric charges e_q as follows:

$$\mathcal{C}^{(0,0)}_{i,qq} = \mathcal{C}^{(0,0)}_{i,\overline{q}\overline{q}} = e_q^2 \mathrm{C}^{(0,0)}_{i,qq},$$
$$\mathcal{C}^{(1,0)}_{i,qq} = \mathcal{C}^{(1,0)}_{i,\overline{q}\overline{q}} = e_q^2 \mathrm{C}^{(1,0)}_{i,qq},$$
$$\mathcal{C}^{(1,0)}_{i,qg} = \mathcal{C}^{(1,0)}_{i,\overline{q}g} = e_q^2 \mathrm{C}^{(1,0)}_{i,qg},$$
$$\mathcal{C}^{(1,0)}_{i,gq} = \mathcal{C}^{(1,0)}_{i,g\overline{q}} = e_q^2 \mathrm{C}^{(1,0)}_{i,gq},$$
$$\mathcal{C}^{(2,0)}_{i,qq} = \mathcal{C}^{(2,0)}_{i,\overline{q}\overline{q}} = e_q^2 \mathrm{C}^{(2),\mathrm{NS}}_{i,qq} + \left(\sum_{q_k} e_{q_k}^2\right) \mathrm{C}^{(2),\mathrm{PS}}_{i,qq},$$
$$\mathcal{C}^{(2,0)}_{i,qg} = \mathcal{C}^{(2,0)}_{i,\overline{q}g} = e_q^2 \mathrm{C}^{(2,0)}_{i,qg},$$
$$\mathcal{C}^{(2,0)}_{i,gq} = \mathcal{C}^{(2,0)}_{i,g\overline{q}} = e_q^2 \mathrm{C}^{(2,0)}_{i,gq},$$
$$\mathcal{C}^{(2,0)}_{i,q\overline{q}} = \mathcal{C}^{(2,0)}_{i,\overline{q}q} = e_q^2 \mathrm{C}^{(2,0)}_{i,q\overline{q}},$$

$$
\begin{aligned}
\mathcal{C}^{(2,0)}_{i,gg} &= \left(\sum_{q_k} e^2_{q_k}\right) \mathrm{C}^{(2,0)}_{i,gg}\,,\\
\mathcal{C}^{(2,0)}_{i,qq'} &= \mathcal{C}^{(2,0)}_{i,\bar{q}\bar{q}'} = e^2_q \mathrm{C}^{(2),[1]}_{i,qq'} + e'^2_q \mathrm{C}^{(2),[2]}_{i,qq'} + e_q e'_q \mathrm{C}^{(2),[3]}_{i,qq'}\,,\\
\mathcal{C}^{(2,0)}_{i,q\bar{q}'} &= \mathcal{C}^{(2,0)}_{i,\bar{q}q'} = e^2_q \mathrm{C}^{(2),[1]}_{i,qq'} + e'^2_q \mathrm{C}^{(2),[2]}_{i,qq'} - e_q e'_q \mathrm{C}^{(2),[3]}_{i,qq'}\,.
\end{aligned}
\tag{3.41}
$$

where, e'_q is the electric charge of quark (q') of different flavor from quark q and summation is over the number of active flavor light quarks.

CFs	Diagrams
$\mathrm{C}^{(2),\mathrm{NS}}_{i,qq}$	VV [Figs. 3.1,3.2,3.3], RV [Figs. 3.2,3.4], RR [Figs. 3.5], A² [Fig. 3.7], B² [Fig. 3.8], D² [Fig. 3.10], AB [Figs. 3.7 3.8], AC [Figs. 3.7,3.9], AD [Figs. 3.7,3.10], BC [Figs. 3.8,3.9], BD [Figs. 3.8,3.10], CD [Figs. 3.9,3.10]
$\mathrm{C}^{(2),\mathrm{PS}}_{i,qq}$	C² [Fig. 3.9]
$\mathrm{C}^{(2,0)}_{i,q\bar{q}}$	B² [Fig. 3.8], D² [Fig. 3.10], BD [Figs. 3.8,3.10]
$\mathrm{C}^{(2),[1]}_{i,qq'}$	B² [Fig. 3.8]
$\mathrm{C}^{(2),[2]}_{i,qq'}$	D² [Fig. 3.10]
$\mathrm{C}^{(2),[3]}_{i,qq'}$	BD [Figs. 3.8,3.10]
$\mathrm{C}^{(2,0)}_{i,qg}$	RV($q\gamma^* \to g$) [Figs. 3.2,3.4], RR [Fig. 3.5]
$\mathrm{C}^{(2,0)}_{i,gq}$	RV($g\gamma^* \to q$) [Figs. 3.2,3.4], RR [Fig. 3.6]
$\mathrm{C}^{(2,0)}_{i,gg}$	RR($g\gamma^* \to g$) [Fig. 3.6]

Table 3.1: Feynman diagrams contributing to the CFs of individual partonic channels.

In Table 3.1 we have listed the individual Feynman diagrams contributing to the CFs for the different channels at NNLO level. The non-singlet CFs, i.e. $C_{i,qq}^{(2,0),\mathrm{NS}}$ receive contributions from VV diagrams in Figs. 3.1, 3.2 and 3.3, from RV diagrams in Figs. 3.2 and 3.4, and from RR real emission diagrams. The latter consist of diagrams with gluon emissions (Fig: 3.5) as well as the squared diagrams A^2, B^2, D^2 and their interference among themselves along with their interference with C type diagrams, cf. Figs. 3.7, 3.8, 3.9 and 3.10. The pure-singlet CFs, i.e. $C_{i,qq}^{(2,0),\mathrm{PS}}$, are obtained from the RR diagrams C^2 in Figs. 3.9. CFs in partonic channels with other flavor combinations for initial and fragmenting quarks/anti-quarks arise from RR diagrams. $C_{i,q\bar{q}}^{(2,0)}$ originates from diagrams of type B and D in Figs. 3.8 and 3.10, while $\mathcal{C}_{i,qq'}^{(2,0)}$ where $q \neq q'$ is sub-divided into three parts according to the interaction of the virtual photon with different quark flavors: $C_{i,qq'}^{(2,0),[1]}$ with B^2 in Fig. 3.8, $C_{i,qq'}^{(2,0),[2]}$ with D^2 in Fig. 3.10, $C_{i,qq'}^{(2,0),[3]}$ with interference between diagrams B and D.

Finally, for the assembly of all partonic CFs from (3.41) to the SIDIS SFs, cf. eq. (2.17), it is useful to introduce functions H_{ab} for the combination of PDFs and FFs in as follows:

$$
\begin{aligned}
H_{qq} &= f_q(x)D_q(z) + f_{\bar{q}}(x)D_{\bar{q}}(z)\,,\\
H_{q\bar{q}} &= f_q(x)D_{\bar{q}}(z) + f_{\bar{q}}(x)D_q(z)\,,\\
H_{qg} &= f_q(x)D_g(z) + f_{\bar{q}}(x)D_g(z)\,,\\
H_{gq} &= f_g(x)D_q(z) + f_g D_{\bar{q}}(z)\,,\\
H_{gg} &= f_g(x)D_g(z)\,,\\
H^{\pm}_{qq'} &= f_q(x)D_{q'}(z) \pm f_q(x)D_{\bar{q}'}(z) \pm f_{\bar{q}}(x)D_{q'}(z) + f_{\bar{q}}(x)D_{\bar{q}'}(z)\,.
\end{aligned}
\tag{3.42}
$$

With the perturbative expansion of the SFs in eq. (2.17) as $F_i = \sum_{l=0} a_s^l F_i^{(l,0)}$ we obtain then to NNLO,

$$
F_i^{(0,0)} = \sum_q e_q^2\, H_{qq}\,,
\tag{3.43}
$$

$$F_i^{(1,0)} = \sum_q e_q^2 \left(H_{qq} \hat{\otimes} \mathrm{C}_{i,qq}^{(1,0)} + H_{qg} \hat{\otimes} \mathrm{C}_{i,qg}^{(1,0)} + H_{gq} \hat{\otimes} \mathrm{C}_{i,gq}^{(1,0)} \right), \tag{3.44}$$

$$\begin{aligned} F_i^{(2,0)} &= \sum_q e_q^2 \Big(H_{qq} \hat{\otimes} \mathrm{C}_{i,qq}^{(2,0),\mathrm{NS}} + H_{q\bar{q}} \hat{\otimes} \mathrm{C}_{i,q\bar{q}}^{(2,0)} + H_{qg} \hat{\otimes} \mathrm{C}_{i,qg}^{(2,0)} + H_{gq} \hat{\otimes} \mathrm{C}_{i,gq}^{(2,0)} \Big) \\ &+ \Big(\sum_{q_k} e_{q_k}^2 \Big) \Big(H_{qq} \hat{\otimes} \mathrm{C}_{i,qq}^{(2,0),\mathrm{PS}} + H_{gg} \hat{\otimes} \mathrm{C}_{i,gg}^{(2,0)} \Big) \\ &+ \sum_q \sum_{q' \neq q} \Big(e_q^2 \, H_{qq'}^{+} \hat{\otimes} \mathrm{C}_{i,qq'}^{(2,0),[1]} + e_{q'}^2 \, H_{qq'}^{+} \hat{\otimes} \mathrm{C}_{i,qq'}^{(2,0),[2]} + e_q e_{q'} H_{qq'}^{-} \hat{\otimes} \mathrm{C}_{i,qq'}^{(2,0),[3]} \Big). \end{aligned} \tag{3.45}$$

where $\hat{\otimes}$ denotes the convolution of $\mathrm{C}_{i,ab}^{(l,0)}$ with H_{ab} in both variables x and z.

Our results for the CFs have been subject to the following checks. In the threshold expansion around $(x', z') \to 1$ our results for $\mathrm{C}_{i,ab}^{(l,0)}$, $i = 1, 2$ are in complete agreement with predictions for all '+'-distributions in $w = x', z'$, $\mathcal{D}_j(w) = (\ln^j(1-w)/(1-w))_+$ and terms to proportional delta functions $\delta(1-w)$ in the unpolarized SFs $F_{1,2}$ in refs. [70, 232] (see also [141, 233]). Also, the complete results have also been checked by the independent computation of refs. [177, 178], finding also perfect agreement for the full NNLO CFs. Results for NNLO QCD correction to Polarised SF (g_1) can be found in [30, 170, 171].

3.3 Phenomenology

In this section, We demonstrate the phenomenological impact of the new higher-order QCD corrections to SIDIS for the EIC at the center-of-mass energy of $\sqrt{s} = 140$ GeV. Beyond LO in QCD, the cross section receives contributions from various partonic channels, i.e. all individual sub-processes discussed in Sec. 3.1.

The hadron level structure function F_1 is computed according to eq. (2.17) as a convolution of the CFs with the corresponding PDFs and FFs for the specific parton-level sub-process. The SIDIS structure functions depend on the three scaling variables x, y and z. The momentum squared transferred, Q^2, depends on the center-of-mass energy of the scattering (s) through $Q^2 = xys$. In the following, we plot the structure function F_1 as a

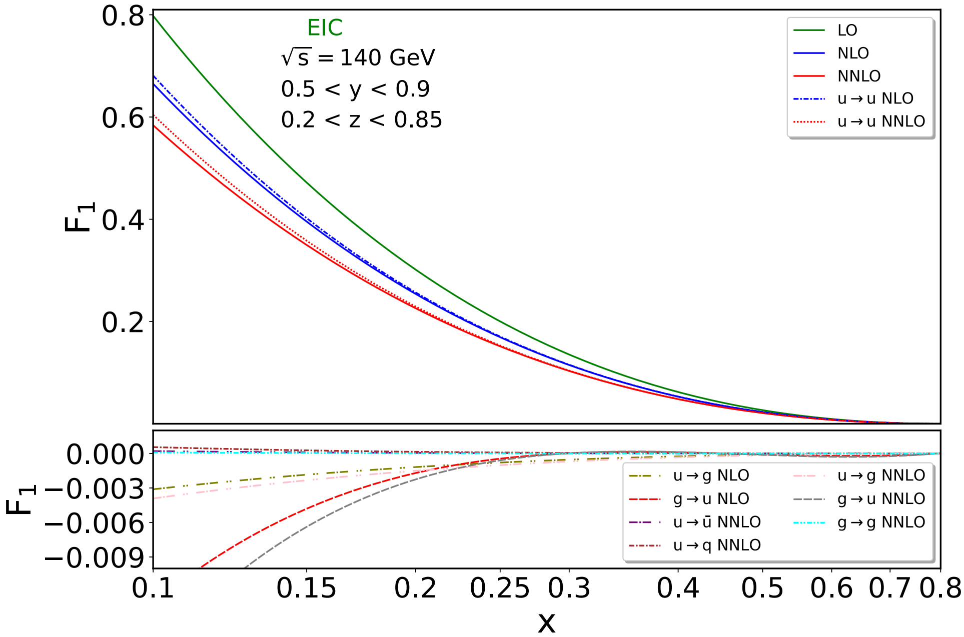

Figure 3.11: Contributions from all partonic channels to the structure function F_1 as a function of x for the EIC at $\sqrt{s} = 140$ GeV.

function of one of these scaling variables, either by fixing the other two variables or by integrating the SFs in some kinematic range.

Starting with the relative contributions of the various partonic channels to F_1 at the EIC with $\sqrt{s} = 140$ GeV, we present in Fig. 3.11 results at successive perturbative orders as a function of x, after integrating over z in the range between 0.2 and 0.85 and y in the range 0.5 to 0.9. Similarly, in Fig. 3.12, we show the contributions from various sub-processes to F_1 through NNLO as a function of z, after integration of x between 0.1 and 0.8 and of y between 0.5 and 0.9.

We observe that the contributions from the coefficient functions $C^{(l,0)}_{1,qq}$, $l = 1, 2$ dominate the perturbative expansion, i.e. they are much larger than those from the coefficient functions of the other partonic sub-processes. We have set both the renormalization and the factorization scale equal to the central scale $\mu_F = \mu_R = Q$. For F_1, we use the `NNPDF31` PDF sets [234] at LO, NLO and NNLO, respectively. The FFs are taken from the `NNFF10PIp` set [235] at the corresponding perturbative orders.

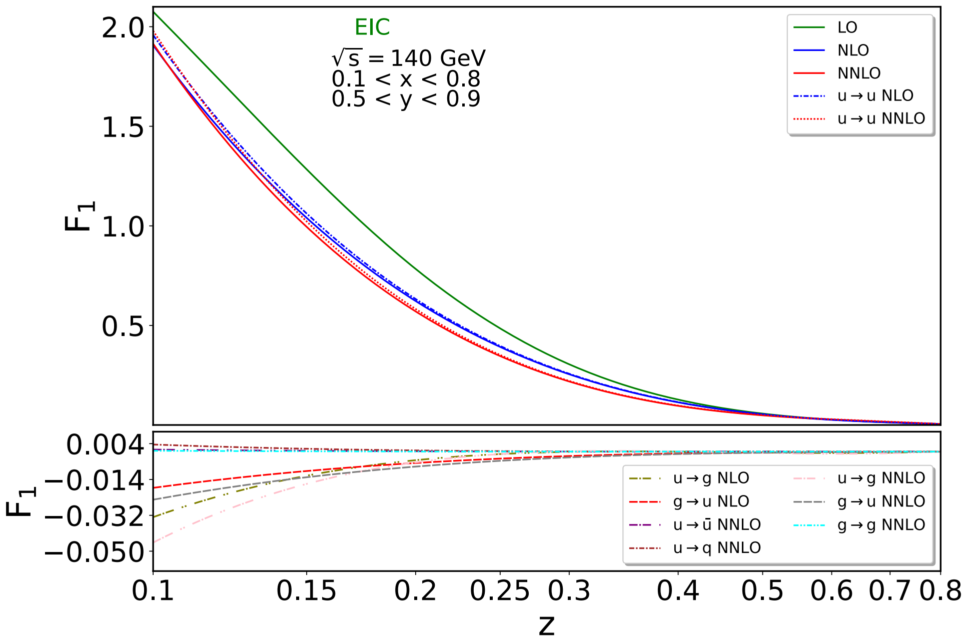

Figure 3.12: Contributions from different partonic channels to F_1 as a function of z for the EIC at $\sqrt{s} = 140$ GeV.

From Figs. 3.11 and 3.12, we find that the total perturbative corrections at order a_s as well as a_s^2 are negative over a wide range of x and z. As a result, the NLO contribution is smaller than that of the LO, and the NNLO prediction is less than that of the NLO in the ranges of x and z. For larger values of x and z, however, the NLO contribution becomes larger than the LO prediction. Similarly, both the NLO and NNLO corrections become larger than LO beyond $z = 0.7$. The exact values of x and z at which this transition occurs depend on the choice of PDFs and FFs as well as the choices of the integration regions.

In order to quantify the impact of the NLO and NNLO contributions with respect to LO, we introduce the K-factor defined as

$$K_{F_1}^{\mathrm{(N)NLO}} = \frac{F_1^{\mathrm{(N)NLO}}}{F_1^{\mathrm{LO}}} . \tag{3.46}$$

These K-factors for F_1 are plotted as a function of x in Fig. 3.13, after integrating y and z in the ranges $0.5 < y < 0.9$ and $0.2 < z < 0.85$. Similarly, Fig. 3.14 shows the K-factors

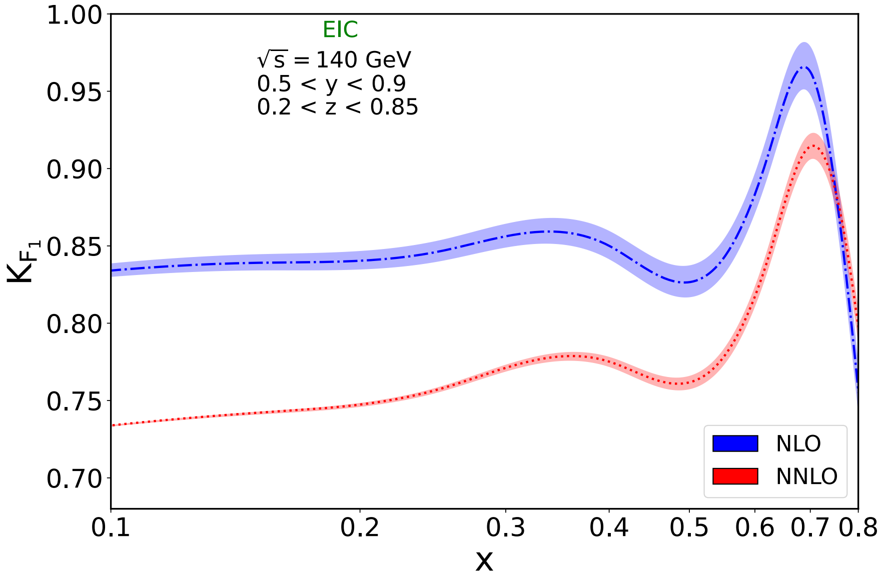

Figure 3.13: NLO and NNLO K-factors for F_1 as a function of x for the EIC at $\sqrt{s} = 140$ GeV.

as a function of z, after integration over $0.5 < y < 0.9$ and $0.1 < x < 0.8$. The same sets of PDFs and FFs as in Figs. 3.11 and 3.12 are used.

The bands for K-factors correspond to variation of the renormalization scale μ_R^2 in the interval $[Q_{avg}^2/2, 2Q_{avg}^2]$ while keeping the factorization scale $\mu_F = Q_{avg}$, where $Q_{avg}^2 = xy_{avg}s$ for Fig. 3.13 and $Q_{avg}^2 = x_{avg}y_{avg}s$ for Fig. 3.14. We find that theoretical uncertainties from scale variation decrease when going from NLO to NNLO accuracy, even though the scale dependence is already moderate at NLO.

In Fig. 3.15 we show the dependence of F_1 on the renormalization and factorization scales for six different values of Q^2. The allowed range of x for a given Q^2 is obtained by requiring $0.5 < y < 0.9$. The scales are varied independently by a factor of two around the central value Q^2, following the standard seven-point scale variation procedure.

The large uncertainty bands of the LO predictions arise mainly from the significant factorization scale dependence of the PDFs and FFs. The inclusion of higher-order corrections significantly reduces this dependence. A comparison of uncertainty bands for the NLO

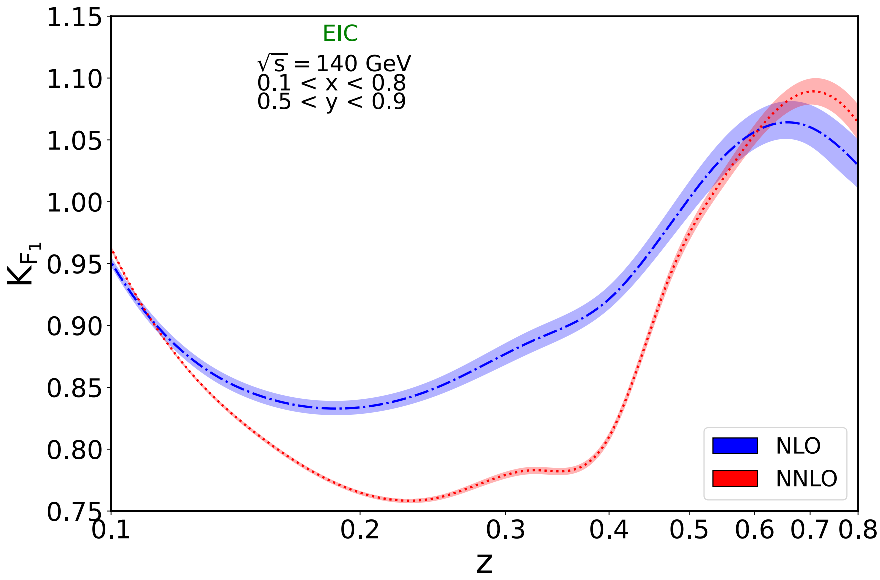

Figure 3.14: Same as Fig. 3.13, now as a function of z.

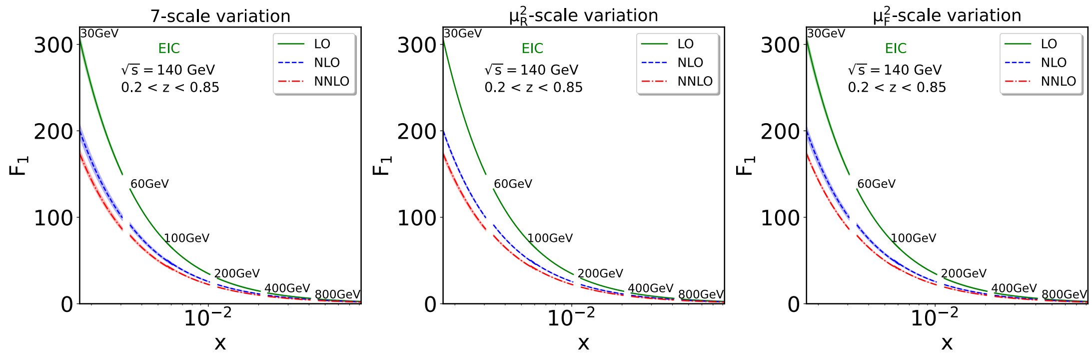

Figure 3.15: Scale variation of F_1 as a function of x for six different values of Q^2.

and NNLO predictions demonstrates a clear reduction of the residual scale dependence at NNLO.

Finally, in order to investigate the impact of different PDF and FF sets on the predictions for F_1 at NNLO, we consider the ratio

$$R_{F_1}^{\mathrm{PDF}} = \frac{F_1^{\mathrm{PDF}}}{F_1^{\mathrm{NNPDF}}} \,. \tag{3.47}$$

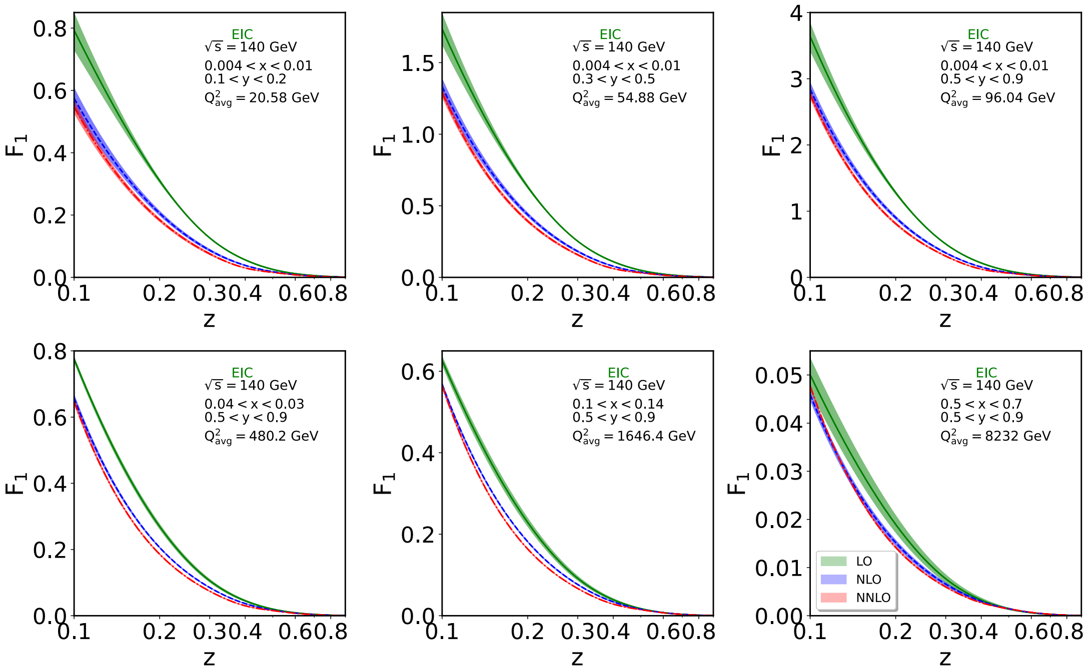

Figure 3.16: Scale variation of F_1 as a function of z for six different values of Q^2_{avg}.

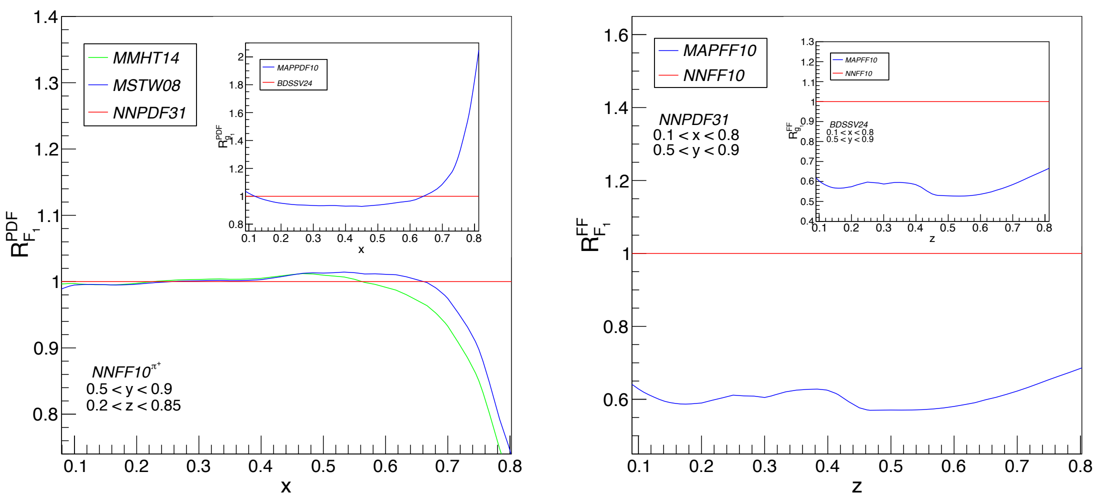

Figure 3.17: NNLO predictions for the SIDIS structure function F_1 for π^+ production. Left panel: Different choices of PDF sets in ratio to predictions with `NNPDF31` PDFs and fixed FFs `NNFF10`. Right panel: Different choices of FFs sets in ratio to predictions obtained with `NNFF10`, keeping the PDFs fixed.

$$R^{\mathrm{FF}}_{F_1} = \frac{F_1^{\mathrm{FF}}}{F_1^{\mathrm{NNFF}}}. \tag{3.48}$$

The PDF variation is illustrated in the left panel of Fig. 3.17, where we have integrated over the ranges $0.2 < z < 0.85$ and $0.5 < y < 0.9$. Similarly, the right panel shows the effect of different FFs parameterizations including NNFF10 and MAPFF10 [236] as a function of z, after integration over $0.1 < x < 0.8$ and $0.5 < y < 0.9$. For both ratios we set $\mu_F^2 = \mu_R^2 = Q_{avg}^2$, where $Q_{avg}^2 = x y_{avg} s$ for the left panel and $Q_{avg}^2 = x_{avg} y_{avg} s$ for the right panel.

The predictions for F_1 obtained using the unpolarized PDF sets `MMHT` [237] and `MSTW` [238] show noticeable deviations from those based on `NNPDF` in certain regions of large x. Similarly, sizable differences are observed when different FFs parameterizations are used. This highlights the importance of future EIC measurements of SIDIS structure functions in order to further constrain PDFs and FFs in the relevant kinematic region.

Chapter 4

NNLO QCD⊗QED Corrections to Unpolarized and Polarized SIDIS

Contents

In this chapter, we extend the NNLO QCD framework developed in Chapter 3 to include pure QED and mixed QCD⊗QED corrections to the SIDIS structure functions F_1, F_2 and g_1. We begin with the motivation for including electromagnetic contributions, then describe the additional partonic sub-processes and amplitudes that arise. We next explain how QED and mixed QCD⊗QED coefficient functions (CFs) can be obtained systematically from QCD results via Abelianization. Finally, we discuss the phenomenological impact of these corrections.

4.1 Motivation

The goal of this section is to establish why purely QCD calculations are insufficient for the level of precision required by modern and future experiments, and to motivate the specific QED and mixed QCD⊗QED contributions that are computed in the rest of the chapter. We also define the perturbative expansion in both couplings that organizes all subsequent results.

The theoretical description of semi-inclusive deep-inelastic scattering (SIDIS) has traditionally focused on perturbative QCD corrections. With the increasing precision of modern and upcoming experiments, however, purely QCD calculations are no longer sufficient for achieving the level of theoretical accuracy required for reliable phenomenological studies. In particular, electromagnetic interactions can give rise to additional contributions that become relevant when aiming at percent-level precision.

QED corrections arise naturally in the perturbative expansion of SIDIS cross sections once the electromagnetic coupling is treated on the same footing as the strong coupling. These corrections originate from photon emission, photon-initiated processes and photon in the loop at the partonic level. Furthermore, QED effects also enter through the evolution of PDFs and FFs, where photon radiation leads to additional splitting channels. Consequently, the consistent inclusion of QED corrections requires both the computation of the corresponding coefficient functions and the use of PDF and FF sets that incorporate QED evolution.

In addition to pure QED effects, mixed QCD⊗QED contributions appear in the perturbative expansion. These terms arise from diagrams involving both strong and electromagnetic interactions and therefore represent the interference between QCD and QED dynamics. Although formally suppressed by the electromagnetic coupling, such contributions can become phenomenologically relevant in precision studies, especially in kinematic regions where the QCD corrections are already under good theoretical control.

The inclusion of QED and mixed QCD⊗QED corrections is also important in view of future high-precision measurements at facilities such as the EIC. The expected experimental accuracy will make it possible to probe subtle effects in the flavor and spin structure of the nucleon, and therefore theoretical predictions must incorporate all relevant perturbative contributions. For SIDIS, the CFs at NNLO in QCD have been completed [169,171,177–181]. Building upon these developments, we present the first results on the impact of NNLO QED and mixed QCD⊗QED contributions on unpolarized and polarized SIDIS. These contributions are essential for enhancing the precision of theoretical predictions, reducing uncertainties resulting from renormalization and factorization scales, and are particularly relevant for upcoming high-precision experiments such as the EIC [39] at BNL and China.

The SFs of SIDIS also receive contributions from electroweak interactions via vector bosons such as $Z, W^{\pm}$, as well as from additional photons, with the simplest corrections arising from photons-namely, quantum electrodynamic (QED) effects. There have been several studies where QED and mixed QCD⊗QED corrections are considered for observables in DIS, see [19,20,150,239–246].

QED radiative corrections to the leptonic part largely factorize, a fact exploited in analytic resummations [247] and in formalisms based on lepton distribution functions [248–252]. At the HERA collider, these effects were systematically treated in the experimental analysis through dedicated Monte-Carlo generators for QED radiation [253–255]. Non-factorizable contributions such as two-photon exchange and leptonic-hadronic interference are known to be numerically negligible in DIS (well below 0.1% [256]) and lie beyond the accuracy relevant for a factorized parton-level calculation. In this work, we also incorporate QED as well as mixed QCD⊗QED corrections to F_1, F_2 and g_1 at NNLO accuracy within the established single-photon exchange framework used in global PDF fits and perturbative QCD analyses.

The perturbative expansion of the SIDIS cross section in both the strong and electromagnetic couplings is given by

$$\sigma = \sigma^{(0,0)} + a_s\,\sigma^{(1,0)} + a_e\,\sigma^{(0,1)} + a_s^2\,\sigma^{(2,0)} + a_e^2\,\sigma^{(0,2)} + a_s a_e\,\sigma^{(1,1)} + \cdots \tag{4.1}$$

with $a_s = \alpha_s/(4\pi) = g_s^2/(16\pi^2)$ and $a_e = \alpha_e^2/4\pi = e^2/(16\pi^2)$ in terms of strong coupling g_s and electric charge e. The cross sections $\sigma^{(m,n)}$ denote the contributions at order $\mathcal{O}(a_s^m, a_e^n)$. In this chapter, we focus on the pure QED corrections at $\mathcal{O}(a_e^2)$ as well as the mixed QCD⊗QED contributions at $\mathcal{O}(a_s a_e)$ to the SFs F_1, F_2 and g_1.

Having established why electromagnetic corrections must be included and how they are organized in the double expansion of eq. (4.1), the next step is to identify all additional partonic subprocesses that contribute beyond the pure QCD case. These are listed in the following section.

4.2 QED and QCD⊗QED Amplitudes at NNLO

In this section, we enumerate the new partonic subprocesses that arise when photons enter as initial or final state particles at NLO and NNLO. These are the QED and mixed QCD⊗QED analogues of the VV, RV, and RR classes already classified for pure QCD in Chapter 3, and they constitute the complete set of diagrams that must be computed to obtain the electromagnetic corrections to the CFs.

The LO, NLO, and NNLO QCD sub-processes have been listed in Section 3.1 of Chapter 3. Here we list only the additional sub-processes that arise when QED and mixed QCD⊗QED corrections are included. The additional sub-processes at NLO involving photons are:

$$q(\bar{q}) + \gamma^* \to q(\bar{q}) + \gamma\,, \tag{4.2}$$

$$\gamma + \gamma^* \to q + \bar{q}\,. \tag{4.3}$$

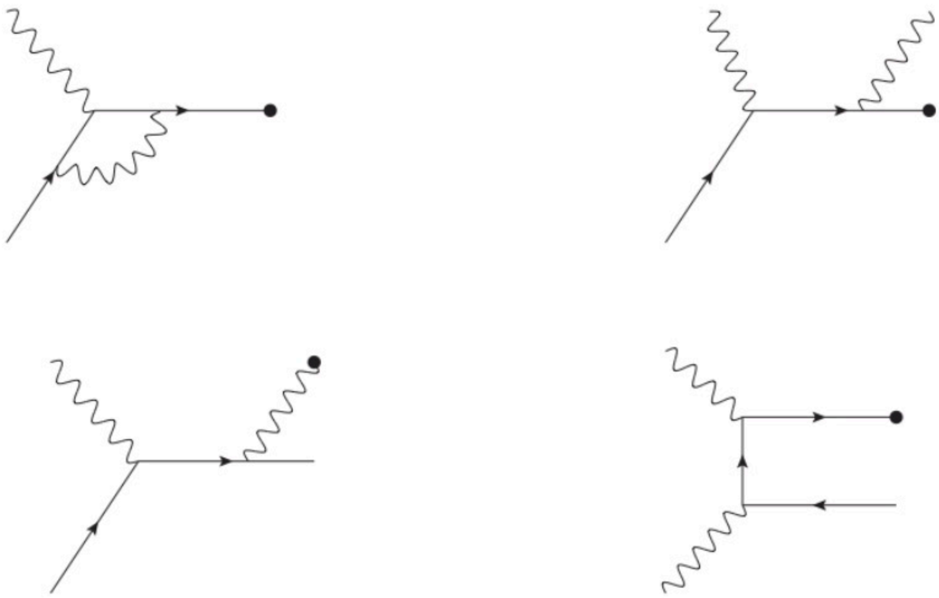

Figure 4.1: Sub-processes at NLO. These diagrams are for QED correction.

At NNLO, the VV contributions include two-loop diagrams with both QED and mixed QCD⊗QED insertions:

$$q(\bar{q}) + \gamma^* \to q(\bar{q}) + \text{two loops}\,, \tag{4.4}$$

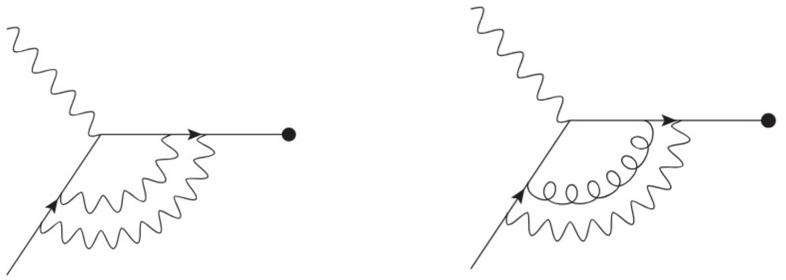

Figure 4.2: Representative two-loop (VV) diagrams contributing to the NNLO pure QED and NNLO mixed QCD⊗QED corrections.

The additional RV sub-processes with photons read:

$$q(\bar{q}) + \gamma^* \to q(\bar{q}) + \gamma + \text{one loop}\,, \tag{4.5}$$

$$\gamma + \gamma^* \to q + \bar{q} + \text{one loop}\,. \tag{4.6}$$

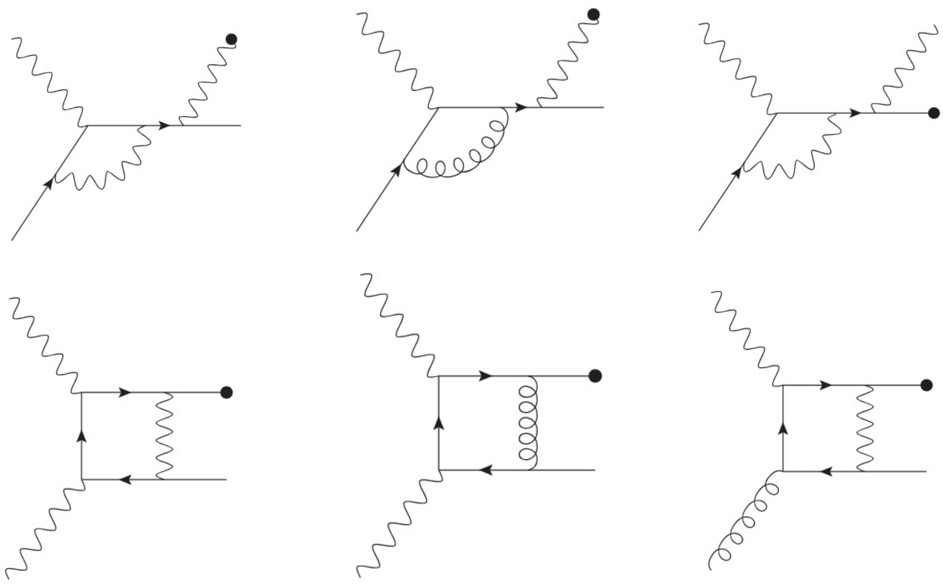

Figure 4.3: Additional RV diagrams (one-loop with one real emission) at NNLO, contributing to NNLO pure QED and NNLO mixed QCD⊗QED.

The additional RR sub-processes with photons are:

$$q(\bar{q}) + \gamma^* \to q(\bar{q}) + \gamma + \gamma\,, \tag{4.7}$$

$$g + \gamma^* \to \gamma + q + \bar{q}\,, \tag{4.8}$$

$$\gamma + \gamma^* \to g + q + \bar{q}\,, \tag{4.9}$$

$$\gamma + \gamma^* \to \gamma + q + \bar{q}\,, \tag{4.10}$$

$$q(\bar{q}) + \gamma^* \to q(\bar{q}) + g + \gamma\,. \tag{4.11}$$

Any one of the final-state partons can fragment into the observed hadron H′.

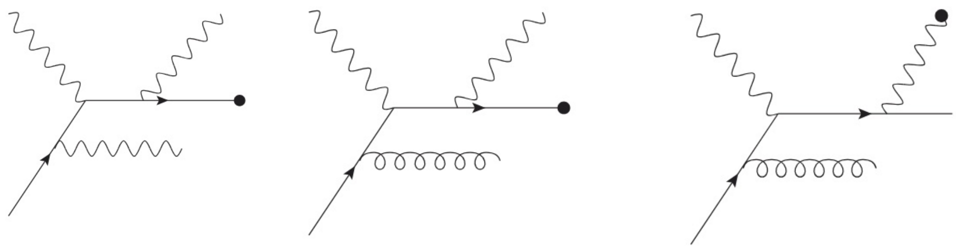

Figure 4.4: RR diagrams: emissions of two photons and one photon plus one gluon. Contributing to NNLO pure QED and NNLO mixed QCD⊗QED.

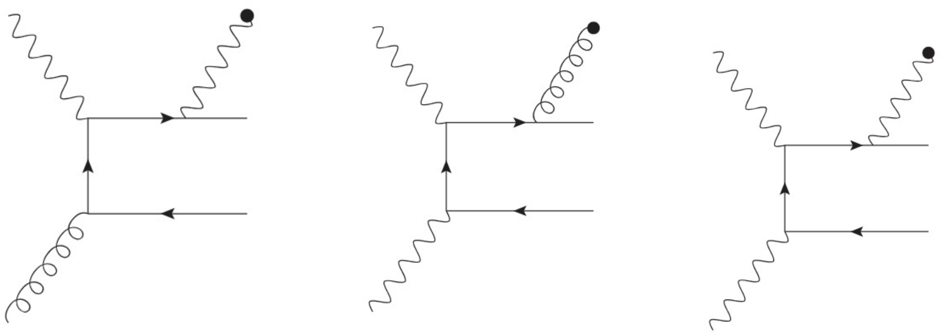

Figure 4.5: RR diagrams: gluon and photon initiated processes. Contributing to NNLO pure QED and NNLO mixed QCD⊗QED.

A summary of all partonic sub-processes contributing at NLO and NNLO, classified by interaction type, is given in Table 4.1.

With all additional amplitudes organized into VV, RV, and RR classes, we have the complete set of matrix elements needed for the QED and mixed QCD⊗QED computation.

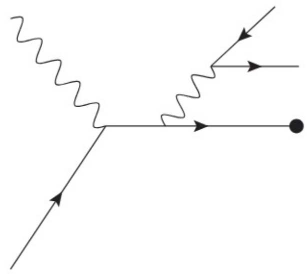

Figure 4.6: RR diagrams: A type. Contributing to NNLO pure QED and NNLO mixed QCD⊗QED.

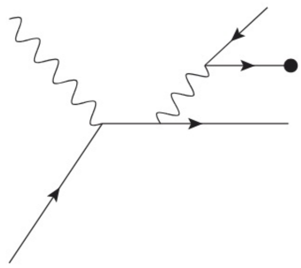

Figure 4.7: RR diagrams: B type. Contributing to NNLO pure QED and NNLO mixed QCD⊗QED.

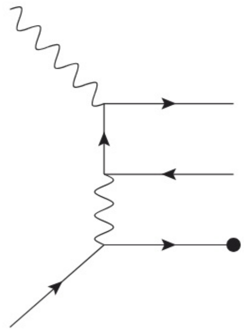

Figure 4.8: RR diagrams: C type. Contributing to NNLO pure QED and NNLO mixed QCD⊗QED.

The next section describes the methodology for processing these amplitudes: how the couplings are renormalized, how the γ_5 ambiguity is resolved for the polarized case, and how mass factorization is extended to include photon channels.

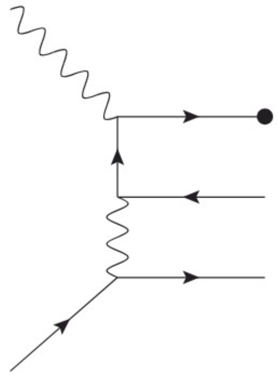

Figure 4.9: RR diagrams: D type. Contributing to NNLO pure QED and NNLO mixed QCD⊗QED.

4.3 Methodology

We describe all the technical extensions to the pure QCD framework of Chapter 3 that are required for the QED and mixed QCD⊗QED computation. This covers the extended coupling renormalization, the γ_5 prescription and the associated scheme transformation for the polarized case, the master integrals, the extended mass factorization including photon AP kernels, and the resulting explicit forms of the finite CFs at each order.

The general framework for computing SIDIS structure functions, the collinear factorization formula, the definition of partonic cross sections,the calculations of MIs and the mass factorization procedure has been laid out in Chapter 3. Here we describe the extensions required for the QED and mixed QCD⊗QED case.

4.3.1 Extended Coupling and Renormalization

The perturbative expansion of the unpolarized (polarized) CFs now runs in powers of both a_s and a_e, cf. eq. (4.1):

$$(\Delta)\mathcal{C}_{I,ab} = \sum_{i,j=0}^{\infty} a_s^i(\mu_R^2)\, a_e^j(\mu_R^2)\, (\Delta)\mathcal{C}_{I,ab}^{(i,j)}(\mu_R^2)\,. \tag{4.12}$$

Order	Process	Contribution type
NLO	$q+\gamma^* \to q$ (1-loop)	QCD, QED
	$q+\gamma^* \to q+g(\gamma)$	QCD (QED)
	$g(\gamma)+\gamma^* \to q+\bar{q}$	QCD (QED)
NNLO	$q+\gamma^* \to q$ (2-loop)	QCD, QED, QCD⊗QED
	$q+\gamma^* \to q+g(\gamma)$ (1-loop)	QCD, QED, QCD⊗QED
	$g(\gamma)+\gamma^* \to q+\bar{q}$ (1-loop)	QCD, QED, QCD⊗QED
	$q+\gamma^* \to q+g(\gamma)+g(\gamma)$	QCD (QED)
	$q+\gamma^* \to q+g+\gamma$	QCD⊗QED
	$q+\gamma^* \to q+q+\bar{q}$	QCD, QED, QCD⊗QED
	$q+\gamma^* \to q+q'+\bar{q}'$	QCD, QED
	$g(\gamma)+\gamma^* \to q+\bar{q}+g(\gamma)$	QCD (QED)
	$g(\gamma)+\gamma^* \to q+\bar{q}+\gamma(g)$	QCD⊗QED

Table 4.1: Partonic subprocesses contributing at NLO and NNLO, classified by contribution type. All final-state partons can hadronize; q' denotes a quark of different flavor from q.

UV divergences are removed by renormalization of both bare couplings $\hat{a}_s$ and $\hat{a}_e$ at the scale μ_R. Let Z_{a_c} denote the renormalization factor for coupling a_c, $c = s, e$. The bare couplings are related to the renormalized ones as

$$\hat{a}_c S_\varepsilon = a_c(\mu_R^2)\, Z_{a_c}\left(a_s(\mu_R^2), a_e(\mu_R^2), \varepsilon\right)\left(\frac{\mu^2}{\mu_R^2}\right)^{\varepsilon/2}, \tag{4.13}$$

where μ is an arbitrary mass scale introduced to keep $\hat{a}_c$ dimensionless in d dimensions and $S_\varepsilon = \exp\left[\frac{\varepsilon}{2}(\gamma_E - \ln 4\pi)\right]$. The Z_{a_c} factors satisfy renormalization group equations

$$\mu_R^2 \frac{d}{d\mu_R^2} \ln Z_{a_c} = -\frac{1}{a_c(\mu_R^2)}\beta_{a_c}\left(a_s(\mu_R^2), a_e(\mu_R^2)\right), \tag{4.14}$$

where the β functions admit expansions $\beta_{a_s} = -\sum_{i,j=0}^{\infty}\beta_{ij}^{(s)}\, a_s^{i+2}a_e^j$ and $\beta_{a_e} = -\sum_{i,j=0}^{\infty}\beta_{ij}^{(e)}\, a_e^{j+2}a_s^i$. The relevant one-loop coefficients are $\beta_{00}^{(s)} = \frac{11}{3}C_a - \frac{4}{3}T_f n_f$ and $\beta_{00}^{(e)} = -\frac{4}{3}\left(N\sum_q^{n_f} e_q^2 + \sum_l^{n_L} e_l^2\right)$, where $C_a = N$, $C_f = (N^2-1)/(2N)$, $T_f = 1/2$, and e_q, e_l are the electric charges of quark q and lepton l.

4.3.2 γ_5 Prescription and Scheme Transformation

The spin-dependent squared amplitudes $(\Sigma|(\Delta)M_{ab}|^2_{\mu\nu})$ in eq. (2.24) involve either the Dirac matrix γ_5 or the Levi-Civita tensor $\epsilon_{\mu\nu\rho\sigma}$, arising from helicity-dependent quark wavefunctions or gluon/photon polarization states; see, e.g., [257]. Since both are intrinsically 4-d objects, we adopt Larin's scheme [258] to define γ_5 in $d = 4 + \varepsilon$ dimensions:

$$\not{p}_a \gamma_5 = -\frac{i}{6}\, \epsilon_{\mu\nu\sigma\lambda} p_a^{\mu} \gamma^{\nu} \gamma^{\sigma} \gamma^{\lambda}\,. \tag{4.15}$$

The product of two Levi-Civita tensors is expressed as a determinant of Kronecker deltas in d dimensions,

$$\epsilon_{\mu_1\nu_1\lambda_1\sigma_1}\, \epsilon^{\mu_2\nu_2\lambda_2\sigma_2} = \begin{vmatrix} \delta^{\mu_2}_{\mu_1} & \delta^{\nu_2}_{\mu_1} & \delta^{\lambda_2}_{\mu_1} & \delta^{\sigma_2}_{\mu_1} \\ \delta^{\mu_2}_{\nu_1} & \delta^{\nu_2}_{\nu_1} & \delta^{\lambda_2}_{\nu_1} & \delta^{\sigma_2}_{\nu_1} \\ \delta^{\mu_2}_{\lambda_1} & \delta^{\nu_2}_{\lambda_1} & \delta^{\lambda_2}_{\lambda_1} & \delta^{\sigma_2}_{\lambda_1} \\ \delta^{\mu_2}_{\sigma_1} & \delta^{\nu_2}_{\sigma_1} & \delta^{\lambda_2}_{\sigma_1} & \delta^{\sigma_2}_{\sigma_1} \end{vmatrix}. \tag{4.16}$$

The QCD contributions in Larin's scheme are converted to the $\overline{\text{MS}}$ scheme via a finite renormalization constant [142, 143, 259, 260] that restores the axial Ward identity and simultaneously transforms the polarized PDFs; see also [170, 179] for a detailed discussion in SIDIS. Currently, no analogous renormalization scheme exists for the QED and mixed QCD⊗QED contributions. We determine the finite renormalization constants for these cases from those of QCD via Abelianization (see Section 4.4). The results for $\Delta\mathcal{C}_{1,ab}$ up to NNLO in the $\overline{\text{MS}}$ scheme are included in the ancillary file of [173].

4.3.3 Master Integrals and Phase Space

The phase space parameterizations and the IBP reduction to master integrals (MIs) are identical to those described in Chapter 3, Section 3.1. The MIs needed for pure QED and mixed QCD⊗QED contributions coincide with those already computed for pure QCD. Details are available in [170, 175, 176].

4.3.4 Mass Factorization with QED

The soft IR divergences cancel between virtual and real emission contributions by the KLN theorem [58, 59]. Residual collinear singularities are factorized into (un)polarized PDFs and FFs via the mass factorization formula:

$$(\Delta)\hat{\mathcal{C}}_{I,ab}(x,z,\varepsilon) = (\Delta)\Gamma_{c\leftarrow a}(x,\varepsilon) \otimes (\Delta)\mathcal{C}_{I,cd}(x,z,\varepsilon) \,\tilde{\otimes}\, \tilde{\Gamma}_{b\leftarrow d}(z,\varepsilon)\,, \tag{4.17}$$

extended now to include photon channels. For QCD⊗QED interactions, the AP kernels include pure QED and mixed QCD⊗QED corrections up to two-loop order as detailed in [228, 239–241, 252, 261].

The AP kernels are expanded in powers of a_s and a_e:

$$\begin{aligned}\mathbb{\Gamma}_{c\leftarrow d}(\xi,\mu_F^2,\varepsilon) = \delta_{cd}\delta(1-\xi) + \sum_{l=1}^{\infty} a_s^l(\mu_F^2)\, \mathbb{\Gamma}_{c\leftarrow d}^{(l,0)}(\xi,\varepsilon) + \sum_{l=1}^{\infty} a_e^l(\mu_F^2)\, \mathbb{\Gamma}_{c\leftarrow d}^{(0,l)}(\xi,\varepsilon) \\ + \sum_{l=1}^{\infty}\sum_{m=1}^{\infty} a_s^l(\mu_F^2)\, a_e^m(\mu_F^2)\, \mathbb{\Gamma}_{c\leftarrow d}^{(l,m)}(\xi,\varepsilon)\,,\end{aligned} \tag{4.18}$$

where $\mathbb{\Gamma} \in \{\Gamma, \Delta\Gamma, \tilde{\Gamma}\}$, subject to the renormalization group evolution equation with splitting functions $\mathbb{P} \in \{P, \Delta P, \tilde{P}\}$:

$$\mathbb{P}_{ce} = \sum_{l=1}^{\infty} a_s^l(\mu_F^2)\, \mathbb{P}_{ce}^{(l,0)} + \sum_{l=1}^{\infty} a_e^l(\mu_F^2)\, \mathbb{P}_{ce}^{(0,l)} + \sum_{\substack{l\geq 1\\ m\geq 1}} a_s^l(\mu_F^2)\, a_e^m(\mu_F^2)\, \mathbb{P}_{ce}^{(l,m)}\,. \tag{4.19}$$

The AP kernels $\Gamma^{(l,m)}_{c\leftarrow d}$ in QED ($l = 0$, $m = 1$) are:

$$\Gamma^{(0,1)}_{q\leftarrow q} = \tfrac{1}{\varepsilon}\mathbb{P}^{(0,1)}_{qq}, \qquad \Gamma^{(0,1)}_{\gamma\leftarrow\gamma} = \tfrac{1}{\varepsilon}\mathbb{P}^{(0,1)}_{\gamma\gamma},$$

$$\Gamma^{(0,1)}_{\bar{q}\leftarrow\gamma} = \Gamma^{(0,1)}_{q\leftarrow\gamma} = \tfrac{1}{\varepsilon}\mathbb{P}^{(0,1)}_{q\gamma}, \qquad \Gamma^{(0,1)}_{q\leftarrow\bar{q}} = 0,$$

$$\Gamma^{(0,1)}_{\gamma\leftarrow\bar{q}} = \Gamma^{(0,1)}_{\gamma\leftarrow q} = \tfrac{1}{\varepsilon}\mathbb{P}^{(0,1)}_{\gamma q},$$

and at NNLO in QED ($l = 0$, $m = 2$) and at mixed NNLO QCD⊗QED ($l = 1$, $m = 1$):

$$\Gamma^{(0,2)}_{q\leftarrow q} = \Gamma^{(0,2),\mathrm{S}}_{q\leftarrow q} + \Gamma^{(0,2),\mathrm{NS}}_{q\leftarrow q}, \qquad \Gamma^{(0,2)}_{\bar{q}\leftarrow q} = \Gamma^{(0,2)}_{q\leftarrow\bar{q}},$$

$$\Gamma^{(0,2)}_{q\leftarrow\bar{q}} = \Gamma^{(0,2),\mathrm{S}}_{q\leftarrow\bar{q}} + \Gamma^{(0,2),\mathrm{NS}}_{q\leftarrow\bar{q}}, \qquad \Gamma^{(0,2),\mathrm{S}}_{q\leftarrow\bar{q}} = \Gamma^{(0,2),\mathrm{S}}_{q\leftarrow q},$$

$$\Gamma^{(0,2)}_{\bar{q}'\leftarrow q} = \Gamma^{(0,2)}_{q'\leftarrow q} = \Gamma^{(0,2),\mathrm{S}}_{q\leftarrow q}, \qquad \{\text{for } q' \neq q\}$$

$$\Gamma^{(1,1)}_{q\leftarrow q} = \Gamma^{(1,1),\mathrm{S}}_{q\leftarrow q} + \Gamma^{(1,1),\mathrm{NS}}_{q\leftarrow q}, \qquad \Gamma^{(1,1)}_{\bar{q}\leftarrow q} = \Gamma^{(1,1)}_{q\leftarrow\bar{q}},$$

$$\Gamma^{(1,1)}_{q\leftarrow\bar{q}} = \Gamma^{(1,1),\mathrm{S}}_{q\leftarrow\bar{q}} + \Gamma^{(1,1),\mathrm{NS}}_{q\leftarrow\bar{q}}, \qquad \Gamma^{(1,1),\mathrm{S}}_{q\leftarrow\bar{q}} = \Gamma^{(1,1),\mathrm{S}}_{q\leftarrow q},$$

$$\Gamma^{(1,1)}_{\bar{q}'\leftarrow q} = \Gamma^{(1,1)}_{q'\leftarrow q} = \Gamma^{(1,1),\mathrm{S}}_{q\leftarrow q}, \qquad \{\text{for } q' \neq q\}$$

and are related to the splitting functions as:

$$\Gamma^{(0,2),\mathrm{NS}}_{q\leftarrow\bar{q}} = \frac{1}{2\varepsilon}\mathbb{P}^{(0,1),-}_{qq}, \qquad \Gamma^{(0,2),\mathrm{S}}_{q\leftarrow q} = \frac{1}{2\varepsilon}\mathbb{P}^{(0,1),\mathrm{S}}_{qq} + \frac{1}{2\varepsilon^2}\left(\mathbb{P}^{(0,1)}_{q\gamma} \otimes \mathbb{P}^{(0,1)}_{\gamma q}\right),$$

$$\Gamma^{(0,2),\mathrm{NS}}_{q\leftarrow q} = \frac{1}{2\varepsilon}\mathbb{P}^{(0,1),\mathrm{NS}}_{qq} + \frac{1}{2\varepsilon^2}\left(2\beta^e_{00}\mathbb{P}^{(0,1)}_{qq} + \mathbb{P}^{(0,1)}_{qq} \otimes \mathbb{P}^{(0,1)}_{qq}\right),$$

$$\Gamma^{(0,2)}_{\gamma\leftarrow\gamma} = \frac{1}{2\varepsilon}\mathbb{P}^{(0,1)}_{\gamma\gamma} + \frac{1}{2\varepsilon^2}\left(2\beta^e_{00}\mathbb{P}^{(0,1)}_{\gamma\gamma} + 2n_f\left(\mathbb{P}^{(0,1)}_{\gamma q} \otimes \mathbb{P}^{(0,1)}_{q\gamma}\right) + \mathbb{P}^{(0,1)}_{\gamma\gamma} \otimes \mathbb{P}^{(0,1)}_{\gamma\gamma}\right),$$

$$\Gamma^{(0,2)}_{\bar{q}\leftarrow\gamma} = \Gamma^{(0,2)}_{q\leftarrow\gamma} = \frac{1}{2\varepsilon}\mathbb{P}^{(0,1)}_{q\gamma} + \frac{1}{2\varepsilon^2}\left(2\beta^e_{00}\mathbb{P}^{(0,1)}_{q\gamma} + \mathbb{P}^{(0,1)}_{q\gamma} \otimes \mathbb{P}^{(0,1)}_{\gamma\gamma} + \mathbb{P}^{(0,1)}_{qq} \otimes \mathbb{P}^{(0,1)}_{q\gamma}\right),$$

$$\Gamma^{(0,2)}_{\gamma\leftarrow\bar{q}} = \Gamma^{(0,2)}_{\gamma\leftarrow q} = \frac{1}{2\varepsilon}\mathbb{P}^{(0,1)}_{\gamma q} + \frac{1}{2\varepsilon^2}\left(2\beta^e_{00}\mathbb{P}^{(0,1)}_{\gamma q} + \mathbb{P}^{(0,1)}_{\gamma\gamma} \otimes \mathbb{P}^{(0,1)}_{\gamma q} + \mathbb{P}^{(0,1)}_{\gamma q} \otimes \mathbb{P}^{(0,1)}_{qq}\right),$$

$$
\begin{aligned}
\Gamma^{(1,1)}_{q\leftarrow q} &= \frac{1}{2\varepsilon}\mathbb{P}^{(1,1)}_{qq} + \frac{1}{2\varepsilon^2}\left(\mathbb{P}^{(1,0)}_{qq}\otimes\mathbb{P}^{(0,1)}_{qq} + \mathbb{P}^{(0,1)}_{qq}\otimes\mathbb{P}^{(1,0)}_{qq}\right),\\
\Gamma^{(1,1)}_{\bar{q}\leftarrow g} = \Gamma^{(1,1)}_{q\leftarrow g} &= \frac{1}{2\varepsilon}\mathbb{P}^{(1,1)}_{qg} + \frac{1}{2\varepsilon^2}\left(\mathbb{P}^{(0,1)}_{qq}\otimes\mathbb{P}^{(1,0)}_{qg}\right),\\
\Gamma^{(1,1)}_{\bar{q}\leftarrow \gamma} = \Gamma^{(1,1)}_{q\leftarrow \gamma} &= \frac{1}{2\varepsilon}\mathbb{P}^{(1,1)}_{q\gamma} + \frac{1}{2\varepsilon^2}\left(\mathbb{P}^{(1,0)}_{qq}\otimes\mathbb{P}^{(0,1)}_{q\gamma}\right),\\
\Gamma^{(1,1)}_{g\leftarrow \bar{q}} = \Gamma^{(1,1)}_{g\leftarrow q} &= \frac{1}{2\varepsilon}\mathbb{P}^{(1,1)}_{gq} + \frac{1}{2\varepsilon^2}\left(\mathbb{P}^{(1,0)}_{gq}\otimes\mathbb{P}^{(0,1)}_{qq}\right),\\
\Gamma^{(1,1)}_{\gamma\leftarrow \bar{q}} = \Gamma^{(1,1)}_{\gamma\leftarrow q} &= \frac{1}{2\varepsilon}\mathbb{P}^{(1,1)}_{\gamma q} + \frac{1}{2\varepsilon^2}\left(\mathbb{P}^{(0,1)}_{\gamma q}\otimes\mathbb{P}^{(1,0)}_{qq}\right).
\end{aligned}
$$

The required expressions for splitting functions $\mathbb{P}^{(l,m)}_{ab}$ up to NNLO are collected in Appendix D.

4.3.5 Coefficient Functions at QED and Mixed QCD⊗QED

The perturbative expansion of the parton-level cross sections $(\Delta)\hat{\mathcal{C}}_{i,ab}$ reads:

$$
\begin{aligned}
(\Delta)\hat{\mathcal{C}}_{i,ab} = (\Delta)\hat{\mathcal{C}}^{(0,0)}_{i,ab} &+ \hat{a}_s\left(\frac{Q^2}{\mu_R^2}\right)^{\frac{\varepsilon}{2}}(\Delta)\hat{\mathcal{C}}^{(1,0)}_{i,ab} + \hat{a}_e\left(\frac{Q^2}{\mu_R^2}\right)^{\frac{\varepsilon}{2}}(\Delta)\hat{\mathcal{C}}^{(0,1)}_{i,ab}\\
&+ \hat{a}_s^2\left(\frac{2\beta^s_{00}}{\varepsilon}\right)\left(\frac{Q^2}{\mu_R^2}\right)^{\frac{\varepsilon}{2}}(\Delta)\hat{\mathcal{C}}^{(1,0)}_{i,ab} + \hat{a}_e^2\left(\frac{2\beta^e_{00}}{\varepsilon}\right)\left(\frac{Q^2}{\mu_R^2}\right)^{\frac{\varepsilon}{2}}(\Delta)\hat{\mathcal{C}}^{(0,1)}_{i,ab}\\
&+ \hat{a}_s^2\left(\frac{Q^2}{\mu_R^2}\right)^{\varepsilon}(\Delta)\hat{\mathcal{C}}^{(2,0)}_{i,ab} + \hat{a}_e^2\left(\frac{Q^2}{\mu_R^2}\right)^{\varepsilon}(\Delta)\hat{\mathcal{C}}^{(0,2)}_{i,ab} + \hat{a}_s\,\hat{a}_e\left(\frac{Q^2}{\mu_R^2}\right)^{\varepsilon}(\Delta)\hat{\mathcal{C}}^{(1,1)}_{i,ab}\\
&+ O(\hat{a}_s^3,\hat{a}_e^3)\,.
\end{aligned}
\tag{4.20}
$$

Substituting the AP kernels into eq. (4.17) we extract the finite CFs order by order:

$$
\begin{aligned}
(\Delta)\mathcal{C}_{i,ab} = (\Delta)\mathcal{C}^{(0,0)}_{i,ab} &+ a_s(\mu_R^2)\,(\Delta)\mathcal{C}^{(1,0)}_{i,ab} + a_e(\mu_R^2)\,(\Delta)\mathcal{C}^{(0,1)}_{i,ab}\\
&+ a_s^2(\mu_R^2)\,(\Delta)\mathcal{C}^{(2,0)}_{i,ab} + a_e^2(\mu_R^2)\,(\Delta)\mathcal{C}^{(0,2)}_{i,ab} + a_s(\mu_R^2)\,a_e(\mu_R^2)\,(\Delta)\mathcal{C}^{(1,1)}_{i,ab} + O(a_s^3,a_e^3)\,.
\end{aligned}
\tag{4.21}
$$

For equal scales $\mu_R = \mu_F$, the pure QED CFs and mixed QCD⊗QED CFs are found to be (showing only the new QED and QCD⊗QED channels; the QCD channels are listed in Chapter 3):

at LO:

$$(\Delta)\mathcal{C}^{(0,0)}_{i,qq}(x',z') = \delta(1-x')\,\delta(1-z'),$$

at NLO, QED:

$$\begin{aligned}
(\Delta)\mathcal{C}^{(0,1)}_{i,qq}(x',z') &= \left(\frac{Q^2}{\mu_F^2}\right)^{\frac{\varepsilon}{2}} (\Delta)\hat{\mathcal{C}}^{(0,1)}_{i,qq}(x',z') - \delta(1-x')\,\tilde{\Gamma}^{(0,1)}_{q\leftarrow q}(z') - (\Delta)\Gamma^{(0,1)}_{q\leftarrow q}(x')\,\delta(1-z'),\\
(\Delta)\mathcal{C}^{(0,1)}_{i,q\gamma}(x',z') &= \left(\frac{Q^2}{\mu_F^2}\right)^{\frac{\varepsilon}{2}} (\Delta)\hat{\mathcal{C}}^{(0,1)}_{i,q\gamma}(x',z') - \delta(1-x')\,\tilde{\Gamma}^{(0,1)}_{\gamma\leftarrow q}(z'),\\
(\Delta)\mathcal{C}^{(0,1)}_{i,\gamma q}(x',z') &= \left(\frac{Q^2}{\mu_F^2}\right)^{\frac{\varepsilon}{2}} (\Delta)\hat{\mathcal{C}}^{(0,1)}_{i,\gamma q}(x',z') - (\Delta)\Gamma^{(0,1)}_{q\leftarrow\gamma}(x')\,\delta(1-z'),
\end{aligned} \tag{4.22}$$

at NNLO, QED:

$$\begin{aligned}
(\Delta)\mathcal{C}^{(0,2)}_{i,qq}(x',z') = \left(\frac{Q^2}{\mu_F^2}\right)^{\varepsilon} (\Delta)\hat{\mathcal{C}}^{(0,2)}_{i,qq}(x',z') &+ \frac{2\beta^e_{00}}{\varepsilon}\left(\frac{Q^2}{\mu_F^2}\right)^{\varepsilon} (\Delta)\hat{\mathcal{C}}^{(1,0)}_{i,qq} - (\Delta)\mathcal{C}^{(0,1)}_{i,qq}(x',z')\tilde{\otimes}\tilde{\Gamma}^{(0,1)}_{q\leftarrow q}(z')\\
&- (\Delta)\mathcal{C}^{(0,1)}_{i,q\gamma}(x',z')\tilde{\otimes}\tilde{\Gamma}^{(0,1)}_{q\leftarrow\gamma}(z') - \delta(1-x')\,\tilde{\Gamma}^{(0,2)}_{q\leftarrow q}(z') - (\Delta)\Gamma^{(0,1)}_{q\leftarrow q}(x')\,\tilde{\Gamma}^{(0,1)}_{q\leftarrow q}(z')\\
&- (\Delta)\Gamma^{(0,1)}_{q\leftarrow q}(x')\otimes(\Delta)\mathcal{C}^{(0,1)}_{i,qq}(x',z') - (\Delta)\Gamma^{(0,1)}_{\gamma\leftarrow q}(x')\otimes(\Delta)\mathcal{C}^{(0,1)}_{i,\gamma q}(x',z')\\
&- (\Delta)\Gamma^{(0,2)}_{q\leftarrow q}(x')\,\delta(1-z'),
\end{aligned}$$

$$(\Delta)\mathcal{C}^{(0,2)}_{i,q\gamma}(x',z') = \left(\frac{Q^2}{\mu_F^2}\right)^{\varepsilon} (\Delta)\hat{\mathcal{C}}^{(0,2)}_{i,q\gamma}(x',z') + \frac{2\beta^e_{00}}{\varepsilon}\left(\frac{Q^2}{\mu_F^2}\right)^{\varepsilon} (\Delta)\hat{\mathcal{C}}^{(0,1)}_{i,q\gamma} - (\Delta)\Gamma^{(0,1)}_{q\leftarrow q}(x')\,\tilde{\Gamma}^{(0,1)}_{\gamma\leftarrow q}(z')$$

$$- (\varDelta)\varGamma^{(0,1)}_{q\leftarrow q}(x') \otimes (\varDelta)\mathcal{C}^{(0,1)}_{i,q\gamma}(x',z') - (\varDelta)\mathcal{C}^{(0,1)}_{i,q\gamma}(x',z')\tilde{\otimes}\tilde{\varGamma}^{(0,1)}_{\gamma\leftarrow\gamma}(z')$$
$$- (\varDelta)\mathcal{C}^{(0,1)}_{i,qq}(x',z')\tilde{\otimes}\tilde{\varGamma}^{(0,1)}_{\gamma\leftarrow q}(z') - \delta(1-x')\,\tilde{\varGamma}^{(0,2)}_{\gamma\leftarrow q}(z'),$$

$$(\varDelta)\mathcal{C}^{(0,2)}_{i,\gamma q}(x',z') = \left(\frac{Q^2}{\mu_F^2}\right)^{\varepsilon}(\varDelta)\hat{\mathcal{C}}^{(0,2)}_{i,\gamma q}(x',z') + \frac{2\beta^e_{00}}{\varepsilon}\left(\frac{Q^2}{\mu_F^2}\right)^{\varepsilon}(\varDelta)\hat{\mathcal{C}}^{(0,1)}_{i,\gamma q} - (\varDelta)\mathcal{C}^{(0,1)}_{i,\gamma q}(x',z')\tilde{\otimes}\tilde{\varGamma}^{(0,1)}_{q\leftarrow q}(z')$$
$$- (\varDelta)\varGamma^{(0,1)}_{\gamma\leftarrow\gamma}(x') \otimes (\varDelta)\mathcal{C}^{(0,1)}_{i,\gamma q}(x',z') - (\varDelta)\varGamma^{(0,1)}_{q\leftarrow\gamma}(x')\,\tilde{\varGamma}^{(0,1)}_{q\leftarrow q}(z')$$
$$- (\varDelta)\varGamma^{(0,1)}_{q\leftarrow\gamma}(x') \otimes (\varDelta)\mathcal{C}^{(0,1)}_{i,qq}(x',z') - (\varDelta)\varGamma^{(0,2)}_{q\leftarrow\gamma}(x')\,\delta(1-z'),$$

$$(\varDelta)\mathcal{C}^{(0,2)}_{i,\gamma\gamma}(x',z') = \left(\frac{Q^2}{\mu_F^2}\right)^{\varepsilon}(\varDelta)\hat{\mathcal{C}}^{(0,2)}_{i,\gamma\gamma}(x',z') - (\varDelta)\mathcal{C}^{(0,1)}_{i,\gamma q}(x',z')\tilde{\otimes}\tilde{\varGamma}^{(0,1)}_{\gamma\leftarrow q}(z') - (\varDelta)\varGamma^{(0,1)}_{q\leftarrow\gamma}(x')\,\tilde{\varGamma}^{(0,1)}_{\gamma\leftarrow q}(z')$$
$$- (\varDelta)\varGamma^{(0,1)}_{q\leftarrow\gamma}(x') \otimes (\varDelta)\mathcal{C}^{(0,1)}_{i,q\gamma}(x',z'),$$

$$(\varDelta)\mathcal{C}^{(0,2)}_{i,q\bar{q}}(x',z') = \left(\frac{Q^2}{\mu_F^2}\right)^{\varepsilon}(\varDelta)\hat{\mathcal{C}}^{(0,2)}_{i,q\bar{q}}(x',z') - (\varDelta)\mathcal{C}^{(0,1)}_{i,qg}(x',z')\tilde{\otimes}\tilde{\varGamma}^{(0,1)}_{g\leftarrow q}(z')$$
$$- (\varDelta)\varGamma^{(0,1)}_{\gamma\leftarrow q}(x') \otimes (\varDelta)\mathcal{C}^{(0,1)}_{i,\gamma q}(x',z') - (\varDelta)\varGamma^{(0,2)}_{\bar{q}\leftarrow q}(x')\,\delta(1-z') - \delta(1-x')\tilde{\varGamma}^{(0,2)}_{\bar{q}\leftarrow q}(z'),$$

$$(\varDelta)\mathcal{C}^{(0,2)}_{i,qb}(x',z') = \left(\frac{Q^2}{\mu_F^2}\right)^{\varepsilon}(\varDelta)\hat{\mathcal{C}}^{(0,2)}_{i,qb}(x',z') - (\varDelta)\mathcal{C}^{(0,1)}_{i,qg}(x',z')\tilde{\otimes}\tilde{\varGamma}^{(0,1)}_{\gamma\leftarrow b}(z')$$
$$- (\varDelta)\varGamma^{(0,1)}_{\gamma\leftarrow b}(x') \otimes (\varDelta)\mathcal{C}^{(0,1)}_{i,\gamma q}(x',z') - (\varDelta)\varGamma^{(0,2)}_{b\leftarrow q}(x')\,\delta(1-z') - \delta(1-x')\tilde{\varGamma}^{(0,2)}_{b\leftarrow q}(z'),$$

at NNLO, QCD⊗QED:

$$(\varDelta)\mathcal{C}^{(1,1)}_{i,qq}(x',z') = \left(\frac{Q^2}{\mu_F^2}\right)^{\varepsilon}(\varDelta)\hat{\mathcal{C}}^{(1,1)}_{i,qq}(x',z') - (\varDelta)\varGamma^{(1,0)}_{q\leftarrow q}(x') \otimes (\varDelta)\mathcal{C}^{(0,1)}_{i,qq}(x',z')$$
$$- (\varDelta)\varGamma^{(0,1)}_{q\leftarrow q}(x') \otimes (\varDelta)\mathcal{C}^{(1,0)}_{i,qq}(x',z') - (\varDelta)\varGamma^{(1,0)}_{q\leftarrow q}(x')\,\tilde{\varGamma}^{(0,1)}_{q\leftarrow q}(z') - (\varDelta)\varGamma^{(0,1)}_{q\leftarrow q}(x')\,\tilde{\varGamma}^{(1,0)}_{q\leftarrow q}(z')$$
$$- (\varDelta)\mathcal{C}^{(0,1)}_{i,qq}(x',z')\tilde{\otimes}\tilde{\varGamma}^{(1,0)}_{q\leftarrow q}(z') - (\varDelta)\mathcal{C}^{(1,0)}_{i,qq}(x',z')\tilde{\otimes}\tilde{\varGamma}^{(0,1)}_{q\leftarrow q}(z') - (\varDelta)\varGamma^{(1,1)}_{q\leftarrow q}(x')\,\delta(1-z')$$
$$- \delta(1-x')\,\tilde{\varGamma}^{(1,1)}_{q\leftarrow q}(z'),$$

$$
\begin{aligned}
(\Delta)\mathcal{C}^{(1,1)}_{i,qg}(x',z') = \left(\frac{Q^2}{\mu_F^2}\right)^{\varepsilon} &(\Delta)\hat{\mathcal{C}}^{(1,1)}_{i,qg}(x',z') - (\Delta)\Gamma^{(0,1)}_{q\leftarrow q}(x') \otimes (\Delta)\mathcal{C}^{(1,0)}_{i,qg}(x',z') \\
&- (\Delta)\Gamma^{(0,1)}_{q\leftarrow q}(x')\,\tilde{\Gamma}^{(1,0)}_{g\leftarrow q}(z') - (\Delta)\mathcal{C}^{(0,1)}_{i,qq}(x',z')\tilde{\otimes}\tilde{\Gamma}^{(1,0)}_{g\leftarrow q}(z') - \delta(1-x')\,\tilde{\Gamma}^{(1,1)}_{g\leftarrow q}(z'),
\end{aligned}
$$

$$
\begin{aligned}
(\Delta)\mathcal{C}^{(1,1)}_{i,q\gamma}(x',z') = \left(\frac{Q^2}{\mu_F^2}\right)^{\varepsilon} &(\Delta)\hat{\mathcal{C}}^{(1,1)}_{i,q\gamma}(x',z') - (\Delta)\Gamma^{(1,0)}_{q\leftarrow q}(x') \otimes (\Delta)\mathcal{C}^{(0,1)}_{i,q\gamma}(x',z') \\
&- (\Delta)\Gamma^{(1,0)}_{q\leftarrow q}(x')\,\tilde{\Gamma}^{(0,1)}_{\gamma\leftarrow q}(z') - (\Delta)\mathcal{C}^{(1,0)}_{i,qq}(x',z')\tilde{\otimes}\tilde{\Gamma}^{(0,1)}_{\gamma\leftarrow q}(z') - \delta(1-x')\,\tilde{\Gamma}^{(1,1)}_{\gamma\leftarrow q}(z'),
\end{aligned}
$$

$$
\begin{aligned}
(\Delta)\mathcal{C}^{(1,1)}_{i,gq}(x',z') = \left(\frac{Q^2}{\mu_F^2}\right)^{\varepsilon} &(\Delta)\hat{\mathcal{C}}^{(1,1)}_{i,gq}(x',z') - (\Delta)\Gamma^{(1,0)}_{q\leftarrow g}(x') \otimes (\Delta)\mathcal{C}^{(0,1)}_{i,qq}(x',z') \\
&- (\Delta)\Gamma^{(1,0)}_{q\leftarrow g}(x')\,\tilde{\Gamma}^{(0,1)}_{q\leftarrow q}(z') - (\Delta)\mathcal{C}^{(1,0)}_{i,gq}(x',z')\tilde{\otimes}\tilde{\Gamma}^{(0,1)}_{q\leftarrow q}(z') - (\Delta)\Gamma^{(1,1)}_{q\leftarrow g}(x')\,\delta(1-z'),
\end{aligned}
$$

$$
\begin{aligned}
(\Delta)\mathcal{C}^{(1,1)}_{i,\gamma q}(x',z') = \left(\frac{Q^2}{\mu_F^2}\right)^{\varepsilon} &(\Delta)\hat{\mathcal{C}}^{(1,1)}_{i,\gamma q}(x',z') - (\Delta)\mathcal{C}^{(0,1)}_{i,\gamma q}(x',z')\tilde{\otimes}\tilde{\Gamma}^{(1,0)}_{q\leftarrow q}(z') \\
&- (\Delta)\Gamma^{(0,1)}_{q\leftarrow \gamma}(x')\,\tilde{\Gamma}^{(1,0)}_{q\leftarrow q}(z') - (\Delta)\Gamma^{(0,1)}_{q\leftarrow \gamma}(x') \otimes (\Delta)\mathcal{C}^{(1,0)}_{i,qq}(x',z') - (\Delta)\Gamma^{(1,1)}_{q\leftarrow \gamma}(x')\,\delta(1-z'),
\end{aligned}
$$

$$
(\Delta)\mathcal{C}^{(1,1)}_{i,q\bar{q}}(x',z') = \left(\frac{Q^2}{\mu_F^2}\right)^{\varepsilon} (\Delta)\hat{\mathcal{C}}^{(1,1)}_{i,q\bar{q}}(x',z') - (\Delta)\Gamma^{(1,1)}_{\bar{q}\leftarrow q}(x')\,\delta(1-z') - \delta(1-x')\,\tilde{\Gamma}^{(1,1)}_{\bar{q}\leftarrow q}(z'),
$$

$$
\begin{aligned}
(\Delta)\mathcal{C}^{(1,1)}_{i,\gamma g}(x',z') = \left(\frac{Q^2}{\mu_F^2}\right)^{\varepsilon} &(\Delta)\hat{\mathcal{C}}^{(1,1)}_{i,\gamma g}(x',z') - (\Delta)\mathcal{C}^{(0,1)}_{i,\gamma q}(x',z')\tilde{\otimes}\tilde{\Gamma}^{(1,0)}_{g\leftarrow q}(z') - (\Delta)\Gamma^{(0,1)}_{q\leftarrow \gamma}(x')\,\tilde{\Gamma}^{(1,0)}_{g\leftarrow q}(z') \\
&- (\Delta)\Gamma^{(0,1)}_{q\leftarrow \gamma}(x') \otimes (\Delta)\mathcal{C}^{(1,0)}_{i,qg}(x',z'),
\end{aligned}
$$

$$
\begin{aligned}
(\Delta)\mathcal{C}^{(1,1)}_{i,g\gamma}(x',z') = \left(\frac{Q^2}{\mu_F^2}\right)^{\varepsilon} &(\Delta)\hat{\mathcal{C}}^{(1,1)}_{i,g\gamma}(x',z') - (\Delta)\mathcal{C}^{(1,0)}_{i,gq}(x',z')\tilde{\otimes}\tilde{\Gamma}^{(0,1)}_{\gamma\leftarrow q}(z') - (\Delta)\Gamma^{(1,0)}_{q\leftarrow g}(x')\,\tilde{\Gamma}^{(0,1)}_{\gamma\leftarrow q}(z') \\
&- (\Delta)\Gamma^{(1,0)}_{q\leftarrow g}(x') \otimes (\Delta)\mathcal{C}^{(0,1)}_{i,q\gamma}(x',z'). \qquad (4.23)
\end{aligned}
$$

Mass factorization for the polarized SF g_1 needs additional care due to the prescription for γ_5 in Larin's scheme, which requires the use of the spin-dependent AP kernels computed in same scheme. Given that the hadronic cross sections (here, g_1) are scheme independent, an additional finite scheme transformation is in order to convert the AP kernels and the finite CF from Larin's to the conventional $\overline{\rm MS}$ scheme. With polarised PDFs Δf_a^L and polarised CF $\Delta\mathcal{C}^L_{1,ab}(\mu_F^2)$ defined in Larin's scheme (denoted by the superscript L), the mass factorization for g_1 reads

$$g_1 = \sum_{a,b} \Delta f_a^L(\mu_F^2) \otimes \Delta\mathcal{C}^L_{1,ab}(\mu_F^2) \tilde{\otimes} D_b(\mu_F^2)\,. \tag{4.24}$$

Here the FFs D_b and the time-like AP kernels ($\tilde{\Gamma}_{c\leftarrow d}$) for handling the final state collinear singularities are already taken in the $\overline{\rm MS}$ scheme, since the final state spins are summed. With a scheme transformation [260] through the finite renormalization constants Z_{ab}, known in the literature [142, 259, 260, 262], for PDFs

$$\Delta f_a(\mu_F^2) = Z_{ca}(\mu_F^2) \otimes \Delta f_c^L(\mu_F^2) \tag{4.25}$$

and for CF,

$$\Delta\mathcal{C}_{1,ab}(\mu_F^2) = \left(Z^{-1}(\mu_F^2)\right)_{ad} \otimes \Delta\mathcal{C}^L_{1,db}(\mu_F^2)\,. \tag{4.26}$$

g_1 in eq. (4.24) can be expressed in terms of $\overline{\rm MS}$ quantities:

$$g_1 = \sum_{a,b} \Delta f_a(\mu_F^2) \otimes \Delta\mathcal{C}_{1,ab}(\mu_F^2) \tilde{\otimes} D_b(\mu_F^2)\,. \tag{4.27}$$

For extraction of the CF $\Delta\mathcal{C}^L_{1,ab}$ in Eq. (4.24) requires the polarized AP kernels in Larin's scheme, which can derived from the polarized space-like AP kernels ($\Delta\Gamma_{c\leftarrow d}$) in the $\overline{\rm MS}$ scheme through the relation Z_{ab} by $\Delta\Gamma^L = Z^{-1} \otimes \Delta\Gamma$. This leads to the scheme transformation for the splitting functions

$$\Delta P^L = Z^{-1} \otimes \Delta P \otimes Z + 2\beta_{a_s}\, Z \otimes \frac{dZ^{-1}}{da_s} + 2\beta_{a_e}\, Z \otimes \frac{dZ^{-1}}{da_e}\,, \tag{4.28}$$

The beta functions β_{a_s} and β_{a_e} are defined in eq. (1.21).

The symmetric matrix valued Z-factor, e.g. given in [142, 259, 260], reads

$$Z_{ab} = 1 + \sum_{l+m=1}^{\infty} a_s^l a_e^m z_{ab}^{(l,m)} , \tag{4.29}$$

More details about finite renormalization constants Z_{ab} are provided in Appendix D.4. Eq. (4.28) provides the spin dependent space-like splitting functions in Larin's scheme:

$$\begin{aligned}
\Delta P_{cd}^{L,(1,0)} &= \Delta P_{cd}^{(1,0)} , \\
\Delta P_{cd}^{L,(0,1)} &= \Delta P_{cd}^{(0,1)} ,
\end{aligned} \tag{4.30}$$

$$\begin{aligned}
\Delta P_{qq}^{L,(2,0)} &= \Delta P_{qq}^{(2,0)} + 2\beta_{00}^{s}\, z_{qq}^{(1,0)} , \\
\Delta P_{qg}^{L,(2,0)} &= \Delta P_{qg}^{(2,0)} - \Delta P_{qg}^{(1,0)} \otimes z_{qq}^{(1,0)} , \\
\Delta P_{gq}^{L,(2,0)} &= \Delta P_{gq}^{(2,0)} + \Delta P_{gq}^{(1,0)} \otimes z_{qq}^{(1,0)} , \\
\Delta P_{gg}^{L,(2,0)} &= \Delta P_{gg}^{(2,0)} ,
\end{aligned} \tag{4.31}$$

$$\begin{aligned}
\Delta P_{qq}^{L,(0,2)} &= \Delta P_{qq}^{(0,2)} + 2\beta_{00}^{e}\, z_{qq}^{(0,1)} , \\
\Delta P_{q\gamma}^{L,(0,2)} &= \Delta P_{q\gamma}^{(0,2)} - \Delta P_{q\gamma}^{(0,1)} \otimes z_{qq}^{(0,1)} , \\
\Delta P_{\gamma q}^{L,(0,2)} &= \Delta P_{\gamma q}^{(0,2)} + \Delta P_{\gamma q}^{(0,1)} \otimes z_{qq}^{(0,1)} , \\
\Delta P_{\gamma\gamma}^{L,(0,2)} &= \Delta P_{\gamma\gamma}^{(0,2)} ,
\end{aligned} \tag{4.32}$$

$$\begin{aligned}
\Delta P_{qq}^{L,(1,1)} &= \Delta P_{qq}^{(1,1)} + 2\beta_{00}^{s}\, z_{qq}^{(0,1)} + 2\beta_{00}^{e}\, z_{qq}^{(1,0)} , \\
\Delta P_{qg}^{L,(1,1)} &= \Delta P_{qg}^{(1,1)} , \\
\Delta P_{gq}^{L,(1,1)} &= \Delta P_{gq}^{(1,1)} , \\
\Delta P_{gg}^{L,(1,1)} &= \Delta P_{gg}^{(1,1)} , \\
\Delta P_{q\gamma}^{L,(1,1)} &= \Delta P_{q\gamma}^{(1,1)} , \\
\Delta P_{\gamma q}^{L,(1,1)} &= \Delta P_{\gamma q}^{(1,1)} , \\
\Delta P_{g\gamma}^{L,(1,1)} &= \Delta P_{g\gamma}^{(1,1)} , \\
\Delta P_{\gamma g}^{L,(1,1)} &= \Delta P_{\gamma g}^{(1,1)} , \\
\Delta P_{\gamma\gamma}^{L,(1,1)} &= \Delta P_{\gamma\gamma}^{(1,1)} .
\end{aligned} \tag{4.33}$$

Likewise, cf. eq. (4.26), the CF in the $\overline{\text{MS}}$ scheme read,

$$
\begin{aligned}
\Delta C^{(0)}_{1,qq} &= \Delta C^{L,(0)}_{1,qq} = \delta(1-x')\delta(1-z')\,,\\
\Delta C^{(1)}_{1,qq} &= \Delta C^{L,(1)}_{1,qq} + (-z^{(1)}_{qq}) \otimes \Delta C^{L,(0)}_{1,qq}\,,\\
\Delta C^{(1)}_{1,qg} &= \Delta C^{L,(1)}_{1,qg}\,,\\
\Delta C^{(1)}_{1,gq} &= \Delta C^{L,(1)}_{1,gq}\,,\\
\Delta C^{(2,0)}_{1,qq} &= \Delta C^{L,(2)}_{1,qq} + (-z^{(1)}_{qq}) \otimes \Delta C^{L,(1)}_{1,qq}\\
&\quad + \left(z^{(1)}_{qq} \otimes z^{(1)}_{qq} - z^{(2,0)}_{qq}\right) \otimes \Delta C^{L,(0)}_{1,qq}\,,\\
\Delta C^{(2,0)}_{1,q\bar{q}} &= \Delta C^{L,(2)}_{1,q\bar{q}} + \left(-z^{(2,0)}_{q\bar{q}}\right) \otimes \Delta C^{L,(0)}_{1,\bar{q}\bar{q}}\,,\\
\Delta C^{(2,0)}_{1,qq'} &= \Delta C^{L,(2)}_{1,qq'} + \left(-z^{(2,0)}_{qq'}\right) \otimes \Delta C^{L,(0)}_{1,q'q'}\,,\\
\Delta C^{(2,0)}_{1,qg} &= \Delta C^{L,(2)}_{1,qg} + (-z^{(1)}_{qq}) \otimes \Delta C^{L,(1)}_{1,qg}\,,\\
\Delta C^{(2,0)}_{1,gq} &= \Delta C^{L,(2)}_{1,gq}\,, \quad \Delta C^{(2,0)}_{1,gg} = \Delta C^{L,(2)}_{1,gg}\,.
\end{aligned} \tag{4.34}
$$

Expressions for $z^{(l)}_{ab}$ are provided in Appendix (D), and the CF in the $\overline{\text{MS}}$ scheme in an ancillary file of [173]. Note that the flavor-nonsinglet CF of polarized SF g_1 SIDIS agree with those of the SF F_3, cf. [174]. The latter requires an additional renormalization of the axial-vector current and a kinematics independent finite renormalization transformation from the Larin to the $\overline{\text{MS}}$ scheme [209, 258]. We find full agreement for the respective CFs, which provides a strong independent check on our computation.

For the removal of initial-state collinear singularities we use the QCD space-like splitting functions $(\Delta)\mathrm{P}^{(i,0)}_{ab}$ with $i = 1, 2$ [31, 226, 227, 230, 231, 260, 263–267], the space-like splitting functions $(\Delta)\mathrm{P}^{(0,j)}_{ab}$ with $j = 1, 2$ for QED and $(\Delta)\mathrm{P}^{(1,1)}_{ab}$ for the mixed QCD⊗QED, all available in the literature [239–241]. The time-like splitting functions needed to remove final-state collinear singularities are known for QCD [230, 231]. For QED and mixed QCD⊗QED, we derive them here by requiring finite CFs; the results are given in

Appendix D:

$$\begin{aligned}\mathrm{LO}: &\tilde{\mathrm{P}}^{(0,1)}_{qq}, \tilde{\mathrm{P}}^{(0,1)}_{q\gamma}, \tilde{\mathrm{P}}^{(0,1)}_{\gamma q}, \tilde{\mathrm{P}}^{(0,1)}_{\gamma\gamma} \\ \mathrm{NLO}: &\tilde{\mathrm{P}}^{(0,2)}_{\gamma q}, \tilde{\mathrm{P}}^{(1,1)}_{gq}, \tilde{\mathrm{P}}^{(1,1)}_{\gamma q}, \tilde{\mathrm{P}}^{(0,2),\mathrm{NS}}_{qq}, \tilde{\mathrm{P}}^{(0,2),\mathrm{S}}_{qq}, \tilde{\mathrm{P}}^{(0,2)}_{q\bar{q}}\end{aligned} \tag{4.35}$$

Using Larin's scheme with the polarized space-like splitting functions and the unpolarized time-like splitting functions in $\overline{\mathrm{MS}}$, we obtain the QED and mixed QCD⊗QED CFs for g_1. The polarized $\overline{\mathrm{MS}}$ splitting functions derived for QED and mixed QCD⊗QED evolution are in complete agreement with [241, 261]:

$$\begin{aligned}\mathrm{LO} \quad &: \quad \varDelta\mathrm{P}^{(0,1)}_{qq}, \varDelta\mathrm{P}^{(0,1)}_{q\gamma}, \varDelta\mathrm{P}^{(0,1)}_{\gamma q}, \varDelta\mathrm{P}^{(0,1)}_{\gamma\gamma} \\ \mathrm{NLO} \quad &: \quad \varDelta\mathrm{P}^{(0,2)}_{q\gamma}, \varDelta\mathrm{P}^{(1,1)}_{qg}, \varDelta\mathrm{P}^{(1,1)}_{q\gamma}, \varDelta\mathrm{P}^{(0,2),\mathrm{NS}}_{qq}, \varDelta\mathrm{P}^{(0,2),\mathrm{S}}_{qq}, \varDelta\mathrm{P}^{(0,2)}_{q\bar{q}}\end{aligned}$$

The finite CFs can be expressed in terms of double and single distributions as well as regular terms, cf. [170] for details. The convolution with PDFs and FFs gives $(g_1)F_1 = \sum_{i+j=0} a_s^i a_e^j (g_1)F_1^{(i,j)}$. Since the QCD results $F_I^{(i,0)}$ have been presented in Chapter 3, we give here the expressions for pure QED and mixed QCD⊗QED:

$$(g_1)F_1^{(0,1)} = \sum_q e_q^4 \Big((\varDelta)H_{qq} \hat{\otimes} (\varDelta)\mathcal{C}^{(0,1)}_{1,qq} + (\varDelta)H_{q\gamma} \hat{\otimes} (\varDelta)\mathcal{C}^{(0,1)}_{1,q\gamma} + (\varDelta)H_{\gamma q} \hat{\otimes} (\varDelta)\mathcal{C}^{(0,1)}_{1,\gamma q} \Big), \tag{4.36}$$

$$\begin{aligned}(g_1)F_1^{(0,2)} = &\sum_q e_q^6 \Big((\varDelta)H_{qq} \hat{\otimes} (\varDelta)\mathcal{C}^{(0,2)}_{1,qq,[1]} + (\varDelta)H_{q\bar{q}} \hat{\otimes} (\varDelta)\mathcal{C}^{(0,2)}_{1,q\bar{q}} + (\varDelta)H_{q\gamma} \hat{\otimes} (\varDelta)\mathcal{C}^{(0,2)}_{1,q\gamma} + (\varDelta)H_{\gamma q} \hat{\otimes} (\varDelta)\mathcal{C}^{(0,2)}_{1,\gamma q} \Big) \\ &+ \sum_q e_q^4 \Big(N \sum_{q_i} e_{q_i}^2 + \sum_{l_i} e_{l_i}^2 \Big) (\varDelta)H_{qq} \hat{\otimes} (\varDelta)\mathcal{C}^{(0,2)}_{1,qq,[2]} + \sum_q e_q^2 \Big(N \sum_{q_i} e_{q_i}^4 + \sum_{l_i} e_{l_i}^4 \Big) (\varDelta)H_{qq} \hat{\otimes} (\varDelta)\mathcal{C}^{(0,2)}_{1,qq,[3]} \\ &+ \sum_q \sum_{q' \neq q} \Big(e_q^4 e_{q'}^2 (\varDelta)H^+_{qq'} \hat{\otimes} (\varDelta)\mathcal{C}^{(0,2)}_{1,qq',[1]} + e_q^2 e_{q'}^4 (\varDelta)H^+_{qq'} \hat{\otimes} (\varDelta)\mathcal{C}^{(0,2)}_{1,qq',[2]} + e_q^3 e_{q'}^3 (\varDelta)H^-_{qq'} \hat{\otimes} (\varDelta)\mathcal{C}^{(0,2)}_{1,qq',[3]} \Big) \\ &+ \Big(N \sum_{q_i} e_{q_i}^6 + \sum_{l_i} e_{l_i}^6 \Big) \Big((\varDelta)H_{\gamma\gamma} \hat{\otimes} (\varDelta)\mathcal{C}^{(0,2)}_{1,\gamma\gamma} \Big),\end{aligned} \tag{4.37}$$

$$
\begin{aligned}
(g_1)F_1^{(1,1)} = \sum_q e_q^4 \Big(& (\Delta)H_{qq} \hat{\otimes} (\Delta)\mathcal{C}_{1,qq}^{(1,1)} + (\Delta)H_{q\bar{q}} \hat{\otimes} (\Delta)\mathcal{C}_{1,q\bar{q}}^{(1,1)} + (\Delta)H_{qg} \hat{\otimes} (\Delta)\mathcal{C}_{1,qg}^{(1,1)} + (\Delta)H_{gq} \hat{\otimes} (\Delta)\mathcal{C}_{1,gq}^{(1,1)} \\
& + (\Delta)H_{q\gamma} \hat{\otimes} (\Delta)\mathcal{C}_{1,q\gamma}^{(1,1)} + (\Delta)H_{\gamma q} \hat{\otimes} (\Delta)\mathcal{C}_{1,\gamma q}^{(1,1)} \Big) + \Big(\sum_{q_i} e_{q_i}^4 \Big) \Big((\Delta)H_{g\gamma} \hat{\otimes} (\Delta)\mathcal{C}_{1,g\gamma}^{(1,1)} + (\Delta)H_{\gamma g} \hat{\otimes} (\Delta)\mathcal{C}_{1,\gamma g}^{(1,1)} \Big) ,
\end{aligned}
\tag{4.38}
$$

where $\hat{\otimes}$ denotes convolution in both x and z, and the $(\Delta)H_{ab}$ combinations of (polarized) unpolarized PDFs and unpolarized FFs are defined as,

$$
\begin{aligned}
&(\Delta)H_{qq} = (\Delta)f_q(x)D_q(z) + (\Delta)f_{\bar{q}}(x)D_{\bar{q}}(z) , && (\Delta)H_{q\bar{q}} = (\Delta)f_q(x)D_{\bar{q}}(z) + (\Delta)f_{\bar{q}}(x)D_q(z) , \\
&(\Delta)H_{qg} = (\Delta)f_q(x)D_g(z) + (\Delta)f_{\bar{q}}(x)D_g(z) , && (\Delta)H_{q\gamma} = (\Delta)f_q(x)D_\gamma(z) + (\Delta)f_{\bar{q}}(x)D_\gamma(z) , \\
&(\Delta)H_{\gamma q} = (\Delta)f_\gamma(x)D_q(z) + (\Delta)f_\gamma(x)D_{\bar{q}}(z) , && (\Delta)H_{gq} = (\Delta)f_g(x)D_q(z) + (\Delta)f_g(x)D_{\bar{q}}(z) , \\
&(\Delta)H_{gg} = (\Delta)f_g(x)D_g(z) , && (\Delta)H_{\gamma\gamma} = (\Delta)f_\gamma(x)D_\gamma(z) , \\
&(\Delta)H_{g\gamma} = (\Delta)f_g(x)D_\gamma(z) , && (\Delta)H_{\gamma g} = (\Delta)f_\gamma(x)D_g(z) , \\
&(\Delta)H_{qq'}^{\pm} = (\Delta)f_q(x)D_{q'}(z) \pm (\Delta)f_q(x)D_{\bar{q}'}(z) \pm (\Delta)f_{\bar{q}}(x)D_{q'}(z) + (\Delta)f_{\bar{q}}(x)D_{\bar{q}'}(z) .
\end{aligned}
\tag{4.39}
$$

With the extended AP kernels, the complete mass factorization formulae, and the explicit finite CFs for all QED and QCD⊗QED channels in hand, we have achieved the main computational goal of this chapter. Before turning to the numerical results, however, it is important to establish how these new CFs relate to the known QCD results through the Abelianization procedure, which also provides an independent check on all of the above.

4.4 Abelianization

In this section, we describe the Abelianization procedure, which provides a systematic and efficient method to derive QED and mixed QCD⊗QED CFs directly from the known QCD results by removing non-Abelian gluon self-interactions and replacing color factors with electric charge factors. This serves both as an independent cross-check of the direct computation and as a powerful consistency test of the entire framework.

We have computed the QED and mixed QCD⊗QED CFs from scratch, reproducing the same results via an independent Abelianization procedure [19, 20, 239, 242, 268]. This method exploits the structural similarity between QCD and QED by identifying those NNLO QCD diagrams that survive in the Abelian limit,where non-Abelian gluon self-interactions are removed and color factors are replaced by appropriate electric charge factors. By systematically isolating these contributions, one can derive the corresponding pure QED and mixed QCD⊗QED CFs and the associated splitting functions.

The mapping rules are summarized in Table 4.2. The resulting expressions are checked against available results for QED evolution kernels, and consistency with factorization and renormalization group equations is verified. The full agreement between the direct computation and the Abelianization results establishes the robustness of the approach at NNLO accuracy and confirms the correctness of all CFs presented in the previous section.

With the Abelianization check confirming the correctness of all CFs, we are now in a position to assess the phenomenological size of the QED and mixed QCD⊗QED corrections relative to the known NNLO QCD predictions. This is the subject of the next section.

4.5 Phenomenology

The goal of this section is to quantify the numerical impact of the pure QED and mixed QCD⊗QED corrections on the SFs F_1 and g_1 at the EIC, and to assess whether these corrections are phenomenologically relevant at the precision level targeted by future experiments. We present results as ratios to the pure QCD predictions so that the relative size of the electromagnetic contributions is made explicit.

We now illustrate the numerical impact of our $(\Delta)\mathcal{C}_{1,ab}$ results for various centre-of-mass energies $\sqrt{s}$ for a range of x and z values. We examine the effects of pure QED and mixed

Mapping	**Rule**
$qq^{(1,0)} \to qq^{(0,1)}$ $qg^{(1,0)} \to q\gamma^{(0,1)}$ $gq^{(1,0)} \to \gamma q^{(0,1)}$	$C_f \to Q^2_{eu}$
$qq^{(2,0),NS} \to qq^{(0,2),NS}$ $qg^{(2,0)} \to q\gamma^{(0,2)}$ $gq^{(2,0)} \to \gamma q^{(0,2)}$ $gg^{(2,0)} \to \gamma\gamma^{(0,2)}$ $qQ^{(2,0)} \to qQ^{(0,2)}$ $qb^{(2,0)} \to qb^{(0,2)}$	$C_f \to Q^2_{eu}, C_a \to 0, T_f\, n_f \to N\, \sum Q^2_q, T_f \to N\, Q^2_{eu}$
$qq^{(2,0),PS} \to qq^{(0,2),PS}$	$C_f \to Q^2_{eu}, T_f\, \sum Q^2_q \to N\, \sum Q^4_{eu}$
$qq^{(2,0),NS} \to qq^{(1,1)}$ $qQ^{(2,0)} \to qQ^{(1,1)}$	$C^2_f \to 2\, C_f\, Q^2_{eu}$, rest color factor $\to 0$
$qg^{(2,0)} \to qg^{(1,1)}$ $qg^{(2,0)} \to q\gamma^{(1,1)}$ $gq^{(2,0)} \to gq^{(1,1)}$	$C^2_f \to C_f\, Q^2_{eu}$, rest color factor $\to 0$
$\gamma q^{(0,2)} \to \gamma q^{(1,1)}$	$N\, Q^6_{eu} \to C_f Q^4_{eu}$
$gg^{(2,0)} \to g\gamma^{(1,1)}$	$C_f \to Q^2_{eu}, C_a \to 0$
$\gamma\gamma^{(0,2)} \to \gamma g^{(1,1)}$	$Q^4_{eu} \to C_f\, Q^2_{eu}$

Table 4.2: Mapping of QCD color structures to QED and mixed QCD⊗QED analogs via Abelianization.

z	F_1				
	LO	NLO$^{\text{QCD}}$	NLO$^{\text{QCD}\otimes\text{QED}}$	NNLO$^{\text{QCD}}$	NNLO$^{\text{QCD}\otimes\text{QED}}$
0.15	$1.23119^{+4.644\%}_{-4.288\%}$	$1.04009^{+0.952\%}_{-1.202\%}$	$1.04266^{+0.865\%}_{-1.121\%}$	$0.99712^{+0.092\%}_{-0.176\%}$	$0.99894^{+0.175\%}_{-0.077\%}$
0.25	$0.44911^{+5.814\%}_{-5.283\%}$	$0.38139^{+1.341\%}_{-1.620\%}$	$0.38257^{+1.245\%}_{-1.532\%}$	$0.33861^{+0.156\%}_{-0.291\%}$	$0.33962^{+0.156\%}_{-0.211\%}$
0.45	$0.08062^{+7.564\%}_{-6.741\%}$	$0.07737^{+2.583\%}_{-2.825\%}$	$0.07771^{+2.474\%}_{-2.727\%}$	$0.07296^{+0.433\%}_{-0.720\%}$	$0.07329^{+0.393\%}_{-0.597\%}$
0.6	$0.02339^{+8.625\%}_{-7.611\%}$	$0.02469^{+3.588\%}_{-3.767\%}$	$0.02483^{+3.471\%}_{-3.666\%}$	$0.02463^{+1.031\%}_{-1.372\%}$	$0.02479^{+0.885\%}_{-1.234\%}$
0.75	$0.00651^{+10.229\%}_{-8.902\%}$	$0.00682^{+5.019\%}_{-5.069\%}$	$0.00687^{+4.894\%}_{-4.964\%}$	$0.00699^{+1.897\%}_{-2.294\%}$	$0.00705^{+1.731\%}_{-2.141\%}$

Table 4.3: Values of F_1 at various orders at the central scale $\mu^2_R = \mu^2_F = Q^2_{\text{avg}}$ and scale variation $\{\mu^2_R, \mu^2_F\} \in [Q^2_{\text{avg}}/2, 2Q^2_{\text{avg}}]$ as a function of z. (See text for integration ranges of x, y.)

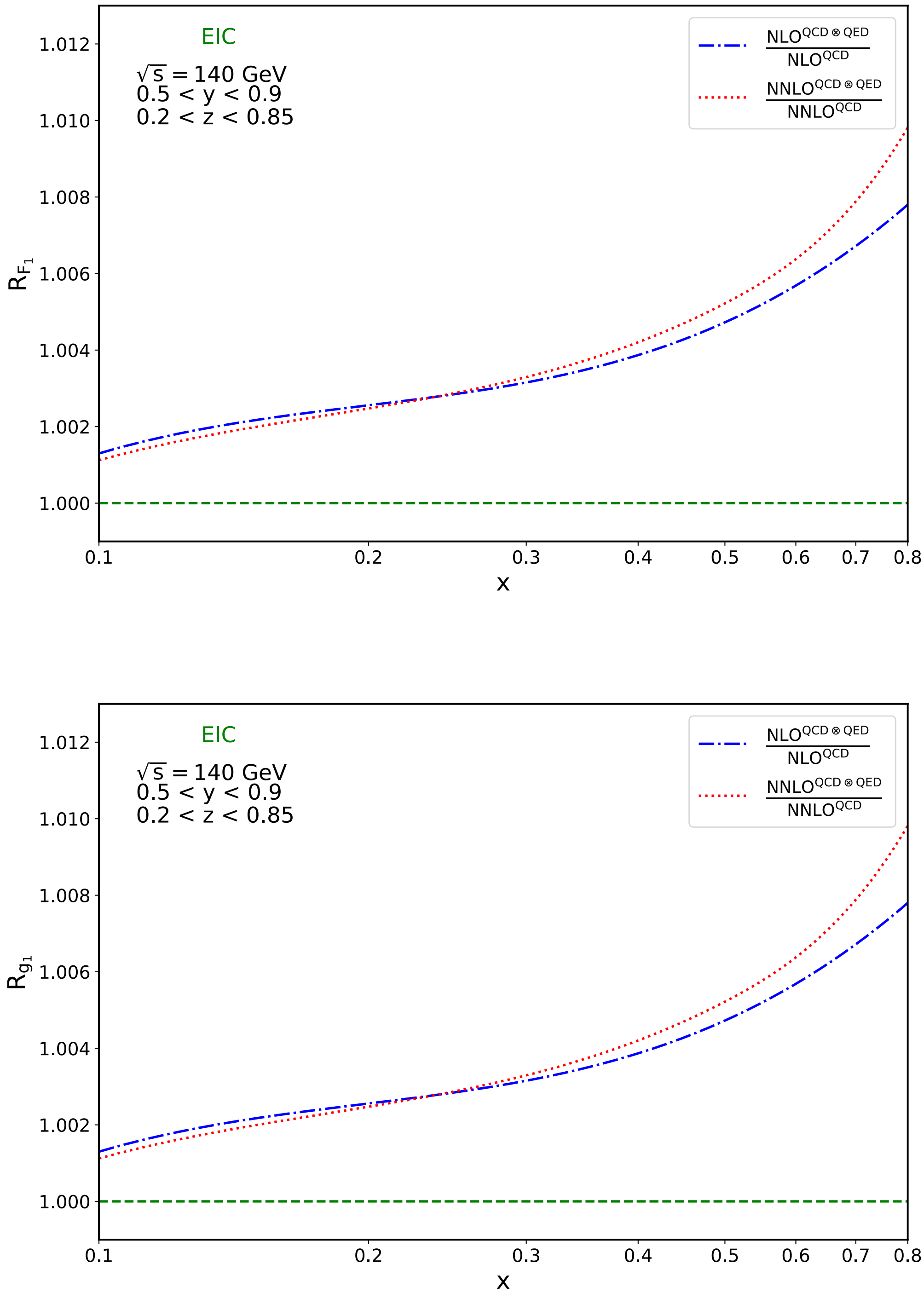

Figure 4.10: Ratio of F_1 (upper panel) and g_1 (lower panel) with QCD⊗QED contributions at NLO and NNLO to those with only QCD corrections at the respective order, as a function of x at the central scale $\mu_R^2 = \mu_F^2 = Q^2_{\rm avg}$ for the EIC at $\sqrt{s} = 140$ GeV. Integration ranges for y and z are indicated in the plots.

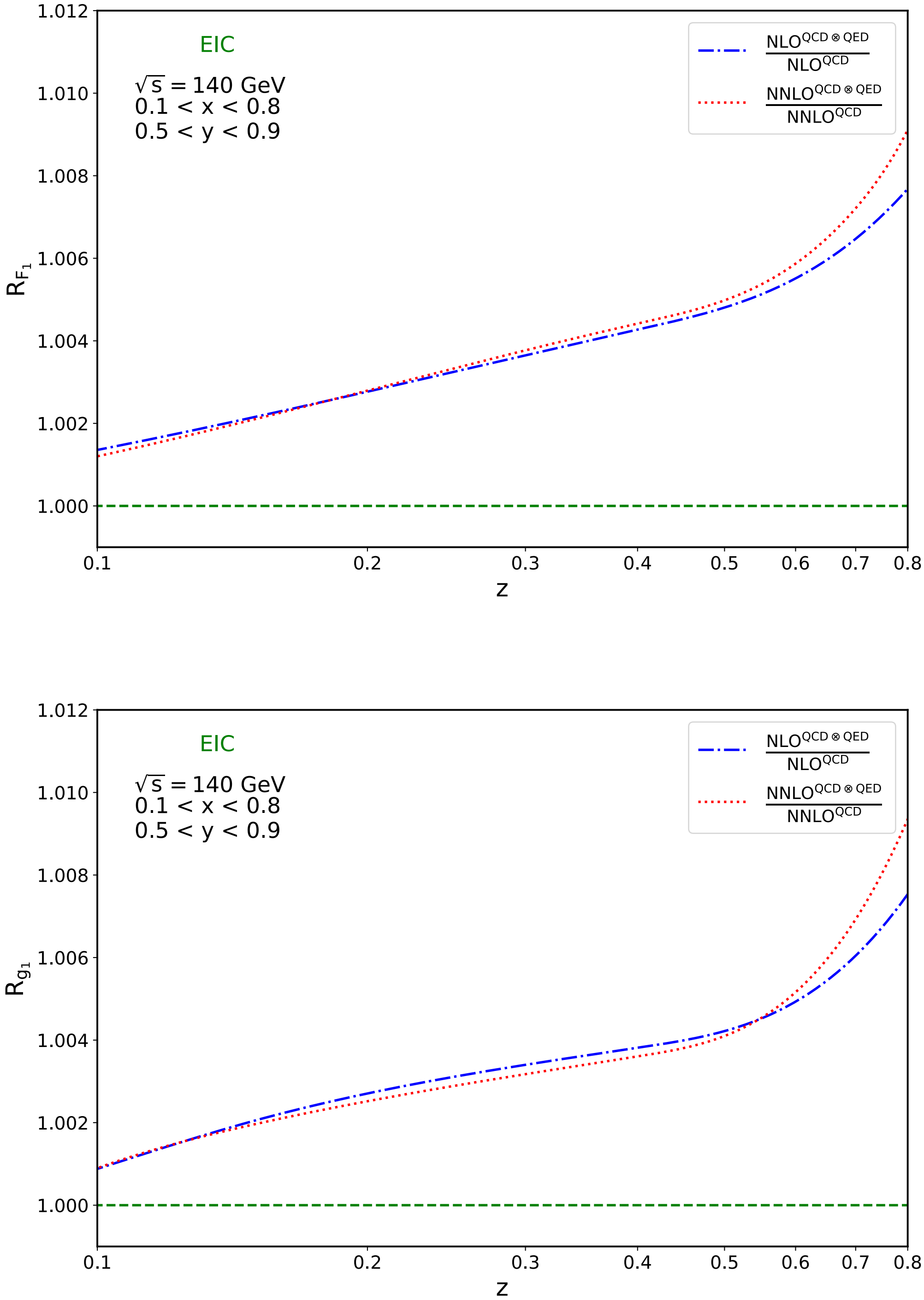

Figure 4.11: Same as Fig. 4.10 for F_1 (upper panel) and g_1 (lower panel) as functions of z.

QCD⊗QED corrections on F_1 and g_1, included alongside the pure QCD terms, providing a more complete description up to $\mathcal{O}(a_e\, a_s)$. In Fig. 4.10, the upper (lower) panel shows

z	g_1				
	LO	NLO$^{\text{QCD}}$	NLO$^{\text{QCD}\otimes\text{QED}}$	NNLO$^{\text{QCD}}$	NNLO$^{\text{QCD}\otimes\text{QED}}$
0.15	$0.59417^{+4.356\%}_{-4.034\%}$	$0.45428^{+0.471\%}_{-0.741\%}$	$0.45525^{+0.467\%}_{-0.653\%}$	$0.42511^{+0.142\%}_{-0.183\%}$	$0.42599^{+0.237\%}_{-0.278\%}$
0.25	$0.22688^{+5.579\%}_{-5.080\%}$	$0.17305^{+0.804\%}_{-1.121\%}$	$0.17353^{+0.702\%}_{-1.026\%}$	$0.14799^{+0.154\%}_{-0.158\%}$	$0.14837^{+0.250\%}_{-0.268\%}$
0.45	$0.04229^{+7.416\%}_{-6.614\%}$	$0.03790^{+2.001\%}_{-2.313\%}$	$0.03806^{+1.888\%}_{-2.212\%}$	$0.03430^{+0.266\%}_{-0.373\%}$	$0.03443^{+0.305\%}_{-0.286\%}$
0.6	$0.01232^{+8.500\%}_{-7.505\%}$	$0.01236^{+3.017\%}_{-3.284\%}$	$0.01242^{+2.896\%}_{-3.178\%}$	$0.01192^{+0.628\%}_{-0.990\%}$	$0.01199^{+0.558\%}_{-0.845\%}$
0.75	$0.00341^{+10.116\%}_{-8.809\%}$	$0.00339^{+4.422\%}_{-4.583\%}$	$0.00342^{+4.293\%}_{-4.473\%}$	$0.00337^{+1.414\%}_{-1.856\%}$	$0.00340^{+1.245\%}_{-1.698\%}$

Table 4.4: Same as Tab. 4.3 for g_1.

results for F_1 (g_1) as a function of x, after integration of y between 0.5 and 0.9 and of z between 0.2 and 0.85. We set $\mu_F = \mu_R = Q_{\text{avg}}$ where $Q^2_{\text{avg}} = x y_{\text{avg}} s$. In Fig. 4.11, results are shown as a function of z, after integration of x between 0.1 and 0.8 and of y between 0.5 and 0.9. We use $n_f = 3$ active quark and lepton flavors throughout.

In Tables 4.3 and 4.4, we present the results of F_1 and g_1 from pure QCD and mixed QCD⊗QED for $z = 0.15, 0.25, 0.45, 0.6, 0.75$ along with percentage uncertainties from scale variation. NLO$^{\text{QCD}\otimes\text{QED}}$ indicates contributions at order a_s from QCD and a_e from QED added to LO; NNLO$^{\text{QCD}\otimes\text{QED}}$ adds to LO the pure QCD contributions up to order a_s^2, pure QED to order a_e^2, and mixed QCD⊗QED up to $a_s a_e$.

For F_1 we use the `LUXqed` PDF sets [234, 269] at LO, NLO and NNLO, extended to include QED effects. For g_1 we use the `BDSSV24NLO` PDF set at LO and NLO, and the `BDSSV24NNLO` PDF set [52] at NNLO. In both cases, the `NNFF10PIp` FF sets [235] are used at the respective orders. The polarized PDFs and unpolarized FFs for photons are set to zero throughout; polarized photon PDFs can be found in [261, 270].

We observe that the dominant contribution comes from the QCD sector, while those from QED and mixed QCD⊗QED are generally small but not negligible, and are expected to be comparable in size to the N^{3}LO QCD corrections. This confirms that electromagnetic corrections must be included for any analysis targeting the precision level of the EIC.

In this chapter, we have achieved the following. Starting from the motivation that percent-level precision at the EIC requires electromagnetic corrections, we enumerated all additional QED and mixed QCD⊗QED subprocesses at NLO and NNLO, extended the mass factorization framework to include photon channels and the new AP kernels, and derived the finite CFs for all relevant partonic channels. The Abelianization procedure provided an independent and successful cross-check of every result. The phenomenological analysis confirms that the QED and mixed QCD⊗QED corrections are numerically small but non-negligible, comparable in size to N^{3}LO QCD corrections, and therefore important for precision studies at future facilities. We have also presented the complete NNLO CFs in the $\overline{\text{MS}}$ scheme, the new time-like QED splitting functions, the polarized QED and QCD⊗QED splitting functions, and the renormalization constant Z required for the scheme transformation, all provided as supplementary material in [173].

Supplementary files are provided with [173], including `Mathematica` notebooks containing the unpolarized CFs $\mathcal{C}^{(i,j)}_{I,ab}$ and polarized CFs $\Delta\mathcal{C}^{(i,j)}_{1,ab}$ in the $\overline{\text{MS}}$ scheme, the required splitting functions, and the renormalization constant Z for the scheme transformation. All CFs are simplified to eliminate θ functions, making all terms real-valued and continuous throughout $0 \le x', z' \le 1$.

Chapter 5

Conclusion

This thesis focuses on advancing the theoretical understanding of semi-inclusive deep-inelastic scattering (SIDIS) through the high-precision computation of higher-order radiative corrections. In this work, we computated full Next-to-Next-to-Leading Order (NNLO) corrections to SIDIS structure functions in QCD, along with extension of this framework to include both pure Quantum Electrodynamics (QED) effects and their interplay with QCD at the same order of accuracy. Taken together, these results represent the contribution to the precision phenomenology of hadronic physics, and are directly relevant for the physics program of the upcoming Electron-Ion Collider (EIC).

In this thesis, we demonstrate the necessity of achieving NNLO accuracy in SIDIS for making reliable and precise theoretical predictions. In the QCD sector, we computed the full set of two-loop virtual corrections, one-loop real-virtual interference terms, and double-real emission contributions, working in $d = 4 + \varepsilon$. Each of these pieces individually contains ultraviolet (UV) and infrared (IR) divergences that appear as poles in ε. We cancel all UV poles through renormalization of the strong coupling, and of all collinear IR poles through mass factorization using the Altarelli-Parisi kernels at every perturbative order. The complete cancellation of UV and IR divergences at every order in coupling constants provide a check of the entire computation. The final coefficient functions are finite, well-defined in the $\overline{\text{MS}}$ scheme, and expressed in terms of generalized polylogarithmic functions.

A technical challenge at NNLO is the computation of Master Integrals (MIs) arising from the double-real emission contribution, which were not available in the literature prior to this work. We reduced all the phase-space integrals to these MIs using integration-by-parts (IBP) identities, and derived their solutions by means of differential equations. The system of coupled differential equations satisfied by the MIs was brought into canonical ε-form through an appropriate basis transformation, after which the solutions were obtained via path-ordered integration and expressed order-by-order in ε in terms of multiple polylogarithms. The boundary conditions were determined in the limit $(x', z') \to (1, 1)$, and the integrability condition of the differential equation system provided an additional check. This represents the first complete determination of the NNLO double-real phase-space master integrals for SIDIS.

On the phenomenological side, we demonstrated the impact of the NNLO QCD corrections to the unpolarized SIDIS structure function F_1 in kinematic configurations relevant to the EIC at $\sqrt{s} = 140$ GeV. The structure function F_1 was evaluated as a convolution of the newly computed coefficient functions with the `NNPDF31` PDF sets and the `NNFF10` FF sets at the respective perturbative orders. We presented predictions for F_1 as a function of both x and z, integrating over appropriate ranges of the remaining kinematic variables. We found that the QCD corrections are sizable over a wide range of x and z: the NLO contribution is negative relative to LO over most of the kinematic range, and the NNLO correction further reduces the prediction, indicating a well-behaved but non-trivial perturbative expansion. At large x and z, however, both NLO and NNLO corrections become positive and dominate over the LO prediction, a behavior that depends sensitively on the choice of PDFs, FFs, and integration regions. The dominant contribution in all cases arises from the quark-to-quark channel coefficient function $C^{(l)}_{1,qq}$ at order $l = 1, 2$. These phenomenological results establish the NNLO QCD framework as essential for precision predictions at the EIC.

Building upon the NNLO QCD framework, we further extended the calculation to include the effects of Quantum Electrodynamics (QED) and of the combined QCD ⊗ QED interaction at NNLO. This is the first complete calculation of pure QED and mixed QCD ⊗ QED coefficient functions for SIDIS at NNLO accuracy, covering both the unpolarized and polarized sectors. The relevant partonic subprocesses at $\mathcal{O}(a_s a_e)$ and $\mathcal{O}(a_e^2)$ include virtual corrections involving both gluon and photon exchange, real-virtual interference between QCD and QED amplitudes, double real emission with simultaneous gluon and photon radiation, as well as photon-initiated and photon-fragmentation channels. The latter require the introduction of the photon parton distribution function of the proton and the photon fragmentation function, which extends the collinear factorization framework to incorporate photon in both the initial and final states.

We computed QED and mixed QCD ⊗ QED contributions in two ways. First, we performed a direct calculation from scratch, treating QED corrections on the same footing as the QCD computation and following the same approach of dimensional regularization, IBP reduction, master integral evaluation, UV renormalization, and mass factorization. Second, we used an Abelianization procedure, which exploits the structural similarity between QCD and QED Feynman diagrams: by identifying those NNLO QCD diagrams that survive in the Abelian limit, where non-Abelian gluon self-interactions are removed and color factors are replaced by appropriate electric charge factors. One can extract the pure QED and mixed QCD ⊗ QED contributions from the known QCD results. The complete agreement between both approaches at the level of the coefficient functions provides a cross-check of our results.

A important outcome of the QED extension is the determination of previously unknown splitting functions and finite renormalization constants in the in QED and mixed QCD ⊗ QED sector. Specifically, the unpolarized time-like and polarized space-like Altarelli-Parisi kernels in the QED and mixed QCD ⊗ QED sectors, required for mass factorization at NNLO, were derived for the first time within this work using the Abelianization procedure.

The treatment of the polarized structure function g_1 requires special care due to the presence of the γ_5 matrix in dimensional regularization. Since γ_5 cannot be defined in a fully anticommuting manner in $d \neq 4$ dimensions, we adopted Larin's prescription, in which γ_5 is expressed in terms of the Levi-Civita tensor contracted with products of Dirac matrices. While this approach provides a consistent computation in $d = 4 + \varepsilon$ dimensions, it introduces a violation of the axial Ward identity that must be corrected by a finite renormalization. The finite renormalization constants in pure QCD are well known in the literature; however, the corresponding constants in the pure QED and mixed QCD $\otimes$ QED sectors were not previously known. In this thesis, we derived these missing finite renormalization constants explicitly for the first time, thereby completing the scheme-conversion framework in the combined strong and electromagnetic sector. This ensures that the polarized coefficient functions $\Delta C_{1,ab}$ are correctly defined in the $\overline{\text{MS}}$ scheme.

The phenomenological impact of the QED and mixed QCD $\otimes$ QED corrections was studied numerically for both F_1 and g_1 in EIC kinematics. For the unpolarized structure function F_1, we used the `LUXqed` PDF sets extended to include QED effects. For the polarized structure function g_1, the `BDSSV24NLO` and `BDSSV24NNLO` PDF sets incorporating QED effects were used at the respective perturbative orders. In both cases, the `NNFF10PIp` FF sets were employed. The numerical results reveal that, although electromagnetic corrections are formally suppressed relative to the dominant QCD contributions, their magnitude in certain regions of phase space is comparable to that of N^{3}LO QCD corrections. The QED and mixed corrections modify the SIDIS structure functions at the sub-percent to percent level. Their inclusion is found to improve the perturbative stability of the predictions and reduce the scale dependence on the renormalization and factorization scales. This reduction in scale dependence is a direct indication that the perturbative series is becoming better controlled as more contributions are included, and it underscores the necessity of incorporating electromagnetic effects for percent-level theoretical precision.

The results of this thesis are directly applicable for the experimental program of the Electron-Ion Collider, which is designed to operate over a wide range of center-of-mass energies and to measure SIDIS observables with unprecedented precision, particularly for polarized beams. The NNLO QCD and QCD $\otimes$ QED coefficient functions derived in this work provide the necessary theoretical input for global QCD analyses at NNLO accuracy, enabling more precise and reliable extractions of PDFs, helicity PDFs, and FFs for hadrons. At NNLO accuracy, the enhanced scale stability and reduced theoretical uncertainties are necessary for isolating the contributions of individual quark flavours and for exploring the nucleon's spin structure in kinematic regimes beyond the reach of current experiments.

The analytical results, multiloop computational methods, and the factorization framework developed in this thesis provide a solid foundation for future theoretical developments. Natural directions for future work include the quark mass, which become relevant for charm and bottom quark contributions at EIC energies; doing NNLO QCD $\otimes$ EW and the eventual calculation of N^{3}LO QCD corrections to SIDIS, which will become necessary as experimental precision at the EIC continues to improve. The Abelianization and master integral techniques developed here are generic and can be applied to a wide class of semi-inclusive processes beyond SIDIS.

In conclusion, our work provides a complete NNLO unpolarized QCD and NNLO unpolarized and polarized QCD $\otimes$ QED description of SIDIS structure functions. Our work is a step toward the high-precision theoretical accuracy that will be required to fully exploit the experimental potential of next-generation scattering facilities, and in particular the Electron-Ion Collider, in unravelling the fundamental dynamics of the strong and electroweak interactions within the nucleon.

Appendix A

IBP Reduction Example

A.1 Overview

This chapter demonstrates a complete example of integration-by-parts (IBP) reduction for RV case using the `LiteRed2` package in Mathematica. The code illustrates the systematic reduction of a 1-loop and 1 emission integral family to a basis of independent master integrals through automated IBP relations.

The IBP method is fundamental in modern perturbative quantum field theory calculations. It utilizes the fact that total derivatives of loop integrals vanish:

$$\int d^d\ell \, \frac{\partial}{\partial \ell_\mu} \, [\text{integrand}] = 0 \tag{A.1}$$

This generates algebraic relations between integrals with different powers of propagators, allowing systematic reduction to a minimal basis.

A.2 Implementation

A.2.1 Code Listing

Listing A.1: Mathematica code for IBP reduction using LiteRed2

```
(* Load required packages *)
<< LiteRed2`;

(* Working directory *)
SetDirectory[NotebookDirectory[]];

(* Dimensionality *)
SetDim[d];

(* Declare vectors and kinematic variables *)
Declare[{l1, k, q, p1}, Vector,{Q2, x', z'}, Number];

(* Kinematic relations *)
sp[p1, p1] = 0;
sp[p1, q]  = Q2/(2 x');
sp[q, q]   = -Q2;

(* Definition of squared scalar products *)
s[a_] := sp[a, a];

(* Propagators *)
Pr1 = l1;
Pr2 = l1 - p1;
Pr3 = l1 + q;
Pr4 = l1 - p1 - q + k;
Pr5 = l1 - p1 + k;
Pr6 = l1 + q - k;

(* Cut propagators *)
```

```
CPr1 := s[k];
CPr2 := s[k - p1 - q];
CPr3 := ((z' - 1) sp[p1, q] + sp[k, p1])/sp[p1, q];

(* Define the integral family *)
NewDsBasis[A1, {CPr1, CPr2, CPr3,
s[Pr1], s[Pr2],s[Pr3], s[Pr6]},
{l1, k}, Directory -> "A1Dir",GenerateIBP -> True];

(* Analyze sectors with the specified cut *)
AnalyzeSectors[ A1,CutDs -> {1, 1, 1, 0, 0, 0, 0}];

(* Search for symmetries *)
FindSymmetries[A1];

(* Set options for the reduction *)
SetOptions[CountMIs];
SetOptions[SolvejSector, NMIs -> Automatic];

(* Solve the IBP system *)
Timing[SolvejSector[UniqueSectors[A1]]];

(* Save the LiteRed basis *)
Disksave[A1];

(* Display the master integrals *)
MIs[A1]
```

A.2.2 Code Description

Package Loading and Setup

The code begins by loading the `LiteRed2` package, which provides automated IBP system generation. The working directory is set via `SetDirectory` and the spacetime dimensionality is defined as d. This working example is for one loop-one emission case in SIDIS. I have given code for one integral family.

Kinematic Configuration

Vectors and kinematic variables are declared:

- Loop momenta: l_1
- External momenta: q, p_1 and k
- Scalar invariants: Q^2, x', z'

The kinematic relations specify:

$$p_1^2 = 0 \quad \text{(massless external particle)} \tag{A.2}$$

$$2p_1 \cdot q = \frac{Q^2}{2x'} \quad \text{(interaction kinematics)} \tag{A.3}$$

$$q^2 = -Q^2 \quad \text{(spacelike momentum transfer)} \tag{A.4}$$

Propagator Definition

Seven propagators define the integral family topology. The first three propagators (CPr1, CPr2, CPr3) appear in the cut specification and correspond to:

$$\text{CPr1} = k^2 \tag{A.5}$$

$$\mathrm{CPr2} = (k - p_1 - q)^2 \tag{A.6}$$

$$\mathrm{CPr3} = ((z' - 1)p_1.q + k.p_1)/(p_1.q) \tag{A.7}$$

$$\tag{A.8}$$

and remaining 4 are actual propagators and corresponds to:

$$\mathrm{Pr1} = l_1 \tag{A.9}$$

$$\mathrm{Pr2} = l_1 - p_1 \tag{A.10}$$

$$\mathrm{Pr3} = l_1 + q \tag{A.11}$$

$$\mathrm{Pr6} = l_1 + q - k \tag{A.12}$$

$$\tag{A.13}$$

Remaining propagators required for other topologies.

Integral Family and IBP Reduction

`NewDsBasis` initializes the integral family A_1 with:

- Cut propagators: `CPr1`, `CPr2`, `CPr3`
- Regular propagators: squared forms of Pr1, Pr2, Pr3, Pr6
- Loop momenta: l_1
- Automatic IBP system generation via `GenerateIBP -> True`

`AnalyzeSectors` identifies topologically distinct sectors. The cut specification `{1,1,1,0,0,0,0}` indicates which propagators are cut propagator (1) or actual propagator (0).

Reduction and Output

`FindSymmetries` detects symmetry relations reducing problem size. `SolvejSector` solves the IBP system for all unique sectors with `NMIs -> Automatic` determining the number of master integrals automatically. The timing of this operation is recorded for performance analysis.

Finally, `Disksave` persists the reduced basis to disk, and `MIs[A1]` displays the list of independent master integrals.

Appendix B

Theoretical Preliminaries

Contents

This appendix collects the kinematic conventions, tensor decompositions, and contraction identities used in the derivation of the deep-inelastic scattering cross sections presented in the main text. We begin by establishing the four-momentum assignments and exact kinematic relations for the process $\ell(k)+H(P) \to \ell(k')+X$, retaining finite lepton mass m_ℓ and nucleon mass M throughout. The leptonic and hadronic tensors are then decomposed in terms of structure functions, and the relevant tensor contractions are evaluated exactly. These results are subsequently used to derive the kinematic coefficients of the structure functions F_1, F_2, and g_1 appearing in the double-differential cross section, including all mass corrections of order M^2/Q^2 and m_ℓ^2/Q^2. The appendix concludes with the complete cross-section formulae and consistency checks in the massless limits. The projection operators used to extract the structure functions at the partonic level are discussed in Appendix C.

B.1 Setup and Conventions

We consider the process $\ell(k) + H(P) \to \ell(k') + X$ mediated by the exchange of a virtual boson (photon, Z, or $W^{\pm}$).

B.1.1 Four-momenta and masses

$$P^\mu = (M, 0, 0, 0) \quad \text{(nucleon, rest frame)} \tag{B.1}$$

$$S^\mu = \lambda_H (0, 0, 0, M) \quad \text{(longitudinal spin vector)} \tag{B.2}$$

$$k^\mu = (E, 0, 0, -k_z) \quad \text{(incoming lepton)} \tag{B.3}$$

$$k'^\mu = k^\mu - q^\mu \quad \text{(outgoing lepton)} \tag{B.4}$$

$$q^\mu = (\nu, 0, 0, -|\vec{q}|) \quad \text{(virtual photon)} \tag{B.5}$$

where $k_z = \sqrt{E^2 - m_\ell^2}$ and the spin vector satisfies

$$S \cdot P = 0, \qquad S^2 = -M^2. \tag{B.6}$$

B.1.2 Kinematic invariants

$$Q^2 = -q^2 > 0 \qquad \text{(photon virtuality)} \tag{B.7}$$

$$x = \frac{Q^2}{2P \cdot q} \qquad \text{(Bjorken } x\text{, parton momentum fraction)} \tag{B.8}$$

$$y = \frac{P \cdot q}{P \cdot k} \qquad \text{(inelasticity)} \tag{B.9}$$

$$s = (P + k)^2 = M^2 + m_\ell^2 + \frac{Q^2}{xy} \qquad \text{(CM energy}^2\text{)} \tag{B.10}$$

Important: The relation $Q^2 = sxy$ is *not* exact. The correct relation is

$$\boxed{Q^2 = xy\left(s - M^2 - m_\ell^2\right)} \tag{B.11}$$

The approximation $Q^2 \approx sxy$ holds only when $s \gg M^2, m_\ell^2$.

B.1.3 Complete kinematic dictionary

The following dot products are **exact** for any M and m_ℓ:

$$P \cdot q = \frac{Q^2}{2x} \tag{B.12}$$

$$P \cdot k = \frac{Q^2}{2xy} \qquad \text{(exact by definition of } y\text{)} \tag{B.13}$$

$$P \cdot k' = \frac{Q^2(1 - y)}{2xy} \tag{B.14}$$

$$k \cdot q = -\frac{Q^2}{2} \qquad \text{(exact for any } m_\ell\text{)} \tag{B.15}$$

$$k' \cdot q = +\frac{Q^2}{2} \tag{B.16}$$

$$k \cdot k' = m_\ell^2 + \frac{Q^2}{2} \tag{B.17}$$

The lepton energy and 3-momentum in the rest frame:

$$E = \frac{P \cdot k}{M} = \frac{Q^2}{2Mxy}, \qquad k_z = \sqrt{E^2 - m_\ell^2} = \frac{Q^2}{2Mxy}\sqrt{1 - \epsilon_\ell^2} \tag{B.18}$$

where we define the dimensionless parameter

$$\boxed{\epsilon_\ell^2 \equiv \frac{4M^2x^2y^2m_\ell^2}{Q^4}} \tag{B.19}$$

B.1.4 Transverse vectors

Current conservation requires all tensor structures to be transverse to q^μ. Define

$$\hat{P}^\mu = P^\mu - \frac{P \cdot q}{q^2} q^\mu = P^\mu + \frac{P \cdot q}{Q^2} q^\mu, \qquad q \cdot \hat{P} = 0 \tag{B.20}$$

$$\hat{P}^2 = M^2 + \frac{Q^2}{4x^2} \tag{B.21}$$

Dot products with leptons:

$$k \cdot \hat{P} = k' \cdot \hat{P} = \frac{Q^2(2-y)}{4xy} \tag{B.22}$$

B.1.5 Spin vector dot products

Using $|\vec{q}|$ derived from $k \cdot q = -Q^2/2$ exactly:

$$k_z |\vec{q}| = E\nu + \frac{Q^2}{2} \implies |\vec{q}| = \frac{Q^2/2Mx + Mxy}{\sqrt{1-\epsilon_\ell^2}} \tag{B.23}$$

The exact spin-vector dot products are:

$$\boxed{S \cdot k} = \lambda_H M k_z = \frac{\lambda_H Q^2}{2xy}\sqrt{1-\epsilon_\ell^2} \tag{B.24}$$

$$\boxed{S \cdot q} = \lambda_H M |\vec{q}| = \frac{\lambda_H}{\sqrt{1-\epsilon_\ell^2}}\left(\frac{Q^2}{2x} + M^2 xy\right) \tag{B.25}$$

$$\boxed{S \cdot k'} = S \cdot k - S \cdot q = \frac{-\lambda_H}{\sqrt{1-\epsilon_\ell^2}}\left(\frac{Q^2(1-y)}{2xy} + M^2 xy + \frac{Q^2\epsilon_\ell^2}{2xy}\right) \tag{B.26}$$

Hence:

$$\boxed{\frac{S \cdot q}{P \cdot q} = \frac{\lambda_H}{\sqrt{1-\epsilon_\ell^2}}\left(1 + \frac{2M^2x^2y}{Q^2}\right)} \tag{B.27}$$

B.2 Leptonic Tensor

For a lepton of mass m_ℓ and helicity $\lambda_\ell = \pm 1$:

$$L^{\mu\nu} = L_S^{\mu\nu} + L_A^{\mu\nu} \tag{B.28}$$

$$L_S^{\mu\nu} = 2\left[k^\mu k'^\nu + k'^\mu k^\nu - g^{\mu\nu}(k \cdot k' + m_\ell^2)\right] \tag{B.29}$$

$$L_A^{\mu\nu} = -2i\lambda_\ell\, \varepsilon^{\mu\nu\alpha\beta} k_\alpha k'_\beta \tag{B.30}$$

The symmetric part $L_S^{\mu\nu}$ contracts with symmetric $W_{\mu\nu}$ structures (F_1, F_2). The antisymmetric part $L_A^{\mu\nu}$ contracts with antisymmetric structures g_1.

B.3 Hadronic Tensor

Setting $g_2 = g_3 = 0$ (longitudinal polarization; these are suppressed by M^2/Q^2), the hadronic tensor is:

$$W_{\mu\nu} = T_{1\mu\nu} F_1 + \frac{\hat{P}_\mu \hat{P}_\nu}{P \cdot q} F_2 + \frac{i\varepsilon_{\mu\nu\alpha\beta} q^\alpha S^\beta}{P \cdot q} g_1 \tag{B.31}$$

where the transverse metric tensor is

$$T_{1\mu\nu} = -g_{\mu\nu} + \frac{q_\mu q_\nu}{q^2} = -g_{\mu\nu} - \frac{q_\mu q_\nu}{Q^2} \tag{B.32}$$

B.3.1 Contraction rules

Since $L_S^{\mu\nu}$ is symmetric and $L_A^{\mu\nu}$ is antisymmetric:

$$L_S^{\mu\nu} \cdot W_{\mu\nu}^{(A)} = 0, \qquad L_A^{\mu\nu} \cdot W_{\mu\nu}^{(S)} = 0 \tag{B.33}$$

Therefore:

- F_1, F_2 : contracted with $L_S^{\mu\nu}$ only

- F_3, g_1: contracted with $L_A^{\mu\nu}$ only (require $\lambda_\ell \neq 0$)

B.4 Key Contractions

B.4.1 $L_S^{\mu\nu} \cdot T_{1\mu\nu}$

$$L_S^{\mu\nu} T_{1\mu\nu} = 2\left[k^\mu k'^\nu + k'^\mu k^\nu - g^{\mu\nu}(k \cdot k' + m_\ell^2)\right]\left(-g_{\mu\nu} - \frac{q_\mu q_\nu}{Q^2}\right) \tag{B.34}$$

Computing term by term (using $k \cdot q = -Q^2/2$, $k' \cdot q = Q^2/2$, $k \cdot k' = m_\ell^2 + Q^2/2$, $g^{\mu\nu} g_{\mu\nu} = 4$):

Term	Expression	Value
1	$2k^\mu k'^\nu(-g_{\mu\nu})$	$-2m_\ell^2 - Q^2$
2	$2k'^\mu k^\nu(-g_{\mu\nu})$	$-2m_\ell^2 - Q^2$
3	$-2g^{\mu\nu}(k \cdot k' + m_\ell^2)(-g_{\mu\nu})$	$+16m_\ell^2 + 4Q^2$
4	$2k^\mu k'^\nu(-q_\mu q_\nu/Q^2)$	$-Q^2/2$
5	$2k'^\mu k^\nu(-q_\mu q_\nu/Q^2)$	$-Q^2/2$
6	$-2g^{\mu\nu}(k \cdot k' + m_\ell^2)(-q_\mu q_\nu/Q^2)$	$+4m_\ell^2 + Q^2$
	Total	$\mathbf{16m_\ell^2 + 2Q^2}$

$$\boxed{L_S^{\mu\nu}\, T_{1\mu\nu} = 16m_\ell^2 + 2Q^2} \tag{B.35}$$

B.4.2 $L_S^{\mu\nu} \cdot \hat{P}_\mu \hat{P}_\nu$ and $T_{2\mu\nu}$

$$L_S^{\mu\nu}\, \hat{P}_\mu \hat{P}_\nu = 4(k \cdot \hat{P})(k' \cdot \hat{P}) - 2(k \cdot k' + m_\ell^2)\hat{P}^2 \tag{B.36}$$

Substituting $k \cdot \hat{P} = k' \cdot \hat{P} = Q^2(2-y)/4xy$, $\hat{P}^2 = M^2 + Q^2/4x^2$, $k \cdot k' + m_\ell^2 = 2m_\ell^2 + Q^2/2$:

$$4(k \cdot \hat{P})^2 = \frac{Q^4(2-y)^2}{4x^2y^2} \tag{B.37}$$

$$\begin{aligned} 2(k \cdot k' + m_\ell^2)\hat{P}^2 &= 2\left(2m_\ell^2 + \frac{Q^2}{2}\right)\left(M^2 + \frac{Q^2}{4x^2}\right) \\ &= 4m_\ell^2 M^2 + \frac{m_\ell^2 Q^2}{x^2} + M^2Q^2 + \frac{Q^4}{4x^2} \end{aligned} \tag{B.38}$$

The Q^4 terms combine:

$$\frac{Q^4(2-y)^2}{4x^2y^2} - \frac{Q^4}{4x^2} = \frac{Q^4}{4x^2y^2}\left[(2-y)^2 - y^2\right] = \frac{Q^4(1-y)}{x^2y^2} \tag{B.39}$$

(using $(2-y)^2 - y^2 = 4 - 4y = 4(1-y)$). Therefore:

$$L_S^{\mu\nu}\,\hat{P}_\mu\hat{P}_\nu = \frac{Q^4(1-y)}{x^2y^2} - M^2Q^2 - \frac{m_\ell^2Q^2}{x^2} - 4m_\ell^2M^2 \tag{B.40}$$

Dividing by $P\cdot q = Q^2/2x$:

$$\boxed{L_S^{\mu\nu}\,T_{2\mu\nu} = \frac{2Q^2(1-y)}{xy^2} - 2xM^2 - \frac{2m_\ell^2}{x} - \frac{8xm_\ell^2M^2}{Q^2}} \tag{B.41}$$

B.4.3 $L_A^{\mu\nu}\cdot\varepsilon_{\mu\nu\alpha\beta}q^\alpha V^\beta$

For any vector V^β:

$$\varepsilon^{\mu\nu\rho\sigma}\varepsilon_{\mu\nu\alpha\beta} = -2\left(\delta^\rho_\alpha\delta^\sigma_\beta - \delta^\rho_\beta\delta^\sigma_\alpha\right) \tag{B.42}$$

$$\begin{aligned} L_A^{\mu\nu}\cdot\frac{i\varepsilon_{\mu\nu\alpha\beta}q^\alpha V^\beta}{P\cdot q} &= \frac{(-2i\lambda_\ell)(i)}{P\cdot q}\,\varepsilon^{\mu\nu\rho\sigma}\varepsilon_{\mu\nu\alpha\beta}\,k_\rho k'_\sigma q^\alpha V^\beta \\ &= \frac{2\lambda_\ell}{P\cdot q}\cdot(-2)\left[(k\cdot q)(k'\cdot V) - (k\cdot V)(k'\cdot q)\right] \end{aligned} \tag{B.43}$$

Using $k' = k - q$:

$$\begin{aligned} (k\cdot q)(k'\cdot V) - (k\cdot V)(k'\cdot q) &= (k\cdot q)(k\cdot V - V\cdot q) - (k\cdot V)(k\cdot q + Q^2) \\ &= -(k\cdot q)(V\cdot q) - Q^2(k\cdot V) \end{aligned} \tag{B.44}$$

Substituting $k \cdot q = -Q^2/2$:

$$\boxed{(k \cdot q)(k' \cdot V) - (k \cdot V)(k' \cdot q) = \frac{Q^2}{2}(V \cdot q) - Q^2(k \cdot V) = Q^2\left[\frac{V \cdot q}{2} - k \cdot V\right]} \tag{B.45}$$

B.5 Derivation of F_1

The F_1 hadronic structure is $W_{\mu\nu}^{(F_1)} = T_{1\mu\nu}F_1$. Contracting with $L_S^{\mu\nu}$:

$$L_S^{\mu\nu}\, W_{\mu\nu}^{(F_1)} = \left(16m_\ell^2 + 2Q^2\right) F_1 \tag{B.46}$$

Applying the prefactor $2\pi y\alpha^2/Q^4$ and factoring out $4\pi\alpha^2/xyQ^2$:

The F_1 coefficient in $\frac{d^2\sigma}{dxdy} \cdot \frac{xyQ^2}{4\pi\alpha^2\eta}$ is:

$$\frac{2\pi y\alpha^2}{Q^4} \cdot (16m_\ell^2 + 2Q^2) \cdot \frac{xyQ^2}{4\pi\alpha^2} = \frac{xy^2}{2Q^2}(16m_\ell^2 + 2Q^2) = xy^2 + \frac{8xm_\ell^2 y^2}{Q^2} \tag{B.47}$$

$$\boxed{\text{Coeff. of } F_1 = xy^2\left(1 + \frac{8m_\ell^2}{Q^2}\right)} \tag{B.48}$$

B.6 Derivation of F_2

The F_2 structure is $W_{\mu\nu}^{(F_2)} = \hat{P}_\mu \hat{P}_\nu/(P \cdot q) \cdot F_2$. Using (B.41):

$$L_S^{\mu\nu}\, W_{\mu\nu}^{(F_2)} = \left(\frac{2Q^2(1-y)}{xy^2} - 2xM^2 - \frac{2m_\ell^2}{x} - \frac{8xm_\ell^2 M^2}{Q^2}\right) F_2 \tag{B.49}$$

Applying the conversion factor $xy^2/2Q^2$:

$$\boxed{\text{Coeff. of } F_2 = \left(1 - y - \frac{x^2y^2M^2}{Q^2} - \frac{m_\ell^2 y^2}{Q^2} - \frac{4x^2y^4m_\ell^2M^2}{Q^4}\right)} \tag{B.50}$$

B.7 Derivation of g_1

The g_1 structure is $W_{\mu\nu}^{(g_1)} = i\varepsilon_{\mu\nu\alpha\beta}q^\alpha S^\beta/(P\cdot q)\cdot g_1$. Using (B.45) with $V^\beta = S^\beta$:

$$\begin{aligned} L_A^{\mu\nu} W_{\mu\nu}^{(g_1)} &= \frac{-4\lambda_\ell}{P\cdot q}\cdot Q^2\left[\frac{S\cdot q}{2} - S\cdot k\right]g_1 \\ &= -8\lambda_\ell x\left[\frac{S\cdot q}{2} - S\cdot k\right]g_1 \end{aligned} \tag{B.51}$$

B.7.1 Evaluate $S\cdot q/2 - S\cdot k$ exactly

$$\begin{aligned} \frac{S\cdot q}{2} - S\cdot k &= \frac{\lambda_H}{2\sqrt{1-\epsilon_\ell^2}}\left(\frac{Q^2}{2x} + M^2xy\right) - \frac{\lambda_H Q^2}{2xy}\sqrt{1-\epsilon_\ell^2} \\ &= \frac{\lambda_H}{\sqrt{1-\epsilon_\ell^2}}\left[\frac{Q^2}{4x} + \frac{M^2xy}{2} - \frac{Q^2}{2xy}(1-\epsilon_\ell^2)\right] \\ &= \frac{\lambda_H}{\sqrt{1-\epsilon_\ell^2}}\cdot\frac{Q^2}{4xy}\left[(y-2) + \frac{2M^2x^2y^2}{Q^2} + 2\epsilon_\ell^2\right] \end{aligned} \tag{B.52}$$

Substituting back:

$$\begin{aligned} L_A^{\mu\nu} W_{\mu\nu}^{(g_1)} &= -8\lambda_\ell x\cdot\frac{\lambda_H}{\sqrt{1-\epsilon_\ell^2}}\cdot\frac{Q^2}{4xy}\left[(y-2) + \frac{2M^2x^2y^2}{Q^2} + 2\epsilon_\ell^2\right]g_1 \\ &= \frac{2\lambda_\ell\lambda_H Q^2}{y\sqrt{1-\epsilon_\ell^2}}\left(2 - y - \frac{2x^2y^2M^2}{Q^2} - \frac{8x^2y^2m_\ell^2M^2}{Q^4}\right)g_1 \end{aligned} \tag{B.53}$$

Applying conversion factor $xy^2/2Q^2$:

$$\boxed{\text{Coeff. of } g_1 = \frac{\lambda_\ell \lambda_H xy}{\sqrt{1-\epsilon_\ell^2}}\left(2 - y - \frac{2x^2y^2M^2}{Q^2} - \frac{8x^2y^2m_\ell^2M^2}{Q^4}\right)} \tag{B.54}$$

B.8 Complete Cross-Section Formulae

B.8.1 Propagator factors η_j

Without decay widths (exact in the stable boson limit):

$$\eta_\gamma = 1 \tag{B.55}$$

$$\eta_{\gamma Z} = \frac{G_F M_Z^2}{2\sqrt{2}\pi\alpha_e} \cdot \frac{Q^2}{Q^2 + M_Z^2} \tag{B.56}$$

$$\eta_Z = \eta_{\gamma Z}^2 \tag{B.57}$$

$$\eta_W = \frac{1}{2}\left(\frac{G_F M_W^2}{2\sqrt{2}\pi\alpha_e}\right)^2 \cdot \frac{Q^4}{(Q^2 + M_W^2)^2} \tag{B.58}$$

B.8.2 Unpolarized cross-section

$$\boxed{\frac{d^2\sigma}{dx\,dy} = \frac{4\pi\alpha_e^2\eta}{xyQ^2}\left\{\left[1 - y - \frac{x^2y^2M^2}{Q^2} - \frac{m_\ell^2y^2}{Q^2} - \frac{4x^2y^4m_\ell^2M^2}{Q^4}\right]F_2 + \left[y^2 + \frac{8m_\ell^2y^2}{Q^2}\right]xF_1\right\}} \tag{B.59}$$

The $\mp$ sign: $-$ for incoming e^+ or $\bar{\nu}$ ($\lambda_\ell = +1$), $+$ for incoming e^- or ν ($\lambda_\ell = -1$).

B.8.3 Polarized cross-section difference

Define $\Delta\sigma = \sigma(\lambda_H = -1, \lambda_\ell) - \sigma(\lambda_H = +1, \lambda_\ell)$.

$$\boxed{\frac{d^2\Delta\sigma}{dx\,dy} = \frac{4\pi\alpha_e^2\eta}{xyQ^2\sqrt{1-\epsilon_\ell^2}}\left\{\ \lambda_\ell\lambda_H\left(2-y-\frac{2x^2y^2M^2}{Q^2}-\frac{8x^2y^2m_\ell^2M^2}{Q^4}\right)x\,g_1\ \right\}} \tag{B.60}$$

B.9 Limits and Checks

B.9.1 Massless lepton: $m_\ell \to 0$ ($\epsilon_\ell \to 0$)

$$\frac{d^2\sigma}{dxdy} \to \frac{4\pi\alpha_e^2\eta}{xyQ^2}\left\{\left(1-y-\frac{x^2y^2M^2}{Q^2}\right)F_2 + y^2xF_1\right\} \tag{B.61}$$

$$\frac{d^2\Delta\sigma}{dxdy} \to \frac{4\pi\alpha_e^2\eta}{xyQ^2}\left\{\lambda_\ell\lambda_H\left(2-y-\frac{2x^2y^2M^2}{Q^2}\right)xg_1\right\} \tag{B.62}$$

B.9.2 Massless lepton and massless nucleon: $m_\ell, M \to 0$

$$\frac{d^2\sigma}{dxdy} \to \frac{4\pi\alpha_e^2\eta}{xyQ^2}\left\{(1-y)F_2 + y^2xF_1\right\} \tag{B.63}$$

$$\frac{d^2\Delta\sigma}{dxdy} \to \frac{4\pi\alpha_e^2\eta}{xyQ^2}\left\{\lambda_\ell\lambda_H(2-y)xg_1\right\} \tag{B.64}$$

The massless limits derived above serve as a consistency check on the general mass-corrected formulae: setting $m_\ell \to 0$ reproduces the standard target-mass-corrected expressions, while the further limit $M \to 0$ reduces to the parton-model result. The kinematic framework established here feeds directly into the partonic calculation, where the hadronic tensor is replaced by its partonic counterpart and the structure functions are extracted using the projection operators described in Appendix C.

Appendix C

Hadronic Projectors

Contents

This appendix presents the hadronic projection operators used to extract individual structure functions directly from the hadronic tensor $W_{\mu\nu}$. Rather than solving it explicitily, one constructs a projector $\mathcal{P}^{\mu\nu}_{(i)}$ such that its contraction with $W_{\mu\nu}$ isolates a single structure function F_i or g_i while annihilating all others. We begin by introducing the symmetric basis tensors that span the hadronic tensor and establishing their contraction identities in n dimensions. The projectors for F_1, F_2, and g_1 are then derived systematically by imposing orthogonality and normalization conditions, and their mutual consistency is verified explicitly. The resulting projectors are collected in a summary table for reference. These operators are applied in the main calculation to extract the partonic structure functions from the perturbatively computed partonic tensor, as described in the main text. The splitting functions that arise in the subsequent mass factorization step are collected in Appendix D.

C.1 Projection Operators

The projection operators allow us to *extract* individual structure functions directly from the hadronic tensor $W_{\mu\nu}$ without solving a coupled system. The strategy is to build a projector $\mathcal{P}^{\mu\nu}_{(i)}$ such that

$$\mathcal{P}^{\mu\nu}_{(i)} W_{\mu\nu} = c_i \cdot F_i \quad (\text{or } c_i \cdot g_i) \tag{C.1}$$

where c_i is a known kinematic factor, while all other structure functions are annihilated.

C.1.1 Basis tensors and their properties

The hadronic tensor is spanned by two symmetric basis tensors:

$$T_1^{\mu\nu} = -g^{\mu\nu} + \frac{q^\mu q^\nu}{q^2} = -g^{\mu\nu} - \frac{q^\mu q^\nu}{Q^2} \tag{C.2}$$

$$T_2^{\mu\nu} = \frac{\hat{P}^\mu \hat{P}^\nu}{P \cdot q} \tag{C.3}$$

Their self-contractions in n dimensions:

$$T_1^{\mu\nu}T_{1\mu\nu} = g^{\mu\nu}g_{\mu\nu} - \frac{q^2}{Q^2} - \frac{q^2}{Q^2} + \frac{(q^2)^2}{Q^4} = n - 1 - 1 + 1 = n - 1 \tag{C.4}$$

$$T_2^{\mu\nu}T_{2\mu\nu} = \frac{\hat{P}^4}{(P\cdot q)^2} = \frac{(M^2 + Q^2/4x^2)^2}{(Q^2/2x)^2} = \frac{(M^2 + Q^2/4x^2)^2\cdot 4x^2}{Q^4} \tag{C.5}$$

Crucially, the two basis tensors are **orthogonal**:

$$T_1^{\mu\nu}T_{2\mu\nu} = \frac{1}{P\cdot q}\left(-\hat{P}^{\mu}\hat{P}_{\mu} + \frac{q^{\mu}\hat{P}_{\mu}q^{\nu}\hat{P}_{\nu}}{Q^2}\right) = \frac{1}{P\cdot q}\left(-\hat{P}^2 + \frac{(q\cdot\hat{P})^2}{Q^2}\right) = \frac{-\hat{P}^2}{P\cdot q} + 0 \neq 0 \tag{C.6}$$

let us compute this carefully. Since $q\cdot\hat{P} = 0$ by construction:

$$T_1^{\mu\nu}T_{2\mu\nu} = \frac{1}{P\cdot q}\left(-g^{\mu\nu} - \frac{q^{\mu}q^{\nu}}{Q^2}\right)\hat{P}_{\mu}\hat{P}_{\nu} = \frac{1}{P\cdot q}\left(-\hat{P}^2 - \frac{(q\cdot\hat{P})^2}{Q^2}\right) = \frac{-\hat{P}^2}{P\cdot q} \tag{C.7}$$

This is *not* zero in general. However, the projectors are constructed so that the unwanted terms cancel. The projectors use a linear combination $\alpha T_1 + \beta T_2$, and α, β are fixed to zero the coefficient of the unwanted structure function.

C.1.2 General symmetric projector

Any symmetric projector can be written as:

$$\mathcal{P}^{\mu\nu} = \alpha\, T_1^{\mu\nu} + \beta\, T_2^{\mu\nu} \tag{C.8}$$

Contracting with the symmetric hadronic tensor:

$W_{\mu\nu}^{(S)} = F_1 T_{1\mu\nu} + \frac{F_2}{P\cdot q}\hat{P}_{\mu}\hat{P}_{\nu}$

$$
\begin{aligned}
\mathcal{P}^{\mu\nu}W^{(S)}_{\mu\nu} &= \alpha F_1\, T_1^{\mu\nu}T_{1\mu\nu} + \frac{\alpha F_2}{P\cdot q}\, T_1^{\mu\nu}\hat{P}_\mu\hat{P}_\nu + \frac{\beta F_1}{P\cdot q}\,\hat{P}^\mu\hat{P}^\nu T_{1\mu\nu}\cdot(P\cdot q) + \frac{\beta F_2}{(P\cdot q)^2}\,\hat{P}^\mu\hat{P}^\nu\hat{P}_\mu\hat{P}_\nu \\
&= \alpha F_1(n-1) + \frac{\alpha F_2\,\hat{P}^2}{P\cdot q}\cdot(-1) - \beta F_1\,\hat{P}^2 + \beta F_2\,\frac{\hat{P}^4}{(P\cdot q)^2}
\end{aligned}
\tag{C.9}
$$

where we used $T_1^{\mu\nu}\hat{P}_\mu\hat{P}_\nu = -\hat{P}^2$ (since $q\cdot\hat{P} = 0$) and $T_{1\mu\nu}\hat{P}^\mu\hat{P}^\nu\cdot(P\cdot q) = -(P\cdot q)\hat{P}^2$.

C.1.3 Projector for F_1

We want $\mathcal{P}^{\mu\nu}_{(F_1)}$ to give F_1 and kill F_2.

Condition to kill F_2:

$$
-\frac{\alpha\hat{P}^2}{P\cdot q} + \beta\frac{\hat{P}^4}{(P\cdot q)^2} = 0 \implies \beta = \frac{\alpha\, P\cdot q}{\hat{P}^2}
\tag{C.10}
$$

Condition to normalize F_1:

$$
\alpha(n-1)-\beta\hat{P}^2 = 1 \implies \alpha(n-1)-\alpha\, P\cdot q\cdot\frac{\hat{P}^2}{\hat{P}^2} = 1 \implies \alpha\,(n-2) = 1 \implies \alpha = \frac{1}{n-2}
\tag{C.11}
$$

Hence $\beta = P\cdot q/[(n-2)\hat{P}^2]$ and defining $\tilde{T}_2^{\mu\nu} = \hat{P}^\mu\hat{P}^\nu/(P\cdot q)$:

$$
\boxed{\mathcal{P}^{\mu\nu}_{(F_1)} = \frac{1}{n-2}\left(T_1^{\mu\nu} + \frac{P\cdot q}{\hat{P}^2}\,\tilde{T}_2^{\mu\nu}\right) = \frac{1}{n-2}\left(-g^{\mu\nu} - \frac{q^\mu q^\nu}{Q^2} + \frac{\hat{P}^\mu\hat{P}^\nu}{\hat{P}^2}\right)}
\tag{C.12}
$$

Verification:

$$
\begin{aligned}
\mathcal{P}^{\mu\nu}_{(F_1)}W^{(S)}_{\mu\nu} &= \frac{1}{n-2}\left[F_1(n-1) - \frac{\hat{P}^2}{P\cdot q}\cdot\frac{P\cdot q}{\hat{P}^2}\cdot F_2 - F_1\hat{P}^2\cdot\frac{1}{\hat{P}^2} + F_2\frac{\hat{P}^4}{(P\cdot q)^2}\cdot\frac{P\cdot q}{\hat{P}^2}\cdot\frac{1}{P\cdot q}\right] \\
&= \frac{1}{n-2}\left[F_1(n-1) - F_2 - F_1 + F_2\right] = \frac{F_1(n-2)}{n-2} = F_1
\end{aligned}
\tag{C.13}
$$

At $n = 4$: $\mathcal{P}^{\mu\nu}_{(F_1)} = \frac{1}{2}\left(-g^{\mu\nu} - q^\mu q^\nu/Q^2 + \hat{P}^\mu \hat{P}^\nu/\hat{P}^2\right)$.

C.1.4 Projector for F_2

We want $\mathcal{P}^{\mu\nu}_{(F_2)}$ to give F_2 and kill F_1.

Condition to kill F_1:

$$\alpha(n-1) - \beta\hat{P}^2 = 0 \implies \beta = \frac{\alpha(n-1)}{\hat{P}^2} \tag{C.14}$$

Condition to normalize F_2:

$$-\frac{\alpha\hat{P}^2}{P\cdot q} + \beta\frac{\hat{P}^4}{(P\cdot q)^2} = 1 \implies -\frac{\alpha\hat{P}^2}{P\cdot q} + \frac{\alpha(n-1)\hat{P}^2}{(P\cdot q)} = 1 \implies \frac{\alpha\hat{P}^2(n-2)}{P\cdot q} = 1 \implies \alpha = \frac{P\cdot q}{(n-2)\hat{P}^2} \tag{C.15}$$

Hence:

$$\boxed{\mathcal{P}^{\mu\nu}_{(F_2)} = \frac{P\cdot q}{(n-2)\hat{P}^2}\left(T_1^{\mu\nu} + \frac{(n-1)\,\hat{P}^\mu\hat{P}^\nu}{\hat{P}^2}\right)} \tag{C.16}$$

In terms of Q^2, x, M using $P\cdot q = Q^2/2x$ and $\hat{P}^2 = M^2 + Q^2/4x^2$:

$$\alpha = \frac{Q^2/2x}{(n-2)(M^2 + Q^2/4x^2)}, \qquad \beta = \frac{(n-1)Q^2/2x}{(n-2)(M^2 + Q^2/4x^2)^2} \tag{C.17}$$

Massless nucleon limit $M \to 0$:

$$\hat{P}^2 \to \frac{Q^2}{4x^2}, \quad \alpha \to \frac{Q^2/2x}{(n-2)Q^2/4x^2} = \frac{2x}{(n-2)}, \quad \mathcal{P}^{\mu\nu}_{(F_2)} \to \frac{2x}{n-2}\left(T_1^{\mu\nu} + \frac{4x^2(n-1)}{Q^2}\hat{P}^\mu\hat{P}^\nu\right) \tag{C.18}$$

C.1.5 Projector for g_1

The g_1 projector uses the antisymmetric tensor with S instead of P:

$$A_S^{\mu\nu} = \frac{i\,\varepsilon^{\mu\nu\alpha\beta} q_\alpha S_\beta}{P \cdot q} \tag{C.19}$$

Self-contraction of A_S:

$$A_S^{\mu\nu} A_{S\mu\nu} = \frac{2(q^2 S^2 - (S \cdot q)^2)}{(P \cdot q)^2} = \frac{2(-Q^2(-M^2) - (S \cdot q)^2)}{(P \cdot q)^2} = \frac{2(Q^2 M^2 - (S \cdot q)^2)}{(P \cdot q)^2} \tag{C.20}$$

Contraction $A_S^{\mu\nu} W_{\mu\nu}^{(g_1)}$:

$$A_S^{\mu\nu} \cdot \frac{i\varepsilon_{\mu\nu\alpha\beta} q^\alpha S^\beta}{P \cdot q}\, g_1 = \frac{Q^2 M^2 - (S \cdot q)^2}{(P \cdot q)^2} \cdot (-2)\, g_1 \tag{C.21}$$

The g_1 projector:

$$\boxed{\mathcal{P}_{(g_1)}^{\mu\nu} = \frac{-i\,\varepsilon^{\mu\nu\alpha\beta} q_\alpha P_\beta}{(n-2)(n-3)\, P \cdot q}} \tag{C.22}$$

C.1.6 Verification: $\mathcal{P}_{(F_1)}$ kills F_2 and vice versa

To ensure the consistency of the projection operators, we verify their orthogonality by applying them to the corresponding hadronic tensors.

$\mathcal{P}_{(F_1)}$ applied to $W^{(F_2)}$:

$$\begin{aligned}
\mathcal{P}_{(F_1)}^{\mu\nu} \cdot \frac{\hat{P}_\mu \hat{P}_\nu}{P \cdot q} &= \frac{1}{n-2} \left(T_1^{\mu\nu} + \frac{P \cdot q}{\hat{P}^2} \tilde{T}_2^{\mu\nu} \right) \frac{\hat{P}_\mu \hat{P}_\nu}{P \cdot q} \\
&= \frac{1}{n-2} \left(\frac{T_1^{\mu\nu} \hat{P}_\mu \hat{P}_\nu}{P \cdot q} + \frac{\hat{P}^4}{(P \cdot q)\hat{P}^2} \right) \\
&= \frac{1}{n-2} \left(\frac{-\hat{P}^2}{P \cdot q} + \frac{\hat{P}^2}{P \cdot q} \right) = 0
\end{aligned} \tag{C.23}$$

$\mathcal{P}_{(F_2)}$ **applied to** $W^{(F_1)} = T_{1\mu\nu}F_1$**:**

$$
\begin{aligned}
\mathcal{P}^{\mu\nu}_{(F_2)} \cdot T_{1\mu\nu} &= \frac{P\cdot q}{(n-2)\hat{P}^2}\left(T_1^{\mu\nu}T_{1\mu\nu} + \frac{(n-1)}{\hat{P}^2}\hat{P}^\mu\hat{P}^\nu T_{1\mu\nu}\right)\\
&= \frac{P\cdot q}{(n-2)\hat{P}^2}\left((n-1) + \frac{(n-1)(-\hat{P}^2)}{\hat{P}^2}\right)\\
&= \frac{P\cdot q}{(n-2)\hat{P}^2}\cdot(n-1)(1-1) = 0
\end{aligned}
\tag{C.24}
$$

C.1.7 Complete projector table

SF	Projector $\mathcal{P}^{\mu\nu}$	Type
F_1	$\frac{1}{n-2}\left(-g^{\mu\nu} - \frac{q^\mu q^\nu}{Q^2} + \frac{\hat{P}^\mu\hat{P}^\nu}{\hat{P}^2}\right)$	Symmetric
F_2	$\frac{P\cdot q}{(n-2)\hat{P}^2}\left(-g^{\mu\nu} - \frac{q^\mu q^\nu}{Q^2} + \frac{(n-1)\hat{P}^\mu\hat{P}^\nu}{\hat{P}^2}\right)$	Symmetric
g_1	$\frac{-i\,\varepsilon^{\mu\nu\alpha\beta}q_\alpha P_\beta}{(n-2)(n-3)\,P\cdot q}$	Antisymmetric

The projectors presented here are valid in $n = 4 + \varepsilon$ dimensions, which is essential for their use within dimensional regularization. At $n = 4$ they reduce to the familiar four-dimensional expressions, but the n-dimensional forms must be retained throughout the intermediate steps of the calculation to correctly capture the ε-dependent terms that contribute after mass factorization. The splitting functions that enter the mass factorization kernels $(\Delta)\Gamma$ are listed in Appendix D.

Appendix D

Splitting Functions

Contents

This appendix collects the space-like unpolarised and polarised and time-like unpolarised splitting functions that enter the mass factorization procedure and the transformation between renormalization schemes. The splitting functions are organized according to their perturbative order in the strong coupling a_s and the electromagnetic coupling a_e, with the superscript notation $P^{(i,j)}$ denoting i powers of a_s and j powers of a_e. We list separately the unpolarized space-like splitting functions in Section D.1, the polarized space-like splitting functions in Section D.2, and the time-like unpolarized splitting functions in Section D.3. The appendix concludes with the finite renormalization constants Z_{ab} that govern the transformation of splitting and coefficient functions from the Larin scheme to the $\overline{\text{MS}}$ scheme. These quantities enter directly into the construction of the physical coefficient functions discussed in the main text. The sector decomposition identities used in evaluating the phase-space integrals over these kernels are presented in Appendix E.

D.1 Space-like Unpolarised Splitting Functions

$$P_{gg}^{(1,0)} = C_A\left\{ -16 + \frac{22}{3}\delta(1-x) + \frac{8}{1-x} + \frac{8}{x} + 8x - 8x^2 \right\} - \frac{8}{3}\delta(1-x)\, n_F T_F \tag{D.1}$$

$$P_{gq}^{(1,0)} = C_F\left\{ -8 + \frac{8}{x} + 4x \right\} \tag{D.2}$$

$$P_{qg}^{(1,0)} = \left\{ 2 - 4x + 4x^2 \right\} \tag{D.3}$$

$$P_{qq}^{(1,0)} = C_F\left\{ -4 + 6\delta(1-x) + \frac{8}{1-x} - 4x \right\} \tag{D.4}$$

$$P_{\gamma\gamma}^{(0,1)} = \sum e_f^2\left\{ -\frac{8}{3}\delta(1-x) \right\} \tag{D.5}$$

$$P_{\gamma q}^{(0,1)} = e_q^2\left\{ -8 + \frac{8}{x} + 4x \right\} \tag{D.6}$$

$$P_{q\gamma}^{(0,1)} = e_q^2 N\left\{ 4 - 8x + 8x^2 \right\} \tag{D.7}$$

$$P_{qq}^{(0,1)} = e_q^2\left\{ -4 + 6\delta(1-x) + \frac{8}{1-x} - 4x \right\} \tag{D.8}$$

$$\begin{aligned} P_{qg}^{(1,1)} = e_q^2 \Big\{ & 28 - 58x + 40x^2 - 8\zeta_2 + 16x\zeta_2 - 16x^2\zeta_2 + 16x\ln(1-x) - 16x^2\ln(1-x) \\ & + 4\ln^2(1-x) - 8x\ln^2(1-x) + 8x^2\ln^2(1-x) + 6\ln x - 8x\ln x + 16x^2\ln x \\ & - 8\ln(1-x)\ln x + 16x\ln(1-x)\ln x - 16x^2\ln(1-x)\ln x + 2\ln^2 x - 4x\ln^2 x \end{aligned}$$

$$+ 8x^2 \ln^2 x \Big\} \tag{D.9}$$

$$\begin{aligned} P_{q\gamma}^{(1,1)} = C_F e_q^2 N \Big\{ & 56 - 116x + 80x^2 - 16\zeta_2 + 32x\zeta_2 - 32x^2\zeta_2 + 32x\ln(1-x) - 32x^2\ln(1-x) \\ & + 8\ln^2(1-x) - 16x\ln^2(1-x) + 16x^2\ln^2(1-x) + 12\ln x - 16x\ln x + 32x^2\ln x \\ & - 16\ln(1-x)\ln x + 32x\ln(1-x)\ln x - 32x^2\ln(1-x)\ln x + 4\ln^2 x - 8x\ln^2 x \\ & + 16x^2\ln^2 x \Big\} \end{aligned} \tag{D.10}$$

$$\begin{aligned} P_{qq,\mathrm{NS}}^{(1,1)} = C_F e_q^2 \Big\{ & -80 + 6\delta(1-x) + 80x - 48\delta(1-x)\zeta_2 + 96\delta(1-x)\zeta_3 - \frac{48\ln x}{1-x} - 32x\ln x \\ & + 32\ln(1-x)\ln x - \frac{64\ln(1-x)\ln x}{1-x} + 32x\ln(1-x)\ln x - 8\ln^2 x - 8x\ln^2 x \Big\} \end{aligned} \tag{D.11}$$

$$\begin{aligned} P_{q\bar{q}}^{(1,1)} = C_F e_q^2 \Big\{ & 64 - 64x + 32\zeta_2 - 32x\zeta_2 - \frac{64\zeta_2}{1+x} + 64\mathrm{Li}_2(-x) - 64x\mathrm{Li}_2(-x) - \frac{128\mathrm{Li}_2(-x)}{1+x} \\ & + 32\ln x + 32x\ln x - 16\ln^2 x + 16x\ln^2 x + \frac{32\ln^2 x}{1+x} + 64\ln x\ln(1+x) \\ & - 64x\ln x\ln(1+x) - \frac{128\ln x\ln(1+x)}{1+x} \Big\} \end{aligned} \tag{D.12}$$

$$P_{qq,S}^{(1,1)} = 0 \tag{D.13}$$

$$\begin{aligned} P_{qg}^{(2,0)} = C_F \Big\{ & 28 - 58x + 40x^2 - 8\zeta_2 + 16x\zeta_2 - 16x^2\zeta_2 + 16x\ln(1-x) - 16x^2\ln(1-x) \\ & + 4\ln^2(1-x) - 8x\ln^2(1-x) + 8x^2\ln^2(1-x) + 6\ln x - 8x\ln x + 16x^2\ln x \\ & - 8\ln(1-x)\ln x + 16x\ln(1-x)\ln x - 16x^2\ln(1-x)\ln x + 2\ln^2 x - 4x\ln^2 x \\ & + 8x^2\ln^2 x \Big\} + C_A \Big\{ -8 + \frac{80}{9x} + 100x - \frac{872}{9}x^2 - 16x\zeta_2 - 8\mathrm{Li}_2(-x) - 16x\mathrm{Li}_2(-x) \\ & - 16x^2\mathrm{Li}_2(-x) - 16x\ln(1-x) + 16x^2\ln(1-x) - 4\ln^2(1-x) + 8x\ln^2(1-x) \end{aligned}$$

$$- 8x^2\ln^2(1-x) + 4\ln x + 32x\ln x + \frac{176}{3}x^2\ln x - 4\ln^2 x - 8x\ln^2 x - 8\ln x\ln(1+x)$$

$$- 16x\ln x\ln(1+x) - 16x^2\ln x\ln(1+x)\Bigg\} \tag{D.14}$$

$$P_{qq,\mathrm{NS}}^{(2,0)} = C_F n_F T_F\Bigg\{ -\frac{16}{9} - \frac{4}{3}\delta(1-x) - \frac{160}{9(1-x)} + \frac{176}{9}x - \frac{32}{3}\delta(1-x)\zeta_2 + \frac{16}{3}\ln x - \frac{32\ln x}{3(1-x)}$$

$$+ \frac{16}{3}x\ln x\Bigg\} + C_F^2\Bigg\{ -40 + 3\delta(1-x) + 40x - 24\delta(1-x)\zeta_2 + 48\delta(1-x)\zeta_3 - \frac{24\ln x}{1-x}$$

$$- 16x\ln x + 16\ln(1-x)\ln x - \frac{32\ln(1-x)\ln x}{1-x} + 16x\ln(1-x)\ln x - 4\ln^2 x - 4x\ln^2 x\Bigg\}$$

$$+ C_A C_F\Bigg\{ -\frac{316}{9} + \frac{17}{3}\delta(1-x) + \frac{536}{9(1-x)} - \frac{220}{9}x + 8\zeta_2 + \frac{88}{3}\delta(1-x)\zeta_2 - \frac{16\zeta_2}{1-x} + 8x\zeta_2$$

$$- 24\delta(1-x)\zeta_3 - \frac{20}{3}\ln x + \frac{88\ln x}{3(1-x)} - \frac{20}{3}x\ln x - 4\ln^2 x + \frac{8\ln^2 x}{1-x} - 4x\ln^2 x\Bigg\} \tag{D.15}$$

$$P_{q\bar{q}}^{(2,0)} = C_F^2\Bigg\{ 32 - 32x + 16\zeta_2 - 16x\zeta_2 - \frac{32\zeta_2}{1+x} + 32\mathrm{Li}_2(-x) - 32x\mathrm{Li}_2(-x) - \frac{64\mathrm{Li}_2(-x)}{1+x}$$

$$+ 16\ln x + 16x\ln x - 8\ln^2 x + 8x\ln^2 x + \frac{16\ln^2 x}{1+x} + 32\ln x\ln(1+x) - 32x\ln x\ln(1+x)$$

$$- \frac{64\ln x\ln(1+x)}{1+x}\Bigg\} + C_A C_F\Bigg\{ -16 + 16x - 8\zeta_2 + 8x\zeta_2 + \frac{16\zeta_2}{1+x} - 16\mathrm{Li}_2(-x) + 16x\mathrm{Li}_2(-x)$$

$$+ \frac{32\mathrm{Li}_2(-x)}{1+x} - 8\ln x - 8x\ln x + 4\ln^2 x - 4x\ln^2 x - \frac{8\ln^2 x}{1+x} - 16\ln x\ln(1+x)$$

$$+ 16x\ln x\ln(1+x) + \frac{32\ln x\ln(1+x)}{1+x}\Bigg\} \tag{D.16}$$

$$P_{qq,S}^{(2,0)} = C_F\Bigg\{ -8 + \frac{80}{9x} + 24x - \frac{224}{9}x^2 + 4\ln x + 20x\ln x + \frac{32}{3}x^2\ln x - 4\ln^2 x - 4x\ln^2 x\Bigg\} \tag{D.17}$$

$$P_{q\gamma}^{(0,2)} = e_q^4 N\Bigg\{ 56 - 116x + 80x^2 - 16\zeta_2 + 32x\zeta_2 - 32x^2\zeta_2 + 32x\ln(1-x) - 32x^2\ln(1-x)$$

$$+ 8\ln^2(1-x) - 16x\ln^2(1-x) + 16x^2\ln^2(1-x) + 12\ln x - 16x\ln x + 32x^2\ln x$$

$$-16\ln(1-x)\ln x+32x\ln(1-x)\ln x-32x^2\ln(1-x)\ln x+4\ln^2 x-8x\ln^2 x+16x^2\ln^2 x\Bigg\}$$

(D.18)

$$P^{(0,2)}_{qq,\mathrm{NS}}=e_q^2\sum e_f^2\Bigg\{-\frac{16}{9}-\frac{4}{3}\delta(1-x)-\frac{160}{9(1-x)}+\frac{176}{9}x-\frac{32}{3}\delta(1-x)\zeta_2+\frac{16}{3}\ln x-\frac{32\ln x}{3(1-x)}$$
$$+\frac{16}{3}x\ln x\Bigg\}+e_q^4\Bigg\{-40+3\delta(1-x)+40x-24\delta(1-x)\zeta_2+48\delta(1-x)\zeta_3-\frac{24\ln x}{1-x}$$
$$-16x\ln x+16\ln(1-x)\ln x-\frac{32\ln(1-x)\ln x}{1-x}+16x\ln(1-x)\ln x-4\ln^2 x-4x\ln^2 x\Bigg\}$$

(D.19)

$$P^{(0,2)}_{q\bar{q}}=e_q^4\Bigg\{32-32x+16\zeta_2-16x\zeta_2-\frac{32\zeta_2}{1+x}+32\mathrm{Li}_2(-x)-32x\mathrm{Li}_2(-x)-\frac{64\mathrm{Li}_2(-x)}{1+x}$$
$$+16\ln x+16x\ln x-8\ln^2 x+8x\ln^2 x+\frac{16\ln^2 x}{1+x}+32\ln x\ln(1+x)-32x\ln x\ln(1+x)$$
$$-\frac{64\ln x\ln(1+x)}{1+x}\Bigg\} \tag{D.20}$$

$$P^{(0,2)}_{qq,S}=e_q^4N\Bigg\{-16+\frac{160}{9x}+48x-\frac{448}{9}x^2+8\ln x+40x\ln x+\frac{64}{3}x^2\ln x-8\ln^2 x-8x\ln^2 x\Bigg\}$$

(D.21)

D.2 Space-like Polarised Splitting Functions

$$\Delta P^{(1,0)}_{gg}=C_A\Bigg\{8+\frac{22}{3}\delta(1-x)+\frac{8}{1-x}-16x\Bigg\}-\frac{8}{3}\delta(1-x)\,n_FT_F \tag{D.22}$$

$$\Delta P^{(1,0)}_{gq}=C_F\Bigg\{8-4x\Bigg\} \tag{D.23}$$

$$\Delta P^{(1,0)}_{qg}=\Bigg\{-2+4x\Bigg\} \tag{D.24}$$

$$\Delta P_{qq}^{(1,0)} = C_F\left\{-4 + 6\delta(1-x) + \frac{8}{1-x} - 4x\right\} \tag{D.25}$$

$$\Delta P_{\gamma\gamma}^{(0,1)} = \sum e_f^2\left\{-\frac{8}{3}\delta(1-x)\right\} \tag{D.26}$$

$$\Delta P_{\gamma q}^{(0,1)} = e_q^2\left\{8 - 4x\right\} \tag{D.27}$$

$$\Delta P_{q\gamma}^{(0,1)} = e_q^2 N\left\{-4 + 8x\right\} \tag{D.28}$$

$$\Delta P_{qq}^{(0,1)} = e_q^2\left\{-4 + 6\delta(1-x) + \frac{8}{1-x} - 4x\right\} \tag{D.29}$$

$$\begin{aligned}\Delta P_{qg}^{(1,1)} = e_q^2\Big\{&4 + 6x + 8\zeta_2 - 16x\zeta_2 + 16\ln(1-x) - 16x\ln(1-x) - 4\ln^2(1-x) + 8x\ln^2(1-x)\\ &- 2\ln x + 32x\ln x + 8\ln(1-x)\ln x - 16x\ln(1-x)\ln x - 2\ln^2 x + 4x\ln^2 x\Big\}\end{aligned} \tag{D.30}$$

$$\begin{aligned}\Delta P_{q\gamma}^{(1,1)} = C_F e_q^2 N\Big\{&8 + 12x + 16\zeta_2 - 32x\zeta_2 + 32\ln(1-x) - 32x\ln(1-x) - 8\ln^2(1-x)\\ &+ 16x\ln^2(1-x) - 4\ln x + 64x\ln x + 16\ln(1-x)\ln x - 32x\ln(1-x)\ln x - 4\ln^2 x\\ &+ 8x\ln^2 x\Big\}\end{aligned} \tag{D.31}$$

$$\begin{aligned}\Delta P_{qq,\mathrm{NS}}^{(1,1)} = C_F e_q^2\Big\{&-80 + 6\delta(1-x) + 80x - 48\delta(1-x)\zeta_2 + 96\delta(1-x)\zeta_3 - \frac{48\ln x}{1-x} - 32x\ln x\\ &+ 32\ln(1-x)\ln x - \frac{64\ln(1-x)\ln x}{1-x} + 32x\ln(1-x)\ln x - 8\ln^2 x - 8x\ln^2 x\Big\}\end{aligned} \tag{D.32}$$

$$\begin{aligned}\Delta P_{q\bar{q}}^{(1,1)} = C_F e_q^2\Big\{&-64 + 64x - 32\zeta_2 + 32x\zeta_2 + \frac{64\zeta_2}{1+x} - 64\mathrm{Li}_2(-x) + 64x\mathrm{Li}_2(-x) + \frac{128\mathrm{Li}_2(-x)}{1+x}\\ &- 32\ln x - 32x\ln x + 16\ln^2 x - 16x\ln^2 x - \frac{32\ln^2 x}{1+x} - 64\ln x\ln(1+x) + 64x\ln x\ln(1+x)\end{aligned}$$

$$+\left.\frac{128\ln x\ln(1+x)}{1+x}\right\} \tag{D.33}$$

$$\varDelta P^{(1,1)}_{qq,S} = 0 \tag{D.34}$$

$$\begin{aligned}\varDelta P^{(2,0)}_{qg} = C_F\Big\{&4+6x+8\zeta_2-16x\zeta_2+16\ln(1-x)-16x\ln(1-x)-4\ln^2(1-x)+8x\ln^2(1-x)\\&-2\ln x+32x\ln x+8\ln(1-x)\ln x-16x\ln(1-x)\ln x-2\ln^2 x+4x\ln^2 x\Big\}\\&+C_A\Big\{48-44x-8\zeta_2-8\mathrm{Li}_2(-x)-16x\mathrm{Li}_2(-x)-16\ln(1-x)+16x\ln(1-x)\\&+4\ln^2(1-x)-8x\ln^2(1-x)+4\ln x+32x\ln x-4\ln^2 x-8x\ln^2 x-8\ln x\ln(1+x)\\&-16x\ln x\ln(1+x)\Big\}\end{aligned} \tag{D.35}$$

$$\begin{aligned}\varDelta P^{(2,0)}_{qq,\mathrm{NS}} = C_F n_F T_F\Big\{&\frac{176}{9}-\frac{4}{3}\delta(1-x)-\frac{160}{9(1-x)}-\frac{16}{9}x-\frac{32}{3}\delta(1-x)\zeta_2+\frac{16}{3}\ln x-\frac{32\ln x}{3(1-x)}\\&+\frac{16}{3}x\ln x\Big\}+C_F^2\Big\{-40+3\delta(1-x)+40x-24\delta(1-x)\zeta_2+48\delta(1-x)\zeta_3-\frac{24\ln x}{1-x}\\&-16x\ln x+16\ln(1-x)\ln x-\frac{32\ln(1-x)\ln x}{1-x}+16x\ln(1-x)\ln x-4\ln^2 x-4x\ln^2 x\Big\}\\&+C_AC_F\Big\{\frac{212}{9}+\frac{17}{3}\delta(1-x)+\frac{536}{9(1-x)}-\frac{748}{9}x+8\zeta_2+\frac{88}{3}\delta(1-x)\zeta_2-\frac{16\zeta_2}{1-x}+8x\zeta_2\\&-24\delta(1-x)\zeta_3-\frac{20}{3}\ln x+\frac{88\ln x}{3(1-x)}-\frac{20}{3}x\ln x-4\ln^2 x+\frac{8\ln^2 x}{1-x}-4x\ln^2 x\Big\}\end{aligned} \tag{D.36}$$

$$\begin{aligned}\varDelta P^{(2,0)}_{q\bar{q}} = C_AC_F\Big\{&16-16x+8\zeta_2-8x\zeta_2-\frac{16\zeta_2}{1+x}+16\mathrm{Li}_2(-x)-16x\mathrm{Li}_2(-x)-\frac{32\mathrm{Li}_2(-x)}{1+x}\\&+8\ln x+8x\ln x-4\ln^2 x+4x\ln^2 x+\frac{8\ln^2 x}{1+x}+16\ln x\ln(1+x)-16x\ln x\ln(1+x)\\&-\frac{32\ln x\ln(1+x)}{1+x}\Big\}+C_F^2\Big\{-32+32x-16\zeta_2+16x\zeta_2+\frac{32\zeta_2}{1+x}-32\mathrm{Li}_2(-x)+32x\mathrm{Li}_2(-x)\\&+\frac{64\mathrm{Li}_2(-x)}{1+x}-16\ln x-16x\ln x+8\ln^2 x-8x\ln^2 x-\frac{16\ln^2 x}{1+x}-32\ln x\ln(1+x)\end{aligned}$$

$$+ 32x\ln x\ln(1+x) + \frac{64\ln x\ln(1+x)}{1+x}\Bigg\} \tag{D.37}$$

$$\Delta P^{(2,0)}_{qq,S} = C_F\Bigg\{4 - 4x - 4\ln x + 12x\ln x - 4\ln^2 x - 4x\ln^2 x\Bigg\} \tag{D.38}$$

$$\Delta P^{(0,2)}_{q\gamma} = e_q^4 N\Bigg\{8 + 12x + 16\zeta_2 - 32x\zeta_2 + 32\ln(1-x) - 32x\ln(1-x) - 8\ln^2(1-x) + 16x\ln^2(1-x)$$
$$- 4\ln x + 64x\ln x + 16\ln(1-x)\ln x - 32x\ln(1-x)\ln x - 4\ln^2 x + 8x\ln^2 x\Bigg\} \tag{D.39}$$

$$\Delta P^{(0,2)}_{qq,\mathrm{NS}} = e_q^2\sum e_f^2\Bigg\{\frac{176}{9} - \frac{4}{3}\delta(1-x) - \frac{160}{9(1-x)} - \frac{16}{9}x - \frac{32}{3}\delta(1-x)\zeta_2 + \frac{16}{3}\ln x - \frac{32\ln x}{3(1-x)}$$
$$+ \frac{16}{3}x\ln x\Bigg\} + e_q^4\Bigg\{-40 + 3\delta(1-x) + 40x - 24\delta(1-x)\zeta_2 + 48\delta(1-x)\zeta_3 - \frac{24\ln x}{1-x}$$
$$- 16x\ln x + 16\ln(1-x)\ln x - \frac{32\ln(1-x)\ln x}{1-x} + 16x\ln(1-x)\ln x - 4\ln^2 x - 4x\ln^2 x\Bigg\} \tag{D.40}$$

$$\Delta P^{(0,2)}_{q\bar{q}} = e_q^4\Bigg\{-32 + 32x - 16\zeta_2 + 16x\zeta_2 + \frac{32\zeta_2}{1+x} - 32\mathrm{Li}_2(-x) + 32x\mathrm{Li}_2(-x) + \frac{64\mathrm{Li}_2(-x)}{1+x}$$
$$- 16\ln x - 16x\ln x + 8\ln^2 x - 8x\ln^2 x - \frac{16\ln^2 x}{1+x} - 32\ln x\ln(1+x) + 32x\ln x\ln(1+x)$$
$$+ \frac{64\ln x\ln(1+x)}{1+x}\Bigg\} \tag{D.41}$$

$$\Delta P^{(0,2)}_{qq,S} = e_q^4 N\Bigg\{8 - 8x - 8\ln x + 24x\ln x - 8\ln^2 x - 8x\ln^2 x\Bigg\} \tag{D.42}$$

D.3 Time-like Unpolarised Splitting Functions

$$\tilde{P}^{(1,0)}_{gg} = C_A\Bigg\{-16 + \frac{22}{3}\delta(1-z) + \frac{8}{1-z} + \frac{8}{z} + 8z - 8z^2\Bigg\} - \frac{8}{3}\delta(1-z)\,n_F T_F \tag{D.43}$$

$$\tilde{P}_{gq}^{(1,0)} = C_F\left\{ -8 + \frac{8}{z} + 4z \right\} \tag{D.44}$$

$$\tilde{P}_{qg}^{(1,0)} = \left\{ 2 - 4z + 4z^2 \right\} \tag{D.45}$$

$$\tilde{P}_{qq}^{(1,0)} = C_F\left\{ -4 + 6\delta(1-z) + \frac{8}{1-z} - 4z \right\} \tag{D.46}$$

$$\tilde{P}_{\gamma\gamma}^{(0,1)} = \sum e_f^2\left\{ -\frac{8}{3}\delta(1-z) \right\} \tag{D.47}$$

$$\tilde{P}_{\gamma q}^{(0,1)} = e_q^2\left\{ -8 + \frac{8}{z} + 4z \right\} \tag{D.48}$$

$$\tilde{P}_{q\gamma}^{(0,1)} = e_q^2 N\left\{ 4 - 8z + 8z^2 \right\} \tag{D.49}$$

$$\tilde{P}_{qq}^{(0,1)} = e_q^2\left\{ -4 + 6\delta(1-z) + \frac{8}{1-z} - 4z \right\} \tag{D.50}$$

$$\begin{aligned}\tilde{P}_{gq}^{(1,1)} = C_F e_q^2\Bigg\{ & -4 + 128\zeta_2 - \frac{128\zeta_2}{z} - 64\zeta_2 z + 36z - 128\mathrm{Li}_2(1-z) + \frac{128\mathrm{Li}_2(1-z)}{z} + 64z\mathrm{Li}_2(1-z) \\ & + 16z\ln(1-z) - 16\ln^2(1-z) + \frac{16\ln^2(1-z)}{z} + 8z\ln^2(1-z) - 64\ln z + 4z\ln z \\ & - 64\ln(1-z)\ln z + \frac{64\ln(1-z)\ln z}{z} + 32z\ln(1-z)\ln z + 8\ln^2 z - 4z\ln^2 z \Bigg\}\end{aligned} \tag{D.51}$$

$$\begin{aligned}\tilde{P}_{\gamma q}^{(1,1)} = C_F e_q^2\Bigg\{ & -4 + 128\zeta_2 - \frac{128\zeta_2}{z} - 64\zeta_2 z + 36z - 128\mathrm{Li}_2(1-z) + \frac{128\mathrm{Li}_2(1-z)}{z} + 64z\mathrm{Li}_2(1-z) \\ & + 16z\ln(1-z) - 16\ln^2(1-z) + \frac{16\ln^2(1-z)}{z} + 8z\ln^2(1-z) - 64\ln z + 4z\ln z \\ & - 64\ln(1-z)\ln z + \frac{64\ln(1-z)\ln z}{z} + 32z\ln(1-z)\ln z + 8\ln^2 z - 4z\ln^2 z \Bigg\}\end{aligned} \tag{D.52}$$

$$\tilde{P}_{qq,\mathrm{NS}}^{(1,1)} = C_F e_q^2\Bigg\{ -80 + 6\delta(1-z) - 48\delta(1-z)\zeta_2 + 96\delta(1-z)\zeta_3 + 80z - 80\ln z + \frac{48\ln z}{1-z} - 48z\ln z$$

$$- 32\ln(1-z)\ln z + \frac{64\ln(1-z)\ln z}{1-z} - 32z\ln(1-z)\ln z + 40\ln^2 z - \frac{64\ln^2 z}{1-z} + 40z\ln^2 z\Bigg\} \tag{D.53}$$

$$\tilde{P}^{(1,1)}_{q\bar{q}} = C_F e_q^2 \Bigg\{ 64 + 32\zeta_2 - 64z - 32\zeta_2 z - \frac{64\zeta_2}{1+z} + 64\mathrm{Li}_2(-z) - 64z\mathrm{Li}_2(-z) - \frac{128\mathrm{Li}_2(-z)}{1+z}$$
$$+ 32\ln z + 32z\ln z - 16\ln^2 z + 16z\ln^2 z + \frac{32\ln^2 z}{1+z} + 64\ln z\ln(1+z) - 64z\ln z\ln(1+z)$$
$$- \frac{128\ln z\ln(1+z)}{1+z}\Bigg\} \tag{D.54}$$

$$\tilde{P}^{(1,1)}_{qq,S} = 0 \tag{D.55}$$

$$\tilde{P}^{(2,0)}_{gq} = C_F^2 \Bigg\{ -4 + 128\zeta_2 - \frac{128\zeta_2}{z} - 64\zeta_2 z + 36z - 128\mathrm{Li}_2(1-z) + \frac{128\mathrm{Li}_2(1-z)}{z} + 64z\mathrm{Li}_2(1-z)$$
$$+ 16z\ln(1-z) - 16\ln^2(1-z) + \frac{16\ln^2(1-z)}{z} + 8z\ln^2(1-z) - 64\ln z + 4z\ln z$$
$$- 64\ln(1-z)\ln z + \frac{64\ln(1-z)\ln z}{z} + 32z\ln(1-z)\ln z + 8\ln^2 z - 4z\ln^2 z\Bigg\}$$
$$+ C_A C_F \Bigg\{ 40 - 96\zeta_2 + \frac{136}{9z} + \frac{128\zeta_2}{z} - 8z + 64\zeta_2 z - \frac{352}{9}z^2 + 128\mathrm{Li}_2(1-z) - \frac{128\mathrm{Li}_2(1-z)}{z}$$
$$- 64z\mathrm{Li}_2(1-z) + 32\mathrm{Li}_2(-z) + \frac{32\mathrm{Li}_2(-z)}{z} + 16z\mathrm{Li}_2(-z) - 16z\ln(1-z) + 16\ln^2(1-z)$$
$$- \frac{16\ln^2(1-z)}{z} - 8z\ln^2(1-z) + 64\ln z - \frac{48\ln z}{z} + 72z\ln z + \frac{64}{3}z^2\ln z + 32\ln(1-z)\ln z$$
$$- \frac{32\ln(1-z)\ln z}{z} - 16z\ln(1-z)\ln z - 16\ln^2 z - \frac{32\ln^2 z}{z} - 24z\ln^2 z + 32\ln z\ln(1+z)$$
$$+ \frac{32\ln z\ln(1+z)}{z} + 16z\ln z\ln(1+z)\Bigg\} \tag{D.56}$$

$$\tilde{P}^{(2,0)}_{qq,\mathrm{NS}} = C_F n_F T_F \Bigg\{ -\frac{16}{9} - \frac{4}{3}\delta(1-z) - \frac{32}{3}\delta(1-z)\zeta_2 - \frac{160}{9(1-z)} + \frac{176}{9}z + \frac{16}{3}\ln z - \frac{32\ln z}{3(1-z)} + \frac{16}{3}z\ln z\Bigg\}$$
$$+ C_A C_F \Bigg\{ \frac{212}{9} + \frac{17}{3}\delta(1-z) + 8\zeta_2 + \frac{88}{3}\delta(1-z)\zeta_2 - 24\delta(1-z)\zeta_3 + \frac{536}{9(1-z)} - \frac{16\zeta_2}{1-z} - \frac{748}{9}z$$
$$+ 8\zeta_2 z - \frac{20}{3}\ln z + \frac{88\ln z}{3(1-z)} - \frac{20}{3}z\ln z - 4\ln^2 z + \frac{8\ln^2 z}{1-z} - 4z\ln^2 z\Bigg\}$$

$$
+ C_F^2 \left\{ -40 + 3\delta(1-z) - 24\delta(1-z)\zeta_2 + 48\delta(1-z)\zeta_3 + 40z - 40\ln z + \frac{24\ln z}{1-z} - 24z\ln z \right.
$$

$$
\left. - 16\ln(1-z)\ln z + \frac{32\ln(1-z)\ln z}{1-z} - 16z\ln(1-z)\ln z + 20\ln^2 z - \frac{32\ln^2 z}{1-z} + 20z\ln^2 z \right\}
$$

(D.57)

$$
\tilde{P}_{q\bar{q}}^{(2,0)} = C_F^2 \left\{ 32 + 16\zeta_2 - 32z - 16\zeta_2 z - \frac{32\zeta_2}{1+z} + 32\mathrm{Li}_2(-z) - 32z\mathrm{Li}_2(-z) - \frac{64\mathrm{Li}_2(-z)}{1+z} \right.
$$

$$
+ 16\ln z + 16z\ln z - 8\ln^2 z + 8z\ln^2 z + \frac{16\ln^2 z}{1+z} + 32\ln z\ln(1+z) - 32z\ln z\ln(1+z)
$$

$$
\left. - \frac{64\ln z\ln(1+z)}{1+z} \right\} + C_A C_F \left\{ -16 - 8\zeta_2 + 16z + 8\zeta_2 z + \frac{16\zeta_2}{1+z} - 16\mathrm{Li}_2(-z) + 16z\mathrm{Li}_2(-z) \right.
$$

$$
+ \frac{32\mathrm{Li}_2(-z)}{1+z} - 8\ln z - 8z\ln z + 4\ln^2 z - 4z\ln^2 z - \frac{8\ln^2 z}{1+z} - 16\ln z\ln(1+z) + 16z\ln z\ln(1+z)
$$

$$
\left. + \frac{32\ln z\ln(1+z)}{1+z} \right\} \tag{D.58}
$$

$$
\tilde{P}_{qq,S}^{(2,0)} = C_F \left\{ -32 - \frac{80}{9z} + 16z + \frac{224}{9}z^2 - 20\ln z - 36z\ln z - \frac{32}{3}z^2\ln z + 4\ln^2 z + 4z\ln^2 z \right\}
$$

(D.59)

$$
\tilde{P}_{\gamma q}^{(0,2)} = e_q^4 \left\{ -4 + 128\zeta_2 - \frac{128\zeta_2}{z} - 64\zeta_2 z + 36z - 128\mathrm{Li}_2(1-z) + \frac{128\mathrm{Li}_2(1-z)}{z} + 64z\mathrm{Li}_2(1-z) \right.
$$

$$
+ 16z\ln(1-z) - 16\ln^2(1-z) + \frac{16\ln^2(1-z)}{z} + 8z\ln^2(1-z)
$$

$$
\left. - 64\ln z + 4z\ln z - 64\ln(1-z)\ln z + \frac{64\ln(1-z)\ln z}{z} + 32z\ln(1-z)\ln z + 8\ln^2 z - 4z\ln^2 z \right\}
$$

(D.60)

$$
\tilde{P}_{qq,\mathrm{NS}}^{(0,2)} = e_q^2 \Sigma e_f^2 \left\{ -\frac{16}{9} - \frac{4}{3}\delta(1-z) - \frac{32}{3}\delta(1-z)\zeta_2 - \frac{160}{9(1-z)} + \frac{176}{9}z + \frac{16}{3}\ln z - \frac{32\ln z}{3(1-z)} + \frac{16}{3}z\ln z \right\}
$$

$$
+ e_q^4 \left\{ -40 + 3\delta(1-z) - 24\delta(1-z)\zeta_2 + 48\delta(1-z)\zeta_3 + 40z - 40\ln z + \frac{24\ln z}{1-z} - 24z\ln z \right.
$$

$$
\left. - 16\ln(1-z)\ln z + \frac{32\ln(1-z)\ln z}{1-z} - 16z\ln(1-z)\ln z + 20\ln^2 z - \frac{32\ln^2 z}{1-z} + 20z\ln^2 z \right\}
$$

(D.61)

$$
\begin{aligned}
\tilde{P}^{(0,2)}_{q\bar{q}} = e_q^4 \Bigg\{ & 32 + 16\zeta_2 - 32z - 16\zeta_2 z - \frac{32\zeta_2}{1+z} + 32\mathrm{Li}_2(-z) - 32z\mathrm{Li}_2(-z) - \frac{64\mathrm{Li}_2(-z)}{1+z} \\
& + 16\ln z + 16z\ln z - 8\ln^2 z + 8z\ln^2 z + \frac{16\ln^2 z}{1+z} + 32\ln z\ln(1+z) - 32z\ln z\ln(1+z) \\
& - \frac{64\ln z\ln(1+z)}{1+z} \Bigg\}
\end{aligned}
\tag{D.62}
$$

$$
\tilde{P}^{(0,2)}_{qq,S} = e_q^4 N \Bigg\{ -64 - \frac{160}{9z} + 32z + \frac{448}{9}z^2 - 40\ln z - 72z\ln z - \frac{64}{3}z^2\ln z + 8\ln^2 z + 8z\ln^2 z \Bigg\}
\tag{D.63}
$$

D.4 Z-Factor

Here, we present the finite renormalization constant Z_{ab} which enters into the transformation of the splitting and coefficient functions from the Larin to $\overline{\mathrm{MS}}$ scheme,

$$
Z^{(i,j)}_{q_\ell q_m} = \delta_{\ell m} Z^{(i,j)}_{qq,V} + Z^{(i,j)}_{qq,S} \quad (i+j \geq 2),
\tag{D.64}
$$

$$
Z^{(i,j)}_{q_\ell \bar{q}_m} = \delta_{\ell m} Z^{(i,j)}_{q\bar{q},V} + Z^{(i,j)}_{qq,S} \quad (i+j \geq 2),
\tag{D.65}
$$

$$
Z^{(i,j)}_{q_\ell \bar{q}_m} = 0 \quad (i+j = 1).
\tag{D.66}
$$

$$
Z^{(1,0)}_{qq} = C_F \Big\{ -8 + 8x \Big\}
\tag{D.67}
$$

$$
Z^{(0,1)}_{qq} = e_q^2 \Big\{ -8 + 8x \Big\}
\tag{D.68}
$$

$$
\begin{aligned}
Z^{(2,0)}_{qQ,V} = C_F^2 \Bigg\{ & 56 - 56x - 16\zeta_2 - 16x\zeta_2 - 32\mathrm{Li}_2(-x) - 32x\mathrm{Li}_2(-x) + 24\ln x + 24x\ln x + 8\ln^2 x + 8x\ln^2 x \\
& - 32\ln x\ln(1+x) - 32x\ln x\ln(1+x) \Bigg\} \\
+ C_A C_F \Bigg\{ & -28 + 28x + 8\zeta_2 + 8x\zeta_2 + 16\mathrm{Li}_2(-x) + 16x\mathrm{Li}_2(-x) - 12\ln x - 12x\ln x \\
& - 4\ln^2 x - 4x\ln^2 x + 16\ln x\ln(1+x) + 16x\ln x\ln(1+x) \Bigg\}
\end{aligned}
\tag{D.69}
$$

$$Z_{qq,V}^{(2,0)} = C_F n_F T_F \left\{ \frac{80}{9} - \frac{80}{9}x + \frac{16}{3}\ln x - \frac{16}{3}x\ln x \right\}$$
$$+ C_F^2 \left\{ -16 + 16x - 16\ln x - 8x\ln x + 16\ln(1-x)\ln x - 16x\ln(1-x)\ln x \right\}$$
$$+ C_A C_F \left\{ -\frac{592}{9} + \frac{592}{9}x + 8\zeta_2 - 8x\zeta_2 - \frac{80}{3}\ln x + \frac{8}{3}x\ln x - 4\ln^2 x + 4x\ln^2 x \right\} \tag{D.70}$$

$$Z_{qq,S}^{(2,0)} = C_F \left\{ 8 - 8x + 12\ln x - 4x\ln x + 4\ln^2 x + 2x\ln^2 x \right\} \tag{D.71}$$

$$Z_{qQ,V}^{(0,2)} = e_q^4 \left\{ 56 - 56x - 16\zeta_2 - 16x\zeta_2 - 32\mathrm{Li}_2(-x) - 32x\mathrm{Li}_2(-x) + 24\ln x + 24x\ln x + 8\ln^2 x \right.$$
$$\left. + 8x\ln^2 x - 32\ln x\ln(1+x) - 32x\ln x\ln(1+x) \right\} \tag{D.72}$$

$$Z_{qq,V}^{(0,2)} = e_q^2 \sum e_f^2 \left\{ \frac{80}{9} - \frac{80}{9}x + \frac{16}{3}\ln x - \frac{16}{3}x\ln x \right\}$$
$$+ e_q^4 \left\{ -16 + 16x - 16\ln x - 8x\ln x + 16\ln(1-x)\ln x - 16x\ln(1-x)\ln x \right\} \tag{D.73}$$

$$Z_{qq,S}^{(0,2)} = e_q^4 N \left\{ 16 - 16x + 24\ln x - 8x\ln x + 8\ln^2 x + 4x\ln^2 x \right\} \tag{D.74}$$

$$Z_{qQ,V}^{(1,1)} = C_F e_q^2 \left\{ 112 - 112x - 32\zeta_2 - 32x\zeta_2 - 64\mathrm{Li}_2(-x) - 64x\mathrm{Li}_2(-x) + 48\ln x + 48x\ln x \right.$$
$$\left. + 16\ln^2 x + 16x\ln^2 x - 64\ln x\ln(1+x) - 64x\ln x\ln(1+x) \right\} \tag{D.75}$$

$$Z_{qq,V}^{(1,1)} = C_F e_q^2 \left\{ -32 + 32x - 32\ln x - 16x\ln x + 32\ln(1-x)\ln x - 32x\ln(1-x)\ln x \right\} \tag{D.76}$$

$$Z_{qq,S}^{(1,1)} = 0 \tag{D.77}$$

The Z-factors listed above complete the set of ingredients required for the scheme transformation. Together with the splitting functions of the preceding sections, they fully determine the mass factorization kernels $(\mathit{\Delta})\mathit{\Gamma}$ and $\tilde{\mathit{\Gamma}}$ at the orders considered in this work. The phase-space integrals over these kernels involve $\mathit{\Theta}$-function constraints whose treatment under dimensional regularization requires a careful $i\delta$ prescription, which is detailed in Appendix E.

Appendix E

Sector Decomposition: $i\delta$ prescription for Θ-functions

Contents

This appendix documents the $i\delta$ prescription used to handle the Θ-function constraints that arise in the phase-space integrals during sector decomposition. In dimensional regularization, products of Θ-functions multiplying singular distributions require a careful analytic continuation to correctly assign the imaginary part of the propagator and resolve the sign ambiguity of the integration variable. The prescription amounts to deforming the argument of each power-law factor by a small imaginary shift $i\delta$, expanding in the sign of the argument using $\Theta(z'-x')$ and $\Theta(x'-z')$, and reading off the phase $(-1 \pm i\varepsilon)^{-\varepsilon/2}$ carried by each sector. We work through seven representative cases that exhaust the distinct kinematic structures encountered in the calculation, presenting the derivation and the final boxed result for each.

E.1 Case (1)

$$\begin{aligned}\left[\frac{z'-x'}{1-x'}\right]^{-\varepsilon/2} &= \left[\frac{z'-x'}{1-x'} + \left\{1 - \frac{i\delta}{1-x'}\right\}\right]^{-\varepsilon/2} \\ &= \left[\left(\frac{z'-x'}{1-x'}\right) + \left\{1 - i\delta\left(\Theta(z'-x') + \Theta(x'-z')\right)\right\}\right]^{-\varepsilon/2}\end{aligned} \tag{E.1}$$

If $z' > x'$:

$$\begin{aligned}&= \left[\left|\frac{z'-x'}{1-x'}\right|(1-i\delta)\right]^{-\varepsilon/2}\Theta(z'-x') \\ &= \left|\frac{z'-x'}{1-x'}\right|^{-\varepsilon/2}\Theta(z'-x')\end{aligned} \tag{E.2}$$

If $x' > z'$:

$$\begin{aligned}&= \left[\left|\frac{x'-z'}{1-x'}\right|(-1+i\delta)\right]^{-\varepsilon/2}\Theta(x'-z') \\ &= \left|\frac{x'-z'}{1-x'}\right|^{-\varepsilon/2}(-1+i\varepsilon)^{-\varepsilon/2}\,\Theta(x'-z')\end{aligned} \tag{E.3}$$

Answer:

$$\boxed{\left|\frac{z'-x'}{1-x'}\right|^{-\varepsilon/2}\left\{\Theta(z'-x') + (-1+i\varepsilon)^{-\varepsilon/2}\,\Theta(x'-z')\right\}} \tag{E.4}$$

E.2 Case (2)

$$\left[\frac{x'-z'}{1-z'}\right]^{-\varepsilon/2} = \left[\left(\frac{x'-z'}{1-z'}\right)\left\{1-\frac{i\delta}{1-z'}\right\}\right]^{-\varepsilon/2}$$
$$= \left[\left(\frac{x'-z'}{1-z'}\right)\{1-i\delta\,(\Theta(z'-x')+\Theta(x'-z'))\}\right]^{-\varepsilon/2} \qquad \text{(E.5)}$$

If $z' > x'$**:**

$$= \left(-\left|\frac{z'-x'}{1-z'}\right|\{1-i\delta\,\Theta(x'-z')\}\right)^{-\varepsilon/2}$$
$$= \left|\frac{z'-x'}{1-z'}\right|^{-\varepsilon/2}(-1+i\varepsilon)^{-\varepsilon/2}\,\Theta(x'-z') \qquad \text{(E.6)}$$

If $x' > z'$**:**

$$= \left(-\left|\frac{x'-z'}{1-z'}\right|\{1-i\delta\}\right)^{-\varepsilon/2}\Theta(z'-z') \qquad \text{(E.7)}$$

Answer:

$$\boxed{\left|\frac{z'-x'}{1-x'}\right|^{-\varepsilon/2}\left[\Theta(z'-x')+(-1+i\varepsilon)^{-\varepsilon/2}\,\Theta(x'-z')\right]} \qquad \text{(E.8)}$$

E.3 Case (3)

$$\left[\frac{z'+x'-1}{z'}\right]^{-\varepsilon/2} = \left[\left(\frac{z'+x'-1}{z'}\right)\left\{1-\frac{i\delta}{z'+x'-1}+\frac{i\delta}{z'}\right\}\right]^{-\varepsilon/2}$$

$$= \left[\left(\frac{z' + x' - 1}{z'} \right) \left\{ 1 + i\delta \left(\frac{x' - 1}{z'(z' + x' - 1)} \right) \right\} \right]^{-\varepsilon/2}$$
$$= \left[\left(\frac{z' + x' - 1}{z'} \right) \{ 1 + i\delta \left(\Theta(z' + x' - 1) \right) + i\delta \left(\Theta(1 - z' - x') \right) \} \right]^{-\varepsilon/2} \tag{E.9}$$

(Note: $(x' - 1)$ and z' are absorbed into δ because $x' - 1 < 0$ and $z' > 0$.)

If $z' + x' - 1 > 0$**:**

$$= \left[\left(\frac{z' + x' - 1}{z'} \right)^{-\varepsilon/2} (1 - i\varepsilon)^{-\varepsilon/2} \, \Theta(z' + x' - 1) \right]$$
$$= \left| \frac{z' + x' - 1}{z'} \right|^{-\varepsilon/2} \Theta(z' + x' - 1) \tag{E.10}$$

If $1 - x' - z' > 0$**:**

$$= \left[- \left(\frac{1 - x' - z'}{z'} \right) \{ 1 + i\delta \} \right]^{-\varepsilon/2} \Theta(1 - z' - x')$$
$$= \left| \frac{1 - x' - z'}{z'} \right|^{-\varepsilon/2} (-1 - i\varepsilon)^{-\varepsilon/2} \, \Theta(1 - z' - x') \tag{E.11}$$

Answer:

$$\boxed{ \left| \frac{z' + x' - 1}{z'} \right|^{-\varepsilon/2} \left\{ \Theta(z' + x' - 1) + (-1 - i\varepsilon)^{-\varepsilon/2} \, \Theta(1 - z' - x') \right\} } \tag{E.12}$$

E.4 Case (4)

$$\left[\frac{z' - x'}{z'(1 - x')} \right]^{-\varepsilon/2} = \left[\frac{z' - x'}{z'(1 - x')} + \left\{ 1 - \frac{i\delta}{1 - x'} + \frac{i\delta}{z'} \right\} \right]^{-\varepsilon/2}$$

$$= \left[\left(\frac{z' - x'}{z'(1 - x')} \right) \left\{ 1 + i\delta \left(\frac{1 - z' - x'}{z'(1 - x')} \right) \right\} \right]^{-\varepsilon/2}$$

$$\Rightarrow \left[\left(\frac{z' - x'}{z'(1 - x')} \right) \{ 1 + i\delta\, \Theta(1 - z' - x) - i\delta\, \Theta(z' + x' - 1) \} \right]^{-\varepsilon/2} \qquad \text{(E.13)}$$

(splitting $z' - x' = (z' - x')[\Theta(z' - x') + \Theta(x' - z')]$)

$$\Rightarrow \left[\left(\frac{z' - x'}{z'(1 - x')} \right) (\Theta(z' - x') + \Theta(x' - z'))\, \{ 1 + i\delta\, \Theta(1 - z' - x) - i\delta\, \Theta(z' + x' - 1) \} \right]^{-\varepsilon/2}$$

$$\Rightarrow \left[\left(\frac{z' - x'}{z'(1 - x')} \right) \{ 1 + i\delta\, \Theta(1 - z' - x')\, \Theta(z' - x') - i\delta\, \Theta(z' + x' - 1)\, \Theta(z' - x') \right.$$

$$\left. + i\delta\, \Theta(1 - z' - x')\, \Theta(x' - z') - i\delta\, \Theta(z' + x' - 1)\, \Theta(x' - z') \} \right]^{-\varepsilon/2} \qquad \text{(E.14)}$$

If $1 - z' - x > 0$ **and** $z' - x' > 0$**:**

$$\left| \frac{z' - x'}{z'(1 - x')} \right|^{-\varepsilon/2} \Theta(1 - z' - x')\, \Theta(z' - x') \qquad \text{(E.15)}$$

If $z' + x' - 1 > 0$ **and** $z' - x' > 0$**:**

$$\left| \frac{z' - x'}{z'(1 - x')} \right|^{-\varepsilon/2} \Theta(z + x' - 1)\, \Theta(z' - x') \qquad \text{(E.16)}$$

If $1 - z' - x' > 0$ **and** $x' - z' > 0$**:**

$$\left| \frac{x' - z'}{z'(1 - x')} \right|^{-\varepsilon/2} (-1 - i\varepsilon)^{-\varepsilon/2}\, \Theta(1 - z' - x')\, \Theta(x' - z') \qquad \text{(E.17)}$$

If $z' + x' - 1 > 0$ **and** $x' - z' > 0$**:**

$$\left| \frac{x' - z'}{z'(1 - x')} \right|^{-\varepsilon/2} (-1 + i\varepsilon)^{-\varepsilon/2}\, \Theta(z' + x' - 1)\, \Theta(x' - z') \qquad \text{(E.18)}$$

Answer:

$$\boxed{\left|\frac{z'-x'}{z'(1-x')}\right|^{-\varepsilon/2}\left\{\Theta(z'-x')+\Theta(x'-z')+(-1-i\varepsilon)^{-\varepsilon/2}\,\Theta(1-z'-x')+(-1+i\varepsilon)^{-\varepsilon/2}\,\Theta(z'+x'-1)\right\}} \tag{E.19}$$

E.5 Case (5)

$$\begin{aligned}\left[\frac{1-z'-x'}{1-x'}\right]^{-\varepsilon/2} &= \left[\left(\frac{1-z'-x'}{1-x'}\right)\left\{1+\frac{i\delta}{1-z'-x'}-\frac{i\delta}{1-x'}\right\}\right]^{-\varepsilon/2}\\ &= \left[\left(\frac{1-z'-x'}{1-x'}\right)\left\{1+i\delta\left(\frac{z'}{(1-z'-x')(1-x')}\right)\right\}\right]^{-\varepsilon/2}\\ &\Rightarrow \left[\left(\frac{1-z'-x'}{1-x'}\right)\{1+i\delta\,\Theta(1-z'-x')-\Theta(z'+x'-1)\}\right]^{-\varepsilon/2}\end{aligned} \tag{E.20}$$

If $1-z'-x'>0$**:**

$$\left|\frac{1-z'-x'}{1-x'}\right|^{-\varepsilon/2}\Theta(1-z'-x') \tag{E.21}$$

If $z'+x'-1>0$**:**

$$\left|\frac{z'+x'-1}{1-x'}\right|^{-\varepsilon/2}(-1+i\varepsilon)^{-\varepsilon/2}\,\Theta(z'+x'-1) \tag{E.22}$$

Answer:

$$\boxed{\left|\frac{1-z'-x'}{1-x'}\right|^{-\varepsilon/2}\left\{\Theta(1-z'-x')+(-1+i\varepsilon)^{-\varepsilon/2}\,\Theta(z'+x'-1)\right\}} \tag{E.23}$$

E.6 Case (6)

$$\left[\frac{1-z'-x'}{(1-x')(1-z')}\right]^{-\varepsilon/2} = \left[\left(\frac{1-z'-x'}{(1-z')(1-x')}\right)\left\{1+\frac{i\delta}{(1-z'-x')}-\frac{i\delta}{(1-x')}-\frac{i\delta}{(1-z')}\right\}\right]^{-\varepsilon/2} \tag{E.24}$$

After simplifying:

$$= \left[\left(\frac{1-z'-x'}{(1-x')(1-z')}\right)\left\{1+i\delta\,\frac{z'(1-x')-(1-z')(1-z'-x')}{(1-z'-x')(1-x')(1-z')}\right\}\right]^{-\varepsilon/2} \tag{E.25}$$

There is sign-ambiguity in $(1-z'-x')$, hence:

$$\Rightarrow \left[\left(\frac{1-z'-x'}{(1-x')(1-z')}\right)\{1+i\delta\,\Theta(1-z'-x')-\Theta(z'+x'-1)\}\right]^{-\varepsilon/2} \tag{E.26}$$

If $1-z'-x'>0$**:**

$$\left|\frac{1-z'-x'}{(1-x')(1-z')}\right|^{-\varepsilon/2}\Theta(1-z'-x') \tag{E.27}$$

If $z'+x'-1>0$**:**

$$\left|\frac{z'+x'-1}{(1-x')(1-z')}\right|^{-\varepsilon/2}(-1+i\varepsilon)^{-\varepsilon/2}\,\Theta(z'+x'-1) \tag{E.28}$$

Answer:

$$\boxed{\left|\frac{1-z'-x'}{(1-x')(1-z')}\right|^{-\varepsilon/2}\left\{\Theta(1-z'-x')+(-1+i\varepsilon)^{-\varepsilon/2}\,\Theta(z'+x'-1)\right\}} \tag{E.29}$$

E.7 Case (7)

$$\left[\frac{(z'-x')(1-z'-x')}{z'(1-z')}\right]^{-\varepsilon/2} = \left[\frac{(z'-x')(1-z'-x')}{z'(1-z')}\cdot\left\{1+i\delta\left(\frac{1}{1-z'-x'}+\frac{1}{z'}-\frac{1}{1-z'}\right)\right\}(1+i\delta)\right]^{-\varepsilon/2}$$
$$= \left[\left(\frac{(z'-x')(1-z'-x')}{z'(1-z')}\right)\left\{\frac{(1-z')(1-z'-x')+z'z'}{(1-z'-x')\,z'(1-z')}\right\}\right]^{-\varepsilon/2}$$
$$\Rightarrow \left[\frac{(z'-x')(1-z'-x')}{z'(1-z')}\left\{1+i\delta\,\frac{x'z'}{(1-z'-x')\,z'(1-z')}\right\}\right]^{-\varepsilon/2}$$
$$\Rightarrow \left[\frac{(z'-x')(1-z'-x')}{z'(1-z')}\,\{1+i\delta\,\Theta(1-z'-x')-i\delta\,\Theta(z'+x'-1)\}\right]^{-\varepsilon/2} \tag{E.30}$$

If $1-z'-x>0$**:** (splitting via $\Theta(z'-x')+\Theta(x'-z')$)

$$\Rightarrow \left[\frac{(z'-x')(1-z'-x')}{z'(1-z')}\,(\Theta(z'-x')+\Theta(x'-z'))\,\{1+i\delta\,\Theta(1-z'-x')-i\delta\,\Theta(z'+x'-1)\}\right]^{-\varepsilon/2}$$
$$\Rightarrow \Bigg[\frac{(z'-x')(1-z'-x')}{z'(1-z')}\,\{1+i\delta\,\Theta(1-z'-x')\,\Theta(z'-x')-i\delta\,\Theta(z'+x'-1)\,\Theta(z'-x')$$
$$+i\delta\,\Theta(1-z'-x')\,\Theta(x'-z')-i\delta\,\Theta(z'+x'-1)\,\Theta(x'-z')\}\Bigg]^{-\varepsilon/2} \tag{E.31}$$

If $(1-z'-x')>0$ **and** $x'>x'$ **(i.e.** $z'>x'$**):**

$$\left|\frac{(z'-x')(1-z'-x')}{z'(1-z')}\right|^{-\varepsilon/2}\Theta(1-z'-x')\,\Theta(z'-x') \tag{E.32}$$

If $1-z'-x'>0$ **and** $x'-z'>0$**:**

$$\left|\frac{(x'-z')(1-z'-x')}{z'(1-z')}\right|^{-\varepsilon/2}(-1-i\varepsilon)^{-\varepsilon/2}\,\Theta(1-z'-x')\,\Theta(x'-z') \tag{E.33}$$

If $z'+x'-1>0$ **and** $x'-z'>0$**:**

(Note: the sign from the power $-\varepsilon/2$ acting on $z' - x' < 0$ and on $1 - z' - x' < 0$ together gives $(-1)^{-\varepsilon/2} \cdot (-1)^{-\varepsilon/2} = (-1 + i\varepsilon)^{-\varepsilon/2}$)

$$\left| \frac{(x' - z')(z' + x' - 1)}{z'(1 - z')} \right|^{-\varepsilon/2} (-1 + i\varepsilon)^{-\varepsilon/2}\, \Theta(z' + x' - 1)\, \Theta(x' - z') \tag{E.34}$$

If $z' + x' - 1 > 0$ **and** $x' - z' > 0$**:**

$$\left| \frac{(x' - z')(z' + x' - 1)}{z'(1 - z')} \right|^{-\varepsilon/2} \Theta(z' + x' - 1)\, \Theta(x' - z') \tag{E.35}$$

Answer:

$$\boxed{\left| \frac{(z' - x')(1 - z' - x')}{z'(1 - z')} \right|^{-\varepsilon/2} \left\{ \begin{aligned} &\Theta(1 - z' - x')\, \Theta(z' - x') \\ &+ \Theta(z' + x' - 1)\, \Theta(x' - z') \\ &+ (-1 - i\varepsilon)^{-\varepsilon/2}\, \Theta(1 - z' - x')\, \Theta(x' - z') \\ &+ (-1 + i\varepsilon)^{-\varepsilon/2}\, \Theta(z' + x' - 1)\, \Theta(x' - z') \end{aligned} \right\}} \tag{E.36}$$

The seven cases presented above cover all the kinematic structures that arise in the sector decomposition of the real-emission phase-space integrals in this calculation. In each case the procedure is the same: introduce the $i\delta$ shift, split the integration domain using Θ-functions, and extract the phase carried by each sector. The resulting expressions, with explicit $(-1 \pm i\varepsilon)^{-\varepsilon/2}$ factors, are then expanded in ε to yield the distributional identities used in the evaluation of the coefficient functions.

Bibliography

[1] D. J. Gross and F. Wilczek, "Ultraviolet Behavior of Nonabelian Gauge Theories," *Phys. Rev. Lett.* **30** (1973) 1343–1346.

[2] D. J. Gross and F. Wilczek, "Asymptotically Free Gauge Theories - I," *Phys. Rev. D* **8** (1973) 3633–3652.

[3] D. J. Gross and F. Wilczek, "ASYMPTOTICALLY FREE GAUGE THEORIES. 2.," *Phys. Rev. D* **9** (1974) 980–993.

[4] H. D. Politzer, "Reliable Perturbative Results for Strong Interactions?," *Phys. Rev. Lett.* **30** (1973) 1346–1349.

[5] H. D. Politzer, "Asymptotic Freedom: An Approach to Strong Interactions," *Phys. Rept.* **14** (1974) 129–180.

[6] **European Muon** Collaboration, J. Ashman *et al.*, "A Measurement of the Spin Asymmetry and Determination of the Structure Function g(1) in Deep Inelastic Muon-Proton Scattering," *Phys. Lett. B* **206** (1988) 364.

[7] J. Ashman, B. Badelek, G. Baum, J. Beaufays, C. Bee, C. Benchouk, I. Bird, S. Brown, M. Caputo, H. Cheung, J. Chima, J. Ciborowski, R. Clifft, G. Coignet, F. Combley, G. Court, G. d'Agostini, J. Drees, M. Düren, N. Dyce, A. Edwards, M. Edwards, T. Ernst, M. Ferrero, D. Francis, E. Gabathuler, R. Gamet, V. Gibson, J. Gillies, P. Grafström, K. Hamacher, D. Harrach, P. Hayman, J. Holt, V. Hughes, A. Jacholkowska, T. Jones, E. Kabuss, B. Korzen, U. Krüner, S. Kullander,

U. Landgraf, D. Lanske, F. Lettenström, T. Lindqvist, J. Loken, M. Matthews, Y. Mizuno, K. Mönig, F. Montanet, E. Nagy, J. Nassalski, T. Niinikoski, P. Norton, F. Oakham, R. Oppenheim, A. Osborne, V. Papavassiliou, N. Pavel, C. Peroni, H. Peschel, R. Piegaia, B. Pietrzyk, U. Pietrzyk, B. Povh, P. Renton, J. Rieubland, A. Rijllart, K. Rith, E. Rondio, L. Ropelewski, D. Salmon, A. Sandacz, T. Schröder, K. Schüler, K. Schultze, T.-A. Shibata, T. Sloan, A. Staiano, H. Stier, J. Stock, G. Taylor, J. Thompson, T. Walcher, J. Toth, L. Urban, W. Wallucks, S. Wheeler, D. Williams, W. Williams, S. Wimpenny, R. Windmolders, W. Womersley, and K. Ziemons, "An investigation of the spin structure of the proton in deep inelastic scattering of polarised muons on polarised protons," *Nuclear Physics B* **328** no. 1, (1989) 1–35. https://www.sciencedirect.com/science/article/pii/0550321389900898.

[8] A. Accardi *et al.*, "Electron Ion Collider: The Next QCD Frontier: Understanding the glue that binds us all," *Eur. Phys. J. A* **52** no. 9, (2016) 268, arXiv:1212.1701 [nucl-ex].

[9] D. Boer *et al.*, "Gluons and the quark sea at high energies: Distributions, polarization, tomography," arXiv:1108.1713 [nucl-th].

[10] G. F. Sterman, *An Introduction to quantum field theory*. Cambridge University Press, 8, 1993.

[11] J. Collins, *Foundations of Perturbative QCD*, vol. 32. Cambridge University Press, 2011.

[12] V. Ravindran, *Perturbative Quantum Chromodynamics*. 2016.

[13] G. Heinrich and A. Olsson, "Perturbative QCD," 9, 2025. arXiv:2509.02790 [hep-ph].

[14] **CTEQ** Collaboration, R. Brock *et al.*, "Handbook of perturbative QCD: Version 1.0" *Rev. Mod. Phys.* **67** (1995) 157–248.

[15] J. C. Romao and J. P. Silva, "A resource for signs and Feynman diagrams of the Standard Model," *Int. J. Mod. Phys. A* **27** (2012) 1230025, arXiv:1209.6213 [hep-ph].

[16] G. 't Hooft and M. J. G. Veltman, "Regularization and Renormalization of Gauge Fields," *Nucl. Phys. B* **44** (1972) 189–213.

[17] G. M. Cicuta and E. Montaldi, "Analytic renormalization via continuous space dimension," *Lett. Nuovo Cim.* **4** (1972) 329–332.

[18] C. G. Bollini and J. J. Giambiagi, "Dimensional Renormalization: The Number of Dimensions as a Regularizing Parameter," *Nuovo Cim. B* **12** (1972) 20–26.

[19] A. A H, P. Banerjee, A. Chakraborty, P. K. Dhani, P. Mukherjee, N. Rana, and V. Ravindran, "NNLO QCD⊕QED corrections to Higgs production in bottom quark annihilation," *Phys. Rev. D* **100** no. 11, (2019) 114016, arXiv:1906.09028 [hep-ph].

[20] A. A H, P. Mukherjee, and V. Ravindran, "Infrared structure of $SU(N) \times U(1)$ gauge theory to three loops," *JHEP* **08** (2020) 156, arXiv:1912.13386 [hep-ph].

[21] G. Abbas, B. Ananthanarayan, I. Caprini, and J. Fischer, "Perturbative expansion of the QCD Adler function improved by renormalization-group summation and analytic continuation in the Borel plane," *Phys. Rev. D* **87** no. 1, (2013) 014008, arXiv:1211.4316 [hep-ph].

[22] V. Ravindran, "On Sudakov and soft resummations in QCD," *Nucl. Phys.* **B746** (2006) 58–76, arXiv:hep-ph/0512249 [hep-ph].

[23] J. C. Collins, D. E. Soper, and G. F. Sterman, "Factorization of Hard Processes in QCD," *Adv. Ser. Direct. High Energy Phys.* **5** (1989) 1–91, arXiv:hep-ph/0409313.

[24] V. N. Gribov and L. N. Lipatov, "Deep inelastic e p scattering in perturbation theory," *Sov. J. Nucl. Phys.* **15** (1972) 438–450.

[25] G. Altarelli and G. Parisi, "Asymptotic Freedom in Parton Language," *Nucl. Phys. B* **126** (1977) 298–318.

[26] Y. L. Dokshitzer, "Calculation of the Structure Functions for Deep Inelastic Scattering and e+ e- Annihilation by Perturbation Theory in Quantum Chromodynamics.," *Sov. Phys. JETP* **46** (1977) 641–653.

[27] V. Sudakov, "Vertex parts at very high-energies in quantum electrodynamics," *Sov. Phys. JETP* **3** (1956) 65–71.

[28] C. W. Bauer, S. Fleming, and M. E. Luke, "Summing Sudakov logarithms in B —> X(s gamma) in effective field theory," *Phys. Rev. D* **63** (2000) 014006, arXiv:hep-ph/0005275.

[29] C. W. Bauer, D. Pirjol, and I. W. Stewart, "Soft collinear factorization in effective field theory," *Phys. Rev. D* **65** (2002) 054022, arXiv:hep-ph/0109045.

[30] S. Goyal, "Precision QCD Studies of Semi-Inclusive Deep Inelastic Scattering at Electron-Ion Collider,".

[31] J. Blümlein, P. Marquard, C. Schneider, and K. Schönwald, "The massless three-loop Wilson coefficients for the deep-inelastic structure functions F_2, F_L, xF_3 and g_1," *JHEP* **11** (2022) 156, arXiv:2208.14325 [hep-ph].

[32] E. Zijlstra and W. van Neerven, "Order-s2 qcd corrections to the deep inelastic proton structure functions f2 and fl," *Nuclear Physics B* **383** no. 3, (1992) 525–574. https://www.sciencedirect.com/science/article/pii/055032139290087R.

[33] S. Moch, J. A. M. Vermaseren, and A. Vogt, "The Longitudinal structure function at the third order," *Phys. Lett. B* **606** (2005) 123–129, arXiv:hep-ph/0411112.

[34] J. Vermaseren, A. Vogt, and S. Moch, "The Third-order QCD corrections to deep-inelastic scattering by photon exchange," *Nucl. Phys. B* **724** (2005) 3–182, arXiv:hep-ph/0504242.

[35] S. Moch, J. A. M. Vermaseren, and A. Vogt, "Third-order QCD corrections to the charged-current structure function F(3)," *Nucl. Phys. B* **813** (2009) 220–258, arXiv:0812.4168 [hep-ph].

[36] D. de Florian, R. Sassot, and M. Stratmann, "Global analysis of fragmentation functions for pions and kaons and their uncertainties," *Phys. Rev. D* **75** (2007) 114010, arXiv:hep-ph/0703242.

[37] **HERMES** Collaboration, A. Airapetian *et al.*, "Quark helicity distributions in the nucleon for up, down, and strange quarks from semi-inclusive deep-inelastic scattering," *Phys. Rev. D* **71** (2005) 012003, arXiv:hep-ex/0407032.

[38] **COMPASS** Collaboration, M. G. Alekseev *et al.*, "Quark helicity distributions from longitudinal spin asymmetries in muon-proton and muon-deuteron scattering," *Phys. Lett. B* **693** (2010) 227–235, arXiv:1007.4061 [hep-ex].

[39] R. Abdul Khalek *et al.*, "Science Requirements and Detector Concepts for the Electron-Ion Collider: EIC Yellow Report," *Nucl. Phys. A* **1026** (2022) 122447, arXiv:2103.05419 [physics.ins-det].

[40] **HERMES** Collaboration, A. Airapetian *et al.*, "Multiplicities of charged pions and kaons from semi-inclusive deep-inelastic scattering by the proton and the deuteron," *Phys. Rev. D* **87** (2013) 074029, arXiv:1212.5407 [hep-ex].

[41] **COMPASS** Collaboration, C. Adolph *et al.*, "Multiplicities of charged kaons from deep-inelastic muon scattering off an isoscalar target," *Phys. Lett. B* **767** (2017) 133–141, arXiv:1608.06760 [hep-ex].

[42] **HERMES** Collaboration, E. C. Aschenauer, H. E. Jackson, S. Joosten, K. Rith, G. Schnell, and C. Van Hulse, “Reply to “Comment on ‘Reevaluation of the parton distribution of strange quarks in the nucleon’”,” *Phys. Rev. D* **92** no. 9, (2015) 098102, `arXiv:1508.04020 [hep-ex]`.

[43] D. de Florian, M. Epele, R. J. Hernández-Pinto, R. Sassot, and M. Stratmann, “Parton-to-kaon fragmentation revisited,” *Physical Review D* **95** no. 9, (May, 2017) . `http://dx.doi.org/10.1103/PhysRevD.95.094019`.

[44] D. P. Anderle, T. Kaufmann, M. Stratmann, and F. Ringer, “Fragmentation functions beyond fixed order accuracy,” *Physical Review D* **95** no. 5, (Mar., 2017) . `http://dx.doi.org/10.1103/PhysRevD.95.054003`.

[45] E. Leader, A. V. Sidorov, and D. B. Stamenov, “Determination of the fragmentation functions from an NLO QCD analysis of the HERMES data on pion multiplicities,” *Phys. Rev. D* **93** no. 7, (2016) 074026, `arXiv:1506.06381 [hep-ph]`.

[46] **NNPDF** Collaboration, V. Bertone, N. P. Hartland, E. R. Nocera, J. Rojo, and L. Rottoli, “Charged hadron fragmentation functions from collider data,” *Eur. Phys. J. C* **78** no. 8, (2018) 651, `arXiv:1807.03310 [hep-ph]`. [Erratum: Eur.Phys.J.C 84, 155 (2024)].

[47] R. Abdul Khalek, V. Bertone, and E. R. Nocera, “Determination of unpolarized pion fragmentation functions using semi-inclusive deep-inelastic-scattering data,” *Physical Review D* **104** no. 3, (Aug., 2021) . `http://dx.doi.org/10.1103/PhysRevD.104.034007`.

[48] J. Ethier, N. Sato, and W. Melnitchouk, “First simultaneous extraction of spin-dependent parton distributions and fragmentation functions from a global qcd analysis,” *Physical Review Letters* **119** no. 13, (Sept., 2017) . `http://dx.doi.org/10.1103/PhysRevLett.119.132001`.

[49] D. de Florian, G. A. Lucero, R. Sassot, M. Stratmann, and W. Vogelsang, "Monte carlo sampling variant of the dssv14 set of helicity parton densities," *Physical Review D* **100** no. 11, (Dec., 2019) . http://dx.doi.org/10.1103/PhysRevD.100.114027.

[50] E. Moffat, W. Melnitchouk, T. Rogers, and N. Sato, "Simultaneous monte carlo analysis of parton densities and fragmentation functions," *Physical Review D* **104** no. 1, (July, 2021) . http://dx.doi.org/10.1103/PhysRevD.104.016015.

[51] **MAP (Multi-dimensional Analyses of Partonic distributions)** Collaboration, V. Bertone, A. Chiefa, and E. R. Nocera, "Helicity-dependent parton distribution functions at next-to-next-to-leading order accuracy from inclusive and semi-inclusive deep-inelastic scattering data," *Phys. Lett. B* **865** (2025) 139497, arXiv:2404.04712 [hep-ph].

[52] I. Borsa, M. Stratmann, W. Vogelsang, D. de Florian, and R. Sassot, "Next-to-Next-to-Leading Order Global Analysis of Polarized Parton Distribution Functions," *Phys. Rev. Lett.* **133** no. 15, (2024) 151901, arXiv:2407.11635 [hep-ph].

[53] D. de Florian, R. Sassot, M. Stratmann, and W. Vogelsang, "Extraction of Spin-Dependent Parton Densities and Their Uncertainties," *Phys. Rev. D* **80** (2009) 034030, arXiv:0904.3821 [hep-ph].

[54] D. de Florian, R. Sassot, M. Stratmann, and W. Vogelsang, "Evidence for polarization of gluons in the proton," *Phys. Rev. Lett.* **113** no. 1, (2014) 012001, arXiv:1404.4293 [hep-ph].

[55] **Particle Data Group** Collaboration, S. Navas *et al.*, "Review of particle physics," *Phys. Rev. D* **110** no. 3, (2024) 030001.

[56] S. Catani and M. H. Seymour, "A General algorithm for calculating jet cross-sections in NLO QCD," *Nucl. Phys. B* **485** (1997) 291–419, arXiv:hep-ph/9605323. [Erratum: Nucl.Phys.B 510, 503–504 (1998)].

[57] S. Catani, "The Singular behavior of QCD amplitudes at two loop order," *Phys. Lett.* **B427** (1998) 161–171, arXiv:hep-ph/9802439 [hep-ph].

[58] T. Kinoshita, "Mass singularities of Feynman amplitudes," *J. Math. Phys.* **3** (1962) 650–677.

[59] T. Lee and M. Nauenberg, "Degenerate Systems and Mass Singularities," *Phys. Rev.* **133** (1964) B1549–B1562.

[60] G. Altarelli, R. K. Ellis, G. Martinelli, and S.-Y. Pi, "Processes Involving Fragmentation Functions Beyond the Leading Order in QCD," *Nucl. Phys. B* **160** (1979) 301–329.

[61] P. Nason and B. R. Webber, "Scaling violation in e+ e- fragmentation functions: QCD evolution, hadronization and heavy quark mass effects," *Nucl. Phys. B* **421** (1994) 473–517. [Erratum: Nucl.Phys.B 480, 755 (1996)].

[62] W. Furmanski and R. Petronzio, "Lepton - Hadron Processes Beyond Leading Order in Quantum Chromodynamics," *Z. Phys. C* **11** (1982) 293.

[63] D. Graudenz, "One particle inclusive processes in deeply inelastic lepton - nucleon scattering," *Nucl. Phys. B* **432** (1994) 351–376, arXiv:hep-ph/9406274.

[64] D. de Florian and Y. Rotstein Habarnau, "Polarized semi-inclusive electroweak structure functions at next-to-leading-order," *Eur. Phys. J. C* **73** no. 3, (2013) 2356, arXiv:1210.7203 [hep-ph].

[65] D. de Florian and R. Sassot, "Phenomenology of forward hadrons in DIS: Fracture functions and its Q**2 evolution," *Phys. Rev. D* **56** (1997) 426–432, arXiv:hep-ph/9703228.

[66] A. Daleo and R. Sassot, "Next-to-leading order evolution of SIDIS processes in the forward region," *Nucl. Phys. B* **673** no. 1–2, (Nov., 2003) 357–384, arXiv:hep-ph/0309073. http://dx.doi.org/10.1016/j.nuclphysb.2003.09.007.

[67] A. Daleo, C. A. Garcia Canal, and R. Sassot, "Order alpha(s)**2 corrections to one particle inclusive processes in DIS," *Nucl. Phys. B* **662** (2003) 334–358, arXiv:hep-ph/0303199.

[68] K.-B. Chen, J.-P. Ma, and X.-B. Tong, "Gluonic contributions to semi-inclusive DIS in the target fragmentation region," *JHEP* **05** (2024) 298, arXiv:2402.15112 [hep-ph].

[69] V. Ravindran, J. Smith, and W. L. van Neerven, "Two-loop corrections to Higgs boson production," *Nucl. Phys.* **B704** (2005) 332–348, arXiv:hep-ph/0408315 [hep-ph].

[70] M. Abele, D. de Florian, and W. Vogelsang, "Approximate NNLO QCD corrections to semi-inclusive DIS," *Phys. Rev. D* **104** no. 9, (2021) 094046, arXiv:2109.00847 [hep-ph].

[71] M. Abele, D. de Florian, and W. Vogelsang, "Threshold resummation at NLL3 accuracy and approximate N3LO corrections to semi-inclusive DIS," *Phys. Rev. D* **106** no. 1, (2022) 014015, arXiv:2203.07928 [hep-ph].

[72] M. Cacciari and S. Catani, "Soft gluon resummation for the fragmentation of light and heavy quarks at large x," *Nucl. Phys. B* **617** (2001) 253–290, arXiv:hep-ph/0107138.

[73] D. P. Anderle, F. Ringer, and W. Vogelsang, "QCD resummation for semi-inclusive hadron production processes," *Phys. Rev. D* **87** no. 3, (2013) 034014, arXiv:1212.2099 [hep-ph].

[74] D. P. Anderle, F. Ringer, and W. Vogelsang, "Threshold resummation for polarized (semi-)inclusive deep inelastic scattering," *Phys. Rev. D* **87** (2013) 094021, arXiv:1304.1373 [hep-ph].

[75] G. F. Sterman and W. Vogelsang, "Crossed Threshold Resummation," *Phys. Rev. D* **74** (2006) 114002, arXiv:hep-ph/0606211.

[76] D. Westmark and J. F. Owens, "Enhanced threshold resummation formalism for lepton pair production and its effects in the determination of parton distribution functions," *Phys. Rev.* **D95** no. 5, (2017) 056024, arXiv:1701.06716 [hep-ph].

[77] P. Banerjee, G. Das, P. K. Dhani, and V. Ravindran, "Threshold resummation of the rapidity distribution for Drell-Yan production at NNLO+NNLL," *Phys. Rev.* **D98** no. 5, (2018) 054018, arXiv:1805.01186 [hep-ph].

[78] R. Hamberg, W. van Neerven, and T. Matsuura, "A complete calculation of the order s2 correction to the drell-yan k-factor," *Nuclear Physics B* **359** no. 2, (1991) 343–405. https://www.sciencedirect.com/science/article/pii/0550321391900645.

[79] V. Ravindran, "Higher-order threshold effects to inclusive processes in QCD," *Nucl. Phys.* **B752** (2006) 173–196, arXiv:hep-ph/0603041 [hep-ph].

[80] A. A H, G. Das, M. C. Kumar, P. Mukherjee, V. Ravindran, and K. Samanta, "Resummed Drell-Yan cross-section at N^{3}LL," *JHEP* **10** (2020) 153, arXiv:2001.11377 [hep-ph].

[81] W. A. Bardeen, A. J. Buras, D. W. Duke, and T. Muta, "Deep Inelastic Scattering Beyond the Leading Order in Asymptotically Free Gauge Theories," *Phys. Rev. D* **18** (1978) 3998.

[82] W. L. van Neerven and E. B. Zijlstra, "Order alpha-s**2 contributions to the deep inelastic Wilson coefficient," *Phys. Lett. B* **272** (1991) 127–133.

[83] S. Moch and J. A. M. Vermaseren, "Deep inelastic structure functions at two loops," *Nucl. Phys. B* **573** (2000) 853–907, arXiv:hep-ph/9912355.

[84] J. Blumlein and H. Bottcher, "QCD analysis of polarized deep inelastic data and parton distributions," *Nucl. Phys. B* **636** (2002) 225–263, arXiv:hep-ph/0203155.

[85] P. M. Nadolsky, D. R. Stump, and C. P. Yuan, "Semiinclusive hadron production at HERA: The Effect of QCD gluon resummation," *Phys. Rev. D* **61** (2000) 014003, arXiv:hep-ph/9906280. [Erratum: Phys.Rev.D 64, 059903 (2001)].

[86] P. J. Rijken and W. L. van Neerven, "Heavy flavor contributions to the Drell-Yan cross-section," *Phys. Rev. D* **52** (1995) 149–161, arXiv:hep-ph/9501373.

[87] S. Dittmaier, A. Huss, and C. Schwinn, "Dominant mixed QCD-electroweak O($\alpha_s\alpha$) corrections to Drell–Yan processes in the resonance region," *Nucl. Phys. B* **904** (2016) 216–252, arXiv:1511.08016 [hep-ph].

[88] S. Dittmaier and M. Huber, "Radiative corrections to the neutral-current Drell-Yan process in the Standard Model and its minimal supersymmetric extension," *JHEP* **01** (2010) 060, arXiv:0911.2329 [hep-ph].

[89] C. Duhr and B. Mistlberger, "Lepton-pair production at hadron colliders at N^{3}LO in QCD," *JHEP* **03** (2022) 116, arXiv:2111.10379 [hep-ph].

[90] X. Chen, T. Gehrmann, N. Glover, A. Huss, T.-Z. Yang, and H. X. Zhu, "Dilepton Rapidity Distribution in Drell-Yan Production to Third Order in QCD," *Phys. Rev. Lett.* **128** no. 5, (2022) 052001, arXiv:2107.09085 [hep-ph].

[91] L. Buonocore, M. Grazzini, S. Kallweit, C. Savoini, and F. Tramontano, "Mixed QCD-EW corrections to $pp \to \ell\nu_\ell + X$ at the LHC," *Phys. Rev. D* **103** (2021) 114012, arXiv:2102.12539 [hep-ph].

[92] M. Kramer, E. Laenen, and M. Spira, "Soft gluon radiation in Higgs boson production at the LHC," *Nucl. Phys. B* **511** (1998) 523–549, arXiv:hep-ph/9611272.

[93] U. Baur and E. W. N. Glover, "Higgs Boson Production at Large Transverse Momentum in Hadronic Collisions," *Nucl. Phys. B* **339** (1990) 38–66.

[94] V. Ravindran, J. Smith, and W. L. Van Neerven, "Next-to-leading order QCD corrections to differential distributions of Higgs boson production in hadron hadron collisions," *Nucl. Phys. B* **634** (2002) 247–290, arXiv:hep-ph/0201114.

[95] D. de Florian and M. Grazzini, "The Structure of large logarithmic corrections at small transverse momentum in hadronic collisions," *Nucl. Phys. B* **616** (2001) 247–285, arXiv:hep-ph/0108273.

[96] R. V. Harlander and W. B. Kilgore, "Next-to-next-to-leading order Higgs production at hadron colliders," *Phys. Rev. Lett.* **88** (2002) 201801, arXiv:hep-ph/0201206 [hep-ph].

[97] A. Pak, M. Rogal, and M. Steinhauser, "Finite top quark mass effects in NNLO Higgs boson production at LHC," *JHEP* **02** (2010) 025, arXiv:0911.4662 [hep-ph].

[98] R. V. Harlander and K. J. Ozeren, "Top mass effects in Higgs production at next-to-next-to-leading order QCD: Virtual corrections," *Phys. Lett. B* **679** (2009) 467–472, arXiv:0907.2997 [hep-ph].

[99] Y. Li, A. von Manteuffel, R. M. Schabinger, and H. X. Zhu, "Soft-virtual corrections to Higgs production at N^{3}LO," *Phys. Rev.* **D91** (2015) 036008, arXiv:1412.2771 [hep-ph].

[100] A. Gehrmann-De Ridder, T. Gehrmann, and E. W. N. Glover, "Antenna subtraction at NNLO," *JHEP* **09** (2005) 056, arXiv:hep-ph/0505111.

[101] M. Czakon, "A novel subtraction scheme for double-real radiation at NNLO," *Phys. Lett. B* **693** (2010) 259–268, arXiv:1005.0274 [hep-ph].

[102] S. Weinzierl, "Subtraction terms at NNLO," *JHEP* **03** (2003) 062, arXiv:hep-ph/0302180.

[103] S. Weinzierl, "Subtraction terms for one loop amplitudes with one unresolved parton," *JHEP* **07** (2003) 052, arXiv:hep-ph/0306248.

[104] S. Frixione and M. Grazzini, "Subtraction at NNLO," *JHEP* **06** (2005) 010, arXiv:hep-ph/0411399.

[105] U. Aglietti, R. Bonciani, G. Degrassi, and A. Vicini, "Two loop light fermion contribution to Higgs production and decays," *Phys. Lett. B* **595** (2004) 432–441, arXiv:hep-ph/0404071.

[106] S. Actis, G. Passarino, C. Sturm, and S. Uccirati, "NLO Electroweak Corrections to Higgs Boson Production at Hadron Colliders," *Phys. Lett. B* **670** (2008) 12–17, arXiv:0809.1301 [hep-ph].

[107] F. Maltoni, Z. Sullivan, and S. Willenbrock, "Higgs-Boson Production via Bottom-Quark Fusion," *Phys. Rev. D* **67** (2003) 093005, arXiv:hep-ph/0301033.

[108] S. Dawson, S. Dittmaier, and M. Spira, “Neutral Higgs boson pair production at hadron colliders: QCD corrections,” *Phys. Rev. D* **58** (1998) 115012, arXiv:hep-ph/9805244.

[109] S. Moch, J. Vermaseren, and A. Vogt, “The Quark form-factor at higher orders,” *JHEP* **08** (2005) 049, arXiv:hep-ph/0507039.

[110] T. Becher and M. Neubert, “On the Structure of Infrared Singularities of Gauge-Theory Amplitudes,” *JHEP* **06** (2009) 081, arXiv:0903.1126 [hep-ph]. [Erratum: JHEP11,024(2013)].

[111] J. Henn, A. V. Smirnov, V. A. Smirnov, M. Steinhauser, and R. N. Lee, “Four-loop photon quark form factor and cusp anomalous dimension in the large-N_c limit of QCD,” *JHEP* **03** (2017) 139, arXiv:1612.04389 [hep-ph].

[112] J. Ablinger, A. Behring, J. Blümlein, A. De Freitas, A. Hasselhuhn, A. von Manteuffel, M. Round, C. Schneider, and F. Wißbrock, “The 3-Loop Non-Singlet Heavy Flavor Contributions and Anomalous Dimensions for the Structure Function $F_2(x, Q^2)$ and Transversity,” *Nucl. Phys. B* **886** (2014) 733–823, arXiv:1406.4654 [hep-ph].

[113] S. Moch, B. Ruijl, T. Ueda, J. A. M. Vermaseren, and A. Vogt, “Low moments of the four-loop splitting functions in QCD,” *Phys. Lett. B* **825** (2022) 136853, arXiv:2111.15561 [hep-ph].

[114] G. Falcioni, F. Herzog, S. Moch, and A. Vogt, “Four-loop splitting functions in QCD – The quark-quark case,” *Phys. Lett. B* **842** (2023) 137944, arXiv:2302.07593 [hep-ph].

[115] G. Falcioni, F. Herzog, S. Moch, and A. Vogt, “Four-loop splitting functions in QCD – The gluon-to-quark case,” *Phys. Lett. B* **846** (2023) 138215, arXiv:2307.04158 [hep-ph].

[116] G. Falcioni, F. Herzog, S. Moch, A. Pelloni, and A. Vogt, "Four-loop splitting functions in QCD – the gluon-gluon case –," *Phys. Lett. B* **860** (2025) 139194, arXiv:2410.08089 [hep-ph].

[117] S. Moch, B. Ruijl, T. Ueda, J. Vermaseren, and A. Vogt, "Additional moments and x-space approximations of four-loop splitting functions in QCD," *Phys. Lett. B* **849** (2024) 138468, arXiv:2310.05744 [hep-ph].

[118] H. Contopanagos, E. Laenen, and G. F. Sterman, "Sudakov factorization and resummation," *Nucl. Phys. B* **484** (1997) 303–330, arXiv:hep-ph/9604313.

[119] N. Kidonakis and G. F. Sterman, "Subleading logarithms in QCD hard scattering," *Phys. Lett. B* **387** (1996) 867–874.

[120] E. Laenen, G. Oderda, and G. F. Sterman, "Resummation of threshold corrections for single particle inclusive cross-sections," *Phys. Lett. B* **438** (1998) 173–183, arXiv:hep-ph/9806467.

[121] B. Mele and P. Nason, "The Fragmentation function for heavy quarks in QCD," *Nucl. Phys. B* **361** (1991) 626–644. [Erratum: Nucl.Phys.B 921, 841–842 (2017)].

[122] P. Mathews, V. Ravindran, and K. Sridhar, "NLO-QCD corrections to dilepton production in the Randall-Sundrum model," *JHEP* **10** (2005) 031, arXiv:hep-ph/0506158 [hep-ph].

[123] P. Banerjee, C. Dey, M. C. Kumar, and V. Ravindran, "Pseudoscalar Higgs boson decay to three parton amplitudes at NNLO to higher orders in the dimensional regulator," *Phys. Rev. D* **111** no. 5, (2025) 054037, arXiv:2411.17611 [hep-ph].

[124] M. C. Kumar, P. Mathews, V. Ravindran, and S. Seth, "Neutral triple electroweak gauge boson production in the large extra-dimension model at the LHC," *Phys. Rev.* **D85** (2012) 094507, arXiv:1111.7063 [hep-ph].

[125] M. C. Kumar, P. Mathews, V. Ravindran, and S. Seth, "Vector boson production in association with KK modes of the ADD model to NLO in QCD at LHC," *J. Phys. G* **38** (2011) 055001, arXiv:1004.5519 [hep-ph].

[126] M. C. Kumar, P. Mathews, V. Ravindran, and A. Tripathi, "Diphoton signals in theories with large extra dimensions to NLO QCD at hadron colliders," *Phys. Lett.* **B672** (2009) 45–50, arXiv:0811.1670 [hep-ph].

[127] M. C. Kumar, P. Mathews, and V. Ravindran, "Extra dimension searches at hadron colliders to next-to-leading order-QCD," *Pramana* **69** (2007) 871–876.

[128] M. Czakon, P. Fiedler, and A. Mitov, "Total Top-Quark Pair-Production Cross Section at Hadron Colliders Through $O(\alpha_S^4)$," *Phys. Rev. Lett.* **110** (2013) 252004, arXiv:1303.6254 [hep-ph].

[129] P. Bärnreuther, M. Czakon, and A. Mitov, "Percent Level Precision Physics at the Tevatron: First Genuine NNLO QCD Corrections to $q\bar{q} \to t\bar{t} + X$," *Phys. Rev. Lett.* **109** (2012) 132001, arXiv:1204.5201 [hep-ph].

[130] B. Mele, P. Nason, and G. Ridolfi, "QCD radiative corrections to Z boson pair production in hadronic collisions," *Nucl. Phys. B* **357** (1991) 409–438.

[131] P. Nason, S. Dawson, and R. K. Ellis, "The Total Cross-Section for the Production of Heavy Quarks in Hadronic Collisions," *Nucl. Phys. B* **303** (1988) 607–633.

[132] T. Gehrmann, A. Huss, J. Niehues, A. Vogt, and D. M. Walker, "Jet production in charged-current deep-inelastic scattering to third order in QCD," *Phys. Lett. B* **792** (2019) 182–186, arXiv:1812.06104 [hep-ph].

[133] E. W. Nigel Glover and J. Pires, "Antenna subtraction for gluon scattering at NNLO," *JHEP* **06** (2010) 096, arXiv:1003.2824 [hep-ph].

[134] A. Denner, "Techniques for calculation of electroweak radiative corrections at the one loop level and results for W physics at LEP-200," *Fortsch. Phys.* **41** (1993) 307–420, arXiv:0709.1075 [hep-ph].

[135] S. Dittmaier and M. Krämer, "Electroweak radiative corrections to W boson production at hadron colliders," *Phys. Rev. D* **65** (2002) 073007, arXiv:hep-ph/0109062.

[136] L. J. Dixon, "Scattering amplitudes: the most perfect microscopic structures in the universe," *J. Phys. A* **44** (2011) 454001, arXiv:1105.0771 [hep-th].

[137] G. F. Sterman and M. E. Tejeda-Yeomans, "Multiloop amplitudes and resummation," *Phys. Lett.* **B552** (2003) 48–56, arXiv:hep-ph/0210130 [hep-ph].

[138] M. Glück, E. Reya, and A. Vogt, "Dynamical parton distributions revisited," *Eur. Phys. J. C* **5** (1998) 461–470, arXiv:hep-ph/9806404.

[139] J. Blumlein and H. Bottcher, "QCD Analysis of Polarized Deep Inelastic Scattering Data," *Nucl. Phys. B* **841** (2010) 205–230, arXiv:1005.3113 [hep-ph].

[140] J. Binnewies, B. A. Kniehl, and G. Kramer, "Next-to-leading order fragmentation functions for pions and kaons," *Z. Phys. C* **65** (1995) 471–480, arXiv:hep-ph/9407347.

[141] V. Ravindran, J. Smith, and W. L. van Neerven, "QCD threshold corrections to di-lepton and Higgs rapidity distributions beyond N^2 LO," *Nucl. Phys.* **B767** (2007) 100–129, arXiv:hep-ph/0608308 [hep-ph].

[142] V. Ravindran, J. Smith, and W. L. van Neerven, "NNLO corrections to massive lepton pair production in longitudinally polarized proton proton collisions," *Nucl. Phys. B* **682** (2004) 421–456, arXiv:hep-ph/0311304.

[143] V. Ravindran, J. Smith, and W. L. van Neerven, “NLO differential distributions of massive lepton pair production in longitudinally polarized proton proton collisions,” *Nucl. Phys. B* **647** (2002) 275–318, `arXiv:hep-ph/0207076`.

[144] T. Ahmed, V. Ravindran, A. Sankar, and S. Tiwari, “Two-loop amplitudes for di-Higgs and di-pseudo-Higgs productions through quark annihilation in QCD,” *JHEP* **01** (2022) 189, `arXiv:2110.11476 [hep-ph]`.

[145] G. Heinrich, “Collider Physics at the Precision Frontier,” *Phys. Rept.* **922** (2021) 1–69, `arXiv:2009.00516 [hep-ph]`.

[146] H. X. Zhu, “On the calculation of soft phase space integral,” *JHEP* **02** (2015) 155, `arXiv:1501.00236 [hep-ph]`.

[147] A. Autieri, S. Camarda, L. Cieri, G. Ferrera, and G. F. R. Sborlini, “Transverse-momentum resummation at mixed QCD⊗QED NNLL accuracy for Z boson production at hadron colliders,” *JHEP* **03** (2026) 113, `arXiv:2511.07324 [hep-ph]`.

[148] S. Camarda, L. Cieri, and G. Ferrera, “Drell–Yan lepton-pair production: qT resummation at N4LL accuracy,” *Phys. Lett. B* **845** (2023) 138125, `arXiv:2303.12781 [hep-ph]`.

[149] A. Autieri, L. Cieri, G. Ferrera, and G. F. R. Sborlini, “Combining QED and QCD transverse-momentum resummation for W and Z boson production at hadron colliders,” *JHEP* **07** (2023) 104, `arXiv:2302.05403 [hep-ph]`.

[150] L. Cieri, G. Ferrera, and G. F. R. Sborlini, “Combining QED and QCD transverse-momentum resummation for Z boson production at hadron colliders,” *JHEP* **08** (2018) 165, `arXiv:1805.11948 [hep-ph]`.

[151] G. Ferrera, G. Somogyi, and F. Tramontano, "Associated production of a Higgs boson decaying into bottom quarks at the LHC in full NNLO QCD," *Phys. Lett. B* **780** (2018) 346–351, arXiv:1705.10304 [hep-ph].

[152] S. Catani, L. Cieri, G. Ferrera, D. de Florian, and M. Grazzini, "Vector boson production at hadron colliders: a fully exclusive QCD calculation at NNLO," *Phys. Rev. Lett.* **103** (2009) 082001, arXiv:0903.2120 [hep-ph].

[153] G. Bozzi, S. Catani, G. Ferrera, D. de Florian, and M. Grazzini, "Production of Drell-Yan lepton pairs in hadron collisions: Transverse-momentum resummation at next-to-next-to-leading logarithmic accuracy," *Phys. Lett.* **B696** (2011) 207–213, arXiv:1007.2351 [hep-ph].

[154] G. Ferrera, M. Grazzini, and F. Tramontano, "Associated WH production at hadron colliders: a fully exclusive QCD calculation at NNLO," *Phys. Rev. Lett.* **107** (2011) 152003, arXiv:1107.1164 [hep-ph].

[155] S. Catani, L. Cieri, D. de Florian, G. Ferrera, and M. Grazzini, "Diphoton production at hadron colliders: a fully-differential QCD calculation at NNLO," *Phys. Rev. Lett.* **108** (2012) 072001, arXiv:1110.2375 [hep-ph]. [Erratum: Phys.Rev.Lett. 117, 089901 (2016)].

[156] S. Pal and S. Seth, "Universality at next-to-leading power for jet associated processes," *Phys. Rev. D* **112** no. 9, (2025) L091505, arXiv:2505.01340 [hep-ph].

[157] M. K. Mandal, P. Mathews, V. Ravindran, and S. Seth, "Three photon production to NLO+PS accuracy at the LHC," *Eur. Phys. J. C* **74** (2014) 3044, arXiv:1403.2917 [hep-ph].

[158] R. K. Ellis and S. Seth, "On Higgs boson plus gluon amplitudes at one loop," *JHEP* **11** (2018) 006, arXiv:1808.09292 [hep-ph].

[159] L. Budge, J. M. Campbell, G. De Laurentis, R. K. Ellis, and S. Seth, "The one-loop amplitudes for Higgs + 4 partons with full mass effects," *JHEP* **05** (2020) 079, arXiv:2002.04018 [hep-ph].

[160] J. M. Campbell, G. De Laurentis, R. K. Ellis, and S. Seth, "The pp $\rightarrow$ W($\rightarrow$ lν) + γ process at next-to-next-to-leading order," *JHEP* **07** (2021) 079, arXiv:2105.00954 [hep-ph].

[161] J. M. Campbell, R. K. Ellis, T. Neumann, and S. Seth, "Transverse momentum resummation at N^{3}LL+NNLO for diboson processes," *JHEP* **03** (2023) 080, arXiv:2210.10724 [hep-ph].

[162] S. Pal and S. Seth, "On Higgs+jet production at next-to-leading power accuracy," *Phys. Rev. D* **109** no. 11, (2024) 114018, arXiv:2309.08343 [hep-ph].

[163] S. Pal and S. Seth, "Soft quark effects on H+jet production at NLP accuracy," *Phys. Lett. B* **860** (2025) 139179, arXiv:2405.06444 [hep-ph].

[164] D. Choudhury, S. Majhi, and V. Ravindran, "QCD corrections to resonant slepton production in hadron colliders," *Nucl. Phys. B* **660** (2003) 343–361, arXiv:hep-ph/0207247.

[165] S. Majhi, P. Mathews, and V. Ravindran, "NNLO QCD corrections to the resonant sneutrino/slepton production at Hadron Colliders," *Nucl. Phys. B* **850** (2011) 287–320, arXiv:1011.6027 [hep-ph].

[166] N. Agarwal, V. Ravindran, V. K. Tiwari, and A. Tripathi, "W^+W^- production in Large extra dimension model at next-to-leading order in QCD at the LHC," *Phys. Rev.* **D82** (2010) 036001, arXiv:1003.5450 [hep-ph].

[167] N. Agarwal, V. Ravindran, V. K. Tiwari, and A. Tripathi, "Next-to-leading order QCD corrections to W^+W^- production at the LHC in Randall Sundrum model," *Phys. Lett.* **B690** (2010) 390–395, arXiv:1003.5445 [hep-ph].

[168] N. Agarwal, P. Banerjee, G. Das, P. K. Dhani, A. Mukhopadhyay, V. Ravindran, and A. Tripathi, "Resummed transverse momentum distribution of pseudo-scalar Higgs boson at NNLO$_A$+NNLL," *JHEP* **12** (2018) 105, arXiv:1805.12553 [hep-ph].

[169] S. Goyal, S.-O. Moch, V. Pathak, N. Rana, and V. Ravindran, "Next-to-Next-to-Leading Order QCD Corrections to Semi-Inclusive Deep-Inelastic Scattering," *Phys. Rev. Lett.* **132** no. 25, (2024) 251902, arXiv:2312.17711 [hep-ph].

[170] S. Goyal, R. N. Lee, S.-O. Moch, V. Pathak, N. Rana, and V. Ravindran, "NNLO QCD corrections to unpolarized and polarized SIDIS," *Phys. Rev. D* **111** no. 9, (2025) 094007, arXiv:2412.19309 [hep-ph].

[171] S. Goyal, R. N. Lee, S.-O. Moch, V. Pathak, N. Rana, and V. Ravindran, "Next-to-Next-to-Leading Order QCD Corrections to Polarized Semi-Inclusive Deep-Inelastic Scattering," *Phys. Rev. Lett.* **133** (2024) 211905, arXiv:2404.09959 [hep-ph].

[172] S. Goyal, S.-O. Moch, V. Pathak, N. Rana, and V. Ravindran, "Soft and virtual corrections to semi-inclusive DIS up to four loops in QCD," arXiv:2506.24078 [hep-ph].

[173] S. Goyal, R. N. Lee, S.-O. Moch, V. Pathak, and V. Ravindran, "NNLO QCD⊗QED corrections to unpolarized and polarized SIDIS," arXiv:2510.18872 [hep-ph].

[174] S. Goyal, S.-O. Moch, V. Pathak, and V. Ravindran, "NNLO QCD corrections to unpolarized and polarized electroweak structure functions in semi-inclusive deep-inelastic scattering," arXiv:2603.30012 [hep-ph].

[175] T. Ahmed, S. Goyal, S. M. Hasan, R. N. Lee, S.-O. Moch, V. Pathak, N. Rana, A. Rapakoulias, and V. Ravindran, "NNLO phase-space integrals for

semi-inclusive deep-inelastic scattering," *Phys. Rev. D* **112** no. 1, (2025) 014020, arXiv:2412.16509 [hep-ph].

[176] L. Bonino, T. Gehrmann, M. Marcoli, R. Schürmann, and G. Stagnitto, "Antenna subtraction for processes with identified particles at hadron colliders," *JHEP* **08** (2024) 073, arXiv:2406.09925 [hep-ph].

[177] L. Bonino, T. Gehrmann, and G. Stagnitto, "Semi-Inclusive Deep-Inelastic Scattering at Next-to-Next-to-Leading Order in QCD," *Phys. Rev. Lett.* **132** no. 25, (2024) 251901, arXiv:2401.16281 [hep-ph].

[178] L. Bonino, T. Gehrmann, M. Löchner, K. Schönwald, and G. Stagnitto, "Polarized Semi-Inclusive Deep-Inelastic Scattering at Next-to-Next-to-Leading Order in QCD," *Phys. Rev. Lett.* **133** no. 21, (2024) 211904, arXiv:2404.08597 [hep-ph].

[179] L. Bonino, T. Gehrmann, M. Löchner, K. Schönwald, and G. Stagnitto, "Polarized Neutral and Charged Current Semi-Inclusive Deep-Inelastic Scattering at NNLO in QCD," arXiv:2510.00100 [hep-ph].

[180] L. Bonino, T. Gehrmann, M. Löchner, K. Schönwald, and G. Stagnitto, "Neutral and charged current semi-inclusive deep-inelastic scattering at NNLO QCD," *JHEP* **10** (2025) 016, arXiv:2506.19926 [hep-ph].

[181] L. Bonino, T. Gehrmann, M. Löchner, K. Schönwald, and G. Stagnitto, "Identified Hadron Production in Deeply Inelastic Neutrino-Nucleon Scattering," arXiv:2504.05376 [hep-ph].

[182] P. Nogueira, "Automatic Feynman graph generation," *J. Comput. Phys.* **105** (1993) 279–289.

[183] J. Kuipers, T. Ueda, J. A. M. Vermaseren, and J. Vollinga, "FORM version 4.0" *Comput. Phys. Commun.* **184** (2013) 1453–1467, arXiv:1203.6543 [cs.SC].

[184] B. Ruijl, T. Ueda, and J. Vermaseren, "FORM version 4.2" arXiv:1707.06453 [hep-ph].

[185] T. Matsuura, S. van der Marck, and W. van Neerven, "The Calculation of the Second Order Soft and Virtual Contributions to the Drell-Yan Cross-Section," *Nucl. Phys. B* **319** (1989) 570–622.

[186] E. B. Zijlstra and W. L. van Neerven, "Order alpha-s**2 QCD corrections to the deep inelastic proton structure functions F2 and F(L)," *Nucl. Phys. B* **383** (1992) 525–574.

[187] P. J. Rijken and W. L. van Neerven, "Higher order QCD corrections to the transverse and longitudinal fragmentation functions in electron - positron annihilation," *Nucl. Phys. B* **487** (1997) 233–282, arXiv:hep-ph/9609377.

[188] V. Ravindran, J. Smith, and W. L. van Neerven, "NNLO corrections to the total cross-section for Higgs boson production in hadron hadron collisions," *Nucl. Phys.* **B665** (2003) 325–366, arXiv:hep-ph/0302135 [hep-ph].

[189] K. G. Chetyrkin and F. V. Tkachov, "Integration by parts: The algorithm to calculate β-functions in 4 loops," *Nucl. Phys. B* **192** (1981) 159–204.

[190] S. Laporta, "High-precision calculation of multiloop Feynman integrals by difference equations," *Int. J. Mod. Phys. A* **15** (2000) 5087–5159, arXiv:hep-ph/0102033.

[191] P. Maierhöfer, J. Usovitsch, and P. Uwer, "Kira—A Feynman integral reduction program," *Comput. Phys. Commun.* **230** (2018) 99–112, arXiv:1705.05610 [hep-ph].

[192] A. V. Smirnov and F. S. Chukharev, "FIRE6: Feynman Integral REduction with modular arithmetic," *Comput. Phys. Commun.* **247** (2020) 106877, arXiv:1901.07808 [hep-ph].

[193] C. Anastasiou, K. Melnikov, and F. Petriello, "A new method for real radiation at NNLO," *Phys. Rev. D* **69** (2004) 076010, arXiv:hep-ph/0311311.

[194] C. Anastasiou, S. Buehler, C. Duhr, and F. Herzog, "NNLO phase space master integrals for two-to-one inclusive cross sections in dimensional regularization," *JHEP* **11** (2012) 062, arXiv:1208.3130 [hep-ph].

[195] C. Anastasiou, L. J. Dixon, K. Melnikov, and F. Petriello, "High precision QCD at hadron colliders: Electroweak gauge boson rapidity distributions at NNLO," *Phys. Rev.* **D69** (2004) 094008, arXiv:hep-ph/0312266 [hep-ph].

[196] C. Anastasiou and K. Melnikov, "Higgs boson production at hadron colliders in NNLO QCD," *Nucl. Phys.* **B646** (2002) 220–256, arXiv:hep-ph/0207004 [hep-ph].

[197] R. N. Lee, "Presenting LiteRed: a tool for the Loop InTEgrals REDuction," arXiv:1212.2685 [hep-ph].

[198] R. N. Lee, "LiteRed 1.4: a powerful tool for reduction of multiloop integrals," *J. Phys. Conf. Ser.* **523** (2014) 012059, arXiv:1310.1145 [hep-ph].

[199] R. N. Lee, "Reducing differential equations for multiloop master integrals," *JHEP* **04** (2015) 108, arXiv:1411.0911 [hep-ph].

[200] T. Matsuura and W. van Neerven, "Second Order Logarithmic Corrections to the Drell-Yan Cross-section," *Z. Phys. C* **38** (1988) 623.

[201] T. Gehrmann, T. Huber, and D. Maitre, "Two-loop quark and gluon form-factors in dimensional regularisation," *Phys. Lett. B* **622** (2005) 295–302, arXiv:hep-ph/0507061.

[202] T. Gehrmann, E. Glover, T. Huber, N. Ikizlerli, and C. Studerus, "Calculation of the quark and gluon form factors to three loops in QCD," *JHEP* **06** (2010) 094, arXiv:1004.3653 [hep-ph].

[203] R. N. Lee, A. V. Smirnov, and V. A. Smirnov, "Analytic Results for Massless Three-Loop Form Factors," *JHEP* **04** (2010) 020, arXiv:1001.2887 [hep-ph].

[204] T. Ahmed, M. Mahakhud, P. Mathews, N. Rana, and V. Ravindran, "Two-loop QCD corrections to Higgs $\to b + \overline{b} + g$ amplitude," *JHEP* **08** (2014) 075, arXiv:1405.2324 [hep-ph].

[205] A. Bhattacharya, M. Mahakhud, P. Mathews, and V. Ravindran, "Two loop QCD amplitudes for di-pseudo scalar production in gluon fusion," *JHEP* **02** (2020) 121, arXiv:1909.08993 [hep-ph].

[206] A. A H, P. Banerjee, A. Chakraborty, P. K. Dhani, P. Mukherjee, N. Rana, and V. Ravindran, "Higgs pair production from bottom quark annihilation to NNLO in QCD," *JHEP* **05** (2019) 030, arXiv:1811.01853 [hep-ph].

[207] P. Banerjee, P. K. Dhani, and V. Ravindran, "Two loop QCD corrections for the process Pseudo-scalar Higgs $\to$ 3 partons," *JHEP* **10** (2017) 067, arXiv:1708.02387 [hep-ph].

[208] T. Ahmed, P. Banerjee, P. K. Dhani, M. Kumar, P. Mathews, N. Rana, and V. Ravindran, "NNLO QCD corrections to the Drell–Yan cross section in models of TeV-scale gravity," *Eur. Phys. J. C* **77** no. 1, (2017) 22, arXiv:1606.08454 [hep-ph].

[209] T. Ahmed, T. Gehrmann, P. Mathews, N. Rana, and V. Ravindran, "Pseudo-scalar Form Factors at Three Loops in QCD," *JHEP* **11** (2015) 169, arXiv:1510.01715 [hep-ph].

[210] T. Ahmed, G. Das, P. Mathews, N. Rana, and V. Ravindran, "Spin-2 Form Factors at Three Loop in QCD," *JHEP* **12** (2015) 084, arXiv:1508.05043 [hep-ph].

[211] D. de Florian, M. Mahakhud, P. Mathews, J. Mazzitelli, and V. Ravindran, "Quark and gluon spin-2 form factors to two-loops in QCD," *JHEP* **02** (2014) 035, arXiv:1312.6528 [hep-ph].

[212] T. Matsuura, *Higher order corrections to the drell-yan process*. PhD thesis, Leiden U., 1989.

[213] G. Somogyi, Z. Trocsanyi, and V. Del Duca, "A Subtraction scheme for computing QCD jet cross sections at NNLO: Regularization of doubly-real emissions," *JHEP* **01** (2007) 070, arXiv:hep-ph/0609042.

[214] P. Banerjee, S. Borowka, P. K. Dhani, T. Gehrmann, and V. Ravindran, "Two-loop massless QCD corrections to the $g + g \to H + H$ four-point amplitude," *JHEP* **11** (2018) 130, arXiv:1809.05388 [hep-ph].

[215] T. Ahmed, A. A H, L. Chen, P. K. Dhani, P. Mukherjee, and V. Ravindran, "Polarised Amplitudes and Soft-Virtual Cross Sections for $b\bar{b} \to ZH$ at NNLO in QCD," *JHEP* **01** (2020) 030, arXiv:1910.06347 [hep-ph].

[216] G. Somogyi, Z. Trocsanyi, and V. Del Duca, "Matching of singly- and doubly-unresolved limits of tree-level QCD squared matrix elements," *JHEP* **06** (2005) 024, arXiv:hep-ph/0502226.

[217] T. Gehrmann and E. Remiddi, "Differential equations for two-loop four-point functions," *Nucl. Phys. B* **580** (2000) 485–518, arXiv:hep-ph/9912329.

[218] T. Gehrmann and R. Schürmann, "Photon fragmentation in the antenna subtraction formalism," *JHEP* **04** (2022) 031, arXiv:2201.06982 [hep-ph].

[219] A. B. Goncharov, "Multiple polylogarithms, cyclotomy and modular complexes," *Math. Res. Lett.* **5** (1998) 497–516, arXiv:1105.2076 [math.AG].

[220] E. Remiddi and J. A. M. Vermaseren, "Harmonic polylogarithms," *Int. J. Mod. Phys. A* **15** (2000) 725–754, arXiv:hep-ph/9905237.

[221] T. Gehrmann and E. Remiddi, "Numerical evaluation of harmonic polylogarithms," *Comput. Phys. Commun.* **141** (2001) 296–312, arXiv:hep-ph/0107173.

[222] D. Maitre, "HPL, a mathematica implementation of the harmonic polylogarithms," *Comput. Phys. Commun.* **174** (2006) 222–240, arXiv:hep-ph/0507152.

[223] S. Buehler and C. Duhr, "Chaplin—complex harmonic polylogarithms in fortran," *Computer Physics Communications* **185** no. 10, (2014) 2703–2713. https://www.sciencedirect.com/science/article/pii/S0010465514001969.

[224] E. Gardi and L. Magnea, "Infrared singularities in QCD amplitudes," *Nuovo Cim. C* **32N5-6** (2009) 137–157, arXiv:0908.3273 [hep-ph].

[225] T. Becher and M. Neubert, "Infrared singularities of scattering amplitudes in perturbative QCD," *Phys. Rev. Lett.* **102** (2009) 162001, arXiv:0901.0722 [hep-ph]. [Erratum: Phys. Rev. Lett.111,no.19,199905(2013)].

[226] S. Moch, J. A. M. Vermaseren, and A. Vogt, "The Three loop splitting functions in QCD: The Nonsinglet case," *Nucl. Phys.* **B688** (2004) 101–134, arXiv:hep-ph/0403192 [hep-ph].

[227] A. Vogt, S. Moch, and J. A. M. Vermaseren, "The Three-loop splitting functions in QCD: The Singlet case," *Nucl. Phys.* **B691** (2004) 129–181, arXiv:hep-ph/0404111 [hep-ph].

[228] A. Mitov, S. Moch, and A. Vogt, "Next-to-Next-to-Leading Order Evolution of Non-Singlet Fragmentation Functions," *Phys. Lett. B* **638** (2006) 61–67, arXiv:hep-ph/0604053.

[229] S. Moch and A. Vogt, "On non-singlet physical evolution kernels and large-x coefficient functions in perturbative QCD," *JHEP* **11** (2009) 099, arXiv:0909.2124 [hep-ph].

[230] A. A. Almasy, S. Moch, and A. Vogt, "On the Next-to-Next-to-Leading Order Evolution of Flavour-Singlet Fragmentation Functions," *Nucl. Phys. B* **854** (2012) 133–152, arXiv:1107.2263 [hep-ph].

[231] H. Chen, T.-Z. Yang, H. X. Zhu, and Y. J. Zhu, "Analytic Continuation and Reciprocity Relation for Collinear Splitting in QCD," *Chin. Phys. C* **45** no. 4, (2021) 043101, arXiv:2006.10534 [hep-ph].

[232] S. Goyal, R. Lee, S.-O. Moch, V. Pathak, N. Rana, and V. Ravindran, ",".

[233] T. Ahmed, M. K. Mandal, N. Rana, and V. Ravindran, "Rapidity Distributions in Drell-Yan and Higgs Productions at Threshold to Third Order in QCD," *Phys. Rev. Lett.* **113** (2014) 212003, arXiv:1404.6504 [hep-ph].

[234] **NNPDF** Collaboration, R. D. Ball *et al.*, "Parton distributions from high-precision collider data," *Eur. Phys. J. C* **77** no. 10, (2017) 663, arXiv:1706.00428 [hep-ph].

[235] **NNPDF** Collaboration, V. Bertone, S. Carrazza, N. P. Hartland, E. R. Nocera, and J. Rojo, "A determination of the fragmentation functions of pions, kaons, and protons with faithful uncertainties," *Eur. Phys. J. C* **77** no. 8, (2017) 516, arXiv:1706.07049 [hep-ph].

[236] **MAP (Multi-dimensional Analyses of Partonic distributions)** Collaboration, R. Abdul Khalek, V. Bertone, A. Khoudli, and E. R. Nocera, "Pion and kaon fragmentation functions at next-to-next-to-leading order," *Phys. Lett. B* **834** (2022) 137456, arXiv:2204.10331 [hep-ph].

[237] L. A. Harland-Lang, A. D. Martin, P. Motylinski, and R. S. Thorne, "Parton distributions in the LHC era: MMHT 2014 PDFs," *Eur. Phys. J.* **C75** no. 5, (2015) 204, arXiv:1412.3989 [hep-ph].

[238] A. D. Martin, W. J. Stirling, R. S. Thorne, and G. Watt, "Parton distributions for the LHC," *Eur. Phys. J. C* **63** (2009) 189–285, arXiv:0901.0002 [hep-ph].

[239] D. de Florian, G. F. R. Sborlini, and G. Rodrigo, "QED corrections to the Altarelli–Parisi splitting functions," *Eur. Phys. J. C* **76** no. 5, (2016) 282, arXiv:1512.00612 [hep-ph].

[240] D. de Florian, G. F. R. Sborlini, and G. Rodrigo, "Two-loop QED corrections to the Altarelli-Parisi splitting functions," *JHEP* **10** (2016) 056, arXiv:1606.02887 [hep-ph].

[241] D. de Florian and L. P. Conte, "Analytical solution for QCD ⊗ QED evolution," arXiv:2505.03520 [hep-ph].

[242] D. de Florian, M. Der, and I. Fabre, "QCD⊕QED NNLO corrections to Drell Yan production," *Phys. Rev. D* **98** no. 9, (2018) 094008, arXiv:1805.12214 [hep-ph].

[243] L. Cieri, D. de Florian, M. Der, and J. Mazzitelli, "Mixed QCD⊗QED corrections to exclusive Drell Yan production using the q_T -subtraction method," *JHEP* **09** (2020) 155, arXiv:2005.01315 [hep-ph].

[244] W. B. Kilgore and C. Sturm, "Two-Loop Virtual Corrections to Drell-Yan Production at order $\alpha_s\alpha^3$," *Phys. Rev. D* **85** (2012) 033005, arXiv:1107.4798 [hep-ph].

[245] A. V. Manohar, P. Nason, G. P. Salam, and G. Zanderighi, "The Photon Content of the Proton," *JHEP* **12** (2017) 046, arXiv:1708.01256 [hep-ph].

[246] R. Bonciani, L. Buonocore, M. Grazzini, S. Kallweit, N. Rana, F. Tramontano, and A. Vicini, "Mixed Strong-Electroweak Corrections to the Drell-Yan Process," *Phys. Rev. Lett.* **128** no. 1, (2022) 012002, arXiv:2106.11953 [hep-ph].

[247] J. Blümlein and H. Kawamura, "Universal higher order singlet QED corrections to unpolarized lepton scattering," *Eur. Phys. J. C* **51** (2007) 317–333, `arXiv:hep-ph/0701019`.

[248] T. Liu, W. Melnitchouk, J.-W. Qiu, and N. Sato, "Factorized approach to radiative corrections for inelastic lepton-hadron collisions," *Phys. Rev. D* **104** no. 9, (2021) 094033, `arXiv:2008.02895 [hep-ph]`.

[249] J. Cammarota, J.-W. Qiu, K. Watanabe, and J.-Y. Zhang, "Factorized QED and QCD contribution to deeply inelastic scattering," *Phys. Rev. D* **112** no. 5, (2025) 056007, `arXiv:2505.23487 [hep-ph]`.

[250] A. D. Martin, R. G. Roberts, W. J. Stirling, and R. S. Thorne, "Parton distributions incorporating QED contributions," *Eur. Phys. J. C* **39** (2005) 155–161, `arXiv:hep-ph/0411040`.

[251] R. D. Ball, V. Bertone, S. Carrazza, L. Del Debbio, S. Forte, A. Guffanti, N. P. Hartland, and J. Rojo, "Parton distributions with qed corrections," *Nuclear Physics B* **877** no. 2, (2013) 290–320. `https://www.sciencedirect.com/science/article/pii/S0550321313005233`.

[252] M. Roth and S. Weinzierl, "QED corrections to the evolution of parton distributions," *Phys. Lett. B* **590** (2004) 190–198, `arXiv:hep-ph/0403200`.

[253] A. Kwiatkowski, H. Spiesberger, and H. J. Möhring, "Heracles: An Event Generator for *ep* Interactions at HERA Energies Including Radiative Processes: Version 1.0," *Comput. Phys. Commun.* **69** (1992) 155–172.

[254] K. Charchula, G. A. Schuler, and H. Spiesberger, "Combined QED and QCD radiative effects in deep inelastic lepton - proton scattering: The Monte Carlo generator DJANGO6," *Comput. Phys. Commun.* **81** (1994) 381–402.

[255] A. Arbuzov, D. Y. Bardin, J. Blümlein, L. Kalinovskaya, and T. Riemann, "Hector 1.00: A Program for the calculation of QED, QCD and electroweak corrections to ep and $l^{\pm}N$ deep inelastic neutral and charged current scattering," *Comput. Phys. Commun.* **94** (1996) 128–184, arXiv:hep-ph/9511434.

[256] H. Spiesberger, "*Radiative corrections to deep inelastic ep scattering at HERA*," 12, 1989. DESY-89-175, https://lib-extopc.kek.jp/preprints/PDF/1990/9003/9003109.pdf.

[257] E. B. Zijlstra and W. L. van Neerven, "Order-α_s^2 corrections to the polarized structure function $g_1(x, Q^2)$," *Nucl. Phys. B* **417** (1994) 61–100. [Erratum: Nucl.Phys.B 426, 245 (1994), Erratum: Nucl.Phys.B 773, 105–106 (2007), Erratum: Nucl.Phys.B 501, 599–599 (1997)].

[258] S. Larin and J. Vermaseren, "The Three loop QCD Beta function and anomalous dimensions," *Phys. Lett. B* **303** (1993) 334–336, arXiv:hep-ph/9302208.

[259] Y. Matiounine, J. Smith, and W. L. van Neerven, "Two loop operator matrix elements calculated up to finite terms for polarized deep inelastic lepton - hadron scattering," *Phys. Rev. D* **58** (1998) 076002, arXiv:hep-ph/9803439.

[260] S. Moch, J. A. M. Vermaseren, and A. Vogt, "The Three-Loop Splitting Functions in QCD: The Helicity-Dependent Case," *Nucl. Phys. B* **889** (2014) 351–400, arXiv:1409.5131 [hep-ph].

[261] D. de Florian and L. P. Conte, "Qed corrections to parton distributions and Altarelli–Parisi splitting functions in the polarized case," *Eur. Phys. J. C* **83** no. 8, (2023) 695, arXiv:2305.14144 [hep-ph].

[262] V. Ravindran, J. Smith, and W. van Neerven, "Nlo differential distributions of massive lepton-pair production in longitudinally polarized proton–proton collisions," *Nuclear Physics B* **647** no. 1, (2002) 275–318. https://www.sciencedirect.com/science/article/pii/S0550321302009392.

[263] R. Mertig and W. L. van Neerven, “The Calculation of the two loop spin splitting functions P(ij)(1)(x),” *Z. Phys. C* **70** (1996) 637–654, arXiv:hep-ph/9506451.

[264] W. Vogelsang, “A Rederivation of the spin dependent next-to-leading order splitting functions,” *Phys. Rev. D* **54** (1996) 2023–2029, arXiv:hep-ph/9512218.

[265] W. Vogelsang, “The Spin dependent two loop splitting functions,” *Nucl. Phys. B* **475** (1996) 47–72, arXiv:hep-ph/9603366.

[266] J. Blümlein, P. Marquard, C. Schneider, and K. Schönwald, “The three-loop unpolarized and polarized non-singlet anomalous dimensions from off shell operator matrix elements,” *Nucl. Phys. B* **971** (2021) 115542, arXiv:2107.06267 [hep-ph].

[267] J. Blümlein, P. Marquard, C. Schneider, and K. Schönwald, “The three-loop polarized singlet anomalous dimensions from off-shell operator matrix elements,” *JHEP* **01** (2022) 193, arXiv:2111.12401 [hep-ph].

[268] A. Ajjath, P. Banerjee, A. Chakraborty, P. K. Dhani, P. Mukherjee, N. Rana, and V. Ravindran, “NNLO QCD⊕QED corrections to Higgs production in bottom quark annihilation,” *Phys. Rev. D* **100** no. 11, (2019) 114016, arXiv:1906.09028 [hep-ph].

[269] **NNPDF** Collaboration, V. Bertone, S. Carrazza, N. P. Hartland, and J. Rojo, “Illuminating the photon content of the proton within a global PDF analysis,” *SciPost Phys.* **5** no. 1, (2018) 008, arXiv:1712.07053 [hep-ph].

[270] D. de Florian, L. P. Conte, and G. F. Volonnino, “The polarized photon distribution function,” *Eur. Phys. J. C* **84** no. 9, (2024) 905, arXiv:2406.03414 [hep-ph].